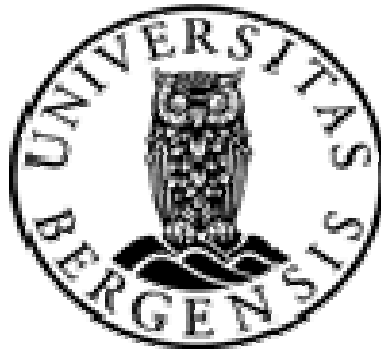


**Master Thesis in Geodynamics**

**Seismotectonics in Central Sudan and Local Site  
Effect in Western Khartoum**



**Alrasheed Warage**  
**Department of Earth Science**  
**University of Bergen, Norway**

**November 2007**



## Table of Contents

Abstract .....	6
Chapter One: Introduction.....	8
1.1 Background Seismicity.....	9
1.2 Background of Tectonics.....	12
PART I: Seismicity and Tectonics of Central Sudan.....	17
Chapter Two: Previous and Present work in the study area(PART I).....	18
2.1 Introducion.....	18
2.2 Study area.....	19
2.3 Previous work in Seismicity of study area.....	19
2.4 Present Study.....	20
Chapter Three: Local Geology and Structure.....	22
Chapter Four: Data and Methods.....	25
4.1 Focal mechanism.....	25
4.1.1 Focal mechanism using ISC Bulletin data.....	26
4.1.2 Focal mechanism using ISC bulletin data and data from Clarke and Browne (1987).....	26
4.1.3 Uncertainty of solution using ISC data.....	27
4.2 Intensity.....	32
4.3 Magnitude.....	34
4.4 Relocation event from macroseismic observation.....	37
4.4.1 Single station method.....	38
4.4.2 Multiple station location.....	40
4.5 Relocation using master event.....	45
4.6 Length of fault rupture.....	47
Chapter Five: Results and Discussions.....	49
Chapter Six: Conclusion.....	51
Refrences of PART I .....	52
PART II: Local site effects in western Khartoum city and Omdurman town.....	57

Chapter Seven: Introduction to PART II.....	58
Chapter Eight: Local seismically around Khartoum.....	61
Chapter Nine: Local Geology of Khartoum area.....	63
9.1 Introduction to Geology.....	63
9.1.1 Basement Complex.....	65
9.1.2 Nubian Sandstone Formation (Mesozoic).....	64
9.1.3 Tertiary volcanoes.....	66
9.1.4 The Gezira Formation.....	66
9.1.5 Superficial deposit (Quaternary).....	68
9.2 Tectonic and structure.....	69
9.3 Other environmental conditions.....	69
Chapter Ten: Methods for empirical estimation of the site effects.....	71
10.1 H/V spectral ratio of strong motion of the earthquake.....	71
10.2 H/V spectral ratio of weak motion.....	76
10.3 H/V spectral ration of noise recording.....	76
Chapter Eleven: Data collection.....	80
11.1 Method and data used.....	80
11.1.1 Measurement Sequence.....	80
11.1.2 Instrument testing.....	81
11.1.3 Data collection.....	89
11.2 Analysis data recording (with SEISAN and JSESAME).....	91
11.2.1 Data Collection.....	91
Chapter Twelve: Analysis of the data and results.....	93
12.1 Analysis of H/V ratio from ambient noise record.....	93
12.1.1 Analysis data recording (with SEISAN and JSESAME).....	93
12.1.2 Result of H/V ratio.....	98
12.1.3 Classification of the spectra computed from the dataset collected in study area.....	106
12.1.4 Spatial distribution of the fundamental site frequency and amplification factor for the western of the Khartoum city.....	122
12.2 Analysis earthquake data for estimate local site effects and results .....	127
12.2.1 Analysis of the H/V ratio for the noise and S-wave recording for weak motion.....	127

12.3 Analysis of Standard Spectral Ratio (SSR method) of weak motion.....	137
Chapter Thirteen: Discussions and Conclusions.....	143
Acknowledgements.....	151
References of PART II.....	152
Appendix A.....	154
Appendix B.....	158
Appendix C.....	161

## **Abstract**

The central part of Sudan is tectonically significant which needs to be studied. In recent years, the central part has grown economically and the population has increased. This results in growing interest to estimate the seismic hazard through tectonic and seismological studies. In the present work we carried out two studies. We used earthquake data to analyze the seismotectonics of the area and conducted a local site effects study in western part of Khartoum.

The first part discusses the seismicity and tectonics of central Sudan. Five significant earthquakes are used which occurred in the area. Earthquakes are relocated and the focal mechanism of the 1966 earthquake is made. We observed that all the events are associated with normal and strike-slip faulting. Focal mechanism of the 1966 earthquake at the south part of central Sudan is interpreted as left lateral strike-slip fault. It has similar focal mechanism as the 1993 earthquake in the northern part of central Sudan. Both of them are conformable with the same stress regimes in that area. However, they do not fit with the orientation of the stress tensor dominated by the Red Sea and East African Rift Systems.

The second part, we have surveyed the site effects in western part of Khartoum city (Omdurman and western Khartoum town). We used the H/V spectral ratio method to calculate the fundamental site frequencies and amplification factors in different sites. The geological conditions of these sites are different, which contains basement rocks mainly granite exposed at the boundaries of the area and covered by Cretaceous and Quaternary sediments in central part of the area. In the study area, we observed that the agreement of the fundamental site frequencies and the amplification factors with the underlying geology was good. The method itself is known to be less reliable for the estimation of the exact amplification factor. Therefore the standard spectral ratio method was used with earthquake data to estimate the amplification factor in Khartoum area. However, this analysis showed poor correlation in the amplification factors. In spite of this, we observed that the H/V ratio and the standard spectral method gave reasonably good correlation for the fundamental sites frequencies. Both methods show good agreement between the sites response and the underlying geology. Furthermore, the H/V spectral ratio results are similar to the analytical

studies conducted by Mohmedazein et al (2006) in central Khartoum. We believe that the present work highlights the importance of local site effects in Khartoum and needs to be taken into account in estimating the earthquake hazard in the area.

# Chapter One

## Introduction

Most of Sudan is classified as low seismic activity and is tectonically stable since the area is an intraplate region. Only the Juba region in southern Sudan and the Suakin city area near the Red sea have high seismic activity. These areas have experienced large earthquakes due to their proximity to the plate boundary. Generally central Sudan is as area characterised with low seismicity. But the area has experienced many infrequent moderate earthquakes; the largest one was in 1966 ( $M_s = 5.6$ ) and located close to Jebel Dumbeir area [*Qureshi and Sadig 1967*]. The Hamrat Elsheikh event in 1993 ( $M_s = 5.5$ ) was located near Khartoum city. Central Sudan is of special interest, because the area is located in relatively stable part of the African land mass away from the East Africa Rift system and Red Sea. Central Sudan is economically important because of the high population density.

Recently, after the installation of Sudanese's seismological network in 2003, there is new better information about seismic activity in parts of central Sudan. And more current geophysical studies are being carried out to investigate the tectonics of the area. Using these recently available data the seismicity of central Sudan is analysed. The study area is divided into two parts. Part I deals with the seismicity and tectonics of southern part of the central Sudan. Part II deals with site effect local in western part of Khartoum city (see figure 1).

In the Part I, we discuss and evaluate the tectonics of southern part of central Sudan using global and local earthquake data. The area has been considered tectonically quiet as it is located far from the activities determining plate boundaries. Most are felt over distance indicating low attenuation typical of stable continental in intensity. One of the objectives of this study is to understand the source of these moderate size earthquakes and to investigate the earthquake generating potentials reveal to the Khartoum city and the town of Elobid.

In Part II, we empirically evaluated the expected local site effects in western Khartoum city - in central Sudan. In this part we have used two datasets. First, we made records of ambient seismic noise in many different sites in western Khartoum and Omdurman. We applied H/V spectral ratio, the so called "Nakamura method" to



calculate the local site response. The second dataset we used were local earthquakes recorded by Sudanese Seismological Network (SSN). We applied different H/V spectral ratio and Standard Spectral Ratio methods (spectral ratio of sedimentary versus bed rock) in order to evaluate the site response in that area.

## 1.2 Background Seismicity

Most of Sudan is classified as country of low seismic activity and is tectonically stable since the area is in an intraplate region. Only the Juba region in southern Sudan and the Suakin city near the Red sea have high seismic activity.. Examples of the larger earthquakes are; 20 May 1990,  $M_s = 7.1 - 7.4$ , one of the largest earthquakes in Africa. It was located near Juba city in southern Sudan. And the main event was followed by several aftershocks of which the largest had magnitude of  $M_s = 7.0$  [D. Giardini and I. Beranzoli 1991]. Another earthquake whose effect caused damage, was the 12 May 1938 ( $M_s = 5.8$ ), which located close to Suakin city near the Red Sea. Both events are associated with the activity rifting areas along the Red sea and East and East African Rift system (EARS). Generally central Sudan is an area of low seismicity. However the area has experienced many infrequent moderate earthquakes; the largest one in 1966 ( $M_s = 5.6$ ) where was located close to Jebel Dumbeir area [Qureshi and Sadig 1967]. The Hamrat Elsheikh event on 1993 ( $M_s = 5.5$ ) was located near Khartoum city.

A catalogue is compiled for these areas; the earthquakes are compiled from, historical data represented by Ambraseys and Adams (1986), East African Seismological Catalog (EAF), Preliminary Determinations of Epicenters (PDE) from USGS, and Sudanese seismological network (SSN). In total 2333 events are compiled (Figure 2), the two areas of seismic activity are delineated in Figure 1. The southern group the include 1966 earthquake which caused strong shaking including the Khartoum city. The northern group have experienced and occasional on low to moderate magnitude events that can give rise to damaging intensities. We categorized seismicity of the northern part of Central Sudan into two subgroups based on the location and also based on the tectonic province. One subgroup is in eastern area of Khartoum and the other is in the western part of the Khartoum (Figure 1). The western subgroup is

exhibit higher intensity and activity than the eastern part. Before the Sudanese Seismological Network started in 2003, the area had three strong earthquake are located at western and southern part of the study area. Earthquakes stroke Kordofan State on August 1, 1993 with magnitude of 5.5 and on November 15, 1993 with Ms 4.3, about 100 km to west of the Khartoum city [ISC catalogue].

Recently they are 22 local events those are located by SSN during the two years from November 2003 and September 2007. Most of them have been located in the eastern and western part of the Khartoum area. Abo Dulige earthquake in November 2004 with Ms =5.3 is located about 149 km east of the Khartoum city. This event was followed by aftershocks with some surface cracks observed [Ayid *et al* 2004]. About 60% of local events take place in the western part. Both of these groups may represent the sources of earthquake where southern part of the Khartoum may be affected.

However, most of the locally recorded events are found close to the epicenter of the Khartoum earthquakes in August 1993, which is associated with a strike slip fault trending NE (see figure 1), based on the seismological data. The majority of the focal mechanisms of events located near Khartoum region are not known yet. All events occur at shallow depths between 5 to 22 km, with magnitudes (Mc) 1.8 to 3.6. At eastern part of Khartoum area the 2004 earthquake is associated with strike slip fault trending NW [Mula *et al* 2005]. Additional geological studies (e.g. gravity and resistivity measurement) were conducted [Mula *et al* 2005] which are help to constrain the focal mechanism of the 2004 event.

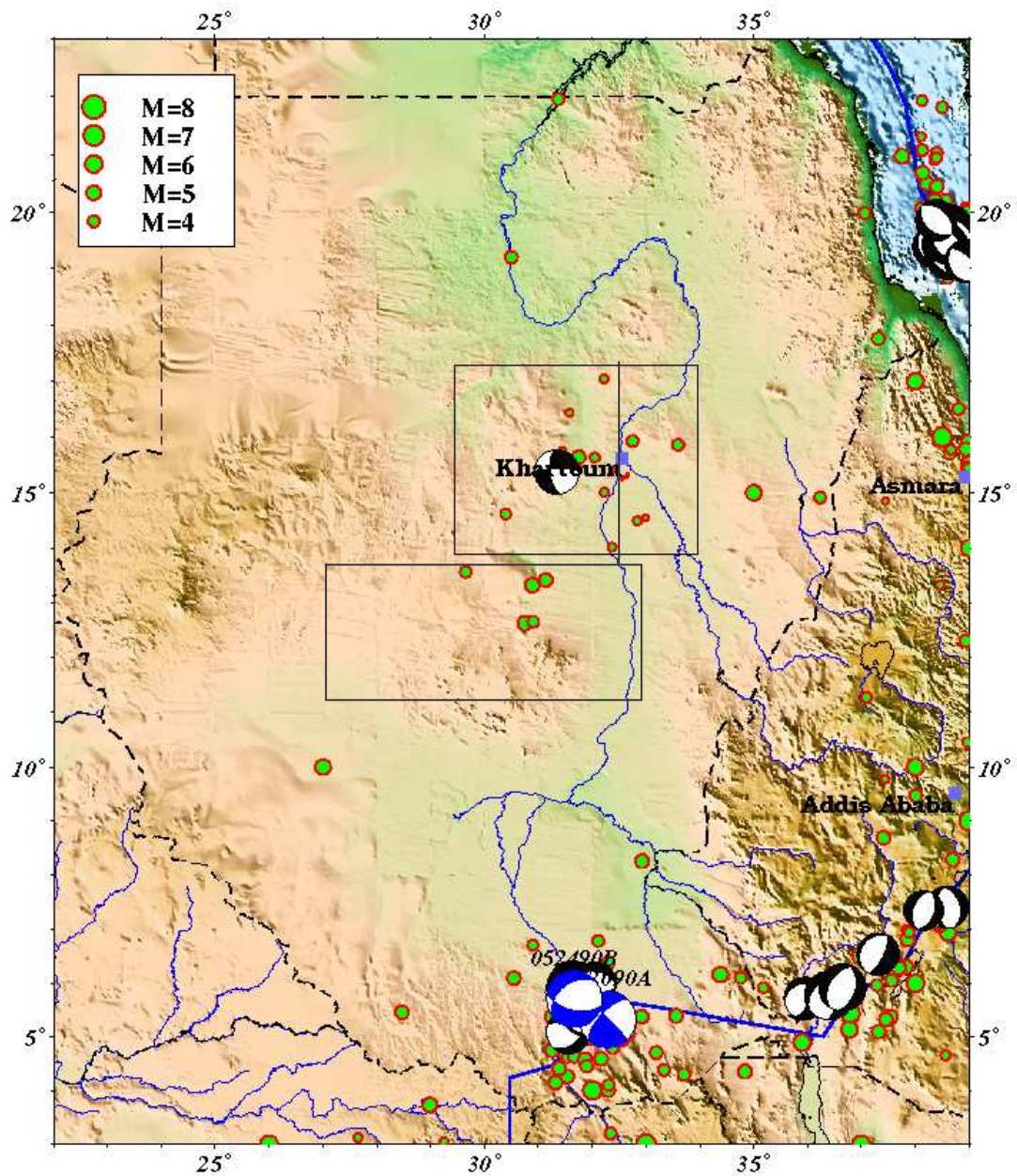


Figure 1- Seismicity map of Sudan area, the two rectangles show the seismicity of the two study areas. Upper and Lower rectangles are shows Part II and Part I respectively. The upper left box shows the legend for event magnitude corresponding to the size of circle. The data come from ISC and SSN, where some of them are recorded recently by the local network seismic SSN.

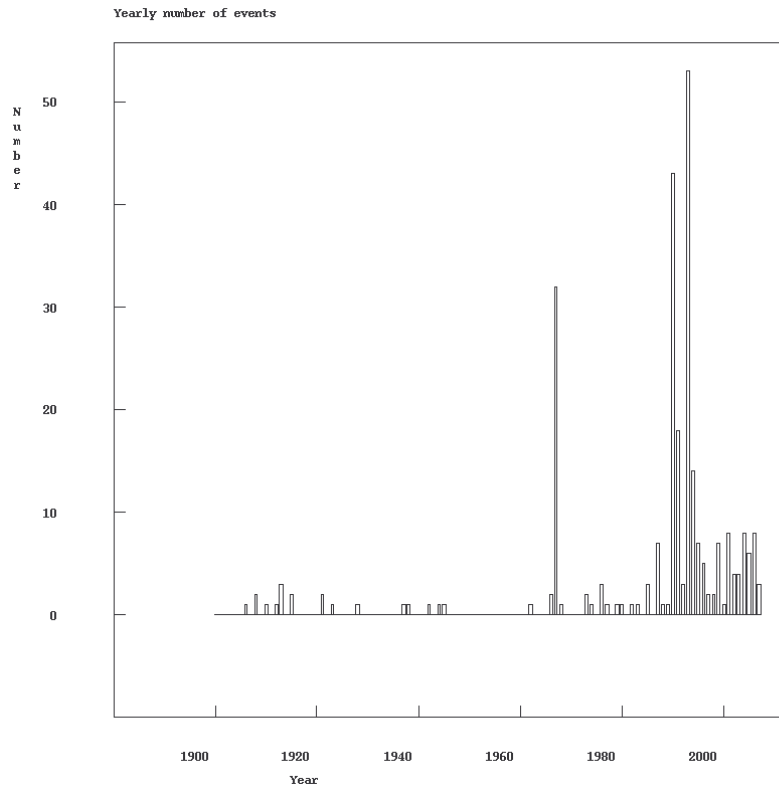


Figure 2. Histogram showing all the events in Sudan during the period from 1910 to 2007. The events are compiled from ISC, EAF, PDE, Ambraseys & Adams 1986 and SSN.

### 1.3 Background Tectonics

Early Cambrian times immediately following the Pan African orogeny, the NE African continental plate has been subjected to various episodes of intercontinental deformation. However, in Sudan stresses imposed during the break up of Gondwana land from the late Triassic to the present were resolved along existing NW –SE- plus N-S and E-W structural orientation (Figure 3). As a result a number of rifts have been formed, some of which appear to have been originated in early Mesozoic basin while others date only from Tertiary [Salama 1985], extending from the western boundaries of Sudan to eastern borders. The Sudanese’s Cenozoic rift systems over a large area and include (a) Bahr el Arab rift (b) White Nile Rift (c) Blue Nile Rift, (d) River Arbara Rift and (e) Wadi El Kuu Rift. All these rifts have contained two or more basins. These rift basin have been the areas for exploration and extensive geophysical research [Sin Oil exploration, 1989; Browne and Fairhead, 1983]

The central Sudan contains two major Cenozoic rifts The White Nile Rift (WNRS) and the Blue Nile Rift (BNRS). These at began to develop in the late Jurassic- Early

Cretaceous during the break up of Gondwanaland and separation of South America from Africa. [W. Bosworth *et al* 1990]. Intracratonic extensional forces that resulted from the opening of the Atlantic, and acted upon and along the African continent facilitated the formation of these basins. Movement along different major fault trends continued and resulted in the formation of several deep fault- bounded troughs. Seismic studies estimated the thickness of sediments in the deepest basins to be 5 km [reported by Robertson Research International (RRI); Geology Research Authority of Sudan (GRAS), 1990; Osman 2006]. The deposition of thick sediments in central Sudan rift is associated with three main rifting phases [Scull, 1988]; each rift phase was contemporaneous with uplift in the source area [Abdall, 1993]. Uplift has apparently taken place in north eastern part of the study area, which contains two basins (Bara and Khartoum) extending from White Nile rift (WNRS) and Blue Nile rift (BNRS), respectively. They are generally trending northwest to southeast. Oil explorations conducted in the region have enabled the subdivision of the rift system into smaller sedimentary basin and sub-basins. The (WNRS) contains basins, such as the Bara basin complex, which is composed of the three major sub-basins named El Beshiri, Umm Ruwaba and Dar Agil. The (BNRS) contain basins such as the Khartoum basin and the Kosit basin complex [W. Bosworth 1992. Oman 2006] (Figures 3.2 and 3). The study region lies south of Central African Shear Zone (CASZ) and forms the northern extension of (WNRS). The CASZ extends from the Cameroon through the Chad to Sudan [Farihead, 1988] (Figure 3). The end of the Umm Ruwaba basin in southern part of study area is associated with Umm Hani Shear Zone (UHSZ) trending NE- SW. It is interpreted by gravity to be active during Late Cretaceous rifting [W. Bosworth 1992]. This indicates that the compression in the area trending N-S at that time. The UHSZ extends from the end of the Umm Ruwaba basin in the west, until the Dinder basin in the east within the southern basins of BNRS. Some crustal extension may have occurred to the north of CASZ in the vicinity of Blue Nile rift [Millegan 1990]. The CASZ is parallel to UHSZ that means the central Sudan is under extensional forces. All these basins were believes to be formed by the shear zones associated with the pull- a part basin in central Sudan. The extensional regime is supported by focal mechanism of the August 1993 earthquake [ISC 1993] (Figure 1). The limit of the extensional system is poorly known. The continental extension of these fracture zones are associated with historical seismicity

[Ambraseys and Adams, 1986], indicating that these fracture zones are weak and still able to dissipate stress into the adjacent continental arc [R. Binks et al 1992].

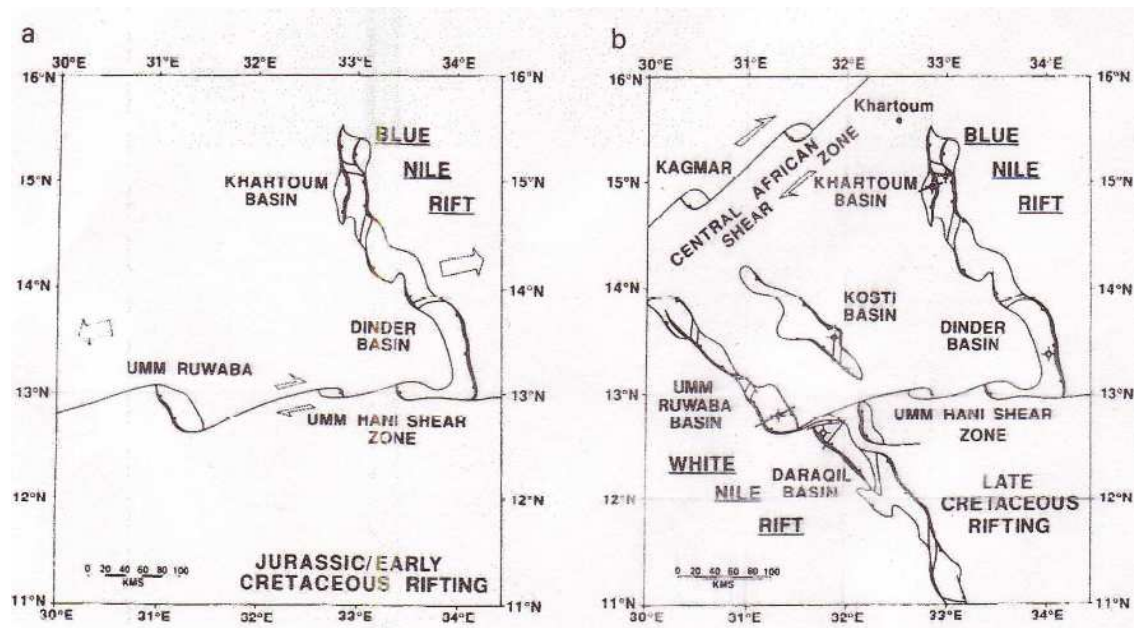


Figure 3, Geometry of rifting recorded in the northern Nile basins of central African rift system, (a) Late Jurassic /Early Cretaceous rifting, confined to basins north of the Umm Hani shear zone, (b) Later Cretaceous Early Tertiary rifting. [W. Bosworth 1992].

The tectonic stresses are presented by World Stress Map (2005) and W. Bosworth et al (1990), suggest N- S extension in response to the ridge push force from the Red Sea, and Atlantic Ocean and East African Refit System (Figure 4). The ridge -push forces play a leading role, while extensional forces from the rift act as modifiers. This is seen in central Sudan, where present day state of stress is a N-S extension with an average orientation of 10°N. The expected stress field based on NW-SE trending Mesozoic- Early Tertiary faults is a NE-SW extension (Figure 3). Inversion of focal mechanism data shows a stress tensor which has near vertical  $\sigma_1$  and sub horizontal  $\sigma_3$  suggesting normal faulting regime [Lostina, 1997] (Figure 5). The geophysical studies such as the gravity indicated many rifts which were formed by extensional forces during the Jurassic- Early Cretaceous age [Fairhead, 1988a; W. Bosworth, 1990]. At that time the extension was E- W oriented, which formed the rifts. The relationship between plate motions and intra-plate stress regimes are determined from focal mechanisms, in situ stress measurement and borehole breakout studies [Zoback et al 1989, and World Stress Map, 2005]. They show that the maximum horizontal stress is sub-parallel to the direction of plate motion. An alternative way of viewing this

relationship is to consider that the poles of rotation, which were describing the progressive opening of an ocean basin, providing the data to map the relative regional stress directions existing at that time. [R.Binks and J.D, Fairhead 1992]. The ductile nature of central Sudan rift could mean that the stress field observed is due to influence of forces from outside the region which also affected the active southern Sudan or East African Rifting System (EARS).

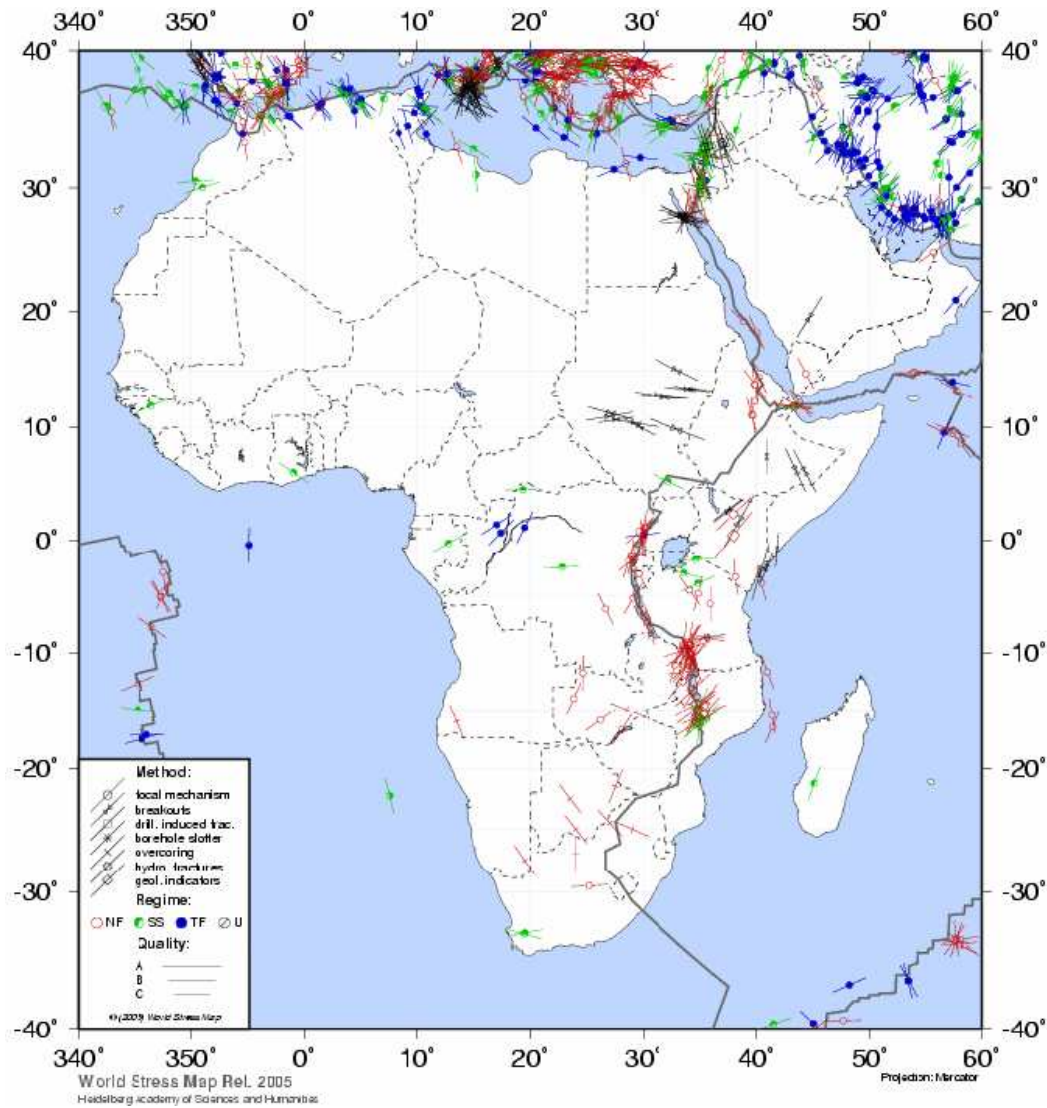


Figure 4, Africa stress map, shows the direction of stress, the down left rectangle shows different methods. In Sudan region we can see the stress made by breakout method in central mostly trend E-W and SE-NW compression, and focal mechanism in southern Sudan [after Geophysical Institute, University of Karlsruhe 2005]

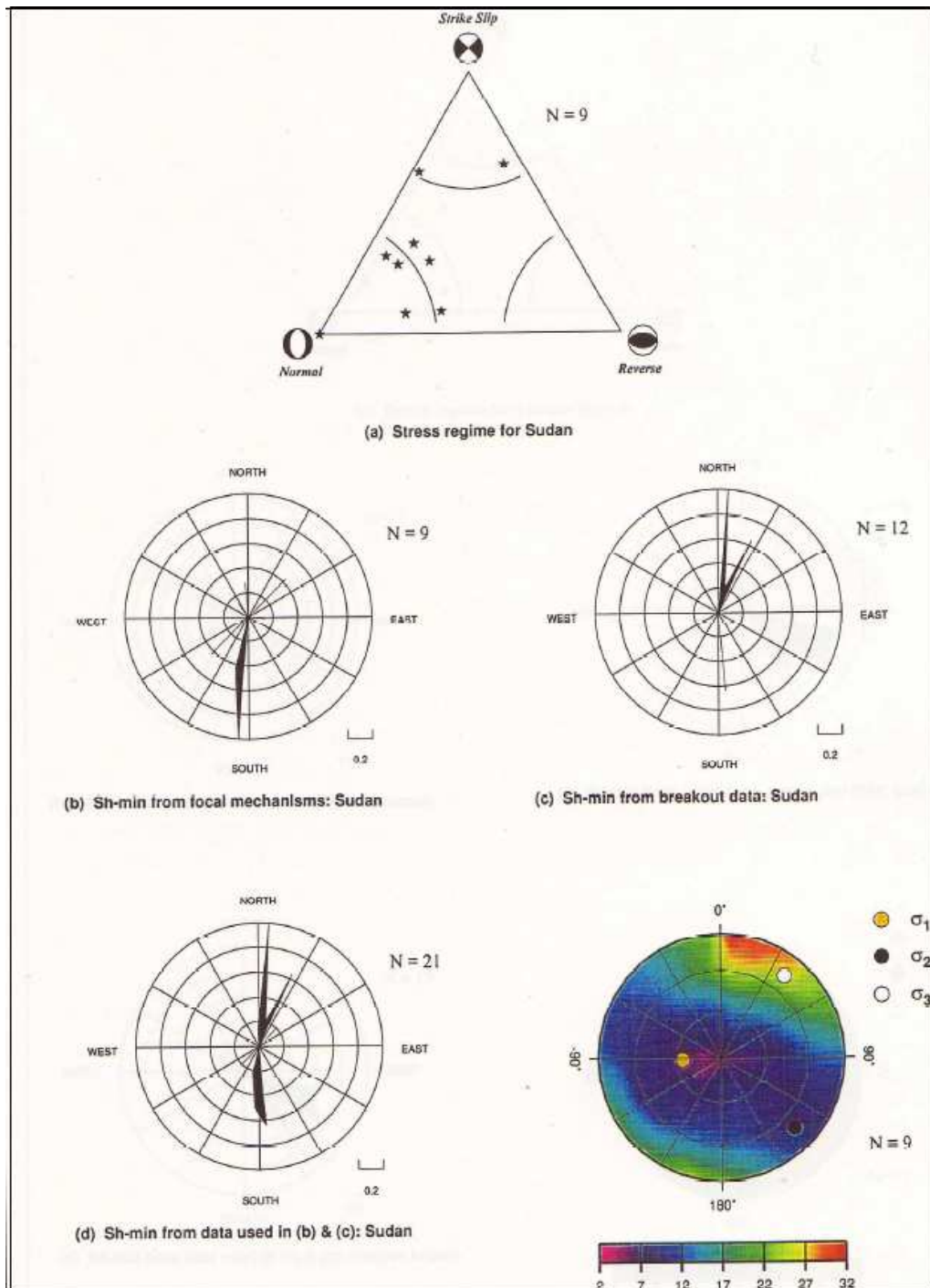


Figure 5, triangular diagram of stress regime (a), rose diagram of minimum horizontal stress ( $Sh_{-}him$ ) direction (b, c and d) and equal area lower hemisphere projection for  $\sigma_1$  stress axis from inversion of focal mechanism (e) for Sudan region.  $N$  is number of events data after [Lostina 1997]



**PART I**

**Seismicity and Tectonics of Central  
Sudan**

## Chapter Two

### Previous and Present Work in the Study Area

#### 2.1 Introduction

Central Sudan experienced historical earthquakes. The instrumental are seismic recordings started since 1966 and this empowered by recent earthquakes recorded by Sudanese Seismic Network (SSN) from 2003 up to now. The seismicity shows two groups of earthquake locations. The first group is located in the north of Kordofan State, between 15N- 16N and 31E-32E, which is near Khartoum, where majority of events have magnitudes 3.0 to 5.5, since 1993. The largest one occurred on August 1, 1993 and December 21, 1994 with magnitudes 5.5 and 5.3, respectively, which resulted in damage in Khartoum city. The Second group is located in the south of North Kordofan State, between 12N-14N and 30E-32E, which is called the Jebel Dumbeir earthquake region. In this study we focus on the southern group since the area has largest earthquakes and following to an area which is least studied. Jebel Dumbier earthquake in 1966, ( $M_s = 5.6$ ), was followed by several aftershocks, and was shaking a large area such as El Obied town and Khartoum city about 380 km from epicentre. The area has different geological settings, which includes a basement complex of granite, a mountain of metamorphic rock and sedimentary basins. Tectonic stresses changed overtime since the extension in Tertiary trending E-W while the present-day stress is in the opposite direction [W. Bosworth *et al* 1990]. The earthquake locate in central Sudan are compiled from (ISC) and (SSN). We will describe relocation of the events, the magnitudes, focal mechanisms, macro seismicity and intensity informations, we also make an attempt to determine the length of surface rupture.

Only a few studies for central Sudan have been carried out [Qureshi and Sadig, 1967., Ambraseys and Adam, 1986., Clark and Browne, 1987]. However, in the current study we will use available earthquake data to assess the tectonics in the southern part. The intension is to obtain better location of the events and study the 1966 earthquake.

## **2.2 Study area**

The study area is located between 12N- 14N and 30E –32E. Five earthquakes were from ISC and SSN, (Figure 2.1). The largest earthquake was occurred on October 9, 1966, Ms=5.6, and was located in central Kordofan. It was followed several by aftershocks [*Qureshi and Sadig 1967*]. The area has different tectonic settings including the sediment basin Bara, metamorphic rocks exposed in the Nubia Mountain and Tertiary volcanics in Jebel Marra in the western part of Sudan and basement rock complex exposed at Dumbier hills (Figure 2.1). This has led to different structures such as normal faults in the Umm Ruwaba basin and strike slip faults occurring around granite Hills. Two big towns like El Obeid, Umm Ruwaba and many villages are scattered in a large agricultural area, and small natural streams is crossing the area, which flows into the White Nile called El Rahid.

## **2.3 Previous work in seismicity of the study area**

Few seismological studies of central Sudan has been carried out, that is because the events have small magnitudes and there were no Sudanese network operational before 2003, also few other geophysical studies have been done.

*Sadig and Qureshi (1967)* were first to describe the 1966 earthquake using primary methods, are intensity data and surface observations. They suggested that fault has a sinistral strike – slip motion, which trend of 20<sup>0</sup>N. *Ambrasey and Adam (1986)* reviewed historic seismicity, and they suggested that there must be a structure in this intraplate region capable of producing medium magnitudes earthquake. A Focal mechanism solution was made by using the relative amplitude method of main event on 1966 [*Clark and Browne 1986*].

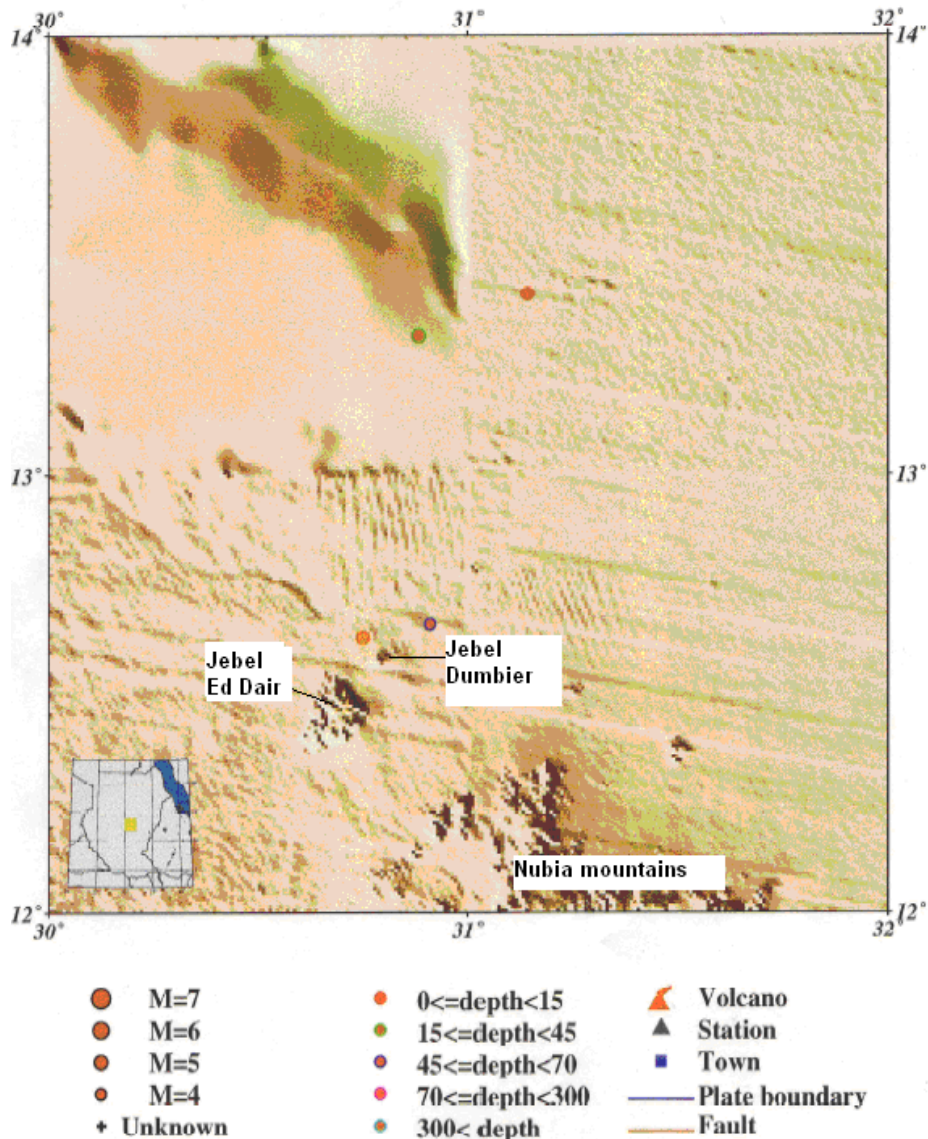


Figure 2.1, Seismicity for part of central Sudan area for the time period 1966 –1987. The data come from IS. In total five events are shown. Magnitude symbols are proportional to size. Shown the topography to the south of events are hills (Nubia, and Ed Dier in west)

## 2.4 Present study

The present study is a reassessment of old and new events in southern part of the central Sudan. We will focus on relocation, focal mechanism, and length of fault rupture and magnitudes. The results will be evaluated the general tectonically of Sudan. Using all available data are come from (ISC) and (SSN). For focal mechanism are used available acquiring from the website and bulletin of ISC (1966).

*Table (1) shows the events in study area are compiled from ISC and SSN*

Event	Time	Location	Magnitude	Depth (km)	No Station recorded
10/09/1966	06:48	12.630N-30.750E	5.1 M <sub>b</sub>	22	137
10/09/1966	10:28	12.620N-30.696E	4.2 M <sub>b</sub>	50	35
17/05/1974	07:31	13.318N-30.884E	4.6 M <sub>b</sub>	33	39
28/7/1987	19:52	13.413N-31.139E	4.6 M <sub>b</sub>	30	32
17/09/2004	17:53	14.613N-30.390E	2.7 M <sub>c</sub>	15	3

## **Chapter Three**

### **Local Geology and Structure**

#### **3.1 Local Geology and Structure**

The study area includes many different geology settings. The basement complex is shallow seated basement rocks of Precambrian age [Vail 1978], reveals area of shallow basement and occurring in boundaries of each sedimentary sub-basin. The basement rock is outcropped around El Obeid and south of El Rahad. They are mainly granites gneiss that is migmatized in Jebel Dumbier, Ed Dair, Hagiart and Nubian mountains. The Nubian mountains have master joints that follow two major's trends NE to SW and NW to SE while in Jebel Dumbier the trend is north to south. Marble and Syenite rocks are recorded in Jebel Ed Daeir south east of El Rahad see modified geology map of Sudan [GRAS 2006] and (Figure 3.1 and 3.2).

Sedimentary rocks are three formations in the study area. The first one is called Nawa formation. Andrew and Karkanis (1945) found in water wells around the Nawa village north of El Rahad [GRAS 2006; Whiteman 1971]. That it consists of sandstone overlying the basement complex. The thickness of the Nawa formation is estimated to be 300 m from water wells [Vail 1978]. The second sediment formation deposited during Jurassic age, and occurring thin basalt lave flow layer. It includes alluvial fan deposit indicating the first stage of rifting [Osman 2006] (Figure 3.2). The third sedimentary formation deposited during rifting phase that initiated in beginning of Mesozoic called Cretaceous unit [Wycisk et al 1990, GRAS 2000]. Cretaceous sediment comprises intercalations of sandstone, mudstone and conglomerates. The top of cretaceous sediment is covered by Umm Rawaba and Khaseeb formation with a thickness around 2.5 km. The last formation is sand Dunes and superficial deposit which cover most all the area except in the southern part of study area. Two normal faults trend NW- SW trendy associated with sub- basin (Figure 3.1).

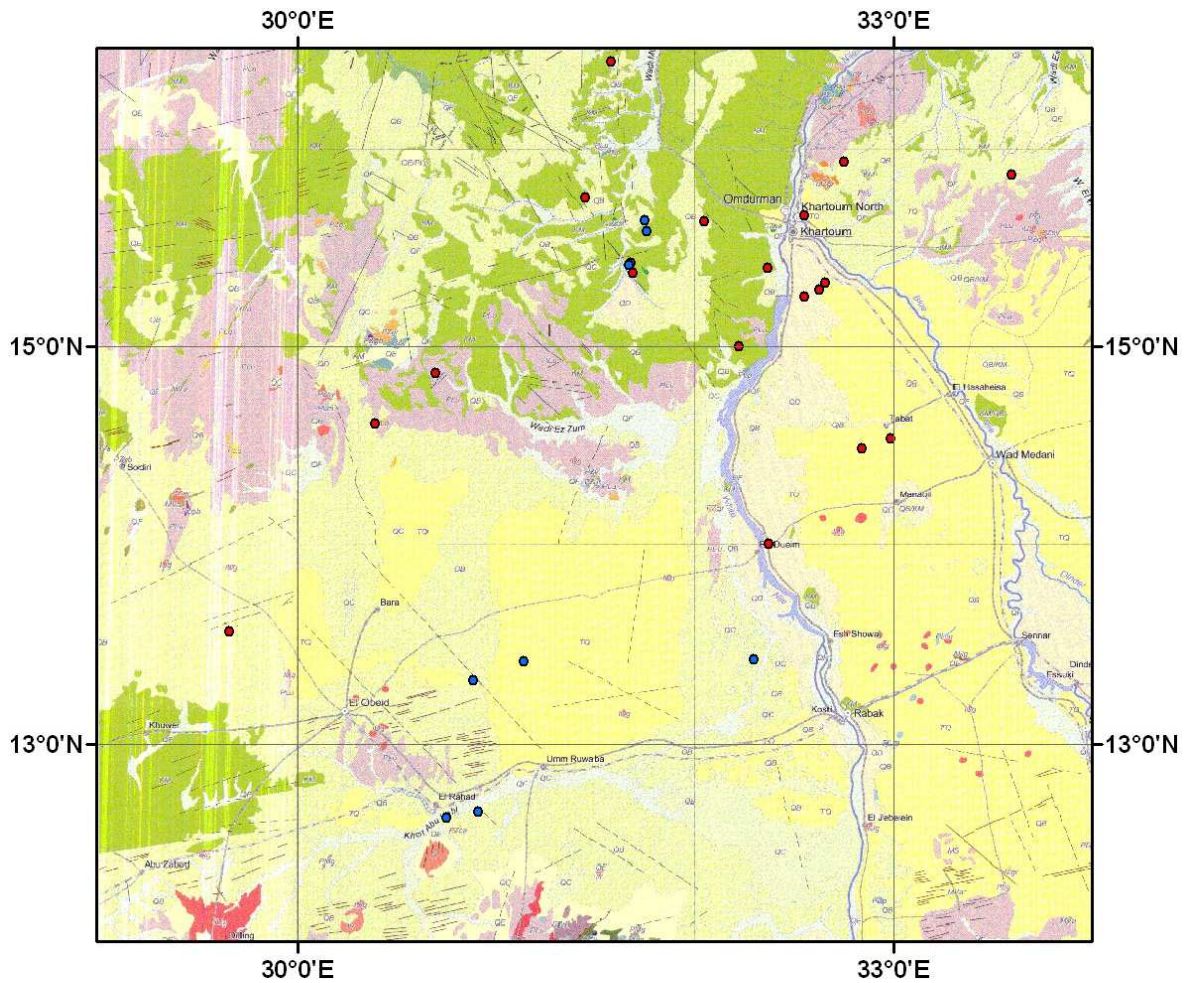

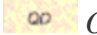

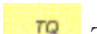











Figure 3.1 Geological map of study area. Different geological formations are visible as blue and red circles shows location of the older and recent earthquake respectively. For each formation on the map we see its corresponding geological complex and the rock type that compose it. The rock type, structure and rivers on the map should be read as follows; Modifier from geological Map of Sudan (GRAS 2006)

-  Recent alluvium and wadi deposit.
-  Older alluvium, raised terraces, younger gravel and sand plains.
-  Quaternary, lacustrine deposit, alluvial fans, dunes and dune fields.
-  Tertiary -Quaternary, Ruwaba formation; Gravel, sand, silt and clay.
-  Cretaceous, fluvial sandstone, lacustrine and mudstone and siltstone.
-  Jurassic sediment, fluvial sandstone.
-  Upper Proterozoic, Basement complex, meta sediments, granite and marble.
-  Late upper Proterozoic Older intrusions including older granite, gabbros, anorthosite and quartz porphyry.
-  Younger intrusions of granite, syenite and gabbro.
-  Blue colour is Nile, River.
-  Black line is Normal fault.
-  Grey colour is fracture;
-  Black line is strike slip fault. .

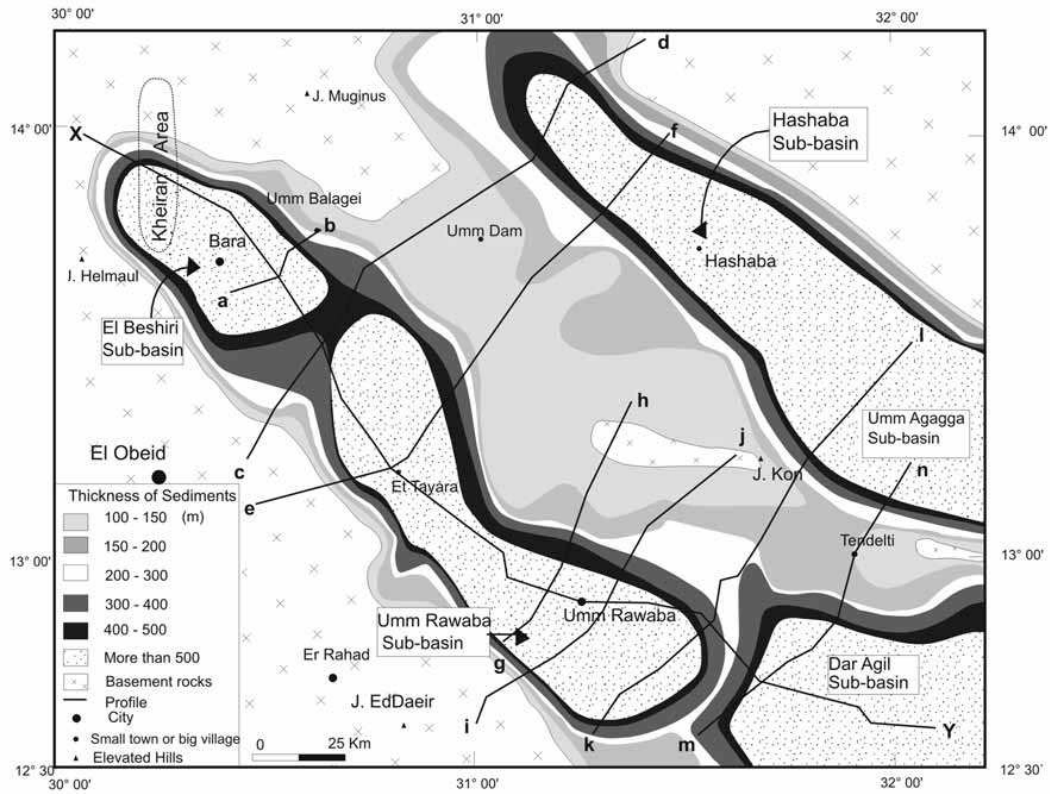


Figure 3.2 The sedimentary sub-basin in the area study and the thickness of the sediments. Shown the basement rocks are surrounding the sub-basin. After [Osman 2006].



## Chapter Four

### Data and Methods

#### 4.1 Focal mechanism

The first motion technique of focal mechanism solution [Seth and Wyession, 2003] is project the polarity of the first arrival at stations on to the focal sphere. The P- wave velocity being used and take off angle. The focal mechanism for the selected event was constrained using FOCMEC program [Snoke et al 1984], which is part of SEISAN software package [Havskov, and Ottemöller 2005]. The program uses polarities see table 4.1 and finds possible solutions with a minimum numbers of wrong polarities for a given grid search. All possible solutions are then plotted on a stereo net with their P and T axes. And then one can choose the best solution by picking the most representative P or T from the possible of P or T solutions. Two focal mechanisms were made with different dataset:

##### *4.1.1 Focal mechanism using ISC Bulletin data*

Polarities from twenty- nine stations were collected for the October 9, 1966 event from the ISC Bulletin are given in table 2. The majority of the stations are in Europe and Asia. The polarities were picked with several stations and send to ISC bulletin. The search was made with a three degrees grad and six polarities did not fit. Consistent strike slip solution was found see figure 4.4c. The two possible solution are; lift lateral strike –slip motion with a trend of  $28^{\circ}$  N and right lateral strike slip motion tend of  $315^{\circ}$  N.

##### *4.1.2 Focal mechanism using ISC Bulletin data and data from Clark and Browne (1976)*

Clerk and Browne (1987) has published two alternative fault plane solution for the 1966 earthquake using both amplitude and polarity data. The 15 polarity data are, all expect three different from the ISC data and based on original readings by Clarke and Browne. In order to improve our solution we have included these in our data set. The total polarities used are 43. The KON station is the different from the polarity of ISC data (Dilatation) and Clark and Browne data (Compression). From the seismogram it

looks like dilatation, so we use dilatation. The precedence of the focal mechanism is the same as the focal mechanism using of ISC data. The result of solution we using the FOCMEC program is also a strike slip solution, where 11 polarities were wrong and the search was made with 3 degrees grid, see Figure 4.5c. The Two possible solution of fault plan are a left lateral motion trending  $54^{\circ}$  N and right lateral motion trending  $330^{\circ}$  N. Comparing the ISC data and ISC + Clark and Browne data solutions, it is seen that they both represent similar strike slip faults with a difference of up to 26 degrees. These two solutions compared to Clark and Browne alternative solution. They are seen that all represent similar strike slip faults. But the different for that the ISC solution in pure strike slip fault while Clark and Browne solution is strike slip fault with normal fault.

#### ***4.1.3 Uncertainty of solution using ISC data***

They are two main sources of uncertainty were observed during the study. The first observation is that the data available is densely concentrated in the centre of the stereonet meaning it uncertain to constrain the solution, with several possible fault plane solutions passing through the centre of the stereonet. This is being due to poor station coverage of African local stations (e.g. AAB) and bad azimuthally coverage. The second observation is that several critical points have incorrect polarity as shown by abundance of mixed polarity reading in the two the northern quadrants. Incorrect polarity reading could result from human error since ISC data contain routine readings from both short and long period records. Some of these errors could also be due to emergent P – wave arrivals that is common on short period records.

In the second solution, stations LIC and JER station have wrong polarity, these uncertainty solutions (Figure 4.5a), where are correct while others now are wrong. The difference in these solutions is five and three degree, which gives an idea about the uncertainty of the solutions (Figure 4.5b).

The ISC and ISC + Clark and Browne are illustrated in figures (4.4c and 4.5c), given similar fault plane solution with a small difference of strike; both of them are pure strike slip fault. Practically in ISC solution one plane trending  $28^{\circ}$ N (lateral strike slip motion) is like the field observations trending  $20^{\circ}$ N (ground surface rupture) [Sadig and Qureshi 1967] than ISC +Clark and Browne solution (1987) (Figure 4.4c and 4.5c).

Our two solutions are different from the two Clark and Browne solutions (1987), The Clark and Browne polarity solution is based on a few points, and is a large deviation from surface rupture direction about 60 degrees to east [*see text of Clark and Browne 1987*]. They also made a solution with amplitude, which represents NNE-SSW normal fault with minor strike slip component.

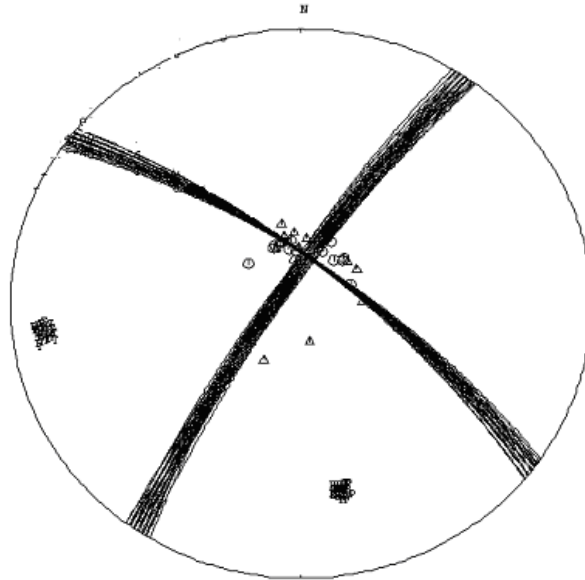
Our solution is based on four times more polarities, therefore considering the most reliable. Since the area had no observation for vertical displacement the strike slip is also the most reliable [*see text Sadig and Qureshi 1967*]. Other reason for strike slip is that in the region close to the study area the August 1993 earthquake occurred and it had a similar focal mechanism as the present study (Figure 1).

The geological structure of the area close to the 1966 earthquake may support our focal mechanism. The master joints in Jebel Dumbeir itself and Jebel El Dira are following a NNE-SSW direction. The normal fault interpreted by Clark and Browne 1987 interprets the normal fault solution as probable since the Jebel Dumbier about 50km to the north has extension (figure 5).

From geology, the extension is in the northeast direction. This is similar to the extension obtained from the fault plane solution. Both of the Hydrogeology studies [Osman 2006] (Figure 5), gravity studies of Umm Hain shear zone and boundary between Umm Ruwaba and Dar Agil sub basin [W. Bosworth 1992] (Figure 3) indicate a structure parallel with the surface break. This also gives support to our solution.

*Table 1, Data used in focal mechanism determination for 048 GMT October 9, 1966 mainshock. The stations have Compressional onsets and dilatational onsets are showing mark by (C) and (D) respectively.*

Station- Code	Polarity	Arrival time of P-wave (hh mm sec)	Distance Km	Delta degree
VAM	D	06 53 52.80	2609	346
RHO	D	06 53 54.40	2650	355
ATH	D	06 54 16.20	2894	347
GRS	C	06 54 53.00	3351	24
SDB	D	06 55 12.80	3587	212
SIM	D	06 55 17.00	3599	4
UZH	C	06 55 49.00	4071	351
VIE	C	06 55 56.50	4172	344
NIE	D	06 55 58.20	4194	349
QUE	D	06 56 00.00	4201	57
IFR	C	06 56 08.00	4310	308
KHC	D	06 56 08.80	4348	342
KRL	C	06 56 23.00	4531	337
DSH	D	06 56 39.00	4726	46
DOU	C	06 56 44.10	4794	335
TAS	C	06 56 50.00	4910	42
KOD	D	06 57 05.00	5099	88
SVE	C	06 57 33.00	5532	21
LHN	C	06 57 40.20	5618	348
TRO	C	06 58 30.30	6395	355
SHL	C	06 58 39.30	6538	68
NOR	C	07 00 01.90	7994	353
BNS	D	06 56 40.20	4761	338
BUR	D	06 57 37.00	5463	336
LHN	C	06 57 40.20	6518	348
KJN	D	06 57 46.60	5724	358
SEM	C	06 58 16.60	6129	36
FRU	C	06 57 25.00	5358	351
MAW	D	07 01 11.90	9275	168



3

Figure 4.4a, The plating for all possible solution of 0648/10/1966 event with 6 error polarity and the grad search is 1 degree.

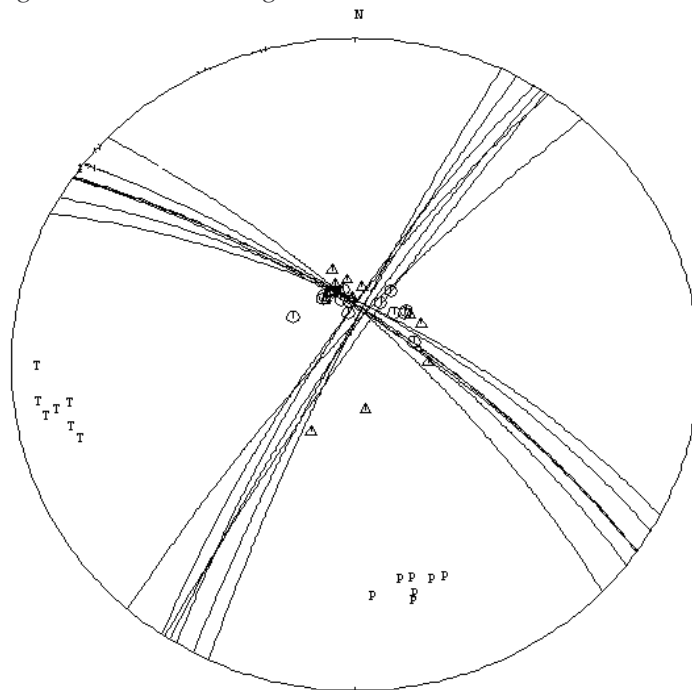


Figure 4.4b, The plating for all possible solution of 0648/10/1966 event with 7 error polarity and the grad search is 3 degree. Show the small different between each solution around Strike/Dip/Rake is (205 to 221)/ (77.8 to 85.4)/ (-15 to -20)

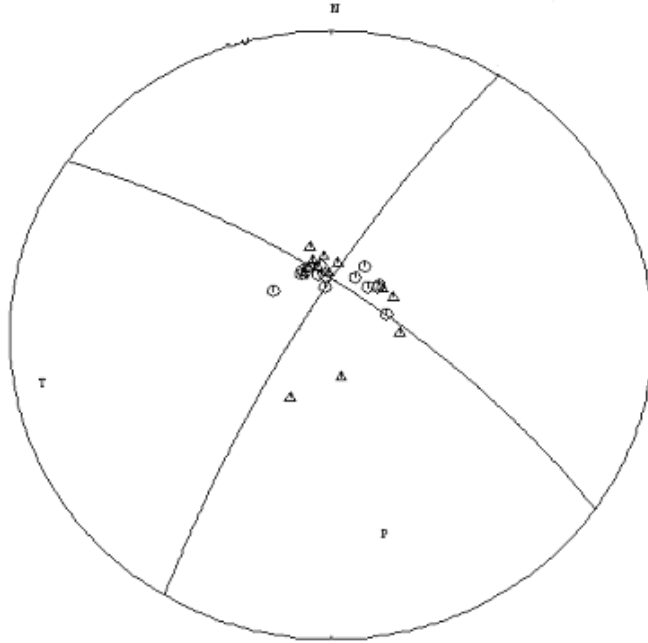


Figure 4.4c, Focal mechanism solution determined in present study with only ISC polarity data, show the possible solution for an event 0648/10/1966 earthquake given by FOCMEC program, the open circle are compression readings, triangle are dilatation readings. P and T are pressure and extension axis respectively, projection is on lower hemisphere equal area stereo net. The two upper solutions are different error polarities and grad search. The last one is best one with less polarity error (6) and grad search (3) degree which given as strike/dip/rake = 208.5/80.2/-17.5.

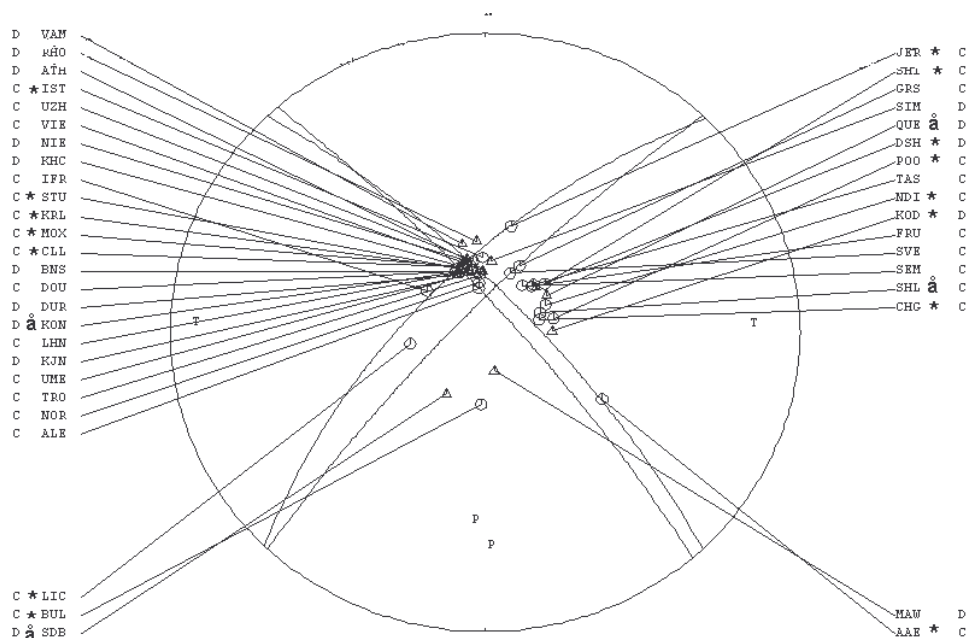


Figure 4.5a, Two solutions with 11 error polarity and 2 degrees research are strike/dip/slip = 224.5/66.0/-10.4 and 223.7/80.58/-15.4, shown the star ship is data fro Clerk and Browne 1986 and the stations without lapel is ISC data and (â) is the stations are the same in to sources.

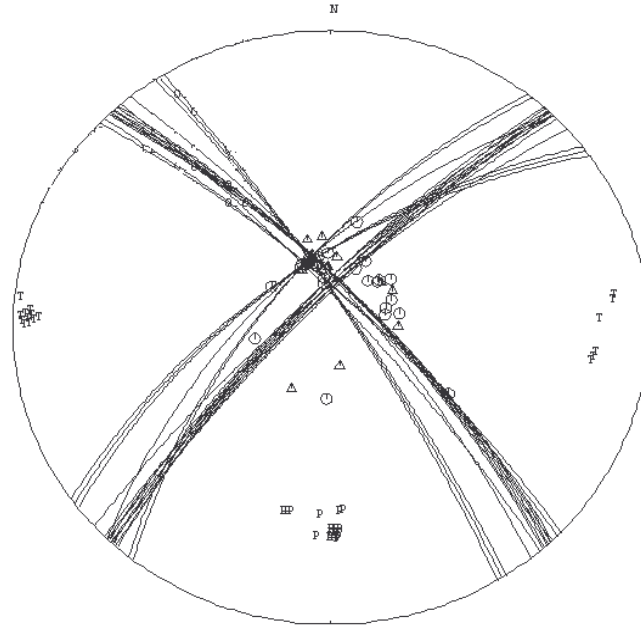


Figure 4.5b, focal mechanism solution of 1966 earthquake; show the many possible solutions with 12 polarity and 3 degrees grad research. These solutions are the different strike about 5 degrees. Show the two polarities in south and west quarts are given idea for uncertainty.

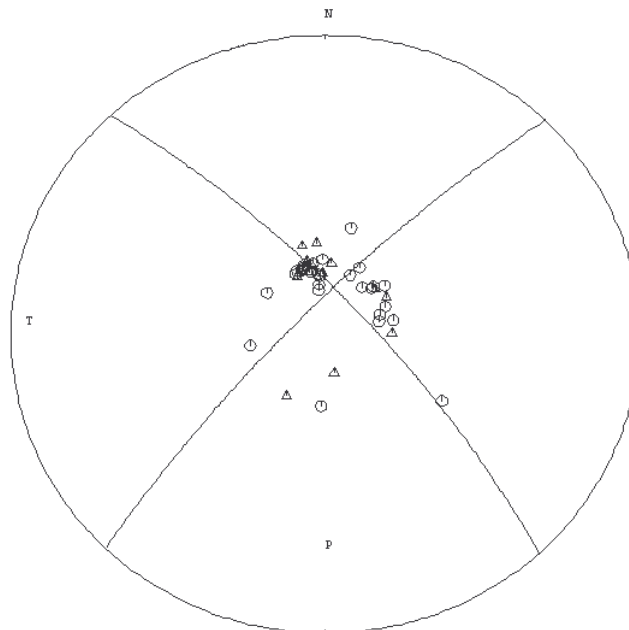


Figure 4.5c, Focal mechanism solution determined in present study include all ISC Bulletin 1966 data and Clark and Browne (1986) data, show the possible solution for an event 0648/10/1966 earthquake by using FOCMEC program, the open circle are compression readings, triangle are dilatation readings. P and T are pressure and extension axis respectively, projection is on lower hemisphere equal area stereo net. The upper one plotting of polarities data with 11-polarity error and grad search is 3 degrees. And second one is finally result without plotting; Strike/Dip/Rake is 234.97/65.4/-14.7.

## 4.2 Intensity

The 1966 earthquake was felt in a large area, with varying intensity from the epicentre to Khartoum city about 380 km far. The highest intensity was close to Jebel Dumbeir area. Two isoseismic maps were published for this event (Figure 4.6 (a and b)). They show high intensity along Semeih, Jebel Dumbeir and Sidra villages (intensity VIII). The shapes of the isoseismic curves are elliptical with long axis parallel to fault rupture trending about  $20^{\circ}$ N. It seems Intensity was affected by the local geology. The El Obid area was experienced higher intensity (V) than the Umm Ruwaba area (IV) about 60 km from epicentre. Thickness of sedimentary rocks over the Basement in Umm Rawaba is about 500 meters while El Obid area, about 90 km from the epicentre, has no sedimentary rocks and has just fractured rocks (Figure 4.6a). This difference in intensity is not shown on the map but it was explained in the text [Qureshi and Sadig 1967]. Due to this reason, all original observations were taken from [Qureshi and Sadig 1967] and a new macroseismic map was made (Figure 4.7). The highest intensity is on basement and the lowest one is on sedimentary rock. This opposes to what we expect. This could be due to some local structures or bad observations. [Adam and Ambraseys 1986] were made reviews of historical seismicity in Sudan area with considering the low intensity observations, which included the 1966 earthquake (Figure 4.6b).

Information about felt area is compiled by *Sadig and Qureshi (1967)* and *Adam and Ambraseys (1986)*. All observations from maps were used. In addition, more observations from the text were added more information. This gives a more complete data set given in table 4.2 and therefore a better intensity, which can be compared with variation of geological features (Figure 4.7). The macroseismic data with different scales were obtained in order to observe variation within the area. The lowest and highest intensity ellipses are elongated northeast to southwest, which is the same as fault rupture trend. The medium levels intensity such as V and IV has shapes of circles. This could be due to geological and topographical effects.



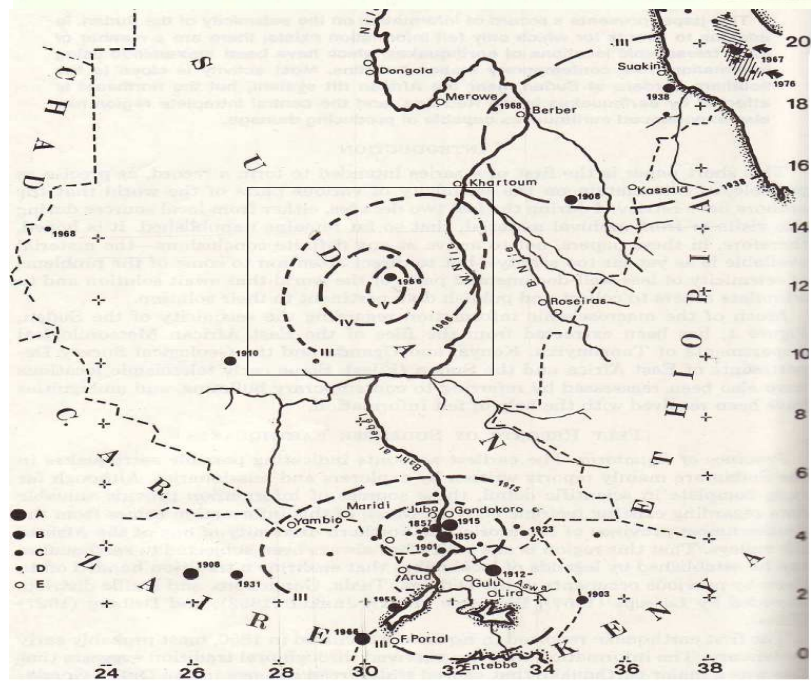
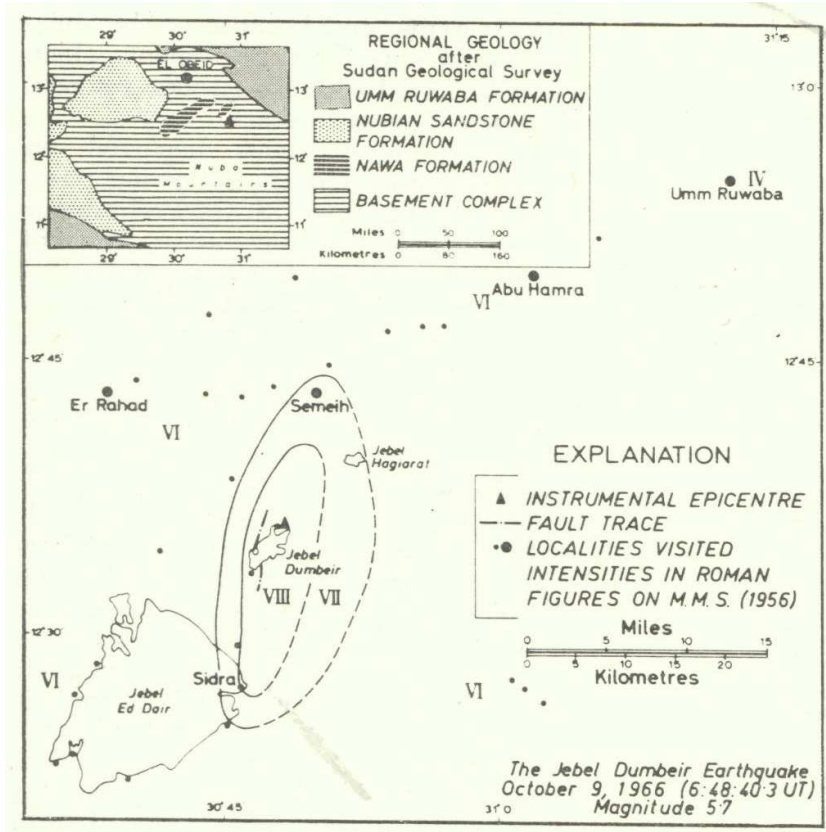


Figure 4.6, Two intensities and isoseismic maps, the upper (a) shown the intensity and fault trace associated with the Jebel Dumbeir Earthquake of October 9, 1966, the inset shows regional geology in central Sudan and epicentre of earthquake [after Qureshi and Sadig 1967]. Down (b) review of intensity of seismicity of Sudan region area felt made by [Adam and Ambraseys 1986]. Both of them made by modified Mercalli scale.

Table 4.2 the sites of the level intensity of 1966 earthquake, these data comiled from [Sadig and Qureshi 1967] and [Adam and Ambraseys 1986] were using Mercalli intensity scale.

Late	long	intensity	site name
14.625	30.000	3.0 EMS	
10.250	29.000	3.0 EMS	
12.875	28.375	3.0 EMS	
13.000	33.000	3.0 EMS	
11.125	30.000	4.0 EMS	
12.000	31.375	4.0 EMS	
12.000	29.125	4.0 EMS	
13.500	30.500	4.0 EMS	
12.904	31.206	4.0 EMS	Umm Ruwabah- under sediment
12.725	30.635	6.0 EMS	Ar Rahad-
12.718	30.836	7.0 EMS	Seimeih- under sediment
12.464	30.743	7.0 EMS	Sidra- granit
13.191	30.215	5.0 EMS	Al obeid-under the basement
12.567	30.783	8.0 EMS	Jebel Dumbeir- synite
12.469	30.765	8.0 EMS	
12.467	30.686	6.0 EMS	Jebel Ed Dair-granit
12.479	30.637	6.0 EMS	
12.449	30.620	6.0 EMS	
12.660	30.867	7.0 EMS	Jebel Hagiarat
12.500	30.823	7.0 EMS	
12.565	30.768	8.0 EMS	
12.823	31.028	6.0 EMS	Abu Hamra
12.583	30.786	8.0 EMS	
12.667	30.824	8.0 EMS	
12.467	31.010	6.0 EMS	
12.633	30.733	6.0 EMS	
12.427	30.740	6.0 EMS	
12.742	30.842	6.0 EMS	
12.823	30.800	6.0 EMS	
12.606	30.793	8.0 EMS	Trace fault( Dumbier)
12.537	30.784	8.0 EMS	Trace fault
12.743	30.798	7.0 EMS	
11.625	30.375	5.0 EMS	
12.500	31.125	5.0 EMS	
12.250	30.125	5.0 EMS	
13.000	30.625	5.0 EMS	
15.250	32.375	3.0 EMS	

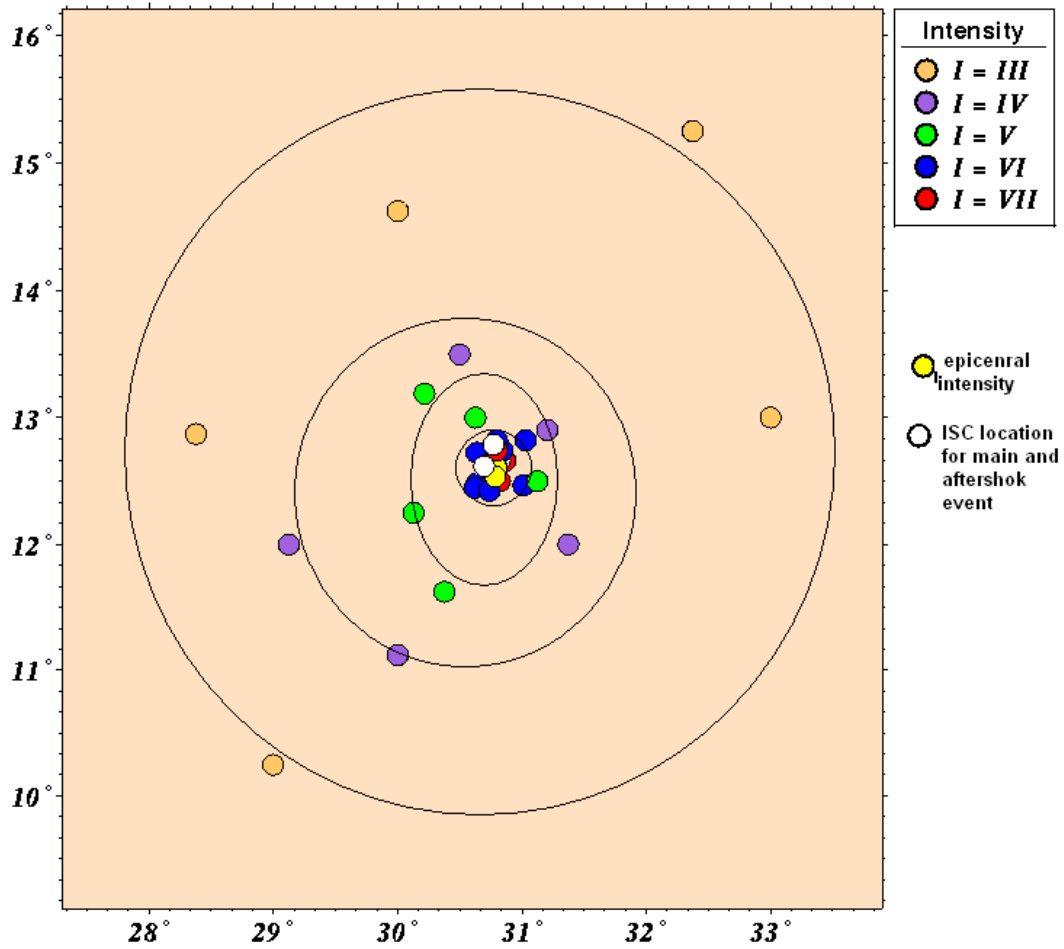


Figure 4.7, Isoseismal map of intensity map and ISC location for the main and aftershock of 1966 earthquake. These data come from reports felt and include data from [Sadig and Quashes 1967]. The yellow circle is intensity epicentre that calculated as the central of highest intensity circle. The white circle is ISC location for main and aftershock.

### 4.3 Magnitude

The surface magnitude has not been published by ISC and an attempt will therefore be made to determine it from the felt area. Both [*Sadig and Qureshi, 1967; Adam and Ambraseys, 1986*] mentioned that the event has an  $M_s$  of 5.7 and 5.6 respectively, but do not give any sources of the calculation.

Several seismologists have published the relationships between magnitude and felt area. Several expressions from different region were used to determining the surface wave magnitude.

Singh et al (1981) have made relationships for different regions in Mexico; we have chosen the relationship to estimate of  $M_s$  for regression of intraplate earthquakes, which is mostly similar to central Sudan. [Singh et al 1981] also the give relation for intensity VII–IV. We chose the relationship for intensity IV since the area for large intensities will be small and therefore uncertain. Also high intensity area is highly affected by hypocentral depth. The relation is;

$$M_s = \log A_{IV} + 1.38 * A_{IV} \quad (1)$$

where  $A_{IV}$  is the area in kilometres square with intensity IV. From Figure 4.7, the intensity for IV is  $5*10^4 \text{ km}^2$ , which gives  $M_s= 5.7$ . This is a same to what is mentioned by *Sadig and Qureshi (1967)*.

Also we used two expressions made by *Trech et al (1993)* with a data set from stable continental interiors. This is a similar tectonic environment a central Sudan region. The first relation gives seismic moment from felt area with III intensity. And second relation gives  $M_s$  from seismic moment. Using equation 2 and data table 4, we get a seismic moment  $10^{24.27}$  dyn-cm, the relation between seismic moment and felt area is:

$$\log(M_0) = 47.34 - 10.81 * \log(A_{felt}) + 1.17 * \log^2(A_{felt}) \quad (2)$$

Where  $M_0$  is seismic moment in (dyn- cm),  $A_{felt}$  is area in ( $\text{km}^2$ ) from the level III intensity.

The relation between,  $M_0$ , and surface magnitude,  $M_s$ , as determined by two steps for interplate earthquake is:

$$\log(M_0) = 22.47 - 0.4 * \log(M_s) + 1.17 * (M_s)^2 \quad (3)$$

where using equation 3, we get  $M_s = 5.5$ .

However, for lower magnitude the moment magnitude  $M_w$  is close to surface wave [Stein and Wyseeisn 2005]. The stand moment magnitude scale calculates by [kanamori 1977] is:

$$M_w = \left[ \frac{1}{1.5} \right] \log M_0 - 10.73 \quad (4)$$

where  $M_w$  is the moment magnitude, gives 5.5.

The  $M_s$  values from intensity relation have an uncertainty of  $\pm 0.3$  [Singh et al 1981]. This is due to unknown in focal depths, regional attention, site response and type of building construction. We used two different relations for  $M_s$  against intensity for interplate area, and we a value of  $M_s 5.5$ . Considering the consistency of  $M_s$  and  $M_w$  values, we believe that  $M_s = 5.5$  is a good estimate.

#### **4.4 Relocation event from macroseismic observation**

The event locate on is the most important to know the sources. The locating process involves determining both hypercentral coordinates and the source origin time. Location determination requires identification of seismic phase and measuring their arrival times, as well as knowing the velocity structure between the hypocenter and seismic station. The location of seismic sources can be given by calculating the travel time for any particular phase to a seismic station anywhere in an arbitrarily complex velocity model. The problem of finding the earthquake location can be usually tackled by three methods depending on available data, single station location, multi phase location and inverse problem.

#### 4.4.1 Single station method

Single station method is used when we have one station with three components recorded. It is used to obtain a crude estimate seismic single. It requires three components recordings of ground motion, since P-wave are vertical and radial polarized, the P-wave motion vector can be used to infer the azimuth to the epicentre. Figure 2.8 displays the nature of P-wave polarization and procedure of location. The vertical motion of the P-wave is upward with positive value. The radial component of the P-wave is directed away from the epicentre. If the vertical component is directed back toward the epicentre, unless the event is at back azimuth such rotated onto single component, both horizontal seismometers will record the radial component of the P-wave. The ratio of amplitudes on the two horizontal components ( $A_E$  and  $A_N$ ) can then be used to find the vector projection of the P- wave along azimuth ( $AZI$ ) to the seismic source.

$$AZI = \arctan \frac{A_E}{A_N} \quad (5)$$

The apparent angle of incidence can be calculated by using the amplitude of vertical components:

$$A_R = \sqrt{(A_E^2) + (A_N^2)} \quad (6)$$

$$I_{app} = \arctan \left( \frac{A_R}{A_Z} \right) \quad (7)$$

Where  $I_{app}$  is the apparent angle of incidence and  $A_Z$  is amplitude of component. [Wiechert 1907] obtained the true incidence angle ( $I_{true}$ ) of P-wave as;

$$I_{True} = \arcsin \left[ \frac{V_P}{V_S} \right] * \sin 0.5 I_{app} \quad (8)$$

The true velocity is important to calculate the local seismic velocity below the observing station by

$$V_{app} = \left[ \frac{V_c}{\sin I} \right] \quad (9)$$

The distance to the seismic source is obtained from the difference between the arrival time of two phases (S and P). The earthquake epicentral distance can be approximated by:

$$D = (t_s - t_p) * 8.0 \quad (10)$$

where  $t_s$  and  $t_p$  is arrival time for S and P wave respectively in second, D is distance in Km. Eq. (10) for “normal medium age” crustal conditions with  $V_p = 5.9$  km/s. For distance  $20^\circ < \Delta < 100^\circ$  the relationship  $\Delta^\circ = \{(t_s - t_p) - 2\} * 10$  still yields reasonably good results with errors  $< 3^\circ$ . Use of the available global travel-time table such as IASP91 [Kennett et al., 1991] and SP6 [Morelli and Dziewonski, 1993] are recommended for calculating for the distance less than 20.

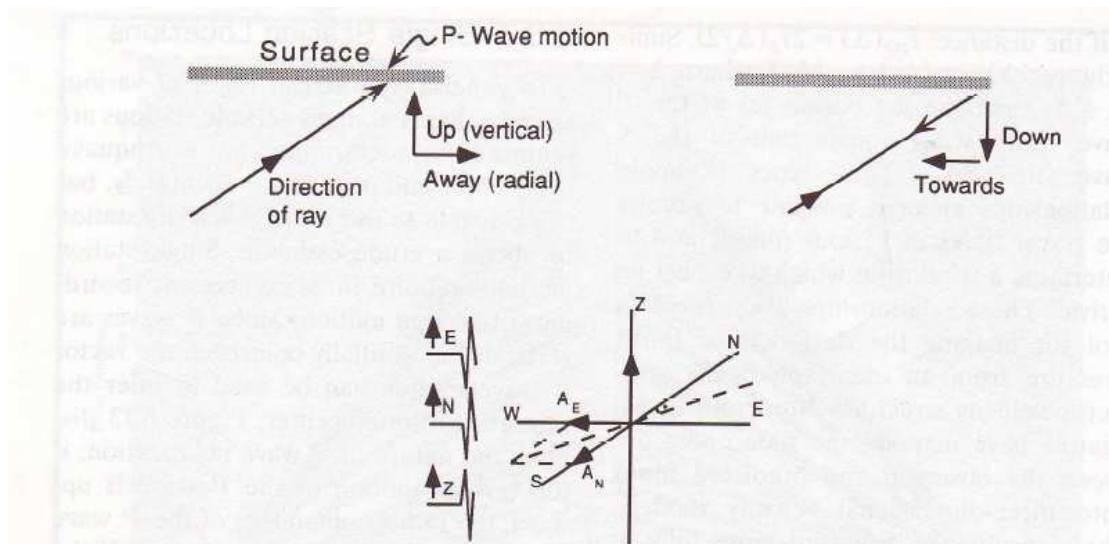


Figure 4.8, Procedure for determining the azimuth to the source of a recorded P-wave by using the three –component vector ground motion and the fact that P-wave motions are polarized in the vertical and radial plane.( after Bath, 1979).

Since the amplitude ration between the components should remain constant not only for the first swing of the P-phase but also for the following oscillation of the same phase, we can with digital data, use the predicted coherence method to automatically calculate back azimuth as well as the angle of incidence. This method is faster and reliable than using the manually readings.

#### 4. 4.2 Multiple station location

When at least three stations are available, a simple manual location can be made from drawing circles with the center at the station locations and the radii equal to the epicentral distances calculated from S- P time. This distance we can calculate by using the same produce of the single station location. Therefore, the circles drawn around the stations with radius epicentral distance. These circles will rarely cross in one point which indicates errors in the observations and/or that we have wrongly assumed a surface focus. If they are not crossing at one point, then we will calculate the epicentral area with boundary at crossing two circles. Or using chord method, which that is to draw the straight line passing through the crossing points between two neighbouring circles.

The last two manuals methods provide insight into location problem, called inverse problem. This is to locating an earthquake and finding its origin time using the arrival time of seismic wave at various stations. The velocity structure is known and then we explore how it can also be estimated from the travel times [Stein and Wysession 2003]. The calculated arrival time  $t_i^c$  at station 'i' can be written as:

$$t_i^c = t(X_i, Y_i, Z_i, X_0, Y_0, Z_0) + t_o \quad (11)$$

where  $t$  is the travel time function of the location of station  $(X_i, Y_i, Z_i)$  and the hypocenter of this equation has 4 unknowns. So from principle 4, the arrival time observation is needed from at least three stations in order to determine the hypocenter and origin time. We have ' $n > 4$ ' observations and ' $n$ ' equations. So the above system of equations is over-determined and has to be solved in such away that the misfit or residual  $r$  at each station is minimized;  $t_i$  is defined as the difference between the observations  $(t_i^o)$  and the calculated travel time  $(t_i^c)$ .

$$t_i = (t_i^o - t_i^c) \quad (12)$$

Since the travel time function is a nonlinear function of the model parameter, it is not possible to solve the equation with any analytical method. However, we can calculate the travel time of all seismic phases to any point by using a model. The method is to perform a grid search over all possible locations and origin time, and compute the



arrival time at each station [Sambridge and Kennett, 1986]. The hypocentral gives the best agreement between the observed and calculated time. This means that some measure of best agreement is needed; particularly many observations are used to find the minimum misfit by using least squares. This is to find the minimum of the sum of the squared residual ( $e$ ) from the  $n$  observation;

$$e = \sum_{i=1}^n (r_i)^2 \quad (13)$$

Where  $r_i$  is residual of station. The root mean squared residual RMS is defined as

$\sqrt{\frac{e}{n}}$  the RMS gives an indication of the fit of the data.

In this study we relocated events considering three different methods preview which depending on the data availability and developed programs. We applied hypercentre location program (HYP) which is part of SEISAN software [Havskov, and Ottemller 2005]. Eight events are collected from ISC and SSN. For six events data available in S-file (arrival time, residual, distance) and for two events data are complied with waveform from SSN.

Two factors led to propose the relocation of the events from ISC; first the ISC using only P- wave arrival, and we want to try using all phase and S-P. Second the ISC used the Bulletin travel time table, which is old and not good for regional P and S while we are using IASP91 travel time table with the Hypocenter program. Since there is no station nearby and no depth phase reported the depth must be fixed. The depth was fixed to five kilometers for four events (Table 4.3), since one of the events had surfers rupture. This was refined location with P, S-P and all phase arrival time.

Figure 4.9, shows the distribution of three relocations of two events of 1966 earthquake, we will discuss the early one on 1966 (main shock), since we know the correct location from felt area, the location accuracy can be evaluated. It seems that the location is close to the true location when only P-phase is used. Using all phase gives a very bad locations indication many misidentified phase. The main shock now lies at about 12.620N, 30.696E, just about 10 kilometres west from the end of the observed fault rupture and more centrally within the isoseismic map. The ISC and

Hypocenter solution with only P-phase are close to each other. However the ISC solution is a bit closer to true epicentre than our hypocenter solution.

The second event was recorded five hours after the mainshock considered as aftershock of 1966 earthquake [*Qureshi and Sadig 1967, Clark and Browne 1986*]. It is relocated following the same procedure as the mainshock. This event is recorded with few station records than the mainshock. The solution of hypocenter gives also better solution when using only P-phase is used. While other phases give unreliable location. The location shifted about 22 kilometres northwest of ISC location. The ISC location lies about 10 kilometres east from surface rupture. Both of hypocenter with P- phase only and ISC location are close to main shock. The ISC location is closer to epicentre than P-phase location. For this reason we preferred an ISC location is better.

Figure 4.10, shows the two relocated events of 1974 and 1987 with different phases used. The figure also shows includes the ISC location. We used 39 and 30 stations record respectively. The solutions with only P-phase move smallest shift from ISC location compare to another phase in both events. The relocation the 1987 event with other phase used is gives up and down location relative to ISC location. The relocations of 1974 event with other phase (s and all phase) are toward to the north of ISC location. We have no absolute solution to compare with, so we assume that the location with smallest shifts represent most reliable solution.

All four events have good result of locations, which are made by ISC. But the aftershock of 1966 is quite interesting to use as relatively event with ISC or our P-phase location of both main and aftershock. See later in master event. The systematic of the P- phase for all event can be give idea about which the fault is activity one. They were seeing all at the line of fault rupture observation on 1966 event.

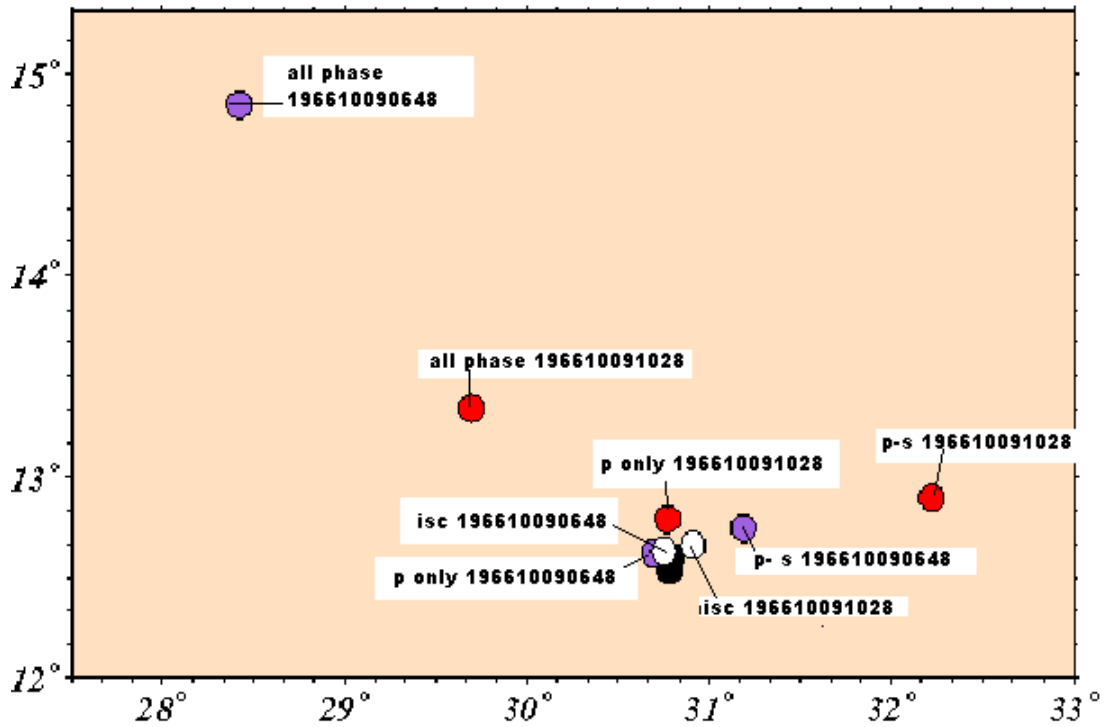


Figure 4.9, Plotting of the relocation of Main and aftershock events of 1966 with different relocation and ISC location

Table 4.3, shows all event in study area with old and new relocations, period between October 9, 1966 to June 23, 2006. The depth is fixed in the last column depending of surface rupture and other factors. The rest of open columns with mark (?), they are data available, from 2004 to 2006 they are not relocated because much accurately than the original data

Time	magnitude	location and depth	Relocation use All phase	Relocation use P-Wave only	Relocation used both P and S-wave	Depth fix km
9/October 1966 6:48	5.1 Mb	12.630N 30.750E Depth 22Km (ISC)	14.841N 28.421E	12.620N 30.696E	12.745N 31.190E	5
9/October 1966 10:28	4.1 Mb	12.660N 30.910E Depth 50Km (ISC)	13.339N 29.696E	12.790N 30.769E	13.640N 32.222E	5
17/March 1974 07:31	4.6 Mb	13.318N 30.884E Depth 33 Km (ISC)	13.603N 30.932	13.385N 30.802E	13.663N 30.838E	5
28/Jul 1987 19:52	4.6 Mb	13.413N 31.139E(ISC) Depth 30 Km (ISC)	13.563N 30.471E	13.769N 30.739E	13.990N 30.937E	5
16/Jul 2002 19:20		13.425N 32.297E Depth 00km	?	?	?	

		(SNSN)				
17/December 2004 17:54	3.2MI	14.866n 30.692E Depth 10 km (SSN)				
6/May 2006 18:53	3.0MI	14.01N 32.373E Depth 0.1km (SSN)				
23/June 2006 09:11	4.0MI	13.563N 29.652E Depth 15.0 km (SSN)				

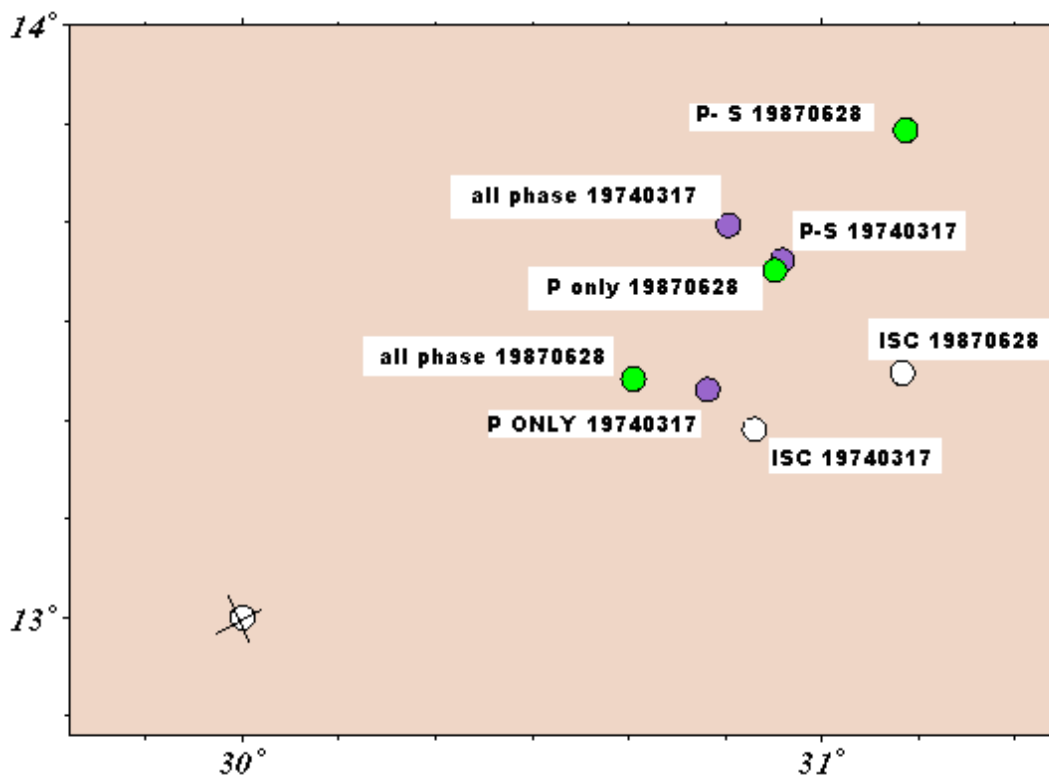


Figure 4.10, Plot shows the distribution of two relocations events on 1974 and 1986 with different phase relocation and ISC location

#### **4.5 Relocation using master event**

The study area has many aftershocks of 1966 earthquake recorded. We used two events in order to get relation between these events as such both events occurring in the same fault. This method is called master event [Stein and Wysession 2003]. The methodology of master event method is to consider particular (often the largest) earthquake in a group as the best located, then located a group of nearby earthquake using travel time correction used at each stations derived from residual at each station for master event.

In this study we used the hypocentre location program. It is part of SEISAN software [Havskov, and Ottemöller 2005]. (Figure 4.11) and Table 4.4 show the result and distributions for location. Twenty nine stations recorded only P-phases in both events are used; only stations with residual less than 2.5 second, were used. These residuals were then used to correct the reading for the aftershock. It turned out that several stations of the aftershocks has residuals larger than 2.0 second, these station were not used and a new location was made, RMS was now 0.6 s. the aftershock was then located 0.120 deg N and 0.115 deg east of the main shock. This distance is almost the same as the distance obtained form the ISC location; however ISC relative location was almost E-W while this one is NE-SW, more in accordance with the observed fault. Master event only improved the relative location a little error in relative location is probably more than 10 km, this is due to inaccurate readings. likely the main shock and aftershock is on the same fault at a distance less than 25 km because the RMS values for all solutions (using different type of wave recorded) are high, could be less than 5 km, if we considering error cannot use this method to get length of fault.

Table 4.4, locations of aftershock relative to main event,(master event method). we used different stations with different residual in second. All possible aftershock locations are occurring in NE from main event, that is the same as relocation and fault trace direction but the ISC solution trend E to W.

Event	Lat	Long	Type of wave used with number of stations	Residual (RMS) <i>sec</i>
The main	12.630	30.750	P-wave only with 29 station	0
Aftershock	12.795	30.768	P-wave only with 24stations	Less than 1.5
Aftershock	12.799	30.773	P- wave with 20 stations	Less than 1
Aftershock	12.750	30.726	P-wave with 17 stations	Less than 0.6

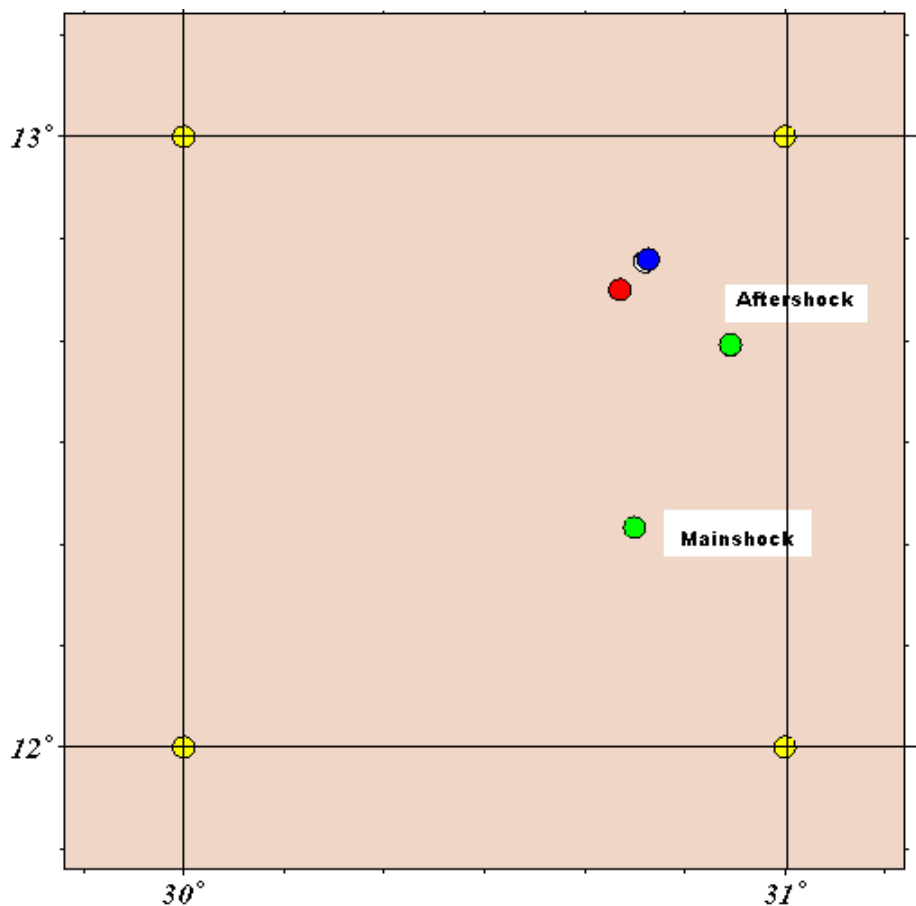


Figure 4.11, Plot shows the main and aftershock event location of 1966 earthquake, and all possible locations of the aftershock as the circle, Red, Blue and White colour. These are refined using master event method.

The relocation shows four earthquakes are occurring in two regions, one associated by strike slip fault supported by fault plant solution, intensity map, and fault trace close to Jebel Dumbier. Another region with two earthquakes (1987, 1974) associated with normal faulting that interpreted by geology map of Sudan 2006 in Umm Ruwaba basin.

#### 4.6 Length of fault rupture

On the seismic moment explained we mentioned in the section 4.3, magnitudes can be used to calculate the length of the fault. In our study on 1966 earthquake we used two relations to calculate the length of fault, one is to find the moment magnitude from Equation (4);

$$M_w = \left(\frac{2}{3}\right) * \log M_0 - 10.73 \quad (4)$$

where the  $M_w$  is moment magnitude, known the  $\log M_0$  from section magnitude and considering the error was given  $M_w = 5.8$ . Wells and Coppersmith (1994) derived empirical relation between the average slip, fault length and moment. Relationship between surface rupture length (SRL) in km and moment magnitude ( $M_w$ ) is:

$$M_w = 5.08 + 1.16 * \log(SRL) \quad (5)$$

Surface rupture length is obtained 4.5 km away the above relation. This is close to the same length observed as fault trace. The average displacement expected was 0.1 m by relation between average displacement (AD) and surface rupture length (SRL) is:

$$\log(AD) = 1.43 + 0.88 * \log(SRL) \quad (6)$$

Where this displacement was not observed while of tension gashes of about 4 cm was observed. There was no obvious vertical displacement, because there was no linear feature crossing the belt. The magnitude of horizontal displacement along the fault could not be estimated well. Since the gash showed only a little distortion at superficial deposit (clay land) which it means the horizontal displacement was small. These observations does not support any evidence of surface fault rupture, they are probably related to surface cracks associated with ground shaking.



## **Chapter Five**

### **Results and Discussions**

In this chapter the results based on the analyses in chapter 3 and 4 are discussed. Here we would like to discuss these results in the light of understanding the seismotectonic of the central Sudan- particularly the area around Jebel Dimebier in the south. Two focal mechanisms are for the 1966 earthquake show pure strike slip faulting (Figures 4.4c and 4.5c). These two solutions are better than those given in Clark and Browne (1986). There are three reasons supporting our results, firstly the new solutions have more polarity data and therefore considered more reliable, secondly since the area has no outcrops with vertical displacement the strike slip solution is more reliable than the mechanism observed by (Clark and Browne 1986. the solution which is strike slip faulting with significant vertical component. Thirdly the distribution of the aftershocks and the isomap of intensities are also conformable with strike of one of the nodal plane in our solution. In addition to these, the observed cracks on the surface have also the same orientation [Sadig and Qureshi 1967]. We therefore believe that our solution is better with the fault plane oriented NE-SW.

The location of the aftershocks using a master event technique shows a trend similar to the orientation of the nodal planes (NE-SW). This supports further our fault plane solution.

In addition the geology of area around this event shows joints oriented NE- SW (Figure 4.3) which is also similar to this trend (Figure 4.2). Moreover the geometry of the sub-basins and the boundary between the Umm Rawaba and Dar Agil sub-basin shows us NE-SW trend (Figure 2.3).

Another indication as mentioned in chapter 3 (section 1.3) is the linear gravity anomaly associated with the Umm Hani shear zone which trend NE- SW. This shear zone is part of the White Nile rift which was active during Mesozoic- Early Tertiary [W. Bosworth1992] (Figure 4). Considering these factors we argue that the fault plane from our solution is the nodal plane trending NE-SW.

The main regional stress field in Sudan is controlled by the opening along the red Sea in the east and influence of the Ethiopian rift in the south. As a result larger parts of central Sudan is under E-W compression [*World Stress Map, 2005, and W. Bosworth et al, 1992*].

On the other hand, the borehole breakouts data shows different orientation than those determined from seismological data such as focal mechanism.

Now, there are two focal mechanisms available in central Sudan; one is the focal mechanism solution of 1966 earthquake in this study and other is the focal mechanism of 1993 earthquake (Figure 1). These earthquakes occurred in the same area and having similar mechanism which further support the solution presented in chapter 4.

However, these solutions are difficult to explain when we consider the main regained stress field based on the bore-hole breakout data. It is likely, that the preview zone of weakness associated with the White Nile and the Blue Nile Rift system play a role here.

## **Chapter Six**

### **Conclusions**

Following is a summary of conclusion bases on the seismitectonic analysis:

- The focal mechanism for the 1966 earthquake obtained in the study, indicates left-lateral faulting along a fault oriented NE-SW ( $17N^0$ )
- The interpretation of this focal mechanism in the extension of the regional is difficult. However, the proposed fault plane fits to the orientation of the earlier zone of weakness associated with the White Nile Rift system.

## References of PART I

N:N Ambraseys and R:D Adams - Reappraisal of major African Earthquake south of 20 N – 1900-1930. () Natural Hazard 4:389-419-1991

Laike M. Asfaw 1992 -Constraining the African poles of rotation - Tectonophysic 209(1992) 55-63- Amsterdam

World stress map – 2003, 2005 Geophysical Institute –University of Karlsruhe  
Dong and H.Shah -Assessment of Global seismic loss Based on Macroeconomic indicators .Natural Hazard 17-269-283-1998- Netherlands

R-Guiraud , W.Bosworth, J-thierry A.Delplanque 2005- Phanerozoic geology evolution of Northern and central Africa And overview (– journal of African sciences 43-83-143

Fekadu Kebede and Ota Kulhanek 1992-Recent seismicity of East African Rift system and its implication – Tectonophysic 209(1992)51-54- Amsterdam

S.J- Gaciri -Lineament map of Kenya 1992- correlation of lineaments to known geology date ( ( tectonophysic 209(1992)139-142) Amsterdam

R.Hofstetter and M.beyth 2003 -Afar depression interpretation of 1960- 2000- earthquakes () Geophys . J. Int (2003)155,715-732

U.Achauer , P.K.H.maguirs , j.Mechie – Wv.Green and kpis 1992 -Some remarks on the structure and geodynamics of the Kenya, Rift (working group-Tectonophysic, 213(1992)257-268-amsterdam

R.M.binks and j .D.Fairhead 1992 -Plate tectonic setting for Mesozoic rift of west and central Sudan (– Tectonophysic 213(1992)141-151 Amsterdam

C:J- Ebner :A:Ibrahim Geo Rundsch 1994 -Multiple episodes of rifting in central and east Africa Are-evolution of gravity data \_ (1994)-183:689-702

W. Borworth 1994- A model for the three dimensional evolution of continental rift basin – north east Africa ((Geol Rundsch(1994)83-671-688

Y\_E\_A. Mohmedzen –J:A Abdalla .A.A.Bdelwahab 2006 - Site response and earthquake design spectra for central Khartoum (Bull earthquake eng (2006)4:277.293

N.N.ambraseys and R.D.adams Seismicity of the Sudan () bulletin of seismological society of America vol.76, No. 2, pp- 483-493- April 1986

R.Qureshi and A:A sadig 1967- Earthquake and associated faulting central Sudan .NARURAL. VOL.215.July 15.1967

lostinas . Chapol 1997-State of stress in East and southern Africa and seismic Hazard analysis of Malawi. (master thesis – UIB- Bergen)

Mc. Hargne, t.R:Heidrick and Livingston 1992 -Development of interior Sudan rifts, central Africa - 0040-1951/92/805-00-1992- Elsevier science Pullisher-1992

William Borworth, M.r. strecker . P.M .Blisnink- Integration of East African paleostress and present day stress data. Implication for continental stress field dynamics ()- journal of geophysical .vol.97.NO .b8.PAGES 11.851-1118-65-12-992

Domenico Giardini and Laura Beranzoli -1992- Waveform modelling of may 20 /1990 Sudan Earthquake – tectonophysic ,209(1992)105-114- Amsterdam

Wiliam Bosworth -Mesozoic and early Tertiary rift tectonic in East Africa () Tectonophysics, 209-(1992)-115-137-Amsterdam.

Marjorie Wilson , Rene Guirand -1992. Magmtism and rifting in western and central Africa from later Jurassic to recent times -Tectonophysics 213(1992) 203-225 – Amsterdam

F.:Kebed ;T.Van eck - Probabilistic seismic hazard assessment for the Horn of Africa based on seismotectonic rationalisation - *Tectonophysics* 270(1997)221-237.

E:L:Wipfler - Transpressive structure in the Neoproterozoic Ariab-Nakasib Belt northeast Sudan. Evidence for suturing by oblique collision () *Journal of African Earth Sciences* .vol.2313.PP.347.362-1996

E. Schrank- Nonmarine cretaceous palaeontology of northern Kordofan, Sudan, With notes on fossil salviniales (water ferns *Geol Rundsch*( 1994) 83-773-786  
E. Calais, C.Ebinger, Cebinger, C .Hartuady, j.M. Nocquet Kinematics of the east African rift from GPS and Earthquake slip vector Data () -website Internet

R:W:girdler and D.A.Mc - 1990-1991 Sudan Earthquake sequence and the extent of east African Rift system .*Connell science* . Vol.264. April 1994

Douglas .B. and Victor Pan -African microplate accretion of Arabian shield () *geological society of America Bulletin* vol.96- p.817-826-6figs- July 1985.

M.B.Katz East African rift and Northeast lineaments- continental spreading – Transform system – *Journal of African earth sciences* vol. 6.NO-1PP. 103-107-1987.

Seismotectonic Regionalization of the Red Sea area and its application to seismic Risk analysis (Roberto pedane, Paolo Lombardo Dimitris) *Natural Hazard* 5.233-247-1992.

Seismic Hazard in east Africa an example of application of in complex and uncertain data (Paivi. M antyniemi, andrzej) -*Natural Hazard* 4.421-40-1991 Netherlands.

Gerhard Franz, Christoph Breitzkreuz, David , A. Coyle Bushra El Hur, Wilhelm Heinrich, Holger Paurlick, dieter Pudlo, Robyn Smith and Gesinne Steiner -The alkaline Meidob volcanic field(Late Cenozoic, northwest Sudan) - *A J* Vol 25, No 2, pp:263-29, 1997

D. C Almond, A. A. Osman and F. Ahmed. The arba” at granite, sudan: a mineralised, pan- Africa intrusion enhanced by hydrothermal metasomatism- vol 24.No 3, pp:335-350 1997

- K. E Ibrahim, M. T. Hussein and I. M. Giddo- Application of combined geophysical and hydrogeological techniques to groundwater exploration: a case study of Shoowak- Wad Elhelew area, Eastern Sudan –vol: 15 no, 1,pp.1-10,1992.
- M. T. Hussein - On the depositional framework of the cretaceous omdurman formation in Khartoum area, Sudan j a vol, 14, pp, 559- 566, 1992.
- W: E: K : Warsi and D. C Almond - Gravity and magnetite signatures of a reworked suture zone :an example from the red sea Hill, Sudan . vol; 14 no pp:361-363,1992.
- E. Klitzsch. Palaeogeographical development and correlation of continental Strata (former Nubian Sandstone) in northeast Africa. Vol; 10., no. ½. Pp- 199-213,1990.
- Valerian Bachtadse , Rainer Zanglein, Jennifer Tait heinrich C. Soffel. - Palaeomagnetism of the permo- carboniferous 280 Ma. Jebel Nehoud ring complex, Kordofan, central Sudan. J A 23(2002)89-97.
- Robert. J. Stern- Crustal evolution in the East African orogen: a neodymium isotopic perspective- J A 34(2002)109-117.
- Mohamed G. Abdelsalam , Jean-paul Liegeois. Robert J. Stern – Review , The Saharan Metacraton J : A 34(2002) 119-136
- A.H. El- Nadi- Late Precambrian volcanism in NE Sudan and evolution of the Nubian Shield. J: A vol, 9, No, ¾, pp.467-480, 1989.
- A:A sadig and F. Ahmed- Gravity signatures over selected ring complexes in the Sudan, and their tectonic significance- Journal of African Earth Science, Vol, 9, No, ¾ , pp. 481-487, 1989.
- D: C . Almond, D.P.F Darbyshire, and F. Ahmed1989- Age limits for major shearing episodes in the Nubian Shield of NE Sudan. Journal of African Earth Science vol, 9, No 3/4 , pp. 489-496,.
- Ahmed. S. Dawoud and Abdelati a. Sadig- structural and gravity Evidence for an Uplifted – Pan – African Granulite terrain in the Sabalka Inlier, Sudan- Journal of African Earth Science - vol. 7, No 5/6, pp. 789-794, 1988.
- G. Franz, H. Puchelt, and P: Pasteels -Petrology, geochemistry and age relation age relations of Triassic and tertiary volcanic rock from Sw Egypt and NW sudan. - Journal of African Earth Science, vol, 6, No. 3, Pp.335-352, 1987.
- P:M. Klemenic -Variable intra- plate igneous activity in central and north- east Sudan.. Journal of African Earth Science, vol. 6, No, 4, pp. 465- 474, 1987.

- R. A. Clark and S. E. Browne, 1987. The Kordofan earthquake, central Sudan – Journal of African Earth Science, vol.6, No, 4, pp. 573- 581,.
- Gisela Prasad -Weathering evidence for surface flow of The Jebel Et Toriya basalt in Sudan.. Journal of African Earth Science, vol. 3, No, 3, pp. 365-370,1985.
- R: B: Salama- Buried troughs, grabens and rifts in Sudan. - Journal of African Earth Science, vol.3, pp,381-390, 1985.
- Laike M, Asfaw. Constraining the African pole of rotation – Tectonophysics, 209(1992)55-63.
- Osman A. E. Abdalla. .Aquifer Systems in Kordofan, Sudan: Subsurface lithological Model- SOUTH AFRICAN JOURNAL OF GEOLOGY, 2006, VOLUME 109 PAGE 445-458.
- T. Denkler . G. Franz. H. Schandelmeier- Tectonometamorphic evolution of the Neoproterozoic Delgo suture zone, Northern Sudan- Geol Rundsch (1994) 83: 578-590.
- R. Hofstetter and M. Beyth. The afar depression: interpretation of the 1090- 2000 earthquakes-Geophys. J. Int.(2003)155, 715-732.
- Faidead, J. D. And Girdler, R. W. 1972. The seismicity of the East African Rift system, Tectonophysics 15(1/2): 115-122*
- .
- Stein, S., and Wysession, M., 2003, An Introduction to Seismology, and Earthquake and Earth Structure, Blackwell Publishing



## **Part II**

### **Local Site Effects in Western Khartoum City and Omdurman Town**

## **Chapter Seven**

### **Introduction to PART II**

In many earthquakes the local geology and soil conditions have had a profound influence on site response. This influence may result in high damage and death-toll, e.g. such as the 1906 San Francisco earthquake, the 1985 Mexico City earthquake, 1898 Loma Prieta earthquake and the 1999 Izmit earthquakes in Turkey. Factors influencing the local modification to the underlying motion are topography and nature of bedrock, and nature, geometry of unconsolidated sediment deposits. Khartoum city is an urban setting located on sedimentary deposits. Local site effect occurs due to the amplification of incoming seismic waves as a result of the impedance contrast between the unconsolidated sediment (soil) and the bedrock. Amplification occurs at frequencies the damping in the soil layer is overcome. In addition, the surface effect (reflected of the seismic wave on the surface) also contribute to the amplification.

In addition, the effect of site response on the built environment is dependent upon the type of building structures. In case where the fundamental frequency of the building corresponds to the fundamental soil layers, resonance phenomenon occurs, giving rise to significant structural damage or collapse. Local site effects therefore should be seen relative to the soil-structure interaction. However, in this thesis only the site response related to the local unconsolidated sediments are addressed. The possible soil structure interactions are considering being outside the scope of this study.

The earthquake in 1993 when was located about 180 km from city, caused severe destruction and two people died. The local site effect in western Khartoum and Omdurman city are of importance especially considering the planned infrastructure in these areas in addition to the dense population.

There are many approaches to evaluate the local site effects. In this part, we empirically evaluated the expected local site effects in western part of Khartoum city and Omdurman town. We used ambient noise and earthquake data to evaluate the local site effects. We applied three methods; first is based on H/V spectral ratio of the

ambient noise, second is based on the H/V spectra of weak motion (local earthquake) and third is based on the standard spectral ratio (sediment versus bedrock) The final results are given separately and compared.

Khartoum is the capital city, and is located in the central part of the Sudan at the junction of White and Blue Niles (see figure 3.1). The city is heavily populated and has high-rise buildings in the centre. The actual population of Khartoum city is 8 million people. This is rapidly increasing and new urban area is growing to the western and southern part of the city. These areas are underlain by soft soil layers. Assessing local site effect is therefore essential in earthquake risk mitigation risk. Khartoum area is classified as seismically low, but eastern and western parts of the study area have moderate earthquakes. The western part of the area has higher seismicity and high intensities than the eastern part. In 1993 an earthquake with  $M_s = 5.5$ , occurred located about 180 km west of Khartoum city. After the installation of the Sudanese seismological network in 2003 the area shows increased activity. In this section, we focus on the local site effect at western part of Khartoum city (including Omdurman town and western part of Khartoum).

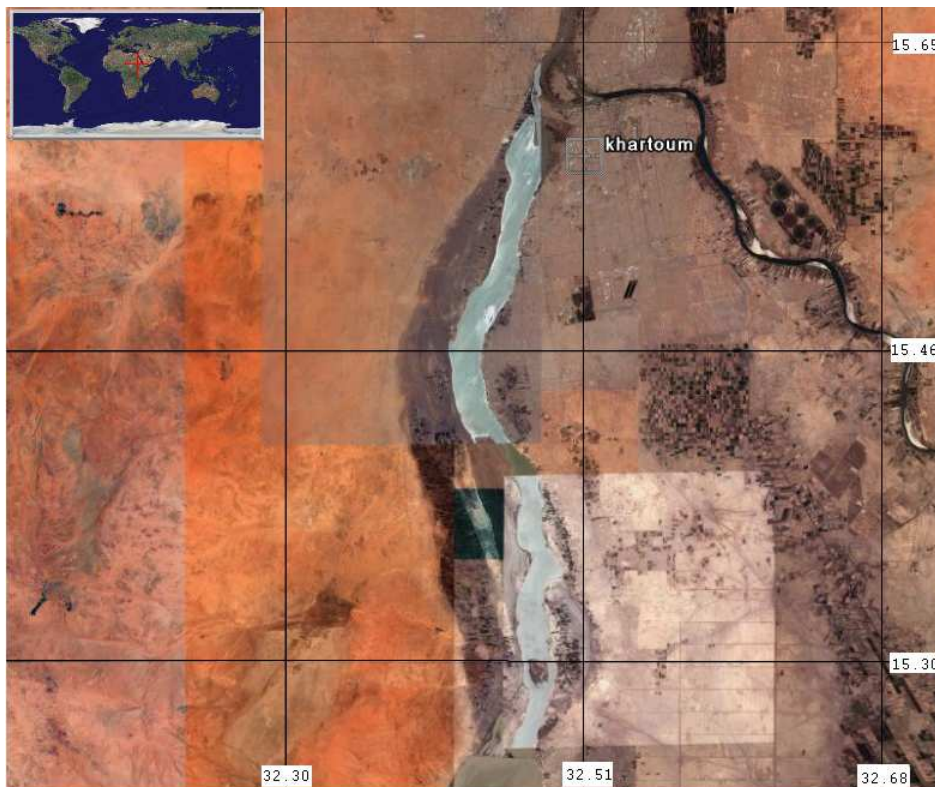


Figure 3-1. Satellite image of Sudan make as cross at upper map with the Khartoum state shown in the central part of the country figure from [Google, 2007].

Since the study area is close to a zone of moderate seismic activity (see later in local seismicity chapter), and since most of the metropolitan area is located on sedimentary deposits (soft clay soil and sandstone) the local site effects are expected to play an important role for the earthquake hazard in the area is significant. The objective of this study area as follows;

- To determine the site response at different sites in western Khartoum city underlain by different formations. The aim of that is to map the fundamental frequency and amplification factors at each site for various sedimentary deposits.
- Evaluate the local site effects in Khartoum basin using both earthquake data as weak motion and ambient noise records to obtain the fundamental frequency and amplification factors.

## Chapter Eight

### Local Seismically Around Khartoum

As we mentioned before in chapter on background seismicity of central Sudan, we can see the area around Khartoum has experienced many infrequent moderate earthquakes. Figure 3.2 shows the distribution of local events. A number of many earthquakes are located close to 1993 earthquake which one have fault plant solution. The temporal distribution of earthquakes detected by SSN is shown in (Figure 8.1) for the period November 2003 to April 2007. The number of events is gradually decreased during 2005, while the network had continued started increasing as the same gradually before 2005 (Figure 8.2). This indicates that there are many events that were missed. This may be due technical problems of SSN stations themselves or the distribution of the stations that is poor.

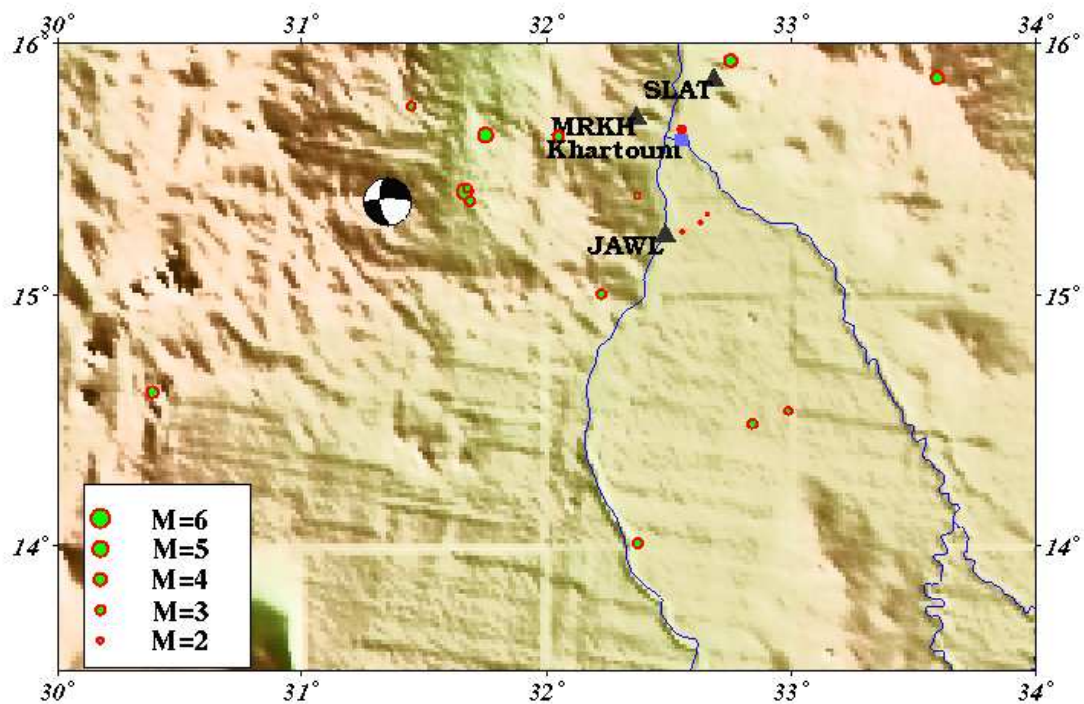


Figure 8.1–Seismicity map of Khartoum area shows the distribution of the events with green circle and explosions with red circle colour. At western part of the Khartoum area had shown Focal mechanism of 1993 earthquake.

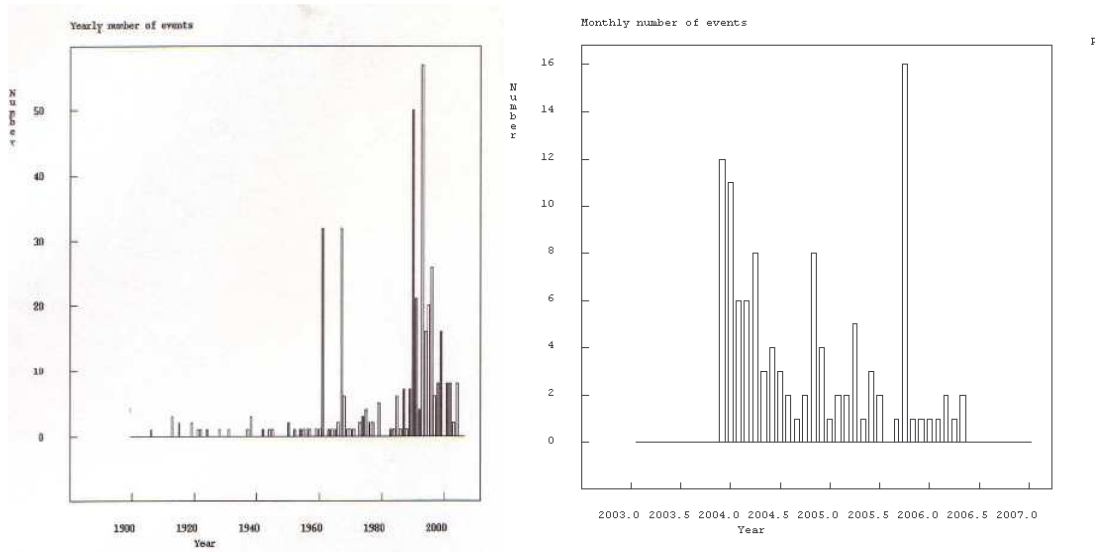


Figure 8.2 Two Histograms showing the distribution of event for two different data base. Right hand shows data come from ISC for the period 1900 to 2003. Increase the number of events up to 1990 to 1992. Lift hand shows the temporal distribution of earthquakes detected by SSN data for the period 2003- 2006.

# Chapter Nine

## Local Geology of Khartoum Area

### 9.1 Introduction to Local Geology

General treatment of geology and illustration of the geological formation based on the geological map of Sudan (GRAS 1988 and 2006) has presented by Andrew (1948), Whiteman (1971) and Vail 1978 and 1982 and authors). Review of published data and additionally observation of the author recorded during the reconnaissance survey carried out.

The principal geology unite (Figure 3), encountered in the study area and the surrounding are summarized, as follows:

- 5-superfical deposit (Quaternary)
- 4-Gezira Formation (Tertiary)
- 3-Volcanics mainly (lat Tertiary)
- 2-Nubian Sandstone Formation (Mesozoic)
- 1-Basement complex Rock (Pre- Cambrian – lower Palaeozoic)

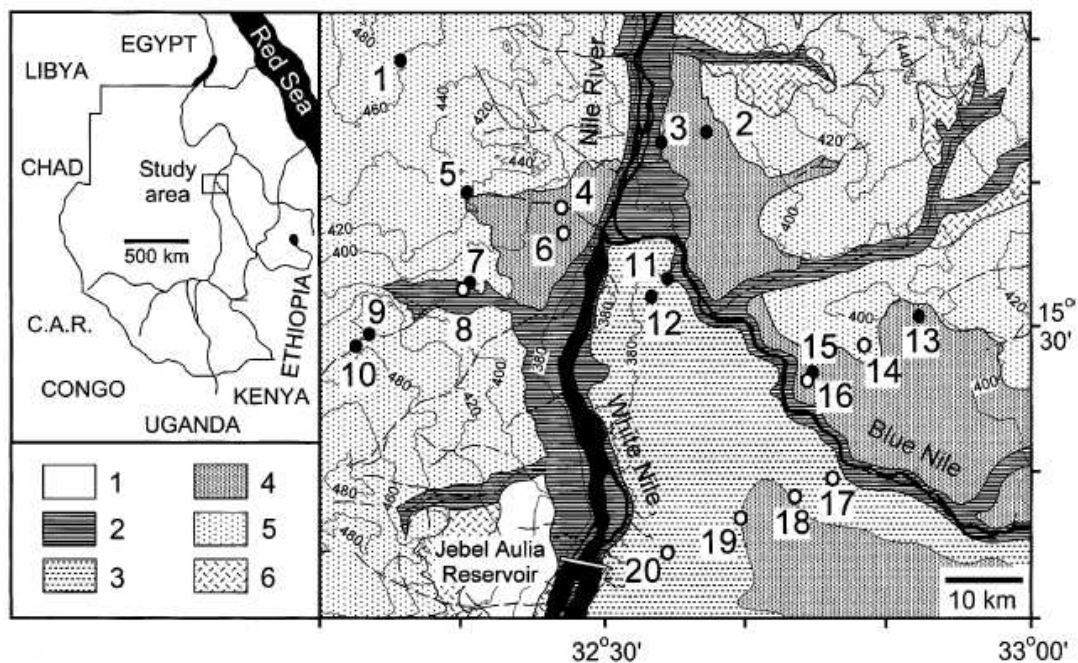


Figure 4, geological map of the study area. Shown all formation unite as number in below the map; 6 Basement complex, 5 Older alluvium, 4 Gezira formation, 3 Omdurman formation, 2 Recent alluvial and 1 Dense. (Modified from Robertson research and GRAS 1988 and 2006). Note, Gezira formation at north western area are adopted to lower Omdurman formation from another research [Farah et al 1997 and Beirir1993]

### ***9.1.1 Basement complex***

The term Basement Complex Pre- Cambrian to early Palaeozoic age (Whiteman 1971) used to embrace all formation older than the Nubian sandstone [Andrew1948]. The basement complex occurs in different place in central Sudan. It is the oldest rock includes igneous, metamorphic and metasedimentary rock. Basement complex is overlain by horizontal and sub-horizontal Palaeozoic and / or Mesozoic sedimentary or igneous rocks.

In the study area the basement protrude and rising above the surrounding plain. It is exposed at two site, one in southern, another in northeastern part of the area. At south the Basement complex is overlain by sedimentary sequence, but small inliers crops out are occurring close to Jebel Mandera in the southern part of the area. It is composed micaceous schist brecciate felsites dykes. Basement rocks are also known the area in borehole at variable depth, where tapped at shallow levels in borehole to the west of J. Aulia [Ibrahim1995].

The basement complex in northern part is occurring with large area, called Sabalok Basement complex. Early it is described by [Down, 1971; Vial 1972; Almond 1977] as a large group of anorogenic igneous complex in Sudan. It is characterized by predominance of acidic rocks (younger granite), shallow level of emplacement, and the common present of structure (Ring of volcanic intrusion and normal and strike slip fault are crossing the area).

### ***9.1.2 Nubian Sandstone Formation (Mesozoic)***

Nubian sandstone formation was used as describe the late cretaceous sandstone in the Nubian Desert in the northern African. Since most study area are covered by sandstone. [Whiteman 1971] the first one proposed the Nubian Sandstone Formation in Sudan. They are unmetamorphosed bedded and usually flat-lying sedimentary rock which are made up of conglomerates, grits, sandstone sandy-mudstone and mudstone, which are considered to be of post Paleozoic and pre Tertiary age. Geologists give different interpretation the Nubian sandstone as different angle. Kheiralla (1966) used the term Nubian sandstone formation for the sedimentary strata of variegated colours around the Khartoum state and divided the Nubian sandstone into five lithological units from Khartoum to Shendi area. Merkhayat Sandstone located northern of Omdurman area which is a part of Nubian sandstone formations, which started as



made up of clastic sedimentary rock largely sandy and conglomerate poorly cemented and another place with high silicified bed. The beds are generally horizontal or gently dipping. The following lithological units were established by Kheiralla (1966):

- 1-Pebble conglomerate
- 2-Intra – formational conglomerate
- 3-Merkhiat sandstone
- 4-Quarzone sandstone
- 5-Mudstone

Husein (1976) and Omer (1975) they are described as sandstone environment, first one suggested that it is a tropical fluvial with the second one proposed a semi dry to tropical paleoclimate and upper Cretaceous age.

[Wycisk et al 1990; Schrank and Awad 1990] adopted the term of Omdurman formation depending on palynological study from subsurface strata. They suggested that in Khartoum area the predominantly sandy Omdurman formation is of Albian to Cenomanian age.

Bireir (1993) based on lithology, grain size, heavy minerals content, geochemistry, clay minerals content, paleogeography and depositional environments, subdivided Omdurman formation into two formations;

- 1-Upper Omdurman formation (outcropping sediments)
- 2-Lower Omdurman formation (subsurface strata)

Upper Omdurman formation is a clastic sedimentary sequence of Khartoum State. It comprises a flat-lying or gently dipping sedimentary rocks lying unconformably on an originally uneven basement surface and characterized by an irregular outcrop pattern [Hussein 1992]. This formation is exposed at Abu Weledat and Ummarahik hills. [Barazi, 1989] located at northwest of Omdurman and Aulia hills in southern of Omdurman is many contain sandstone with various grain size (coarse, medium or fine) cemented by siliceous, kaolinitic and ferruginous materials.

Lower Omdurman formation is represented as the surface and sub-surface strata [Barazi 1989] which are proposed that the depositional environment of the exposed strata is fluvial while sub-surface units display a lacustrine environment. Lower Omdurman formation is composed of fine and less coarse grained, poorly to moderately sorted, siliclastic sediments [Bireir, 1993]. The sediments of this

formation were almost transported as subsided particles which rolling ads and a considerable amount and deposited under fluvio-lacustrine conditions. This processing are gives 72% course-grained sandy where the sandstone is the dominant rock type it is almost friable, except the mudstone horizons which are frequently compacted and hard [Farah et al 1997]. The mudstone can reach more than 90 m thickness, especially in the southern part of Omdurman area. Mudstone clasts and lenses are characteristic of this formation, especially in Omdurman are. This formation shows fining upwards, and stacked- channel sequences, ranging in thickness from 25 to 35m, rapid lateral and vertical changes of facies [Birier, 1993; Farah et al 1997]

### ***9.1.3 Tertiary volcanoes***

Volcanic rocks have been reported in many locations e.g. Jebel Marra at (Whiteman 1971) and Bayuda desert in western and northern of Sudan respectively (Almond et al 1969). (Andrew 1948) correlated that with tertiary volcanic of east African and Ethiopia The area between Khartoum and Shendi regions are observed that, basic volcanic igneous rocks are intrbedded in the Nubian Sandstone Formation [Kheiralla 1966] which are contain mainly basalt and dolerite dykes. The Basalt is occurring at Jebel Toriya (Jebel mean hills) which forms a low hill about 11 km west south of Khartoum (figure 11.4). Extensive geophysical and geological investigations have been carried out [Qureshi et al. 1966] and the petrology of the basalt has been studied in detail [Almond 1967]. On the evidence of centripetally dipping flow banding inclined at moderate to steep angles, suggested that the basalt is an intrusion rather than a flow. Dolerite dyke and basalt reported in north eastern of Khartoum city, as known Sabaloka Igneous complex [Dawoud 1970]. The dolerite dyke of N- S trends was observed in the western parts of the study area. This is found by drill holes in Nubian Sandstone formation. Which were penetrated at variation of depth between Jebel Aulia and Khartoum [Farah et al 1994].

### ***9.1.4 The Gezira Formation***

The triangular area formed by the While Nile and the Blue Nile. It is charatererised by flat and featureless clay. The first one who was introduced by [Anderw 1948] who used this term for the unconsolidated clay, silts, sand and gravels in Gezira area. [Delany 1966, Whiteman 1971; Vail, 1988; Bireir, 1993] believed that the Gezira

formation rest uncomfortably on the Nubian Sandstone formation and is overlain by blown clay and another superficial deposits. Abdel Salam (1966) and Farah et al (1997) classified the Gezira formation in two major formations upper and low Gezira formation (Figure 5). The upper Gezira formation is composed of unconsolidated sands, clays and silts. It is characterized by high percentage of smectite, low percentage of kaolinite and unstable heavy minerals [Birier 1993]. The upper most layer as known the black cotton soil which is dark cracking clay. This cracking is representing by the weathering condition. The thickness of upper Gezira formation is approximately 10 to 90m. At most northern part of the near to Khartoum is thin about 10 to 50m, while it is increasing thickness at southern of Khartoum. The lower Gezira formation consists of interbedded sands and clays. The sands consist predominately of loose, medium and fine grained. The depth of this formation is identified in the borehole data section at depth of 205 to 240m [Birier 1993]. At Khartoum basin the depth that formation is approximately 180 m to 500m [Sun Oil Company 1989, unpublished report]

The thickness of the upper Gezira formation underlines the study area where close to White Nile around 15 to 25 m. Geological Research Authority of Sudan (GRAS) produced map 1988 and 2006 showing the Gezira formation has taken place at part of Omdurman area figure 3. But this part describe by Farah et al (1997) is lower Omdurman sandstone formation with dominated mudstone interbedded layer into sandstone while the Geriza formation between two Nile (White and Blue Nile) is unconsolidated clays, silts, sandstone and gravels see figure 4.

[Abdesalam 1966] Suggested that the main source for the Gezira formation is the Ethiopian volcanic plateau and proposed a fluvio- lacustrine depositional environment while Adamson and Abdulla (1982) suggested fluvial origin. Depending to palynological studies [Awad 1992] is identified the age of the Gezira formation for Oligocene – Miocene. The contact between the upper and lower Gezira formation is transitional. More formation about the different between these formations described by Farwa, 1978; Wycisk et al, 1990; Birier, 1993 Mula et al 1993.

However, the Gezira formation is used in the present work in order to known by the sediment strata and distribution of clay surface layer. We will focus in eastern of the study where located in the eastern bank of white Niles strata. It is employed to designate the interbedded sand and clays which are proposed to gives response site

effect in upper most layers. Considerable the thickness of sedimentary layer will may help to correlation that with the microzonation seismic results.

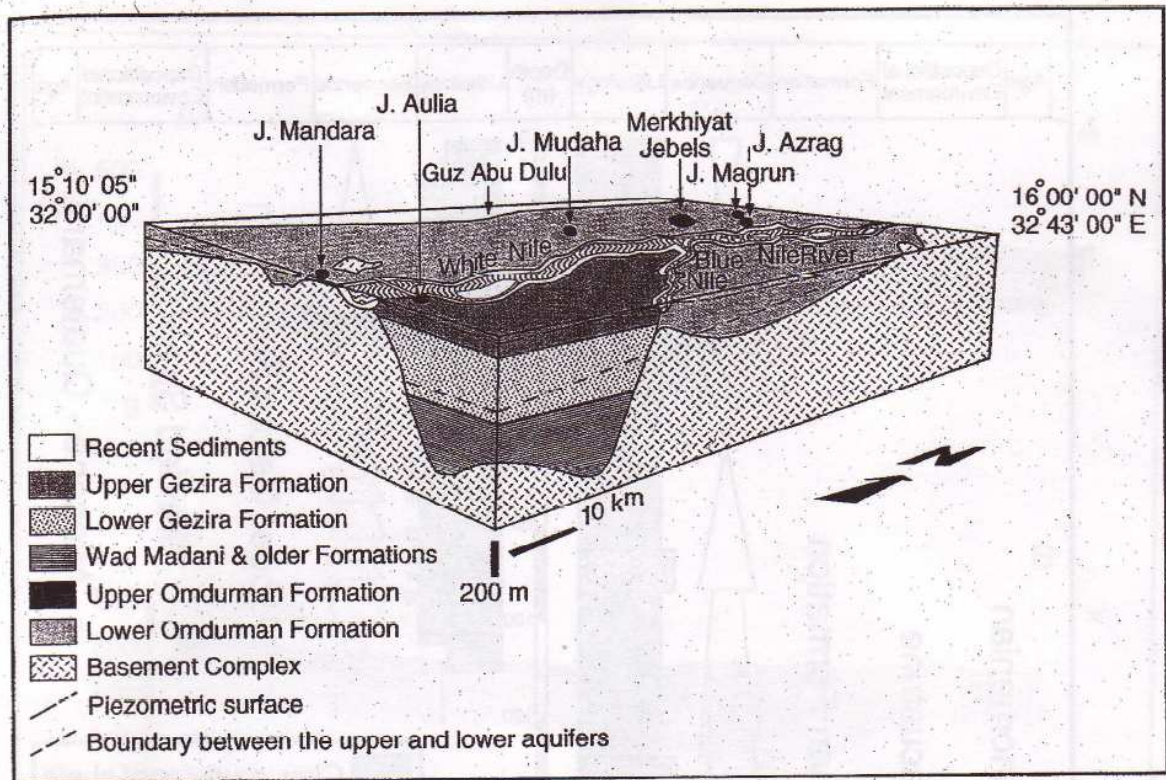


Figure 5 Sketch block diagram of the northern part of the Khartoum basin. Shows the geological and stratigraphical unite study area [after Farah et al 1997]

### 9.1.5 Superficial deposit (Quaternary)

The recent deposits encountered in the study area include windblown sands the White Nile alluvium and Wadi-deposits (streamer channel) [Whiteman 1971]. It is occurring at many places with different characterized. The eolian sands cover most parts of the compresses between White Nile and Kordofan State [Whiteman 1971]. Site are observed along the bank of the White Nile and between the dunes and Wadi deposit, consist of unconsolidated sand, silt sand and gravel and loosely compacted silt, sandy silt and clay (Figure 4). The recent deposits at western bank oh the White Nile and southern of the study area are more compacted and larger area than the one occurring in eastern bank of the White Nile.

## **9.2 Tectonic and structure**

Khartoum basin is one the Blue Nile Rift was formed on early Mesozoic on the central Sudan, in response of sinistral movement of major NS oriented strike–slip fault. The thicknesses of sedimentary sequence generally increase from NE- E (Sabraoka basement) to more than 900m in the W-SW. From southwestern of study area close to north of Aulia Dam where basement rock outcrops and increasing toward in the north western where reach of more than of 900m thickness at Khartoum town (Figure 4-5). The predominantly sands upper and lower Omdurman formations on the western periphery of the northern part of this basin [Shrak and Awad 1990] are interpreted as being deposited in a NW- SE trending zone of subsidence along the trend of the Blue Nile Rift. [Salam, 1985] showed that the Blue Nile Rift is bounded by a series of strike NW- SE, NE –SW and E-W [Hussin 1992] mention that structures it is possible is defaulting of basement complex rejuvenated later during Tertiary created a series of basin. Khartoum basin has repeatedly active in Umm Udam borehole in the northern Gezira Paleozoic deposit occupy a NE channel, and two epicenters of earthquake with shallow depth in this region. The Central African Zone is crossing the Bagbag basin at western Khartoum basin which is suggested to be a border zone of deformation [Ibrahim 1996].

The Nubian sandstone Formation is mainly horizontal or gently dipping rests unconformably on a dissected Basement Complex surface and was later affected by faulting [Farwa 1978].

In the southern part of the study area at Aulia hill a major NW trending fault is observed cutting the Nubian sandstone near to Aulia dam with NE direction thrown down more than 1000m. [Mula 1971 – 1972] reported E-W and younger N-S to NNW faults with down throws normally to E and NE with a displacement of more than 1200 m.

## **9.3 Other environmental conditions**

Most of study area is lying on soft sediments; subsurface layers at some parts are mudstone horizons which are frequently compacted and hard occurring at southern parts of Omdurman area, in the northern part there are mainly mudstone with clasts

and lenses of Cretaceous sandstone layer, with it is hard silicified. These different strata may give different acoustic of ambient wave come from below. The drainage water system in the study area with high population is not allowed to drain into the river Nile, this water remains and recharges into the subsurface layer, this condition may have an effect of underlain by saturated loose to medium dense sand in Khartoum area and mudstone lenses beds in Omdurman, thus they may give different e.g. (acoustic wave). The study areas are specifically urban districts which are economic and historical towns. These factors must be taken into account since there are many buildings under construction such as the new international airport, two bridges and a dam.

## Chapter Ten

### Methods for Empirical Estimation of the Site Effects

The methods for local site effects estimation can be classified into two major groups. The first group the analytical-numerical modelling methods based on the available geotechnical information pertaining to physical parameters of surface structure [Idriss and Seed 1968; Bard 1994., Wald and Mori 2000., Modemedzin et al 2006]. The second group includes analysis of observations or measurements (empirical) of seismic wave records. In the empirical group there are two methods used to obtain the site response; the Standard Spectral Ratio (SSR) method and the Single Station Spectral Ratio (SSSR) methods. The different methods used in the site response evaluation have been discussed in several papers [e.g Aki, 1988; Hartzell, 1992; Aki, 1993; Bard, 1994., Atakan et al 2004].

In this study we will focus on the second group that use natural source. Based on the type of numeral of recording site can be divided into three subgroups;

- 1- H/V standard spectral ratio (SSR).
- 2- H/V spectra on weak - motion data or local earthquake.
- 3- H/V ratio spectra of ambient noise recordings.

In this chapter we will discuss methods based on SSSR an SSR methods. Since we used a particular empirical method to estimate the local site response of the west of Khartoum city, we will highlight the empirical we currently used.

#### 10.1 H/V standard spectral ratio - weak motion data

One of the most common procedures for estimating the site response is called Standard Spectral Ratio (SSR), introduced first by Borcherdt, in (1970). It is still widely used way to estimate the site effect in regions of moderate seismicity. The method involves recording microtremor data from the sites to be investigated. It requires a reference station on hard rock, and stations recording on sediments (soft-soil). It is assumed that signals from the hard rock site are equally amplified well at all frequencies. On the other hand, a soft-soil site amplifies the signal at its resonance frequency, which depends on many factors such as the soil type and the basement configuration. Hence, if the source and the path effects are negligible, then we should

get a flat spectrum at a hard-rock site and spectra showing peaks at resonance frequencies at soft-soil sites. It is assumed that the source of microtremor and the path through which the surface wave's travels to both the sites are identical. This assumption holds true when both sites are very close to each other.

In estimating the site amplification, the large amplitude S- wave part of the seismogram is extracted using a fixed with a pointed window and the extracted data are used to calculate the spectral ratio with respect to the reference station. This method is designed to minimize the source and the path effect. Several researchers have presented the theoretical grounds of this method. Borchardt (1970) had given a simple description of it. The effect on the seismogram can be visualized as follows:

Assume that  $i(t)$  is the source (input) and the output seismogram  $s(t)$ . The ray paths are affected by three elements- earth's crust ( $he(t)$ ), geology of the site ( $hg(t)$ ) and the recording instrument ( $hr(t)$ ). In first approximation each effect on the seismogram can be considered as linear. Hence, the final seismogram may be given as;

$$s(t) = i(t) * he(t) * hg(t) * hr(t) \quad (1)$$

where “\*” denotes the convolution operator. Denoting the Fourier transform of the respective function by capital letters, the expression takes the form;

$$S(f) = I(f) * He(f) * Hg(f) * Hr(f) \quad (2)$$

The ratio of the absolute value of the Fourier transform of a seismogram recorded on the sedimentary layer ( $Ss(f)$ ) to that recorded at a nearby bedrock station ( $Sb(f)$ ).it called SSR provided similar that recording units are used at each site and the travel path through the Earth's crust is essentially the same for sites the station and path effects are considered equal. The ratio for the two sites can be reduced to:

$$\left( \frac{|Ss(f)|}{|Sb(f)|} \right) = \left[ \frac{|Hgs(f)|}{|Hgb(f)|} \right] \quad (3)$$



Bedrock doesn't change the frequency characteristics of the signal as much as a thick sedimentary layer; hence the ratio  $|S_{s(f)}|/|S_{b(f)}|$  will, to a first approximation, be the seismic amplitude response of the sedimentary layer. The ray path contribution between the source and the local site must be small in order for the method to hold [Corinne et al 2004].

The motions from the 1957 and 1906 earthquakes in San Francisco caused great damage, and the geological conditions may have been a factor amplifant [Borcheredt 1970]. The method amplification effect of the local geology could was estimated analyzing the nuclear- explosion recordings. The amplifications for the sedimentary site is better estimated from ground motions generated by nuclear explosion, than from those generated by moderate earthquakes. Therefore, due to the non- linearity, the site effect estimated by SSR techniques may be considered an overestimation or upper limit of the actual site effects at high frequencies, and a slight underestimation at frequencies below to fundamental frequency [Borcheredt 1970].

When using the SSR technique two factors must considered; first, the reference site should be located near enough to the site of test to ensure that differences between each site are only due to site condition, and not to differences in source radiation pattern or travel path, which is generally valid when the hypocentral distance is larger than about 10 times but the distance between the sites Second, the reference site be unaffected by any kind of site effect, which is the case when the reference site is located on an unweathered bedrock [Corinne at el 2004].

[Theodulidis et al 1996] obtained good correlation between strong motion spectral (SSR) and H/V ratio in southern part of California. According to him, this motions give more information about the site effects than the commonly used average shear-wave velocity in the upper 30 m. Suzuki et al (1995), using both microtremor and strong- motion data in Hokkaido, Japan, showed that the frequency from the H/V spectrum seems to correspond well to frequency estimated theoretically from the thickness of the alluvial layer.

We will mention a few studies that give example of H/V ratio derived from strong motion:

The 1994 Northridge earthquake data were used by Huey and Teng (1999) to test the validity, limitation and applicability of this method for site response estimate. According to them, the relationship between H/V ratio and standard spectral ratio is similar below 1.3 Hz. As the frequency becomes higher, the standard spectral ratios yield lower site response value than the H/V ratio even though the geometrical attenuation between two stations has been taken in account.

Lermo and Chavez-Garcia (1993) applied this technique to transfer function for the large amplitude part of *S* -waves for a small sample of earthquake records obtained in three cities in Mexico. They demonstrated that their observations are consistent with estimation of the empirical transfer function as calculated by applying the Haskell method to a layered basin model. Their results show that the H/V ratio can give a robust estimate of the site frequency and amplification.

Edward et al (1997), estimated that the ground amplification for the main shock of the 1994 Northridge earthquake sequence estimated with the H/V method was up to a factor of two less than the amplification observed for the aftershocks. This is an example of the nonlinearity of the problem of the motion amplification. The technique some earthquake studies have demonstrated the nonlinear behaviour of the site response under certain circumstances [Aguirre et al 1995].

Kenichi, et al (1995) estimated the site response from the S-waves and coda wave of strong motion data. Both these wave types give the same amplification values for the 1992 earthquake in Landers- South California. The agreement between S -wave site response and Coda site response estimates is understandable if we assume that Coda wave are dominated by S- waves, as theoretically predicated by Aki (1992).

We will discuss some of the disadvantages of the SSR technique as mentioned by several studies [Brad, 1994; Aki 1995; Huey and Teng 1999]

1. The trigger recording of noise level at different station will some trace not at stations.
2. An appropriate reference site is some traces impossible to find. The best choice for reference site is at the situated on flat crystalline outcrop [Rogers,

1984]. If we have two different reference sites (the crystalline rock outcropping at more than one place in the study area we will get different response, and the site reference sites will have site response that will influence our estimations.

3. The surface effect of the topography effect is some time crysurficant. Due to topographic effects buildings located at hill tops suffered much more damage than the site located at the low sites [Mirzaoglu and Dikmen 2005]. There is also very strong instrumental evidence that surface topography considerably affect the amplitude and frequency content of the ground motion. Theoretical and numerical models made by Pedersen et al (1994) predict complex amplification and de-amplification patterns on hill slopes, resulting in significat motion. Very often, measurement show larger effect than what is predicted by the simulation. A possible explanation is that in many cases weathered rock is found at the top of hills which further reinforces the topographic effect [Pedersen et al 1994].
4. Earthquake parameters such as distance, azimuth, magnitude and thickness of the sediment basin are used for site response estimation. We will take for example the study in Mexico City which explained the effect of the spectrum effect in site response. According to Singh et al (1988) the frequency at which maximum relative amplification occurs varies from site to site in near Mexico City. He suggest that  $f_0 = \beta/4H$  where  $f_0$  = frequency at which maximum relative amplitude occurs,  $\beta$  and  $H$  are the shear wave velocity and thickness of the soft layer. For a given lake bed site the maximum relative amplification and  $f_0$  are roughly constant, independent of magnitude, depth, and azimuth on the source if site at located more than 200km away.
5. The SSR method is both expensive and time consuming [Navarro et al 2001].
6. Quality of data set. The Nonlinear site effects in strong- motions are very common. Reviews from such nonlinear site effect studies may be found in [Nersnev and Wen 1996; Wen et al 2006]. The soil tends to damp more the energy from large amplitude ground motion. The nonlinear amplification means that the site response must also be calibrated as function of the amplitude. Nonlinear amplification at sedimentary sites was inferred by Chin and Aki (1991) and Aki (1993) who report that for sedimentary stations within 50 km of the epicentre of the Loma Prieta earthquake. According Inazki

(2004) to the evaluation of the nonlinear properties of near-surface soil under strong motion may be estimated by using shear wave vibrator as a dynamics loading source.

## 10.2 H/V spectral ratio for weak motion (transfer functions)

This method consists in taking the spectral ratio of the horizontal and the vertical components of the shear wave part of weak motion recordings. This technique is a derivation of Langston's (1979) *receiver-function* method for determining the vertical structure of the crust from the horizontal to vertical spectral ratio of teleseismic P - waves.

Equation (3) computes the ratio of two seismograms at two sites and should correlate with the sedimentary thickness ratio beneath these stations. Let us have two stations one on top of a sediment layer and one station on bedrock and the sediment station SH over a layer with thickness (H). The ratio of the spectra of the seismogram of sediment ( $S_{HS}$ ) station and the bedrock( $S_{HB}$ ) spectrum will be the amplification of the ground amplification from the sedimentary;

$$S_T = \frac{S_{HS}}{S_{HB}} \quad (4)$$

Equation 4 is called transfer function. If we to have a station on the surface and another one deployed in borehole the transfer function way be estimated. This method is costly and the effect of the lateral geometry is not taken in account. In addition the method requires a strong earthquake to occur nearby.

## 10.3 H/V spectral ratio of noise recording

The H/V spectral ratio of the horizontal and the vertical spectra of microtremors was first introduced by Nogoshi and Igarashi (1971), and Nakamura (1989, 2000). It is called (QTS, Quasi – Transfer Spectra). The technique uses fit very well to describe the dynamic characteristics of the ground and structure. The technique uses the ambient seismic noise that is always present in the earth. This source is one of the more advantages of that method. The method is also cheap and easy to use for the site response spectra estimation.

Nakamura (1989, 2000), gives the theoretical base of the H/V method. Dividing the horizontal spectrum of the ground recorded motions on sediment site,  $S_{HS}$ , by the horizontal spectrum of recorded on interface between the bedrock and the sedimentary layer,  $S_{HB}$  will give the transfer function  $S_T$ . Considered to be the reference component.

Nakamura (1989), and Lermo and Chavez-Garcia (1993) used a spectral ratio  $E_s$  to estimate the amplitude effect of the source (including Rayleigh waves)

$$E_s = \frac{S_{VS}}{S_{VB}} \quad (4)$$

where  $S_{VS}$  and  $S_{VB}$  are respectively, the spectra of the vertical motions on the surface and on the bedrock. Originally, Nakamura (1989) assumed that the vertical component of the microtremor spectrum is not amplified by the low-velocity surface layers and estimated the effect of Rayleigh waves on the vertical components of the microtremors by evaluating  $E_s$ . If the effect of the Rayleigh waves is the same on vertical and horizontal components,  $E_s$  can be used to eliminate the effect of Rayleigh waves on the transfer function. In order to compensate for the source effect ( $E_s$ ), Lermo and Chavez-Garcia (1993) introduced a modified site effect function ( $S_{TT}$ ):

$$S_{TT} = \frac{S_T}{E_s} \quad (5)$$

Eq 6, which it is equivalent to;

$$S_{TT} = \left( \frac{S_{HS}}{S_{VS}} \right) / \left( \frac{S_{HB}}{S_{VB}} \right) \quad (6)$$

Nakamura (1989) assumed that the ratio of  $S_{HB}/S_{VB}$  is nearly 1.0 for a wide frequency range, for which he has tried to give several empirical examples using data from microtremor measurements in a borehole. This assumption is reified by several

seismologists. e.g. Huang and Chiu (1998) calculated the ratio  $S_{HB}/S_{VB}$  using both microtremor measurements and earthquake recordings at a bedrock site in Chiawan, Taiwan. The average  $S_{HB}/S_{VB}$  ratios are found to be approximately 1.0. With these empirical proofs, we may consider that a reasonable estimate for the modified site effect function can be derived from the formula;

$$S_{TT} = \frac{S_{HS}}{S_{VS}} \quad (7)$$

Equation 5 suggests that the H/V ratio as defined by this transfer function can be obtained only from the motions the surface. This certainly makes the site effect estimate much easier.

In order to using this method may have many factors we must to be taken into account:

Nakamura (2000) method employs microtremor is well known but there may be some cases when the transfer function calculated from  $S_{Hf}/S_{Hb}$  ratio and from the of borehole structure data show some differences.

[Nogoshi and Igorashi 1971] compared H/V of Rayleigh waves with microtremors H/V of and concluded that microtremor motion was mostly composed of Rayleigh wave. Some of the theoretical studies such as [Lachet and Bard 1994; Konno and Ohmachi, 1998; Bard, 1998] suggested that the peak on H/V can be explained with the fundamental mode of the Rayleigh wave. Many researchers agree on the following arguments: First, H/V is basically related to the ellipticity of the Rayleigh waves, which are predominant in the vertical component. Second, this ellipticity is frequency dependent and exhibits a sharp peak around the fundamental frequency for sites with a high enough impedance contrast between the surface layer and the bedrock layer. Yutaka (2000) reports that the peak in the H/V ratio from microtremor fast of an earthquake cannot be explained with Rayleigh waves; because Rayleigh wave energy is very small for the peak frequency but in the H/V ratio.

The H/V method is attractive because the data can be easily collected and it can be applied in areas of low or even no seismicity. Other researchers have pointed out the correlation between the H/V peak frequency and the fundamental resonance

frequency of the site. They proposed to use the H/V technique as an indicator of underground structures and features. Recently H/V method has been used to estimate the site effect in large urban area (SESAME European project, Site Effect Assessment using Ambient Excitations).

# Chapter Eleven

## Data Collection

### 11.1 Ambient noise data

The method we used to estimate the site response spectra in Omdurman and the east area part of Khartoum city is the H/V spectral ratio technique (called also Nakamura method) for site effects assessment using ambient seismic noise. This method has been mention in methodology section and discussed in chapter ten. This method was refined the software has been developed by European seismologists during the project called Site effects assessment using ambient excitations (SESAME) [Atakan, 2004;2003;2002; Bard 2004; Koller 2004]. More formation about this program and method could be found in the web page <http://sesame-fp5.obs.uif-grenoble.fr/>.

In this chapter we will describe the method just briefly and we will focus on the particular sequence of steps that have to be performed to obtain the site response spectrum at different sites. We will also describe briefly the instrument and software used and at the end we will give description of the data collected during the survey.

#### *11.1.1 Measurement sequence*

The site response spectra from micro tremors were found by calculation the ratio of the spectra of the horizontal (H) and the vertical (V) components of recorded ground motion. The source of that ground motion is the ambient seismic noise present in the ground. In our survey we recorded the ambient noise in different sites and we used the J-SESAME package to compute the spectra ratios [Atakan et al 2004]. It is known that the H/V method gives reliable results for low frequencies. This is one of the disadvantages of the method that it cannot give reliable results at high frequencies. Furthermore, the method has the disadvantage that it does not constrain well the amplification factor the fundamental site frequency. The amplification factor of the high frequencies requires the Standard Spectral Ratio [Atakan et al 1996].

The Nakamura method has the advantage that for short period of time, and low cost reliable result can be obtained. In our survey were used four tools the following equipment;



- 1-Three component seismograph model GBV-316. This instrument was taken from seismology department at the University of Bergen. It is used to make records of the ground motion from ambient seismic noise.
- 2-Computer with installed software to transfer digital data from the sensor into the database folder.
- 3- Global Positioning System receiver (GPS) to determine the exact of location, direction, and elevation of the site of measurement.
- 4- Magnetic compass to determine to orient the instrument.

### ***11.1.2 Instrument testing***

We used three component aseismograph (portable seismic station GeoSIG GBV-316) to record the ground motion. The seismometers are three 4.5Hz geophones, perpendicular to each other. The GeoSIG GBV 316 seismograph has small size, built with low cost. It is very compact complete 16-bit seismograph with built in sensor and battery. External sensors can also be connected. The recording capacity is up to 64 Mb, which at 100 Hz sample rate gives 5 days of continuous recording, although it is more typically used with smaller memory and in triggered mode recording. With GPS it consumes typically 3 W. Communication is by is observed through the serial line [Havskov and Natvik 2004]. The parameters were set up with the acquisition system (Seislog software) and instrumentation specifications used to make good seismic noise recording are given in table 11.1 (shows the most important specifications of the GBV-316 taken for the survey, and Havskov and Alguacil 2004). Before the survey started we made tests to ensure that instrument is working properly. We made test recordings one inside one and outside of laboratory of the University of Bergen and also near the study area. Figure 11.1-11.2, shows the tests of the noise power spectra of the Z-channel of the GeoSIG GBV-316 seismic sensor. These two tests were recorded at two different sites in our study area (hard rock and soft soil on sites). The noise power spectra at the sedimentary site have higher amplitude, due to sediments the amplification of waves generated by sources such as traffic.

<i>Sensor</i>	3 geophone( BGV-316)
Frequency response	4.5 Hz
Sensor generator constant	28 V/(m/s)
Amplifier gain	131*10 <sup>6</sup> counts/V
<i>Digitize</i>	
A/D converter	16 bit
Noise	± bit at gain 1000
Sampling rate	100 sps per channel
Bandwidth	20 Hz
Input rang	±2.5 V DC
Anti aliasing filter	6- poles antis filter at 18.5 Hz
Rs-232	1 sec data buffer or sample per sample
<i>Data recording</i>	
Pre event memory	1 to 30 s
Post event memory	1 to 100 s
Compression factor	2.0
<i>Triggering</i>	
Level triggering	no
Lower band limit	0.1 Hz
Upper band limit	3 Hz
Trigger threshold	0.1 to 100 % full scale
STA/LTA triggering	
STA- base	0.1
LTA base	1
STA/LTA	No
Solid state memory	2 to 64 Mb
<i>Power supply</i>	
Type	External power supply17 to 30 VDC
Internal battery	12 V rechargeable lead acid battery
Battery regulator	Internal
Autonomy	48 hours
Power consumption	1 W at 12 v Dc

Time base	
Clock accuracy	10 ppm(10 min/year)at – 10 <sup>0</sup> C to +50 <sup>0</sup> C
External time interface	GST optional
<i>Communication</i>	
Serial ports	2
Baud rates	2800
Communication protocol	Binary
Protocol securities	Checksum and software handshaking
Communication	PC/RS-232 port or modem
<i>Environment/Housing</i>	
Operational temperature	-20 <sup>0</sup> C to + 70 <sup>0</sup> C
Humidity	0% to 100%(non condensing)
Site	18*18*10 cm
Weight	5.2 kg with the battery
Protection	IP54
Connectors	
RS-232	Communication, parameter setup, data download, time tagged data buffer output
GPS	Continuous or cycled operation
External sensor	Connection of external sensor
Power	External power supply, external battery

*Table (11.1) the main specification of the GBV-316 seismic data acquisition system used in our survey. Modified from [Havskov and Alguacil 2004]*

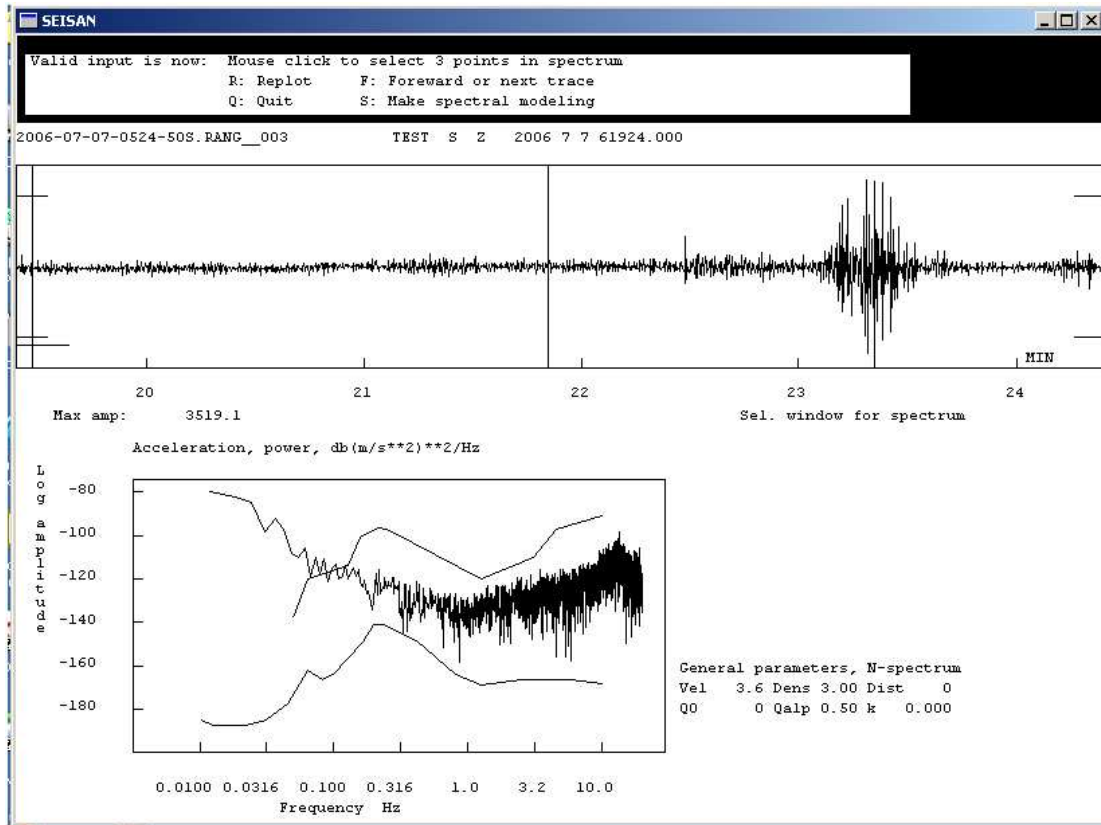


Figure 11.1, power noise spectrum and recording from basement complex rock site in the north eastern Khartoum area. The upper figure shows the seismic noise recording of the Z- component. The lower figure shows the equivalent ground acceleration noise power spectrum for shorted a digitizer using GBV-316 sensor. The smooth curves on top and bottom are the Peterson Lower- Noise and high- Noise models, given as reference.

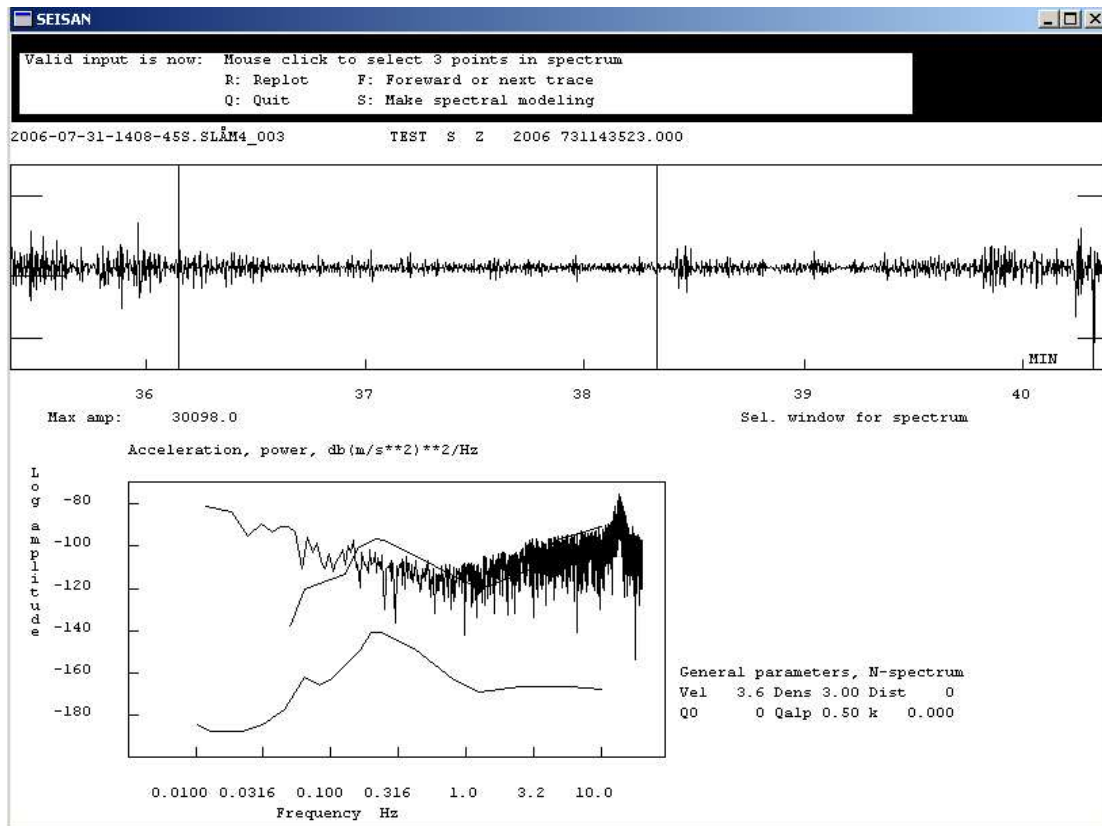


Figure 11.2, Noise spectrum and recording from sediment rock site in the Khartoum basin. The upper figure shows the seismic noise recordings of the Z- component. The lower figure shows, the equivalent ground acceleration noise spectrum for a shorted digitizer, using GBV-316. The smooth curves on top and bottom are the Peterson Lower- Noise and high- Noise models, given as reference.

Below we discuss the sequence of steps that have been performed at each site to obtain the site response spectrum:

We used the Khartoum city map in order to determine the places where we have to do our measurements. Considering the time allocated for the survey we made two plans in order to cover the whole study area. The first plan was across grid in order to cover most of the homogeneously unit in the study area. The second plan is to divide the remaining time to measure details in each unit of smaller scale. The location of each site was extracted from the map, and then we made a time table to visit and to measure as many sites possible. In order to have the best possible measurements we needed to find place as far as possible from heavy traffic streets, buildings under construction, factories, and any industrial sources that may introduce man made noise

in our data. Direct sun light on instruments and pocket computer should be avoided. The variation of temperature in the period between June and mid August affects the response of the instruments and we had to wait for appropriate temperature condition. This was a big problem that took time and high cost for paid new battery, because there is no near electrical recharge and car supply also didn't have enough electrical energy. We stopped measurements when it was raining because the rain generates natural source which as not needed, because the high humidity may damage the sensor.

Once the site was selected we looked for the flat places where the instrument can be site horizontally. We use a magnetic compass to determine the north direction and then we oriented the instrument accordingly. We can see the recording on the screen of laptop pocket computer. We turn on the instrument, connect with the pocket computer by serial line and connect the GPS also by long serial line. The pocket computer must have Seislog program which is the program for seismic data acquisition [Natyvik and Havskov 2004]. This program downloads and installed in order to perform the data acquisition. We have several tests on program in order made sure is working well. We note the site name of each recoding. When they are enough satellite stations receiver by GPS the program will started recording well. If the sky has cloud the GPS well not receive any single from satellite station which it means the program has subsiding recording. Some sites where with low levelling the GPS also has no receiver signal, in this problem we must put the GPS at high level like hall of building or we made construction to be higher about three meters over measurement flat.

The first step is to configure the device and the channels correctly in the Seislog program. That must have three component installed one vertical component and two horizontal components E-W and N- S. We can check if the system is running well by monitoring all channels for some time and performing test by pushing instrument and checking the of display of the sensors. Then we set the system to record for some time we must write the name of the site of measurement in order to identify the data later. In order to get clean records we must set delay time before the start of the record in order to have true to move away from the instrument. Most of our measurements have been of 30 min duration. We used a stop watch to determent the recording time.

During the recording and we should be far from the instrument and make notes on a special field measurement sheet a sample of which is shown in Figure 11.3. The field measurement form was taken from SESAME project [Atakan et al 2004]. In this form we write the most important observations. Date, GMT time, local time, geographical coordinates as given by the GPS, and name of the site. We must note the presence of all nearby source of transient seismic noise. Weather conditions such as wind, rain, temperature should also be noted. Additional to the GPS connect of to the system we used an extra GPS (Garmin TM serial number V 93120003) to determine the location more accurately.

DATE		HOUR		PLACE			
OPERATOR			GPS TYPE and #				
LATITUDE		LONGITUDE		ALTITUDE			
STATION TYPE		SENSOR TYPE					
STATION #		SENSOR #		DISK #			
FILE NAME				POINT #			
GAIN		SAMPL. FREQ      Hz		REC. DURATION      minutes/seconds			
WEATHER		WIND <input type="checkbox"/> none <input type="checkbox"/> weak (5m/s) <input type="checkbox"/> medium <input type="checkbox"/> strong		Measurement (if any): _____			
CONDITIONS		RAIN <input type="checkbox"/> none <input type="checkbox"/> weak <input type="checkbox"/> medium <input type="checkbox"/> strong		Measurement (if any): _____			
		Temperature (approx): _____		Remarks _____			
GROUND		<input type="checkbox"/> earth ( <input type="checkbox"/> hard <input type="checkbox"/> soft)		<input type="checkbox"/> gravel <input type="checkbox"/> sand <input type="checkbox"/> rock <input type="checkbox"/> grass = ( <input type="checkbox"/> short <input type="checkbox"/> tall)			
TYPE		<input type="checkbox"/> asphalt <input type="checkbox"/> cement <input type="checkbox"/> concrete <input type="checkbox"/> paved <input type="checkbox"/> other _____					
		<input type="checkbox"/> dry soil <input type="checkbox"/> wet soil		Remarks _____			
ARTIFICIAL GROUND-SENSOR COUPLING <input type="checkbox"/> no <input type="checkbox"/> yes, type _____							
BUILDING DENSITY <input type="checkbox"/> none <input type="checkbox"/> scattered <input type="checkbox"/> dense <input type="checkbox"/> other, type _____							
TRANSIENTS		MONOCHROMATIC NOISE SOURCES (factories, works, pumps, rivers...)					
		<input type="checkbox"/> no <input type="checkbox"/> yes, type _____					
		NEARBY STRUCTURES (trees, poles, buildings, bridges, underground structures...)					
		(description, height, distance)					
cars		trace	low	moderate	many	very dense	distance
trucks							
pedestrians							
other							
OBSERVATIONS				FREQUENCY: _____ Hz <small>(if computed in the field)</small>			

Figure 11.3 the field measurement sheet and the boxes where we write the name (local and PC), location, local time and GMT, instrument, environment, weather conditions, geology (either outcrop or borehole). From [SESAME H/V user Guidelines, 2005]

After we finish the measurements to for the day the data must be transferred from the pocket to a computer where all waveforms data put in WOR directory of the SEISAN



program. As soon as we finish we must recharge the battery of both instrument and laptop. Usually the instrument battery must have 13V voltage. We have to connect to its power supply to the station to its power supply to charge the battery and to make sure it has enough power fore the measurement. We have two batteries one working and another as extra on case the first one stops working.

The recording duration at each site was approximately 30 min.

### ***11.1.3 Data collection***

The dataset collected during the survey in west of the Khartoum city consists of 147 sites (see figure 11.4). The recording time duration have been done at each site approximated 30 minute length about 80% of total site. Other sites were made with duration10 minute. Figure 7, shows the location of these sites and the different geological units. The survey was made between 2<sup>ed</sup> of June and 13<sup>th</sup> of August 2006. All measurements were collected during the summer holiday. The average temperature was around 30<sup>0</sup> C. These two factors influenced the travel and change plan.

The measurements were done during the day and sometimes during the night. The distance between the sites was about 500m. Transportation of the equipment was a car used. Each day 10 to 20 sites were mentioned. In order to determine most accurately the y location of the site, we were used two GPS receivers one inside the system and another outside (Garmin TM serial number V 93120003). We used both of them to get the best location.

We started with measurements of the basement rock units at the northern part of the area and on the basement complex at the southwestern area. The first day we was made measurement recording on hard and sediment rock in order to test the instrument(see figure 11.1 and11.2).

West of Khartoum city– Geology and site location

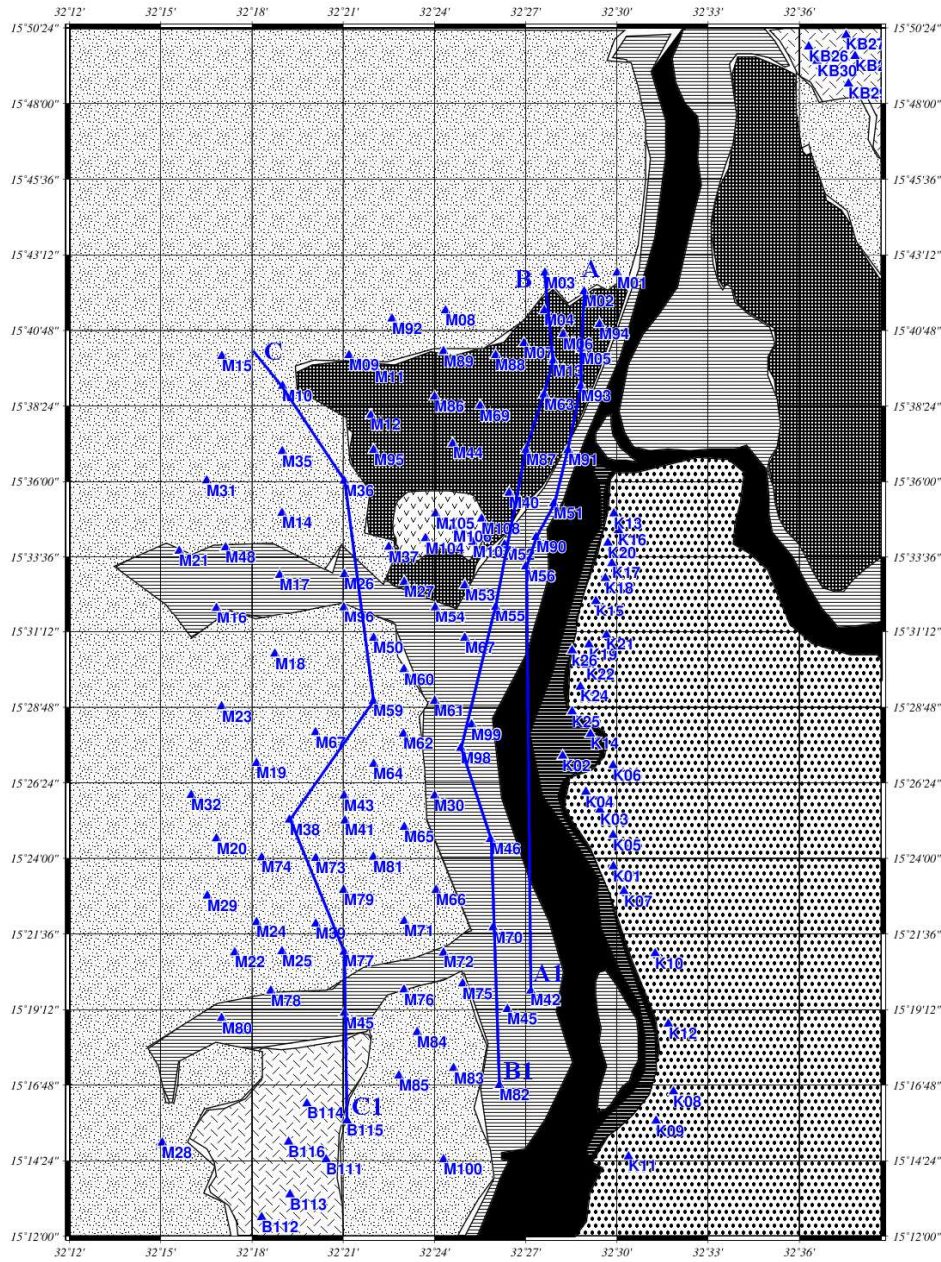
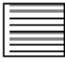

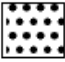
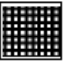
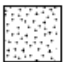





Figure 11.4- Geological map of the study area (West of the Khartoum) and locations of the sites - Blue triangle shows where the measurements were made and three sections crossing some of our measurements (A,B and C). The regions of interest with the geological formations are as follows;

- |   |   |   |  |
|---|---|---|--|
|  | Recent alluvial deposit with consolidated soil. |  | Recent alluvial with unconsolidated soil.        |
|  | Older alluvium.                                 |  | Gezira formation.                                |
|  | Sandstone cretaceous.                           |  | Basalt rock.                                     |
|  | Basement Complex rock.                          |  | Nile River, ; Modified from [GRAS 1988 and 2006] |

## 11.2 Weak motions recorded (local earthquake)

### 11.2.1 Data collection

About 22 earthquakes are shocked the area around Khartoum city for the period between October 1966 and March 2007. There are 12 events from the SSN in the located for the period November 2003 to March 2007. Three stations are placed around Khartoum city. Two of them are located on sediment layer named MRKH and JAWL and one station was located on hard-rock basement complex named SLAT. More information about these local events is given in (table 11.2) and the distributions of the stations and the events are shown in (Figure11.5). Among those events there are 7 earthquakes recorded by all stations while rest of events are recorded and located by one or two stations. In this study we used 6 events divided into two groups depending on there location and distance from the recording stations; the first group contains two earthquakes shown as number (10 and 6) and the second group contains events numbered 2, 3, 4 and 8. Another event is not considered because it is either too close to the stations 4, 9 and 5 or it was far from station but located only by one station such as 1, 12 and 11. Both of them were not good for this method as we need the event to be far from the station and to be recorded by at least two stations.

Table 11.2 Local events were recorded by SSN. Each event number is given in the right column of this liable and is the same as the number in the figure 11.5.

Event number	time	late	long	Depth (km)	Magnitude
1	20031105	15.864	33.598	10	2.9CSSN
2	20031114	15.374	31.688	22	2.8CSSN 3.0LSSN 2.9WSSN
3	20040112	15.424	31.677	15	2.5CSSN 2.5LSSN 2.7WSSN
4	20040214	15.750	31.448	10	2.5CSSN2.5LSSN 2.6WSSN
5	20040702	15.659	32.553	0	1.7LSSN 2.4WSSN
6	20040917	14.613	30.390	15	3.7C SSN3.2LSSN
7	20040321	15.396	32.370	4	2.0CSSN 1.9LSSN 1.8WSSN
8	20040516	15.004	32.225	5	2.4C SSN2.4LSSN 3.0WSSN
9	20060505	15.631	32.048	4	2.2C SSN2.2L SSN3.3WSSN
10	20060623	13.563	29.652	15	3.9CSSN 4.0LSSN 3.7WSSN
11	20060904	16.437	31.580	15	2.6CSSN 2.4LSSN
12	20070311	14.539	32.989	15	2.4C SSN2.5LSSN

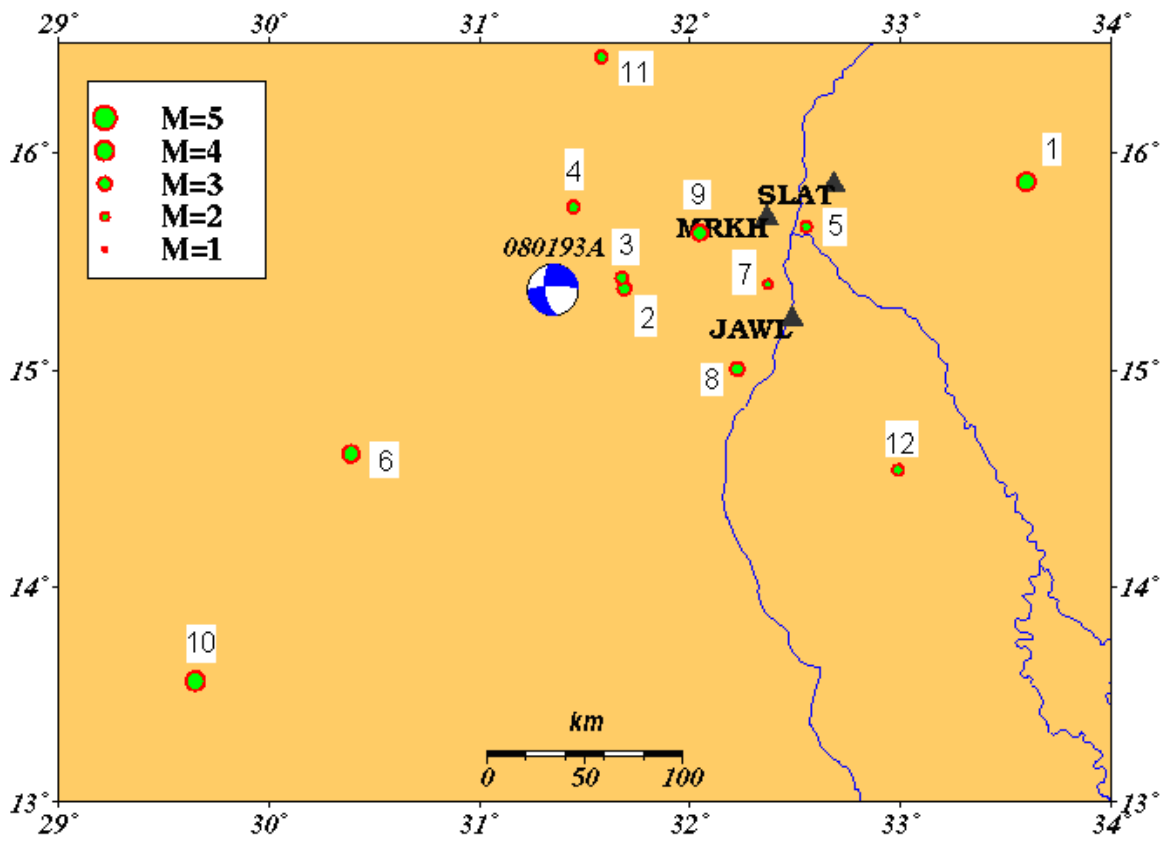


Figure 11.5 Local events around Khartoum region with station named MRKH, SLAT and JAWL. The number of each event is given in Table 7. The focal mechanism liable by 080193 shows earthquake in August 1993.

## Chapter 12

### Analysis of the Data and Results

#### 12.1 Analysis of H/V ratio from ambient noise record

##### 12.1.1 Analysis data recording (with SEISAN and JSESAME)

In order to determine the H/V ratio and fundamental site frequency from the noise recordings we must have Seisolog, Seisan and Jsesame software.

As we mentioned before with Seislog software we recorded data from the instrument into the database folder. With this software we adjusted of recordings site name, duration triggering parameters (STA and LTA, lower and upper band), and also check the recording the screen. However, once all data are in WOR directories in part of SEISAN software. The SEISAN is the earthquake analysis software [*Havskov, and Ottemöller 2005*]. The SEISAN seismic analysis system has many programs to analyze earthquake data both data digital or analog. This software can be installed into the SUN, LINUX and Windows operator systems. We used two programs from SEISAN, DIRF and WAVETOOL. The DIRF program is a used make a file with a numbered list of events named `filenr.lis`. When working with many waveform files with long names, a DIRF is first run, and programs used latter get the file names from the `filenr.lis` file.

WAVETOOL is a program used to convert into different data format. We used this program to convert our data from SEISAN format in to GSE format. Since this format is used by the J-Sesame software. We checked this convert was done will we show the code of format at end to the files.

JSESAME – H/V processing software [*Atakan, et al 2004*] is the software used to process and calculate the H/V ratio from the records of ambient seismic noise. Information for the software could be found in [*Guideline for the implementation of the H/V spectral ratio technique on ambient vibrations SESAME European research project WP12- Deliverable D23.12, Atakan et al 2004*].

The Jsesame software consists of four basic modules, browsing module, window selection, processing module and display module.

We use the manual insert site from the screen menu to create the site name, the measurements are displayed a subfolder. In these subfolders we insert our data file which is the seismic noise waveform files recorded at the site. All these waveform files have to be in GSE format.

When we selected the folder of the corresponding point we inserted the noise record by checking on insert data file on screen menu. Then we went to the director where files have waveforms with GES format only. Once the files have been inserted we were able to plot the seismic noise record one by one. We could also perform different operations on the waveform file such as filtering, windows selection and processing.

In window selection module we could select time windows from the recorded trace with different length either manually or automatically (we can find this option in config in menu screen). If we used both options we must make sure that they only record the most stationary parts of the ambient noise, since the recording can contain transients pulse from specific sources such as traffic, heavy machineries or other sources giving extra waves. The best way to avoid these extra waves is by manual selection. But this option takes time and it is not appropriate for processing large amounts of data.

The automatic window selection algorithm is based on the principle of (STA/LTA) triggering (short term average / long term average) [Havskov and Algvacil 2004]. We followed the simple explanation given by [Kandilarov 2005] which was taken originally from [Havskov and Algvacil 2004]. The principle of it is algorithm method. It averages the signal level over one short and one long time windows. The long time window is representative of the average level of noise. When and where a signal with amplitude is over the average noise level, the short time average (STA) is calculated from the short time window. (STA) will change faster than the long term average (LTA); thus the algorithm can distinguish parts of the signal different from the ambient noise and exclude them from the H/V spectral calculations. There are two thresholds for the (STA/LTA) ratio, upper and lower. Since we would like the ratio to remain below some predefined value usually (1.5- 2) so that there are no energetic

transient in our selected windows. We define an upper threshold, if there is a signal over that threshold, the program will not compute an H/V spectrum for the corresponding time window. We want to avoid abnormally small amplitude that why we must define a lower threshold and we want the signal to drop below that lower threshold, so the corresponding window will not be selected by the algorithm. In order to avoid signal saturation we exclude signals with amplitude above 99.5% of maximum observed amplitude in our noise records.

Optionally we may exclude long term transients which will not affect the (STA/LTA) ratio but will not represent for the true seismic noise. Once a window is selected the algorithm looks for the next window until it covers all recording.

The processing models perform the operation of filtering, removal of the DC component, smoothing spectral computation, and computation of H/V ratio. We used this module in two operations; a filter to calculate how many windows are selected, H/V ratio in order to plot and defined the H/V ratio corresponding to fundamental frequency. The parameter we used to select windows in Jsesame software given in table12.1.

*Table 12.1– parameter we used to select windows in Jsesame software*

Window	
Window length (sec)	10.0
Space between windows(negative for overlapping (sec)	1.0
Windows selection parameter	
Window length for the short term STA in (sec)	1.0
Window length for the long term LTA in (sec)	25.0
Minimum level for STA/LTA in (sec)	0.5
Maximum level for STA/LTA threshold	2.0
Window length for selected window in sec	10-20
Overlap percentage for selected windows	10.0
Level for bad points sec	0.0

The display of the output of the H/V spectra ratio when we used the 10 seconds windows length was clearer than with 20 seconds. An example of that is given in

Figures 12.1, 12.2 and 12.3. We could see on the screen the manual operated options, and the display of the output. In the view output H/V ratio curves are shows the mean in black, mean multiplied and divided by  $10^{\sigma(\log H/V)}$  in red and blue colour. The pink strip shows the frequency range where the data has no significance, due to the sampling rate and the window length. The grey strip represents the mean of the  $f_0$  plus and minus the standard deviation. It is calculated from the  $f_0$  of each individual window. We could also see the spectrum at each horizontal component NS/SV ratio and EW/SV ratio separated.

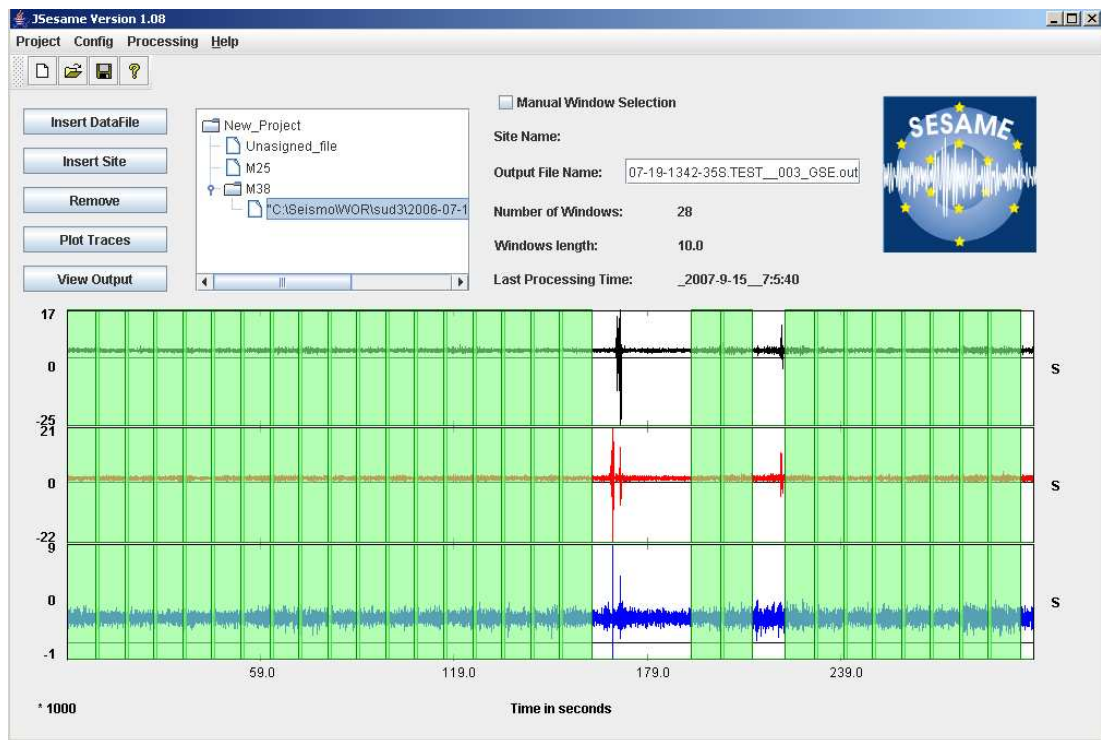


Figure 12.1 General view of graphical user interface of JSESAME, taken from our data processing. We could see the graphical use where different operations can be performed. Selected windows are shown in green, tracing of three component of seismic noise recording, number of windows that have been selected by automatic windows selection, algorithm with window length and structure of organization data.



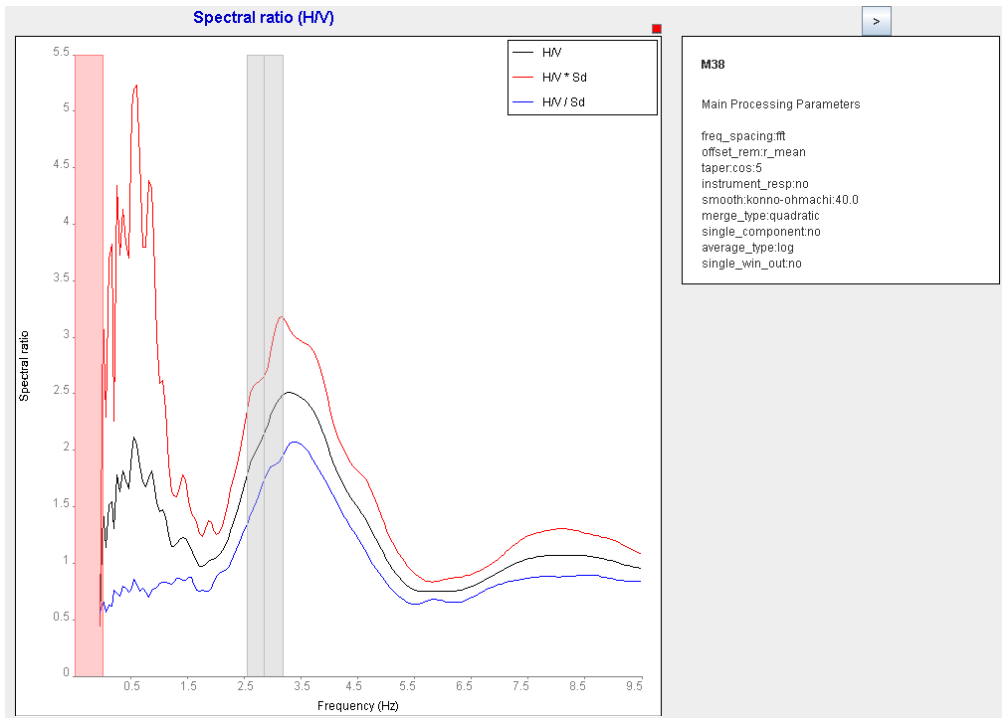


Figure12.2 H/V ratio for the merged horizontal components (mean in black, mean multiplied and divided by  $10^{\sigma(\log H/V)}$  in red and blue). The pink strip shows the frequency range where the data has no significance, due to the sampling rate and the window length. The grey strip represents the mean  $f_0$ , plus and minus the standard deviation. It is calculated from the  $f_0$  of each individual window

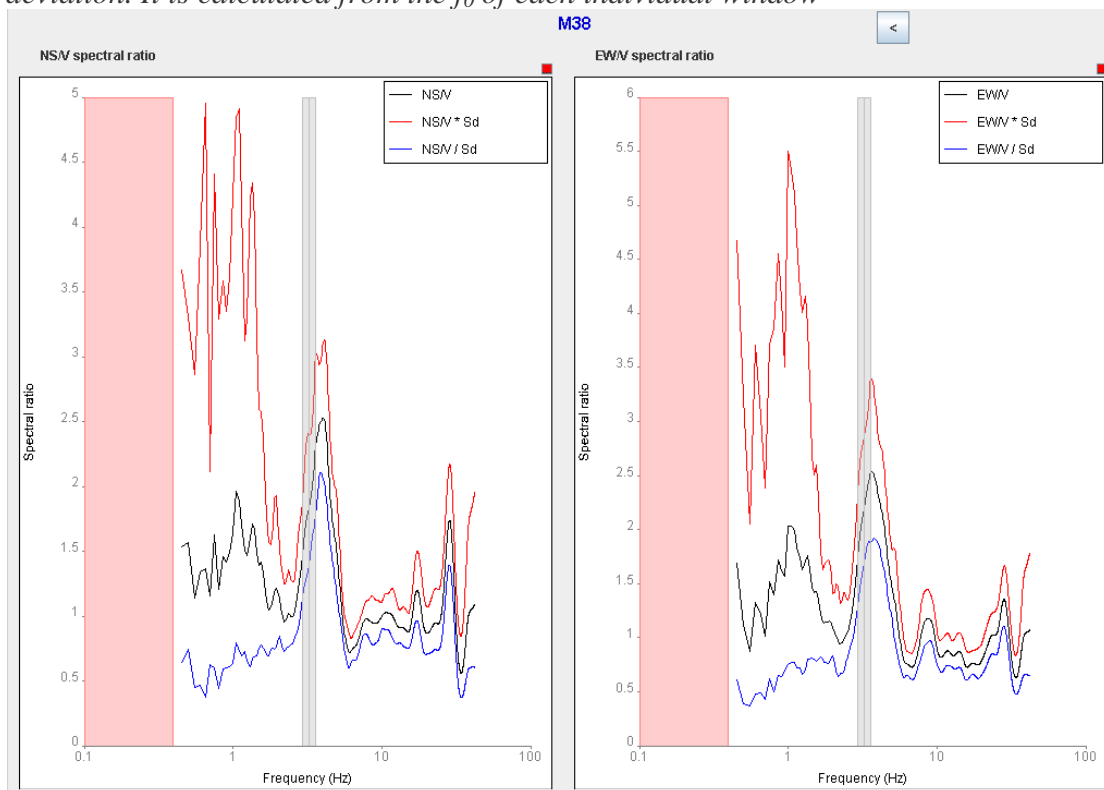


Figure12.3 NS/SV and EW/SV are show in individual horizontal components with vertical.

### ***12.1.2 Result of H/V ratio***

The results of our survey were two maps showing the distribution of frequency and amplification factor for each site. To interpret the site response spectra computed from our survey result. We followed the guidelines available from SESAE project [Atakan et al 2004] to discuss three major factors, windows selected, reliability of the H/V ratio spectra and interpretation of H/V ratio in term of the site characteristic.

#### **Windows selected**

Windows selected is an important factor by which we can evaluate the data collected, since the survey consisted of measuring and recording the ambient seismic noise in urban area and obtaining information about the local site conditions observed. It was observed during survey that conditions were similar in different sites (geological conditions, building density, industrial noise, traffic, and mechanics). In addition to that we also observed within different windows length has similar information in one geological unit, and in one site we had two different number windows length which display different H/V ratio spectra. This is due to factors we mentioned before in chapter five, such as time duration for recording of data, geological similarity of some sites with variation in noise they transmitted, and number of windows selected could affect data quality. All these observations led to categorisation of windows selected from database in term of windows length into two groups.

Figure 12.4 and 12.5 shows two bar diagrams of the number of selected windows per point for the dataset collected in study area with 20 and 10 second length windows respectively. Most of the sites made recording in 30 minute for 88% of all dataset while the rest points in 10 minutes. Therefore, to estimate the average of windows selected in two diagrams we considered the 30 minute recording. However, as we shown from the two diagrams there are different of numbers of windows selected. The number of windows with 10 seconds length is higher than the one with 20 seconds length. We calculated the average of number of windows per point for data collected with 10 seconds length and it was 22, which was three times the average number of windows with 20 second length. This may be due to the fact that most of sites records were made in study area where located on sedimentary formations which generated more noise.

We may conclude that since the average number of selected windows per point in sedimentary formation is higher than in hard rock (basement rock and consolidation sandstone), the quality of data collected in general is good. According to SESAME guidelines and other previous studies; for a reliable computation of site response spectrum we need to have above 10 windows 20 second each [Atakan, et al 2004]. Since the 10 second length windows is recognizing a wide range of recordings (30 to 2 minutes), and as we shown the average number of windows for dataset is higher than what is needed, for these reasons we believe in our results to interpret the site response spectrum for dataset with length of windows 10 seconds.

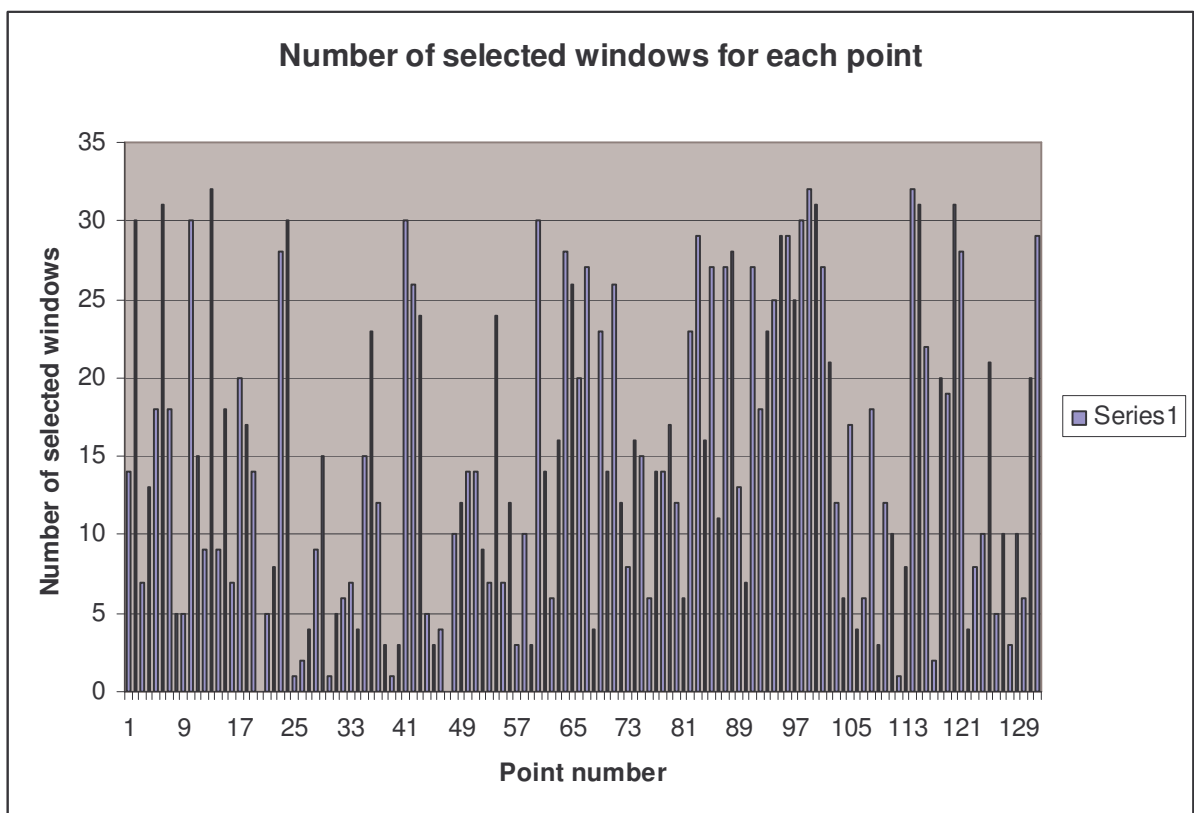


Figure 12.4 13 -Bar diagram showing the number of selected windows for each point for dataset from dataset with 10 second length windows.

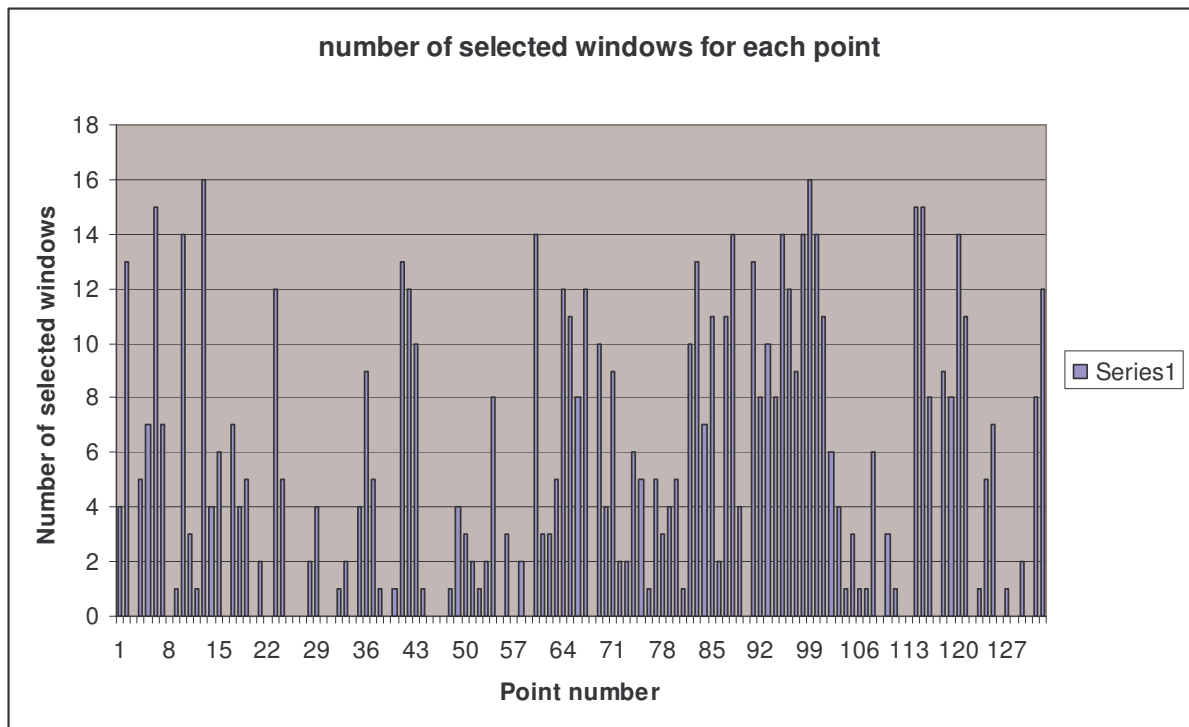


Figure 12.5. Bar diagram showing the number of selected windows for each point from dataset with 20 second length of windows.

### Reliability of H/ V ratio spectra (peak observation)

To establish our interpretation of the site response spectrum we must considering the peak of spectra represented in result of dataset. We observed variation of the behaviour peak in our data spectrum. It is easy to interpreted spectrum we used the available information for noise condition as the site measurement and geological observation (borehole data, and outcrop).

We classification of the spectra computed from the data collected could be classified in three groups follows;

- 1- Site response spectra with a single clear peak.
- 2- Site response with more than one peak.
- 3- Site response having not clear peak.

#### 1- Site response spectra with a single clear peak

The majorities of site response having clear peak single from our dataset is two types; one is peak at low frequency and another one with high frequency. The first one the peak represent at frequency range 5- 0.8 Hz, example for that shown the spectrum

computed from point M38 and M90 are given in figure 15 and 16. The interpretations for these points are easy. We considering the high peak give the fundamental frequency which that is corresponding of amplification factor. This peak reflects due the have sharp between two layers under the point. The fact that the site has peak single in the low frequencies range, which is expected only for the sites overlying thick sediments. We can see these two examples have opposite in the frequencies and amplification, that the one has low frequency with high amplifications.

The second type observed has clear peak with high frequency, this peak as mentioned before in analysis data section is not represent the really site response. We believe these points have thinning of sedimentary layer under the point or may influenced of the high noise generated waves nearby point. That could be happen at points where located in central study area which the area is quarry site. Or may the influenced of method itself which it is building measure the site with have two layer with different contrast. Also these points mainly located on the hard rock (basement complex rock) Example of that given in figure 5.3 which it computed from the point M112.

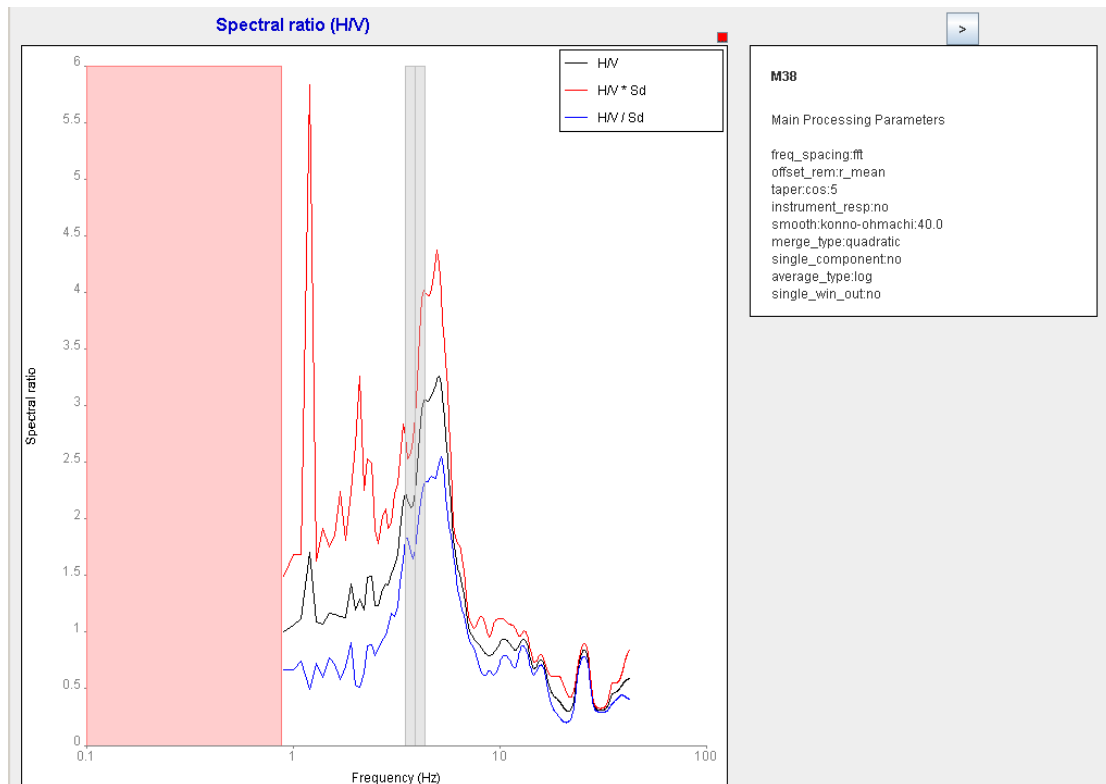


Figure12.6 15. Clear peak single spectrum computed at point M38, it seem the spectrum has one small peak in being, but when we compare to the clean peak around 3 Hz it smaller, we interpret as the high frequency is more common reflected in this point.

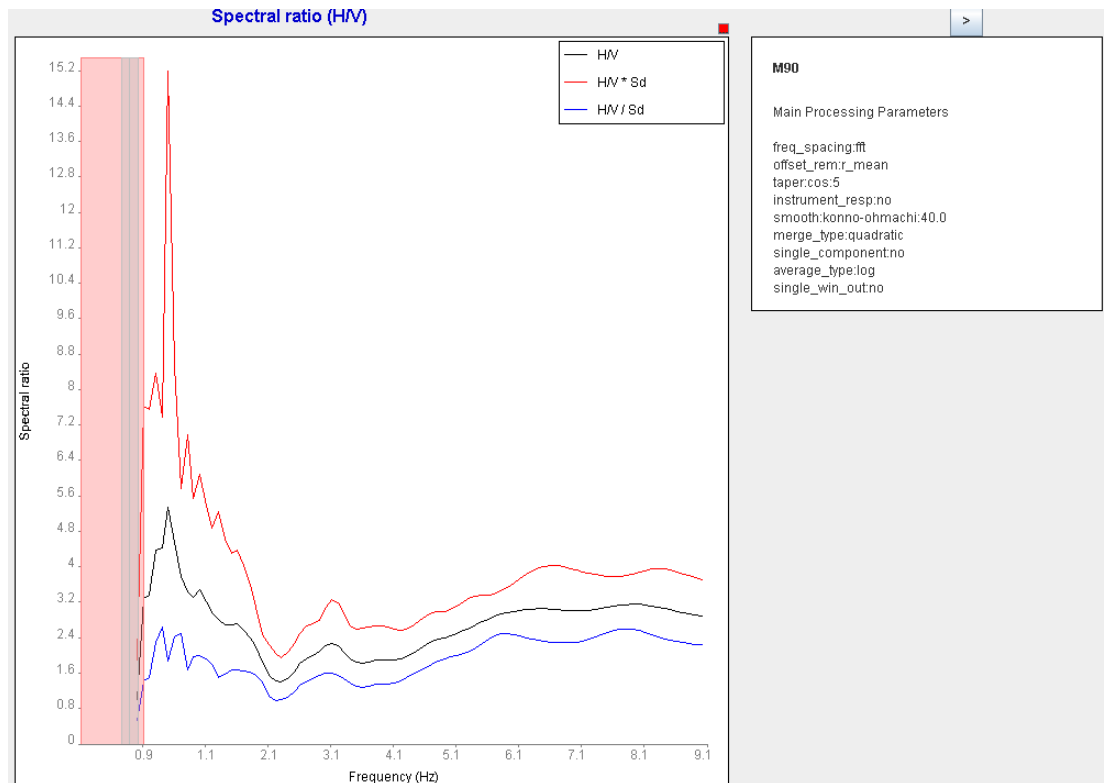


Figure 12.7 16. Clear peak single spectrum computed at point M 90, we could see the clear peak around 1 Hz.

## 2- Site response with more than one peak.

Most of the site response spectrums in our data collection have more than one peak. They are representing at frequencies range 1 to 22 Hz. We interpreted these points by two; one way is from previous work that the peak at high frequencies does not have meaning if the points are occurring on sediment site. Another way is interpreted as first peak in spectra that after check the two horizontal component (EW and NS) spectra separately (see figure 12.9). We chose the peak that it is represented in one horizontal component spectra. If it is not we chose the first one. The reason for that the site response spectrum of that point has reflected more than one different boundary layers under this point. In order to estimate the site response by this method we must have at least two underlying media with different acoustic properties. Another reason could be the presence of seismic noise is come from industrial origin. Figure 12.8 shows example of site response spectrum has more than one peak we could see spectra computed from point kh21.

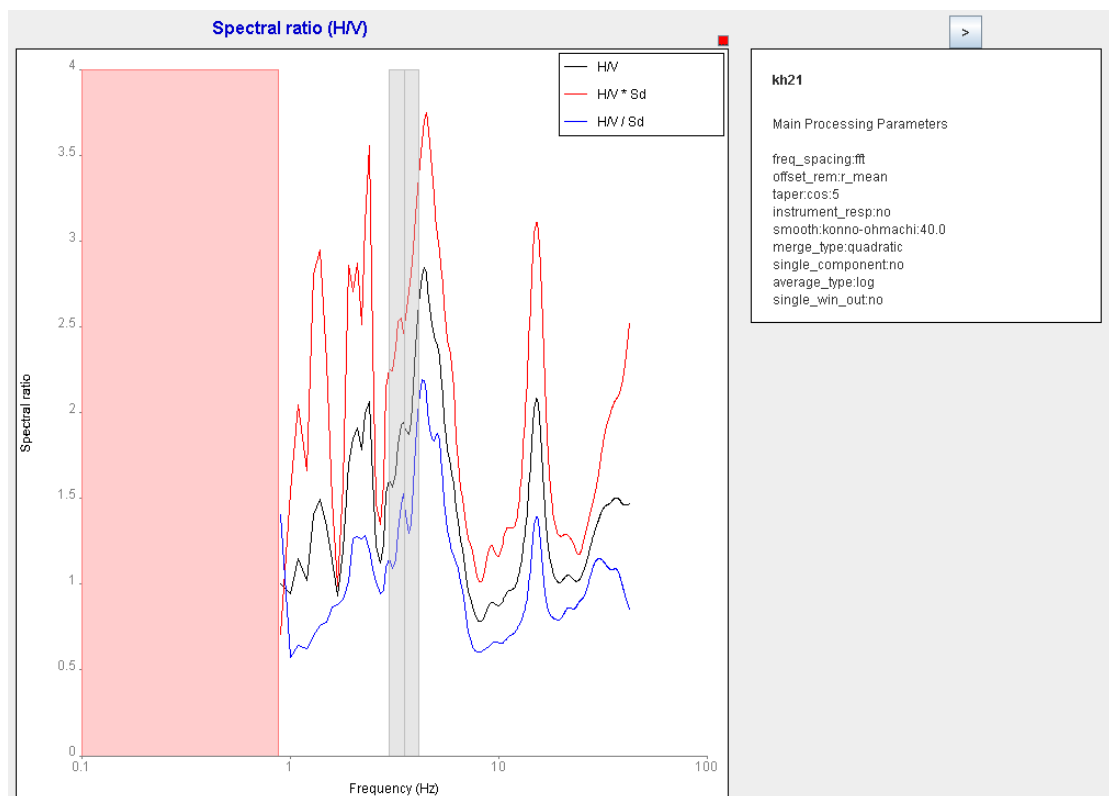


Figure12.8. site response spectrum at point kh27- two distinct peak is visible. There are several such spectra on our dataset from eastern site of while Nile river. We think that possible explanation could be the presence of some underlying structure that is elongated predominantly in one direction and another explanation could be the presence of seismic of industrial origin.

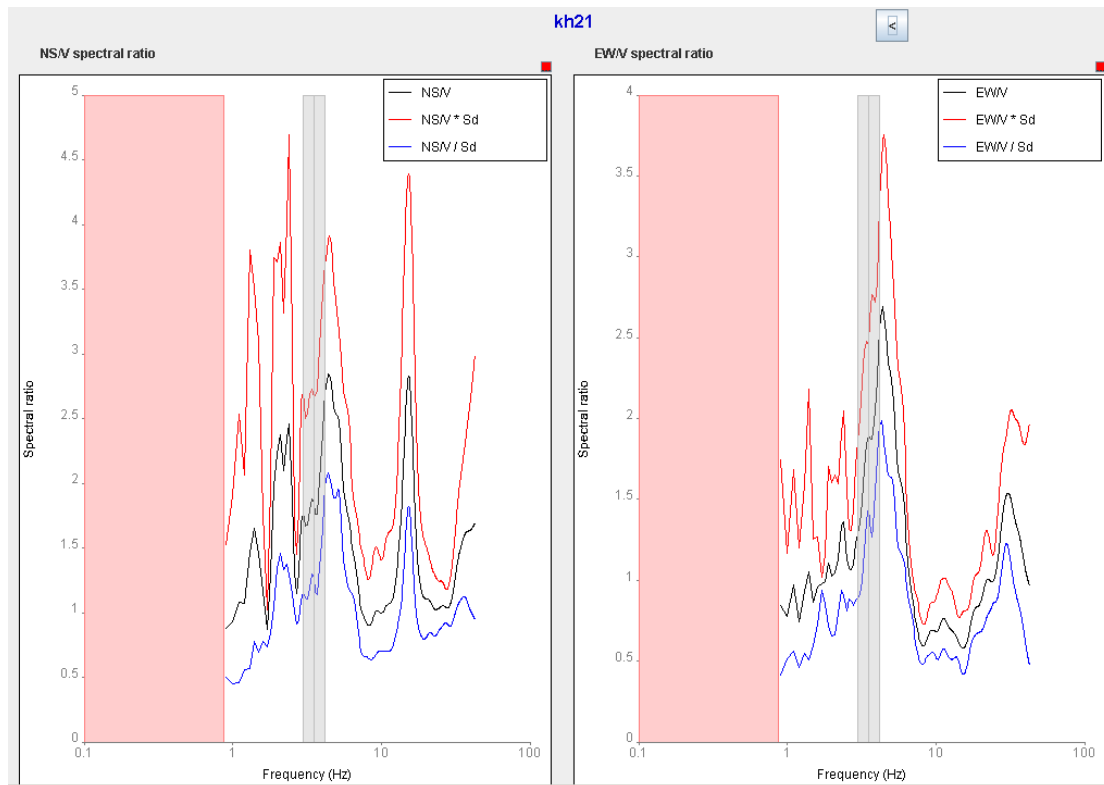


Figure 12.9. NS/SV and EW/SV ratio of the site response spectrum computed from point kh21. As we could see there is substantial difference between the two components. The peak around 3 Hz is visible on the both components while the one at around 12 Hz is seen less amplitude in EW component. Most likely the structure is elongated predominately in NS direction.

### 3- Site response spectra having no clear peak or extensive shape.

There is most of this type with many peaks which is difficult to distinguish between these peaks in our dataset. It is difficult when we have the same shape in NS and EW components either in amplitude or in frequency. The reason for that is the area under that point is more complex or some wave exist the recording from human activity. We interpreted these points by correlation the borehole data nearby measurement site. Figure 12.10 and 12.11 shows the example for this case computed from the point M66.



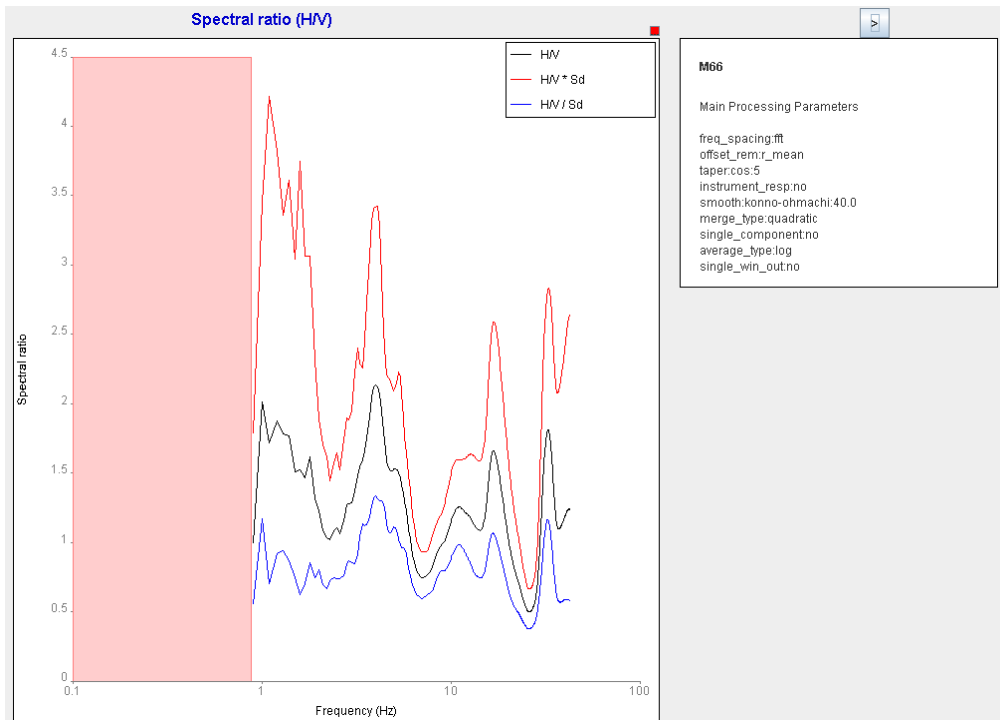


Figure 12.10. Site response spectrum at point M66 – as it can be seen its shape is very complex and no clear can be distinguished.

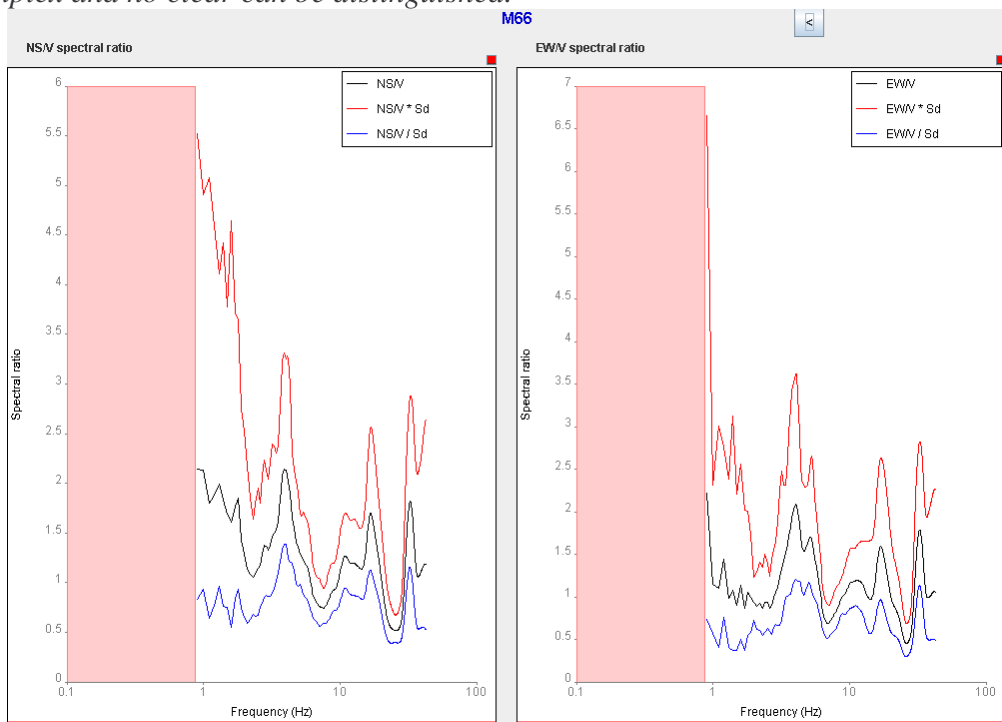


Figure 12.11. The EW/SZ and NS/SZ site response spectrum ratio at point M66. The two components are different and spectrum is difficult to interpret; the point may be occur above some very complex underground structure or close to a source of seismic noise of industrial origin.

For all these above which produce different response even in one unite or rock. We summers cases as concept of this method. We believe that the clear high frequency

peaks observe at the site M114, Kh 29 and M106 as example of anomalies with high frequency overlying hard rocks (basalt and granite) which expected have amplitude around 1, but this concept is not allows had in these areas, may be due to some thin sedimentary layer between the sensor and the rocks that can account for the high frequency. According to Reiter, (1990) observe the proportional between the thickness of the sediment ( $H$ ) and S- wave velocity ( $\beta$ ) in the layer. It is gives the fundamental frequency ( $f$ ) as following the eq 6;

$$f = \frac{\beta}{4H} \quad (6)$$

Eq 6, we can calculate the value of fundamental frequency approximately, where the  $H$  is thickness of the topmost layer and  $\beta$  is velocity of that layer. As we seen if we have big thickness of sediment we expected have low fundamental frequency. When we applied this equation in our study area as we have decrease the thickness of the sediment to word the basement rock at the north eastern or in south western at some place it is fit. Also we can see clear this gradually through the basalt area around point M105, M107 and sandstone at point M40 and into M51 which is increasing the thickness of sedimentary layer. But at the most of our measurements are not fit. That due to two reasons; one is sedimentary layers have different thickness and with also different of consolidation degree. Second is influenced the method itself the computed amplification at some frequency as the site has high fundamental frequency with low amplification is not work well because the influenced the waves and reliability of computed is suspected [Nakamura 2000]. We will describe these variation in next chapters.

### ***12.1.3 Classification of the spectra computed from the dataset collected in study area***

The site response spectra computed from the data collection from study area could be classified in two major different groups each one has subgroup as follows;

- 1- Site response spectra at site of overlying Basement Complex.
- 2- Site response spectra at sites of overlying sedimentary rock

We will describe these two groups with subgroup; we will follow the classical as depending of formation age;

### *Group 1, Site response at site of overlying Basement complex*

The measurements of sites of overlying hard rock have been done at three different locations

#### 1- Site response at Omdurman Basement Complex site

The location of measurements were recording located at southern study with Cambrian granite rock outcrop where close to Awillia Dam. The spectra calculate at these points were different from site to another. The average of amplitude of these points is given in figure A1 around 1.51. Some of them are given flat spectra with H/V ratio of amplitude around 1.5 and another flat with a peak around 2.5 to 4, which are associated with high frequencies. Examples of site response with flat spectra are given in (figure 12.12 and figure 12.13) computed at point M111 and M112. The flat spectra with high frequency peak are shown in (figure 12.13 and 12.14) computed at point M114 and M116.

Since the measurements at recording on Basement sites that should be expected have amplification around 1. For our result this case is not found clear such as point M114, 115 and 116 where the average is 1.5, while at point M111 it is 1.2 or close to what expected.

Since all points are given high amplification that expected this may given by three reasons are;

- Since some of these points are located close to Awillia Dam which is generated high noise one may explanation of the higher average amplification.
- Topographic site effects,
- During the measurement place are current of air higher which probably make extra noise. And the duration time of the recording is short which is not enough can reduces the noise.

we concluded that could be wrong because the method itself is based on estimation of a transfer function between bedrock overlain by a layer with different acoustic properties not in one unite of rock. For this reason and reasons have been happen in field can tell us this method cannot useful to estimate the amplification.

#### 2- Site response of site on Khartoum Basement area

The measurements have been done are located in two different type of rocks, Proterozoic or early Palaeozoic granite with Dolerite dyke close to Silate area and granite close to Sabaloka igneous complex. The spectra calculated at site are shown different spectra. The average amplification of all these sites closes to 1.5. There are two sites with flat response was computed at point Kh30 and kh27 with amplitude 1.2 and 1.3 respectively. Which they are close one what we expected (see figure 12.5 and figure 12.16). On point kh29 located not far from Kh30 has site spectra with peak amplitude around 1.4 (see figure 12.16). This peak may represent by high noise close to measurement place. Other sites were calculated site spectra with high amplitude between 2 to 3, examples Kh28.

Our results of site response spectra are shown the same behaviour as Omdurman site. Which they are again given uncorrected factor of what is should be expected amplification in hard rock. The one explanation it that additional of the reason we mention before in Omdurman case there are high noise generated by Aljayli Oil refinery.

### 3- Site response spectra at site overlying volcanic basalt

Basalt rock sites are located in middle of the study area sitting as intrusion rock. For this case we will discuss the site response of these sites as hard rock. The propos for these measurements is to evaluate how the stable of intrusion rock and in order to compare between Basement and sedimentary spectra rock. The average of the amplification from the site response spectra is computed around 1.3. Most of these sites are representing two different types of site response spectra but all have peak amplitude with higher frequencies. Example for type with flat spectra, peak amplitude and with peak only is shown in (figure 12.18 and figure12.19) computed at point M106 and M104 respectively. Since the area are using as mining (inquiry) may be the reason why have this peak in spectra. Instate of amplification spectra in hard rock may be considering as good result. Since though the points M107, M106 and M105 as similar to what can respected in hard response see appendix.

### *Group 2, Site response spectra at sites of overlying sedimentary rock*

Since many part of our measurement have been done at site located on different type of sedimentary rock. We could classification into five subgroups as following to the age and characteristic of type of rock. We will discuss site response of each one separately;

#### 1- Site response spectra at site overlying by sandstone in Omdurman site

The majority of site response spectra computed from data collection from the Omdurman area have distinct clear peak in frequency rang 0.99 to 10 Hz with amplification around 3 to 5. Among these sites response they are two kinds of spectra either with peak amplitude only close to 1 Hz and another with two peaks or more with high frequencies. Examples of these variations of spectra are shown in (figure 12.20, 12.21, 12.22, 12.23 and 12.24) computed at point M38, M18, M11, M73 and M44 respectively. The one explanation of this variation is that due to reflect of unconsolidated sedimentary underline the surface, or Since our measurements have been done on consolidated sandstone and another site on contraction with consolidated sandstone that can given the reason of variations of peak amplitude. It is expected that the spectra calculated at site located on hard rock should have less amplitude. This case we can recognize through some points such as M44 and M38. While the site responses with contraction with consolidated sandstone are represent higher amplification.

#### 2- Site response spectrum spectra at site overlying Gazira formation in Omdurman area

Since part our measurements have been made at north of basalt site are located on especially geological. The common of sites response spectra computed from the data collection from these sites have more than one peak of amplitude with average amplification around 3. Examples of spectra are shown in (figure 12.25 and 12.26 ) computed at M13 and M65 respectively.

For the amplification around 3 with frequency 2.5 Hz and with more than one peak amplitude, these factors are given scientifically issue in area study. It is the similar spectra what we expected since the area cover by thinning layer

sandstone underline by clay layers, thus tell the variation of these peak in one site response spectra more reliability result.

### 3- Site response spectra at site overlying older alluvium deposit in Khartoum area.

Site response spectrum calculated from collection dataset from Khartoum area are cover by clay underline the cretaceous sandstone have spectra clear peak with frequency around 3. Several such spectra are given in figure 5.18, 5.19 and 5.21 computed at point kh7, kh16 and kh21 respectively. All most sites have site response spectra with amplification around 2.2 but they have different peak of amplification, sine the area has underline unconsolidated sedimentary could be the reason why they have several peaks of amplitude.

### 4- Site response spectra at site overlying recent alluvial in Omdurman site

Most our measurements have been done at recent alluvial sandstone –clay with consolidate rock. Most for these sites are represented different site response spectra either with high or low amplification but both of them have low frequency rang 0.599 to 0.899 Hz. The relation between amplification and frequency it seem reverse proportional. Example of site response given high and low frequency shown in (figure 12.30 and 12.31) computed at point M77 and M93 respectively. About more formation about this relation see appendix. It is expected, that at deep contrast between unconsolidated and consolidated sandstone may given these spectra with lower frequency and high amplification. However, it seem some site response are different as what we expected (high frequency with low amplification) that could be due to interaction hard consolidate layer underline. Furthermore, the significant of these spectra have a few small peaks which could be the behavior of alluvial deposit along the bank of the Nile. Some sandstone layers high consolidate found interline these alluvial sites also can give these different of spectra.

### 5- Site response spectrum at recent alluvial in Khartoum site

Close at east bank of the Nile where deposits of sedimentary has large area. Since Our measurement have been taken place at these area. The majority of site response spectrum shown low frequency with high amplification as such given in (figure 12.32 and 12.33) computed at point kh15 andkh12

respectively. At south of Khartoum area close Nile shown this amplification are increase toward as following to increasing the thickness of alluvial deposit.

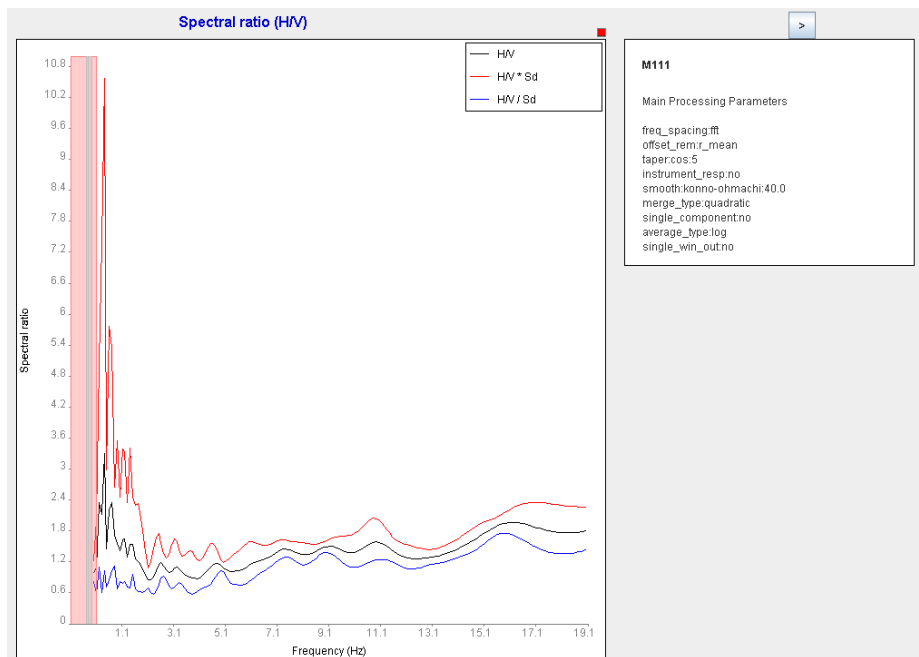


Figure12.12, The spectrum calculated at point M111.it can see the flat site response from overlying rock, the average amplification is 1.5.

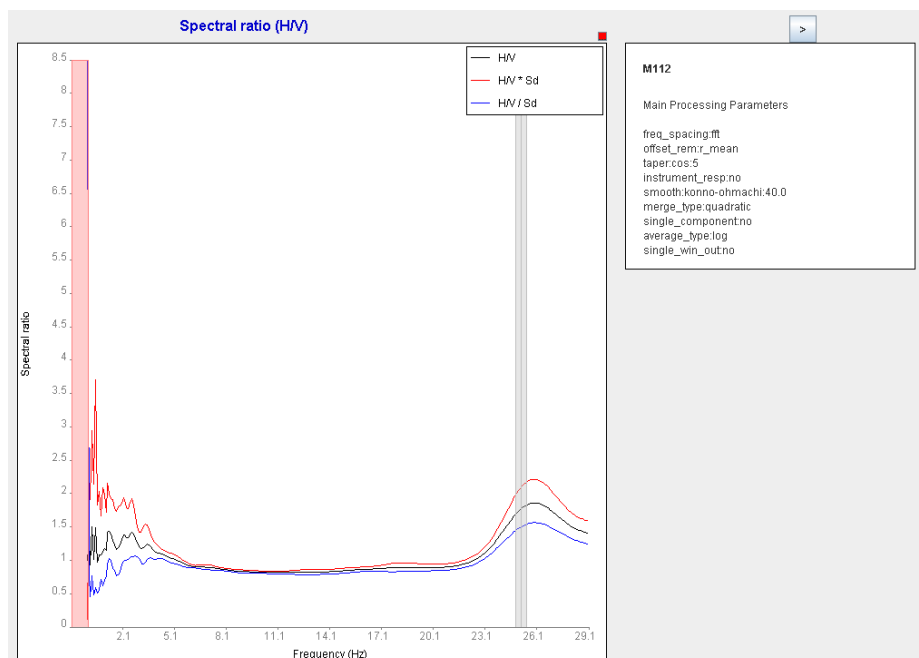


Figure12.12. flat site spectrum computed at point M112 from Omdurman Basement Complex site. The average amplification is around 1.3 or as expected around 1.

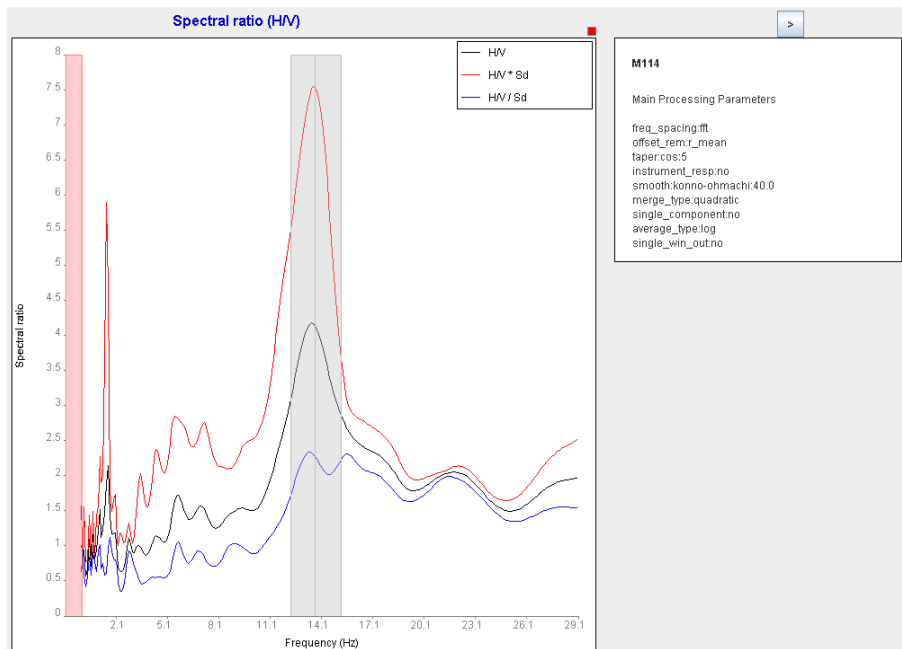


Figure 12.1, site response spectrum at point M114, it is located on Basement rock which clear peak. This peak has specific seismic noise of industrial origin.

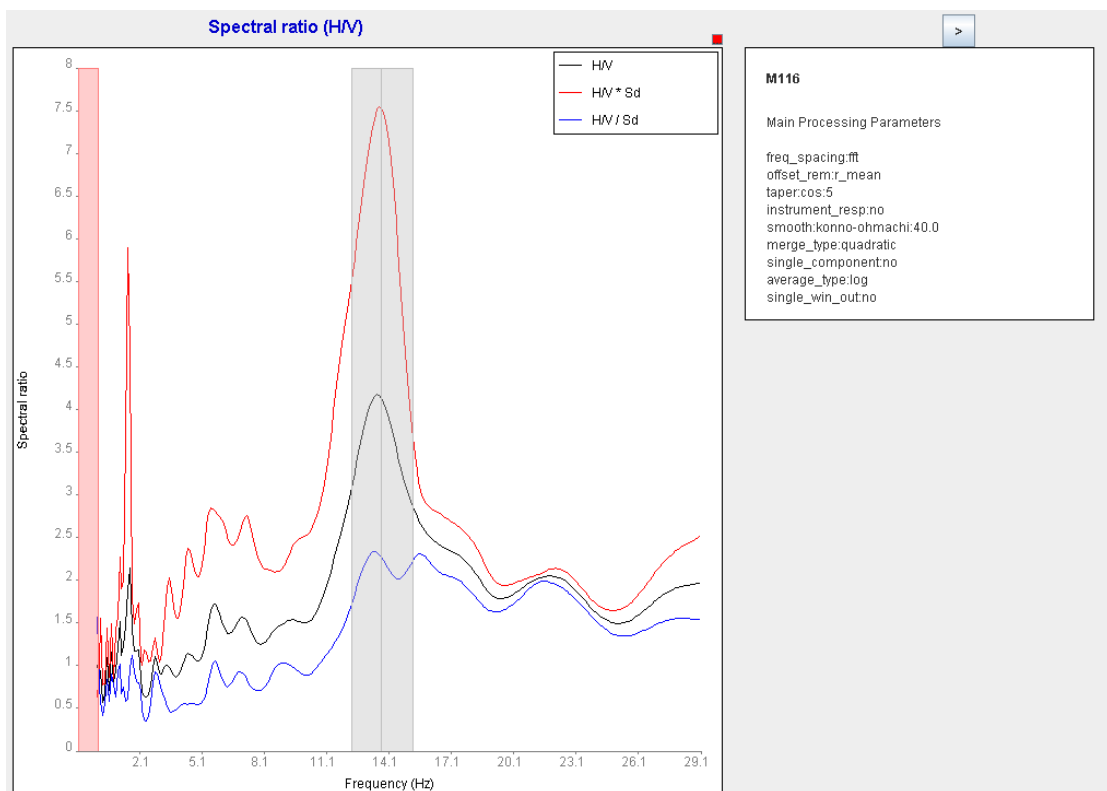


Figure 12.14, flat spectrum with peak calculated at point M116. It seen the average of amplitude is 1.5. Here the peak may make by high seismic noise since the site close to Awillia Dam.



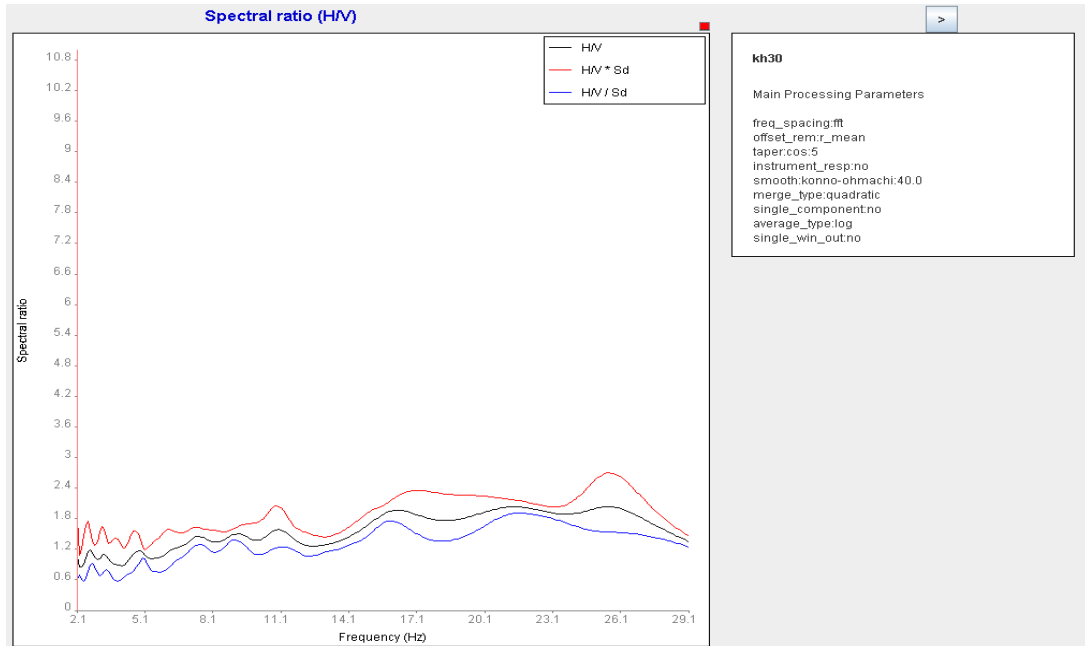


Figure12.15, site response spectrum at point Kh30. It is seem the flat response with the amplification is 1.4.

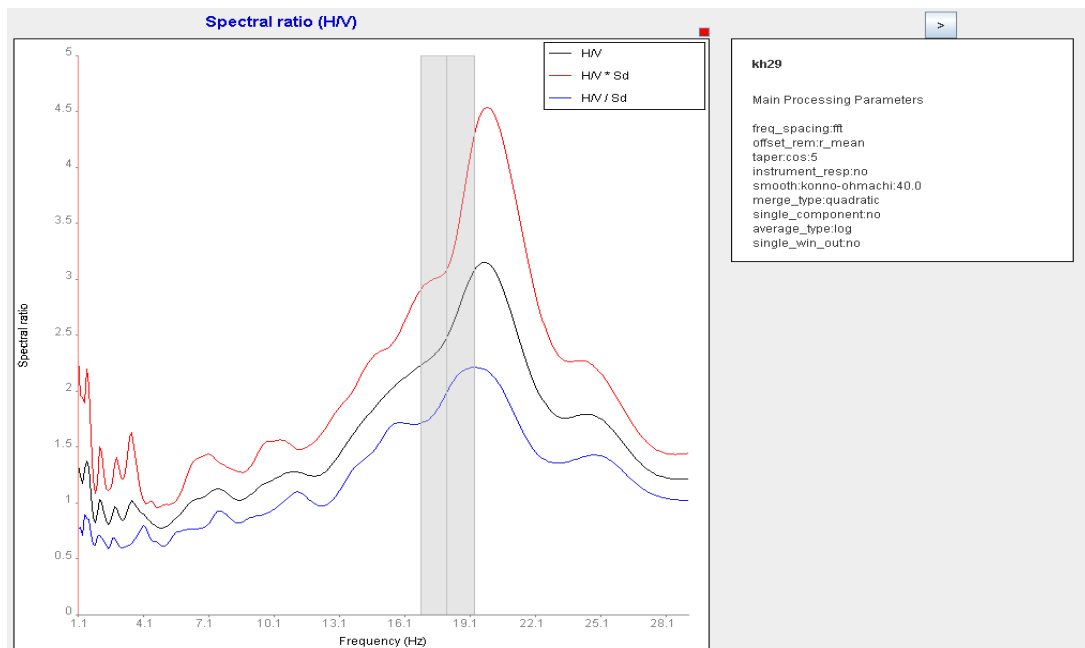


Figure12.16, site response spectrum at point kh29. It is seem the amplification around 1. The peak here may represent by high noise close the measurement area.

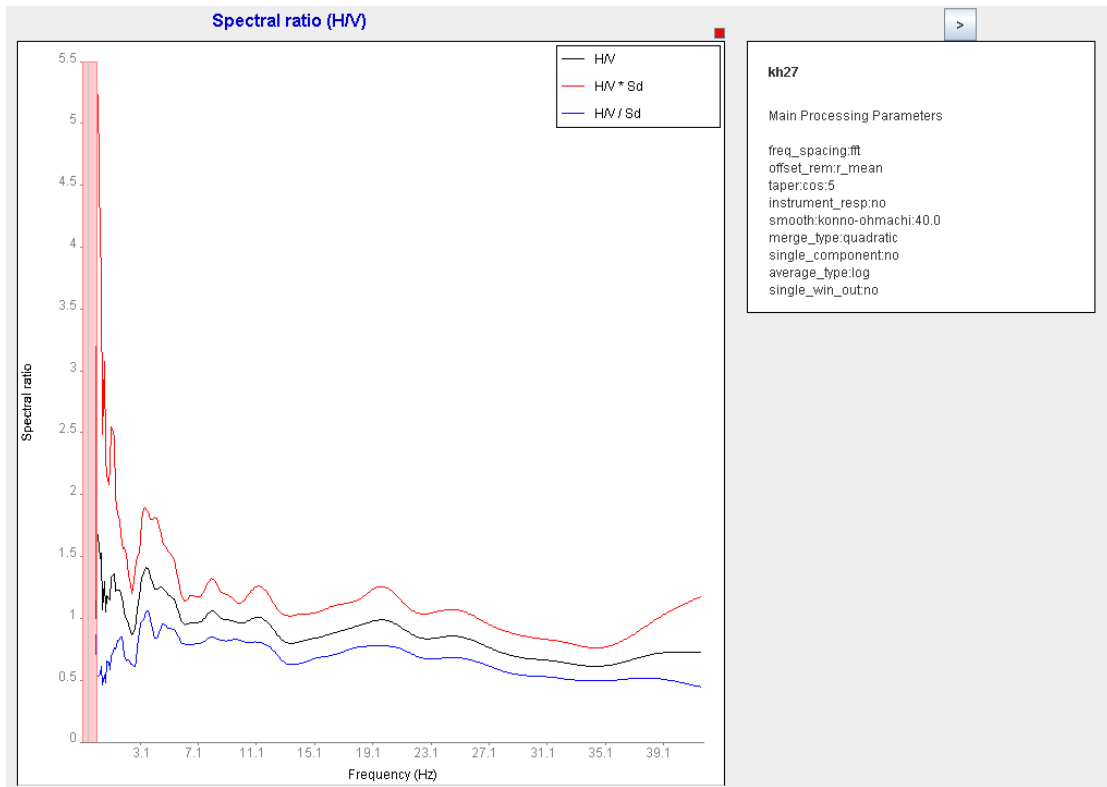


Figure12.17, site response spectrum at point Kh27. It is seem the flat response with the amplification is 1.2.

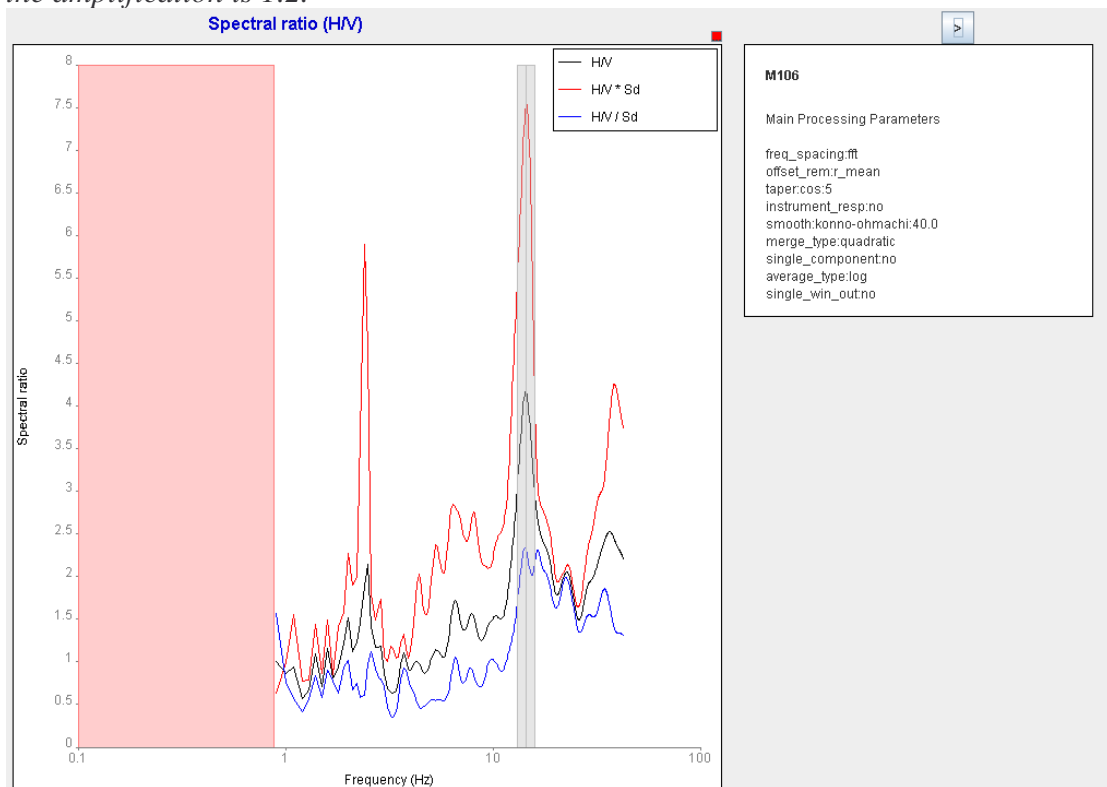


Figure12.18, site response spectrum at point M106. It is seem the flat response with the amplification is 1.1.

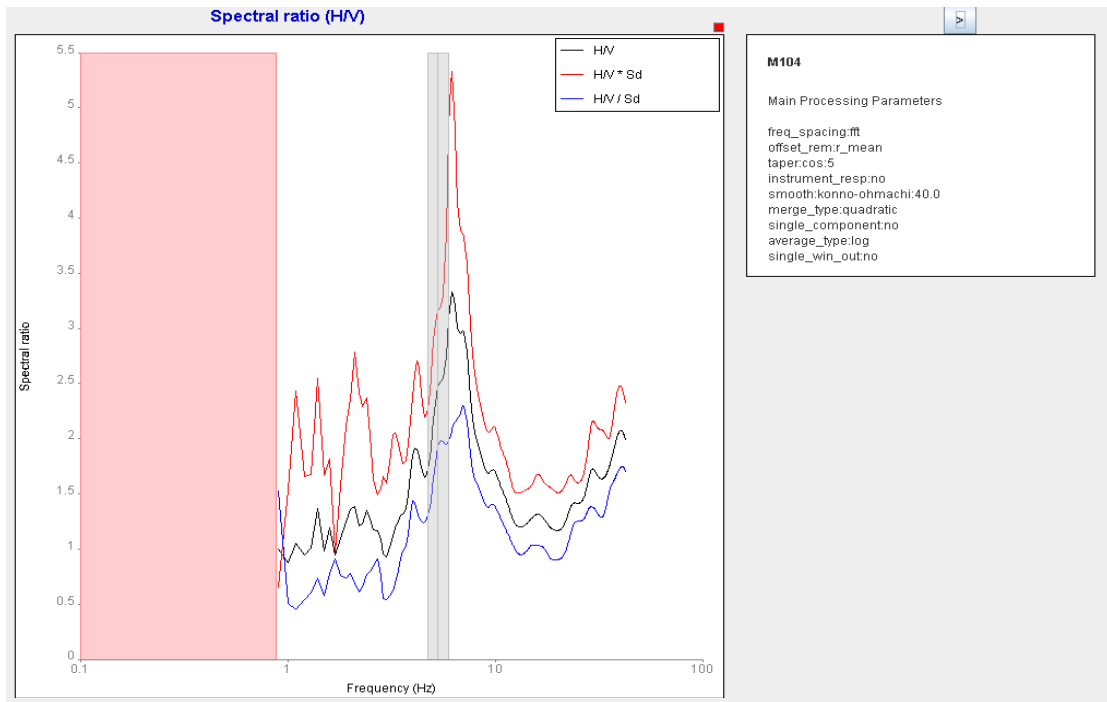


Figure12.19, site response spectrum at point M104. It is seen the flat response with the amplification is 1.2. Please note the first part of spectra take as flat response.

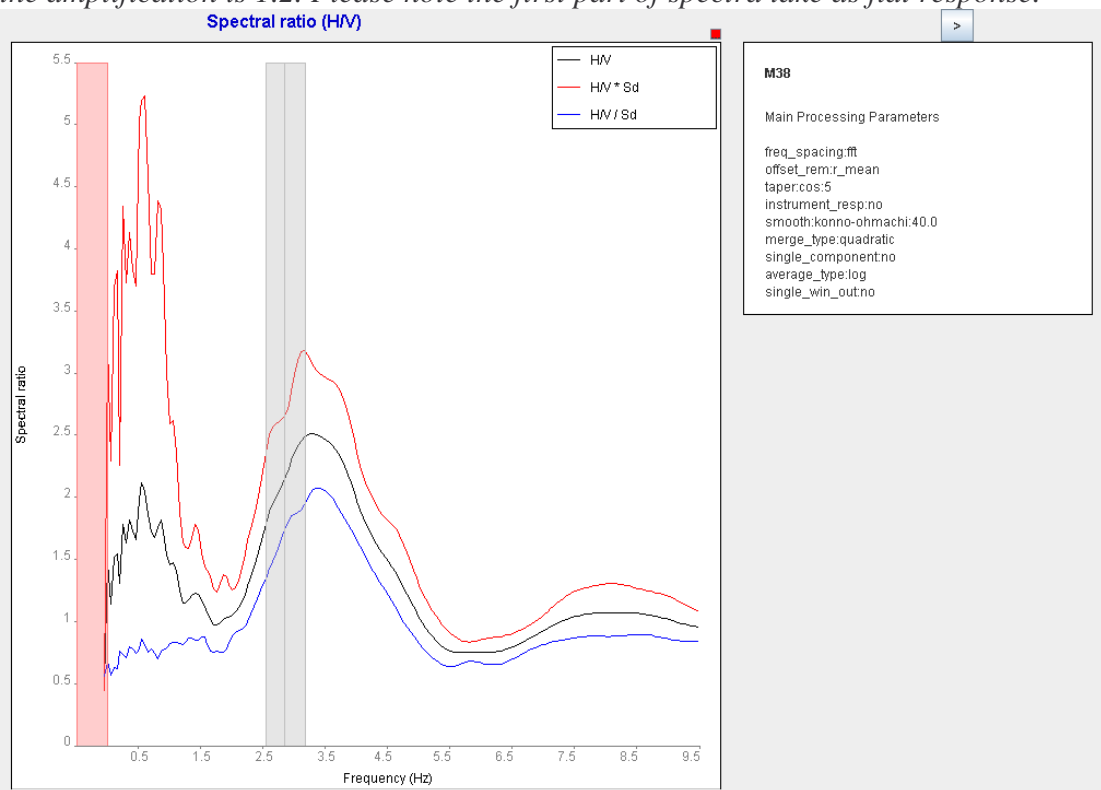


Figure12.20, site response spectrum at point M38. Here it seen two clear peaks which were represented may be by unconsolidated under line sedimentary. The amplification is 2.5 with frequency 2.6 Hz.

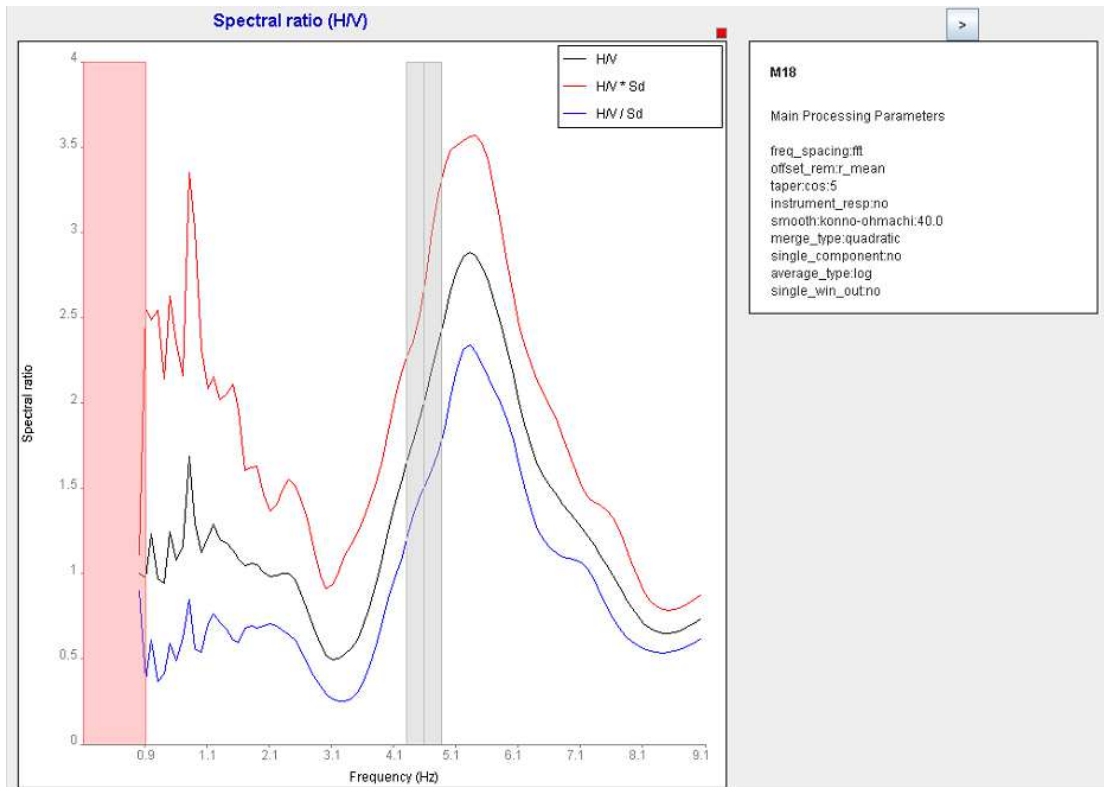


Figure12.21. site response spectrum computed at point M18 from dataset in the sandstone Omdurman having a distinct two peaks clear.

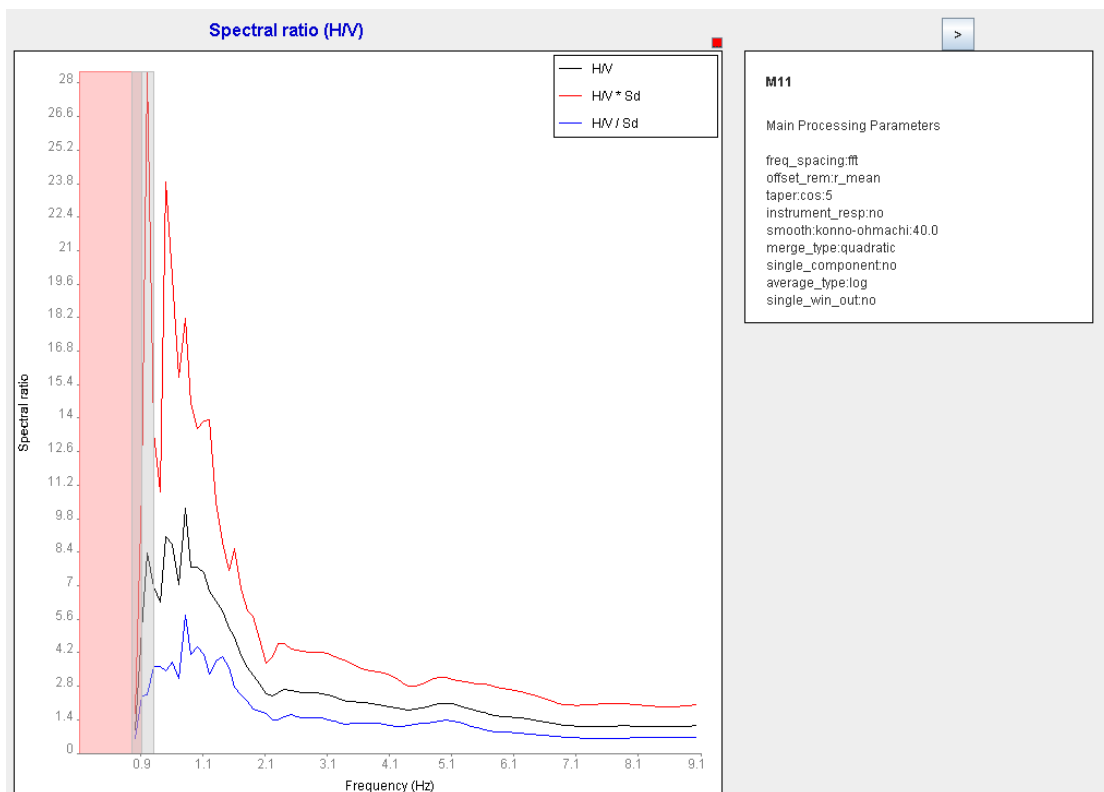


Figure12.22. Site response spectrum computed at point M11 from the Omdurman dataset which has one peak of amplitude around 1 Hz.

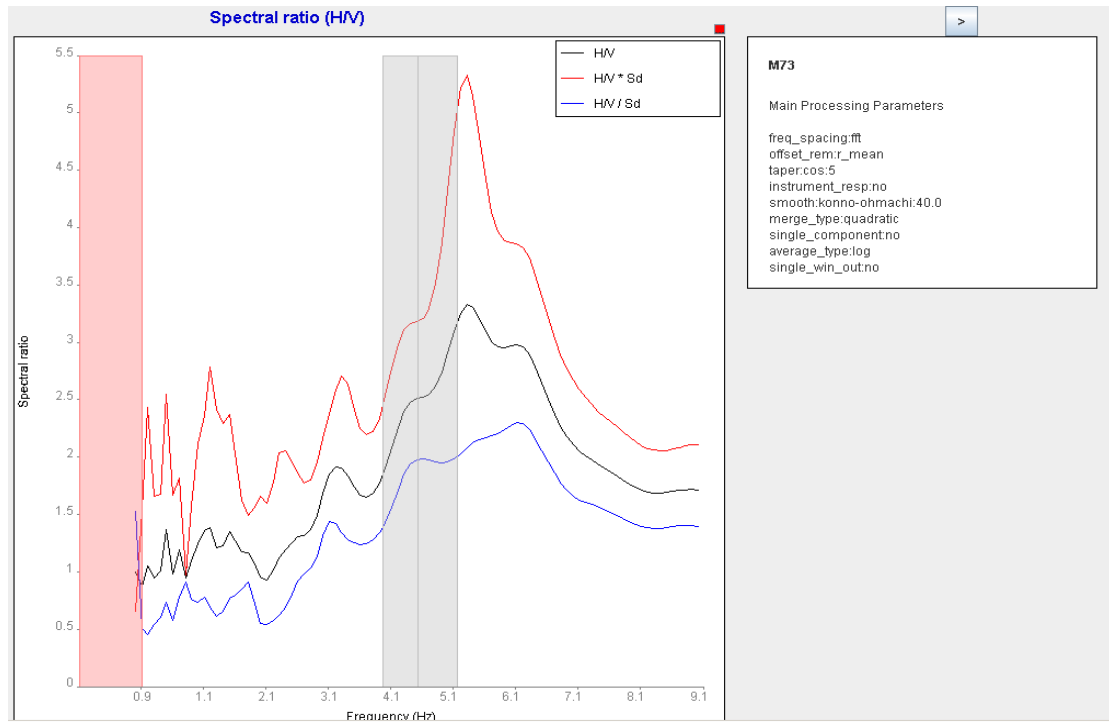


Figure 12.23, Site response spectrum computed at point M73. It is seen have broad band of frequency. Here the amplification is high compare to another which that reflecting to thickness of consolidated sedimentary underlines this site.

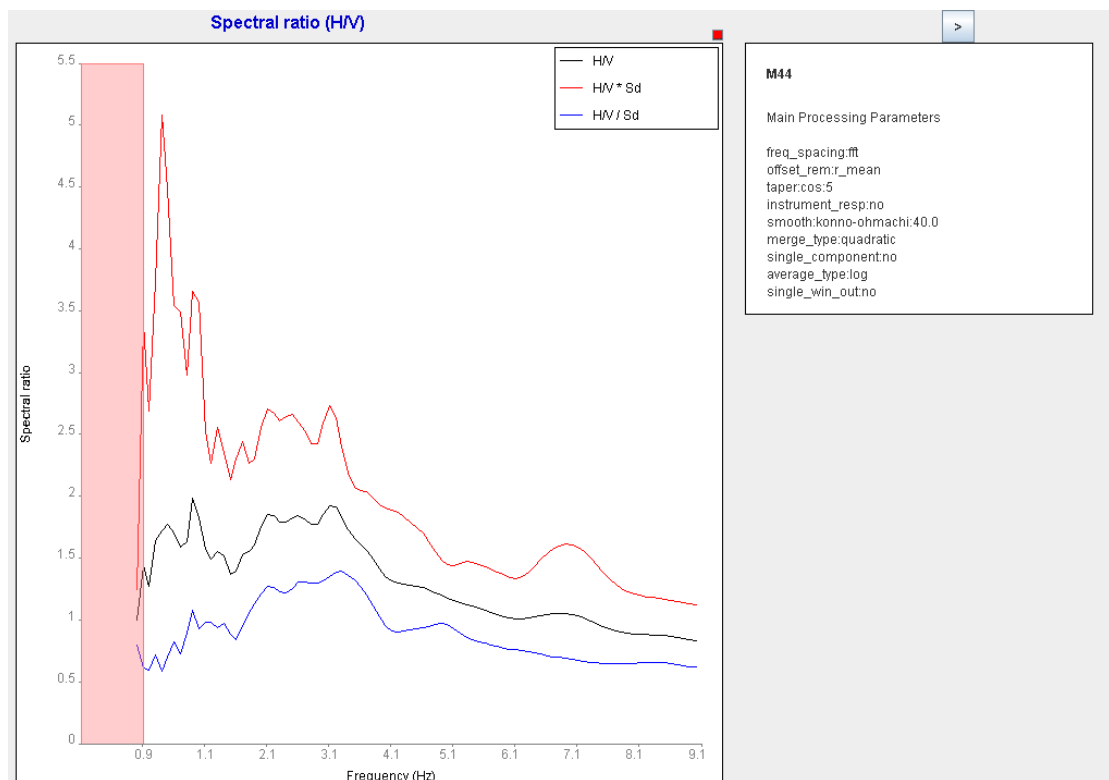


Figure 12.24. Broad band frequency of Site response spectrum computed at point M44. Here we can see the lower amplification compare to another site may be given by consolidated of sandstone.

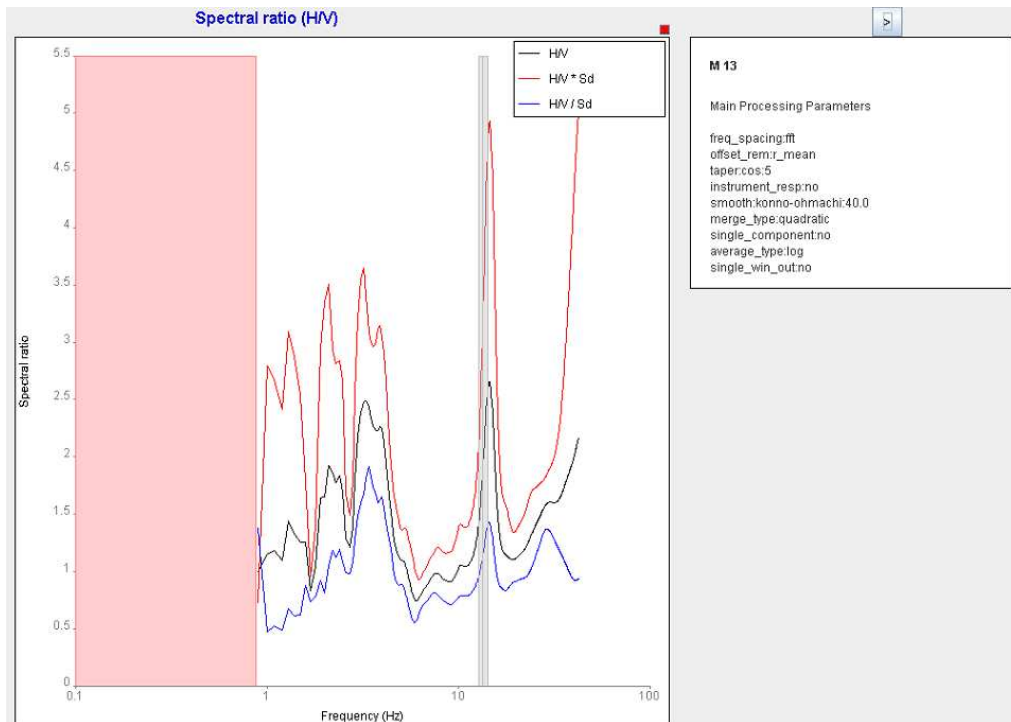


Figure 12.25. site response spectrum at point M13 from the dataset collected in the Gazira formation in Omdurman having more than one peak. Here the first peak may be represent of different strata graphical of underline layers.

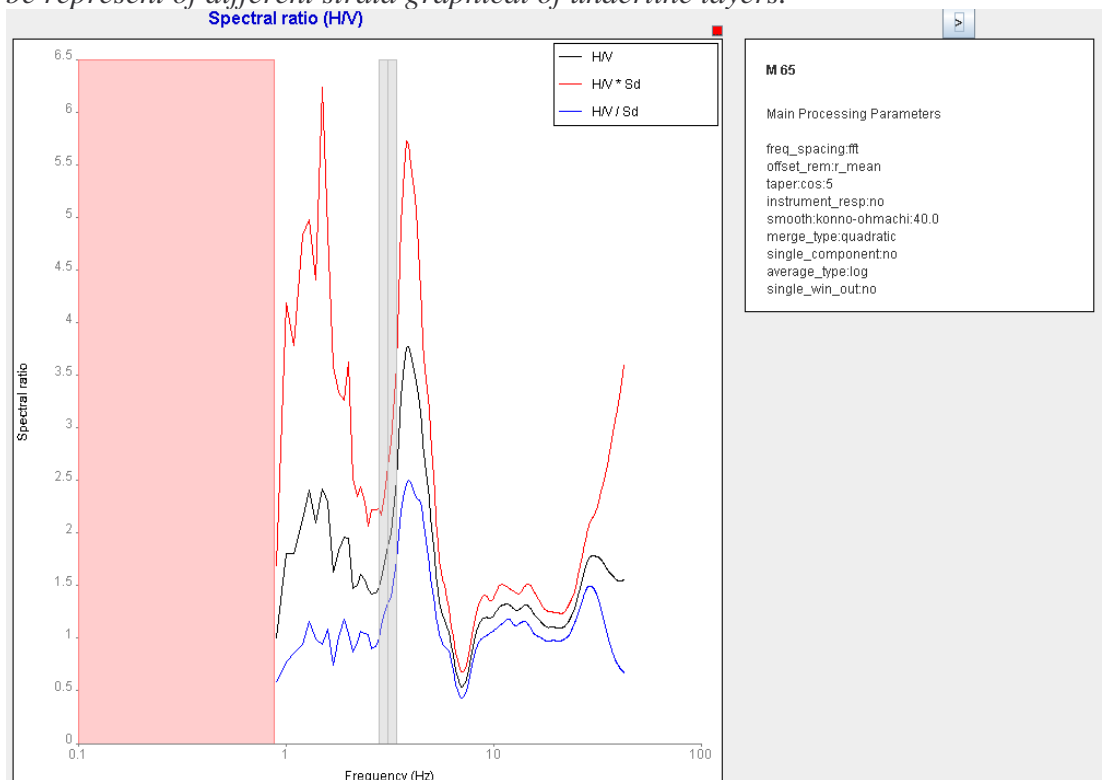


Figure 12.26. site response spectrum computed at point M65 from the dataset collected in Gazira formation in Omdurman site having amplification around 3 with more than one peak.

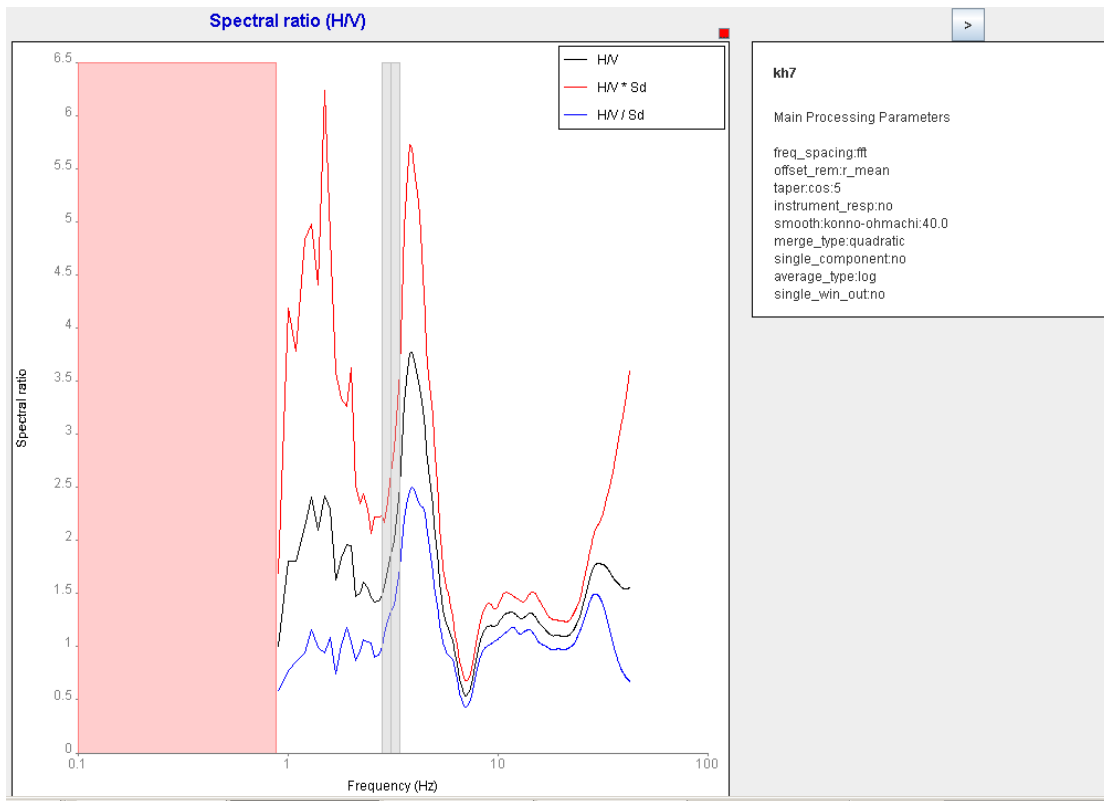


Figure12.27. Site response spectrum computed at point Kh7 from dataset of older alluvium site in Khartoum area. Here we seen clear peak amplitude around 3.7 with frequency 2.5 Hz.

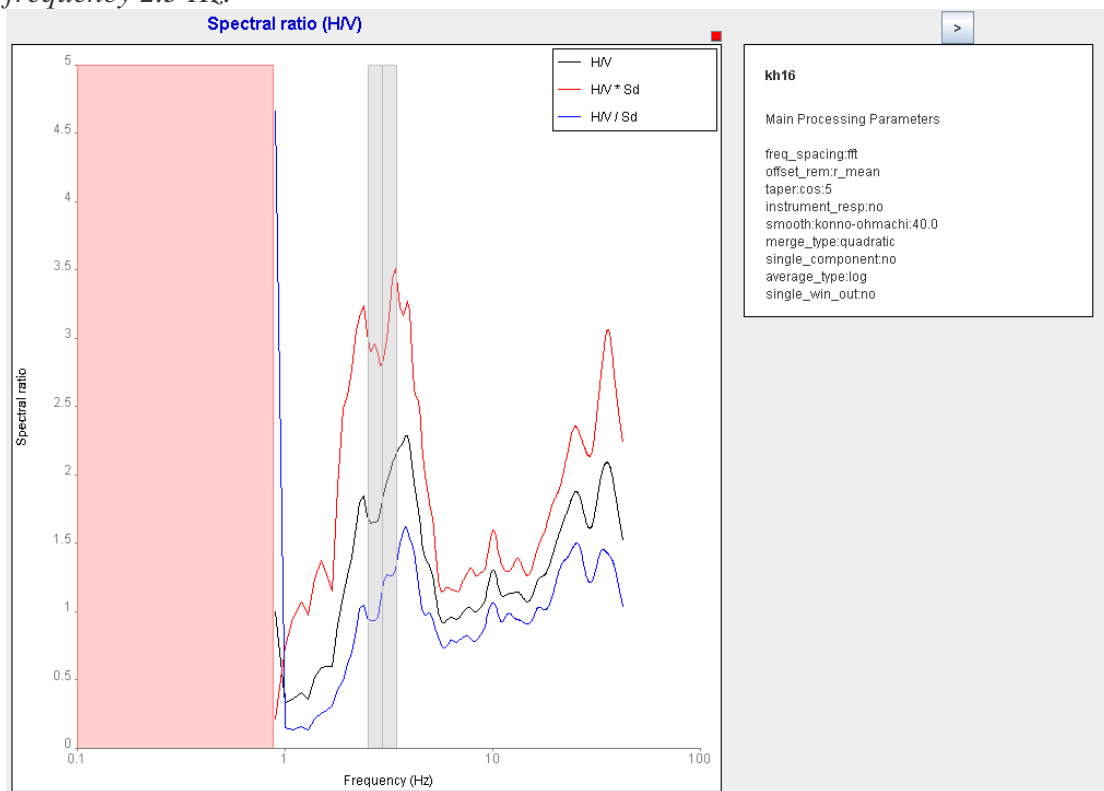


Figure12.28. site response spectrum computed at point kh16 from older alluvium in Khartoum area. Shown here with one peak has different peak may reflect to unconsolidated sedimentary.

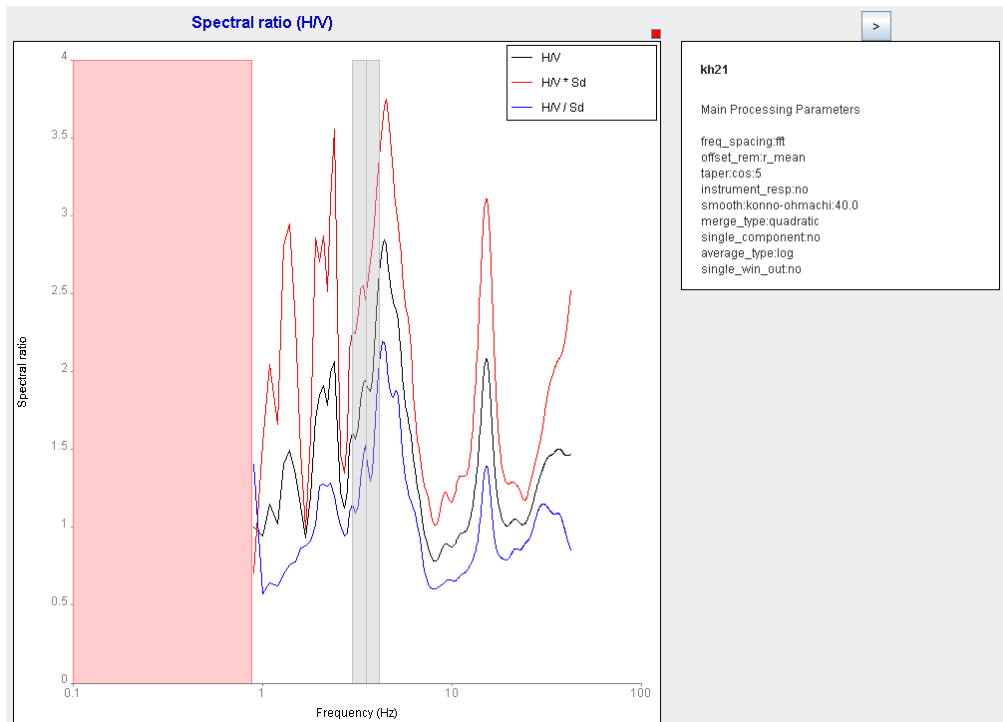


Figure 12.29. site response spectrum has many peaks of amplitude at point kh21. High peak amplitude reflect from two different contrast two layers while the some peak could be due to thickness of unconsolidated layers.

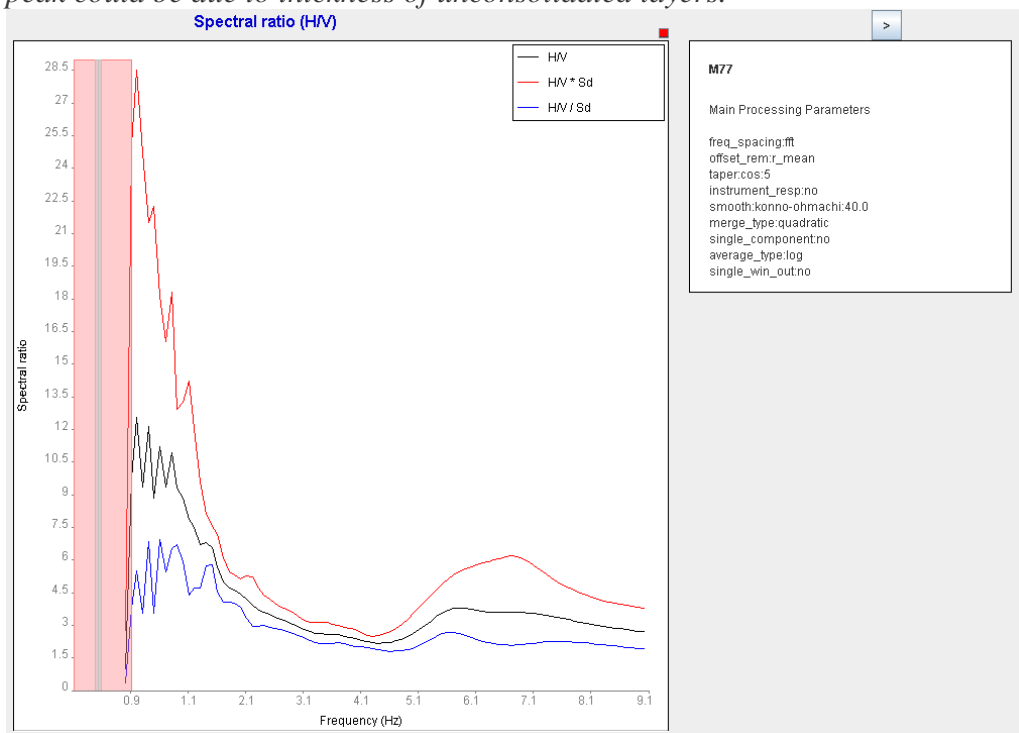


Figure 12.30. site response spectrum at point M77 from dataset from recent alluvial in Omdurman site. Here the amplification is higher about 12.14 than the site has normal sandstone which is covering most of the area study. Fundamental frequency here is representing lower around 0.799 Hz.



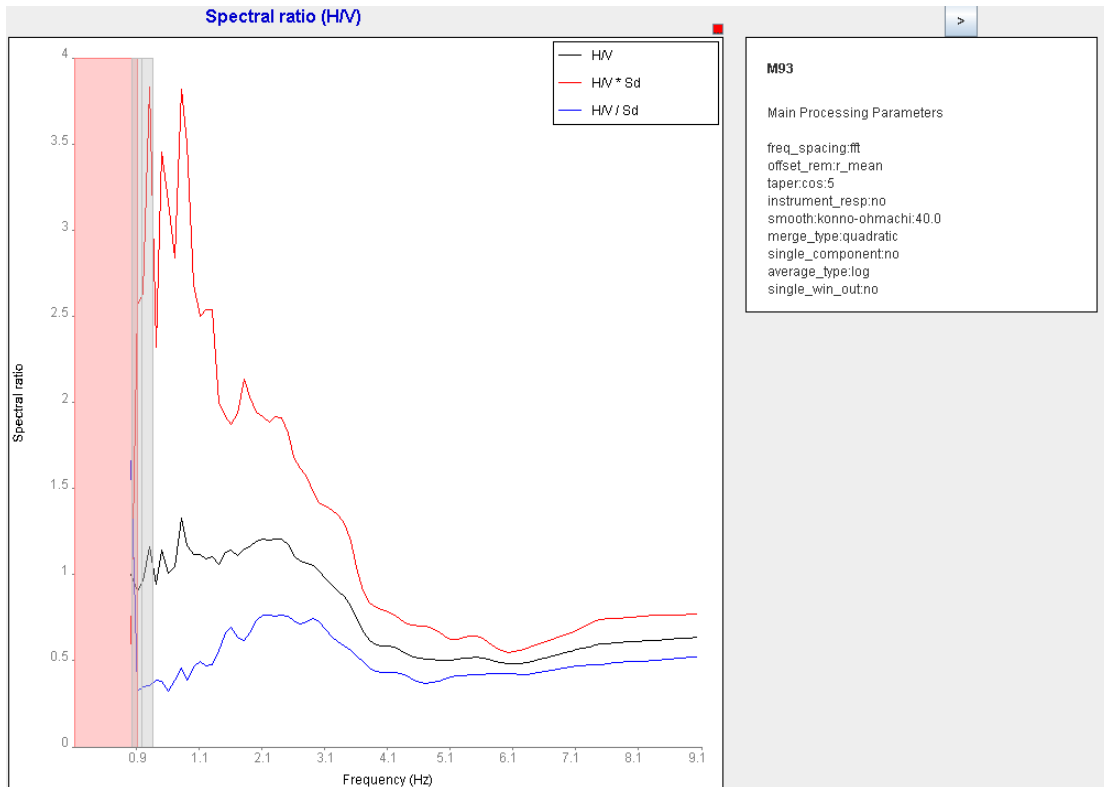


Figure12.31. - Site response spectrum at point M93 from dataset collection from recent alluvial deposit in Omdurman site. Here we can see amplification is lower around 1.4 with higher frequency (0.99 Hz) relatively.

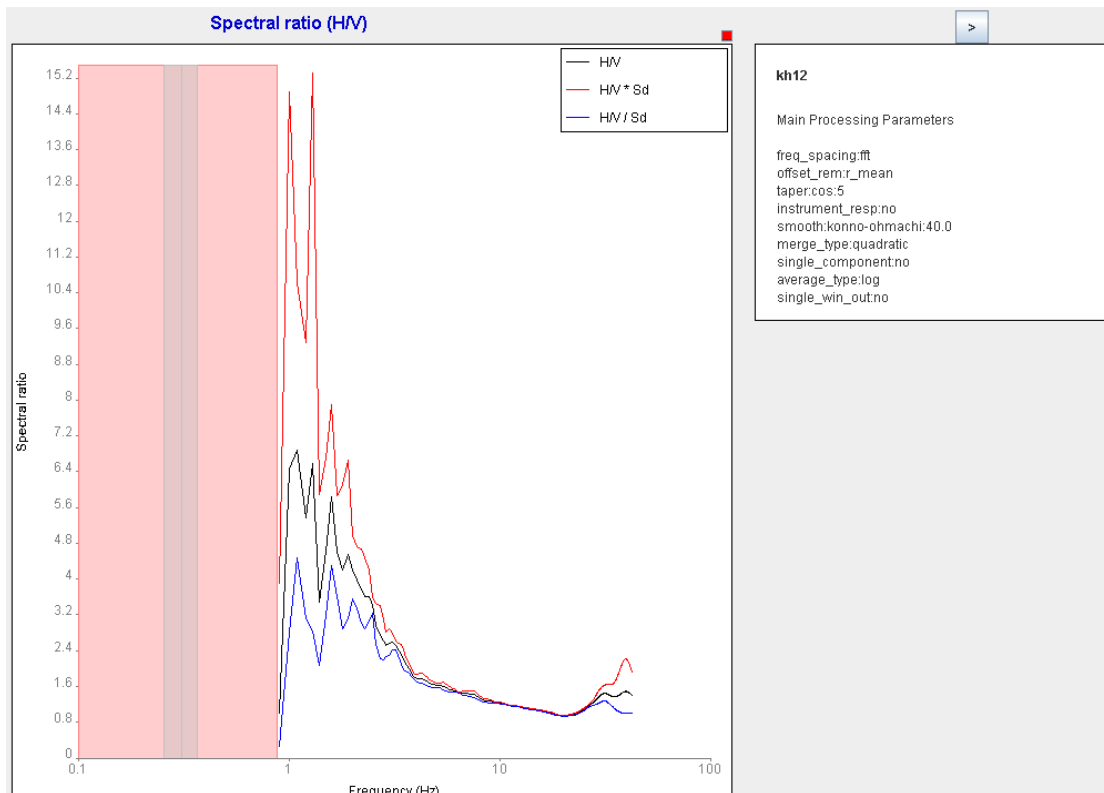


Figure12.32. site response spectrum at point kh12 from the recent alluvial deposit at Khartoum dataset. The amplification is 5.83 with frequency around 0.99 Hz.

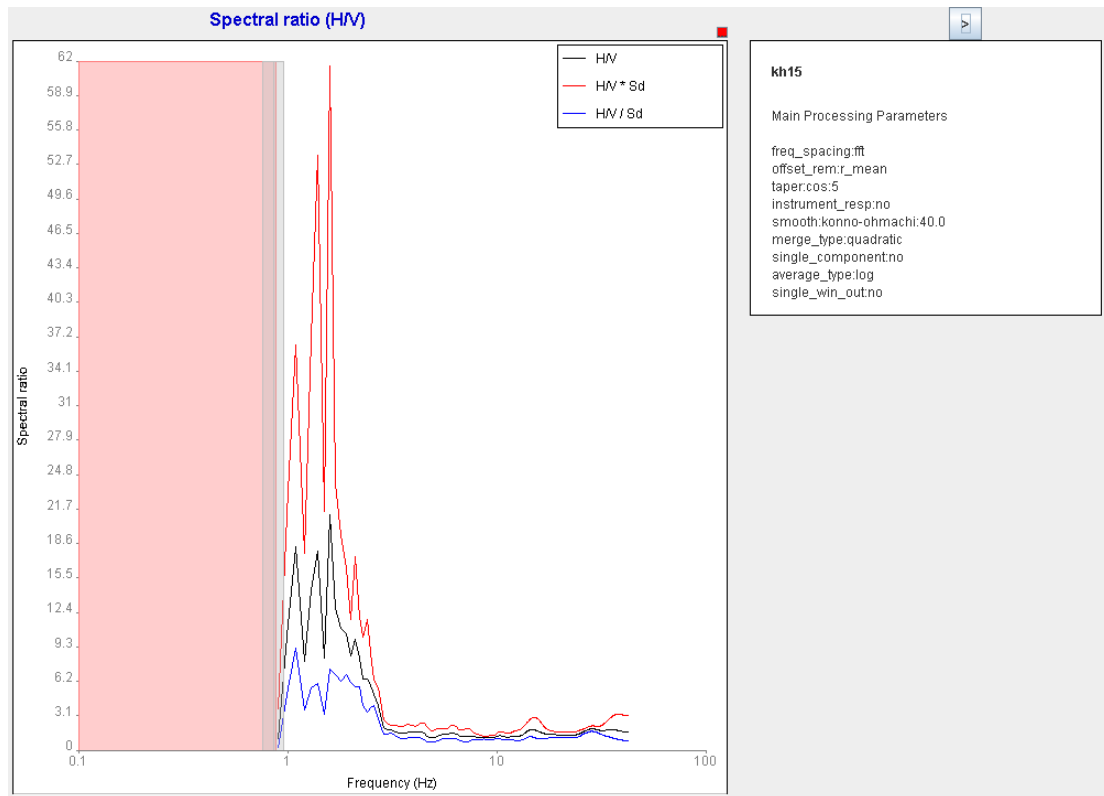


Figure 12.33. site response spectrum at point kh15 from dataset from recent alluvial deposit close to east bank of Nile. Here the amplification ratio is 19 with frequency around 1Hz. Clear peak with small peak reflect thickness of unconsolidated sedimentary, or may be the layers under this point have different layers each one has acoustic wave different.

#### 12.1.4 Spatial distribution of the fundamental site frequency and amplification factor for the western of the Khartoum city

In order to produce a contour map of the spatial distribution of the fundamental frequency and amplification factor, include all points. That mean we include the site response of all formation in order to see the variation of site response for each site in these formation. Figure 21 and 22 shows the spatial distribution of the fundamental frequency and distribution of the amplification factor respectively. It is to be observed that due to inhomogeneous distribution of the measurement points in the area, the map been produce it see has two problem which give poor description; since the area have high value of frequencies or amplification at some part and another place have small values then the interval between two line will influence of lines, either extensive lines contour map if we using small (less one) interval or quite wide if we use interval large than one. In this case we believe use the interval one which it is quite better and gives reliable couture map. The second reason is that some parts of area where no data as

we could see in western, eastern and northern part of the area it gives the interpolation lines. The lines are increasing at that area with no data this values it is not represent the really site response. We mention that the some points with less 1 Hz frequencies are unable to see it. However in order to correlation these two maps with geological formation we made two things one we was put the site name at each site, second the scale of both spatial as the same in geological with site (Figure 9).

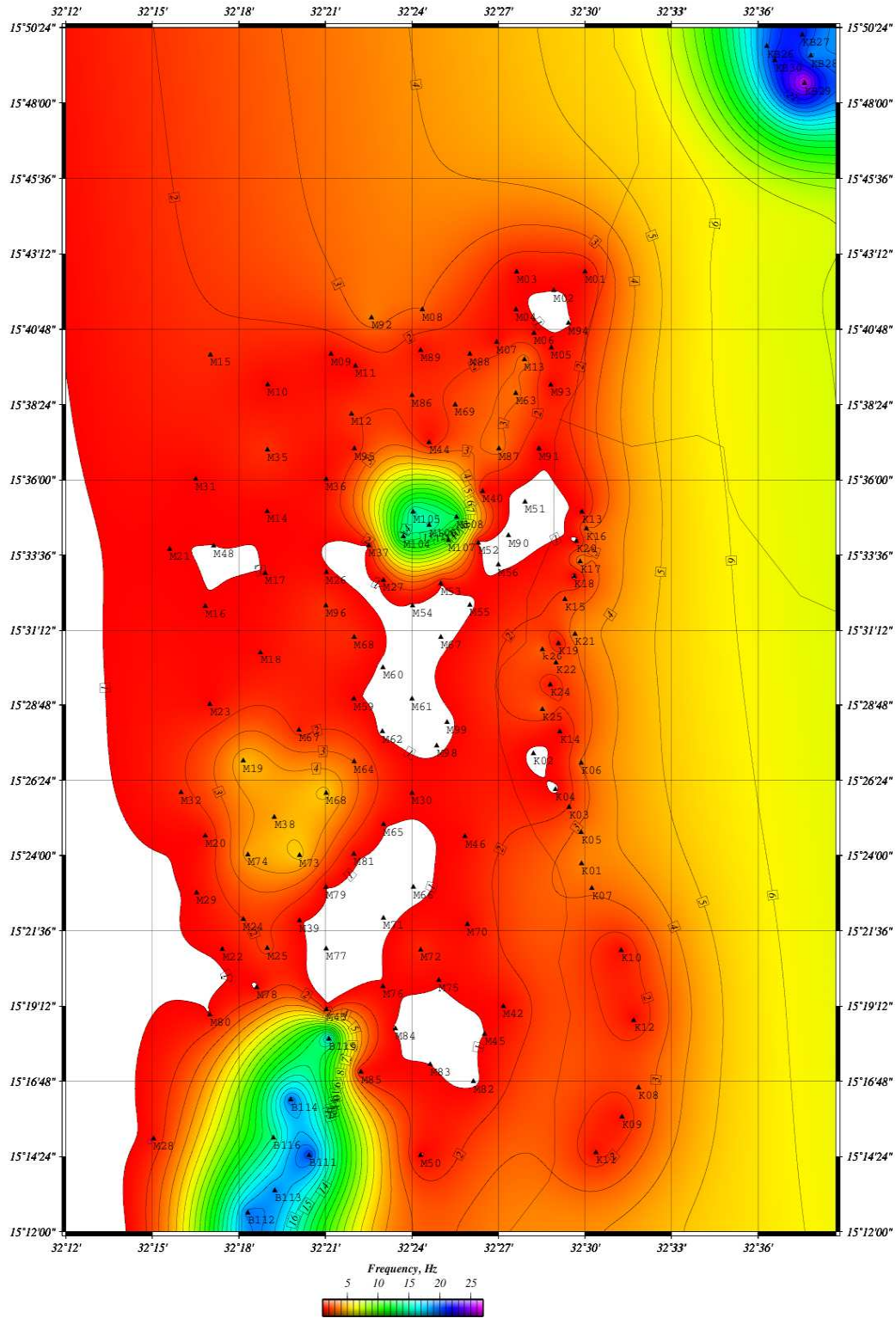
Our first idea was to look for agreement between the spatial of fundamental frequencies and amplification factors in one hand and distribution of sedimentary rocks and basement rocks and another hand. As we could see three anomalies of frequency spatial map are taken different place in study area. First; fundamental with high anomalies located at three parts in area. We was mentioned before in this chapter at section reliably of H/V ratio, these points were measurement overlying hard rock (basalt and granite) as assume that have thin layer under the sensor that may given these anomalies. These points have the fundamental frequencies range 10 to 22 Hz. We can see also that two corner have value increasing out site that mean may the rock increasing that excitedly what we have in geological area see figure 9. For the anomalies in central of the area which is mainly basalt rock we can see the isomap line of the frequencies values as the cycle, is mean the area have limit area. That also corresponding to two geological factors, one is that outcrop for those rocks unite has cycle shape as we see the Google image in figure 3.1 and digital map figure 9. Second is the geophysical in this area produce the shape this rock as intrusion basalt (Qureshi et al. 1966). Second anomalies; the areas have frequency rang 3-6 Hz where are located in three group, northern the central high anomalies (basalt), northern the south anomalies (basement granite) and along eastern bank of White Nile (Khartoum). We could see two group anomalies (north basalt and Khartoum) have similarity of fundamental frequency around 3 Hz even are the same geological but at different place. These two group anomalies may indicator that these areas have site effect. The points at these areas have clear to more peaks in spectrum as we mentioned before may be identified under these points the boundary between two uppermost layers it is sharp. Also most of these sites have more than one peak which is reflected the variation in layers. Third group anomalies in that located northern the south anomalies we see at point M73, M74, M38, M19 and M68 with fundamental frequency range 5 to 6 Hz. This relative high frequency could be due to three reasons since these site are

located on sedimentary rock; one reason is the area has sediment more less high consolidated sandstone in uppermost layer, second reason is our measurement site could effect by near the hills. The normal fault introduce by [Mula 1971] which it may response for high consolidated sandstone, thus may be are response to have high fundamental frequency.

Third anomalies which the site have fundamental frequency range 2 to 0.5 Hz. Two groups we can distinguish for this anomaly. They are distribution at uncertain area along the While Nile River and are recover all study area. The one group with low frequency close to Rive while the another group which with frequency around 2 Hz are represent far at western area. We mentioned before in chapter three, as we know the sediment thickness increases when we go away from basement rock at south and the from the hills at north east, we can see clear the thickness of sediment layer at While Nile river is highest[Farah et al 1997] (see figure 5). We can expect that fundamental site frequency decreasing from the western from the hills in accordance to equation (6) [Reiter 1990]. But the systematic only found at the northern part of Omdurman and Khartoum close to river, while the southern part it quite complex.

Figure 12.34 shows the map of the spatial distribution of the amplification factor in study area. That we can look for relation between the amplification and distributions of geological formation unite. Since we made measurement at hard rock (basement complex as granite rock and occurring at southern and northern area and basalt at central) we expected the amplification factor showed be small while the thickness of the sediment as we go toward the river the amplification factor will be rises. This concept we can agreement at some parts which we could show the small amplification of the sites area located at hard rock especially at corner in northern part and in central close to along the White Nile river while have high anomalies of amplification with increasing of thickness of the sediment. But most of other areas are complete uncorrelated. We showing at some part located on thickness of sediment are no represented high amplification factor. Example for that is area occurring at north, south Omdurman and north riverbank in Khartoum area. Since the area has more than one formation with different types and thickness of layer we might the difficult to estimated the amplification. We believe that the spatial of distribution of amplification is not represent a really site amplification.

*West of Khartoum city– Frequency response*



*Figure 12.34 Map the spatial distribution of the fundamental site frequency of study area.*



## **12.2 Analysis earthquake data for estimate local site effects and results**

As we mentioned early in back ground seismicity and chapter two in this part, western Khartoum area has produce moderated earthquake and most of them are located close western part of Khartoum city. The array from these events as we could see in focal mechanism of August 1993 in Figure 11.5 and focal mechanism of October 1996 earthquake in part I, thus probably have effect in Khartoum area. Furthermore most of local events located close to those two earthquakes. Hence event a magnitude 5.5 earthquake will cause widespread devastation. This devastation could also be caused by local earthquake. In this light we need to carry out site affected of Khartoum city. However in this section we proved the site response in Khartoum basin by using local earthquake data. The method used H/V ratio or Nakamura technique, spectrum Fundamental frequency on spectral ratio and amplification on spectral ratio. We used for analysis data SESAN software [*Havskov, and Ottemöller 2005*].

Full description about this method was given in chapter ten in this part.

### ***12.2.1 Analysis of the H/V ratio for the noise and S-wave recording for weak motion.***

The H/V ratio of noise and S-wave records for two stations (SLAT and MRKH) were calculated by SEISAN software. The purpose of analysis of the H/V ratio of noise and S-wave records the same as for the ambient noise record was described in section 12.1. SPEC program was used where the file contains the parameters that can able to process data and display the result. More information regarding to this issue, can be found in appendix B. Figure (12.36) shows the schematic structure of noise and S-wave analysis for two earthquakes were recorded at two abovementioned stations. The H/V ratio given for each earthquake recording and the summation of two earthquakes could be seen in (Figure 12.37 up to 12.43)

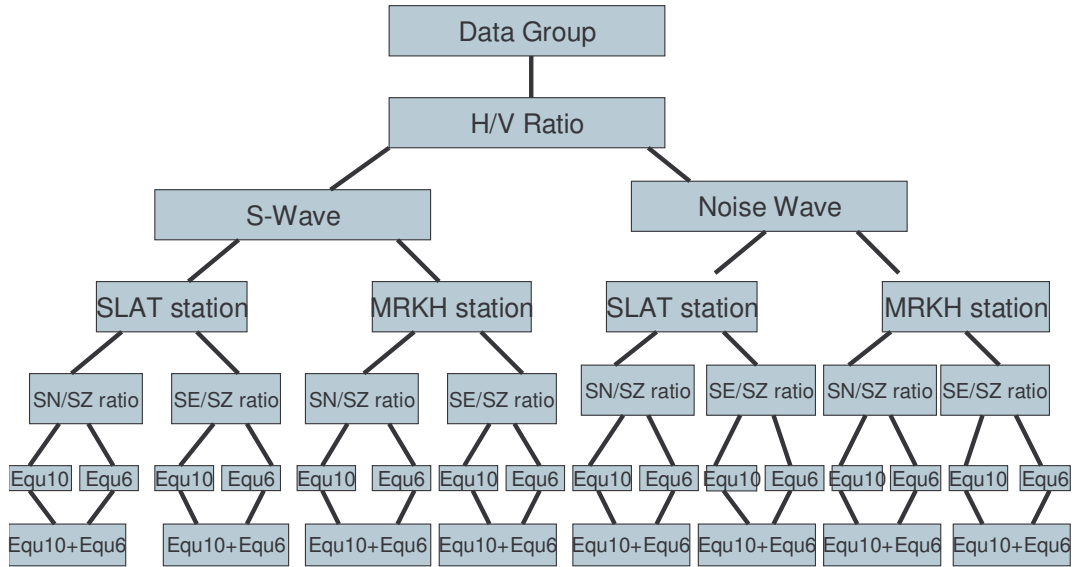


Figure 12.36( a) sketch shows the sturcture of analysis of H/V ratio of the S-wave and Noise recording from two eathquakes data (Number 10 and 6).

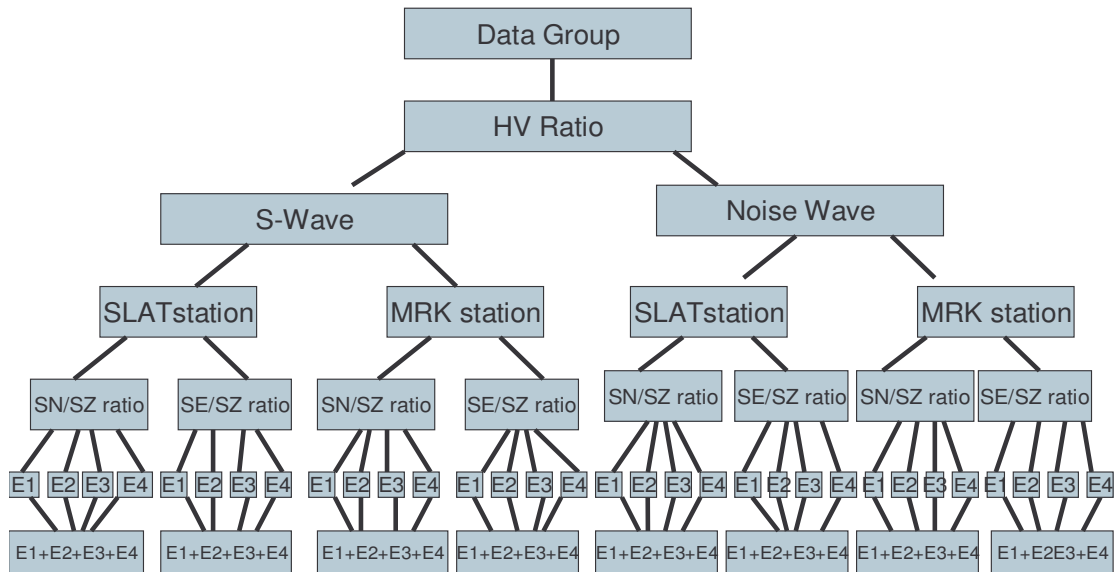


Figure 12.36(b) sketch shows the sturcture of analysis of H/V ratio of the S-wave and Noise recording from two eathquakes data (Number 2, 3, 4, and 8).



Table 1, Result of eight H/V ratio of noise and S-wave of two earthquakes (EQU10+EQU9= 20060911+20040917) for two stations one (MRKH) and (SLAT),

Earthquake	Relative station	H/V ratio of frequency	H/V ratio of amplification
EQU10+EQU6(MRKH S -wave)	S MRKH s-n/S MRKH Z	2.57	3.69
EQU10+EQU6(MRKH S -wave)	S MRKH e-w/S MRKH Z	2.52	3.54
EQU10+EQU6(MRKH) (noise)	S MRKH s-n/S MRKH Z	1.10	2.66
EQU10+EQU6(MRKH) (noise)	S MRKH s-n/S MRKH Z	0.96	1.87
EQU10+EQU6(SLAT) (S -wave)	S SLAT s-n/S SLAT Z	1.02	4.15
EQU10+EQU6(SLAT) (S- wave)	S SLAT e-w/S SLAT Z	0.98	3.06
EQU10+EQU6(SLAT) (noise)	S SLAT s-n/S SLAT Z	1.12	1.90
EQU10+EQU6(SLAT) (noise)	S SLAT e-w/S SLAT Z	1.16	2.56

The results were extracted from the summation of H/V ratio for each station using SN/SZ or SE/SZ ratio and spectral of fundamental frequency ratio and amplification factor were estimated. These results of the summation are given in table 1. We could see the low frequencies ranges between 0.96 to 2.57 Hz are giving amplification factor around 1.9 to 4.15 in that two stations. As we mentioned before in chapter ten the site response spectrum at the site located on bedrock must be flat. At the SLAT station which it is located on bedrock, both of noise and S-waves spectrum show have not flat response (figures 12.37 to 12.39). That may be due to site on the hard rocks exposed at the surface may contain numerous fractures and weathered patches, making it less compact. Such a site may have its own site response spectra that may not be flat. That may be given error to estimated of the site response of that station. The spectrum of site response computed from noise and S-wave from the MRKH station shows amplification factor 2 to 4 have peak at low frequency around 1.1Hz to 2.5Hz (Figures 12.40 up to 12.43). This result may be reliable because both of the noise and S-wave have similar amplification at low frequencies range.

The second group which contains four earthquakes number 2, 3, 4 and 8 are located by MRKH and SLAT station, we could see in figure 11.5. We calculated H/V ratio of noise and S-wave for these earthquakes as the same as was done by used two earthquakes data. However, the results of the analysis of these four events show the same as the results of the two earthquakes. All results are given in appendix B (Figure 12.36(b)).

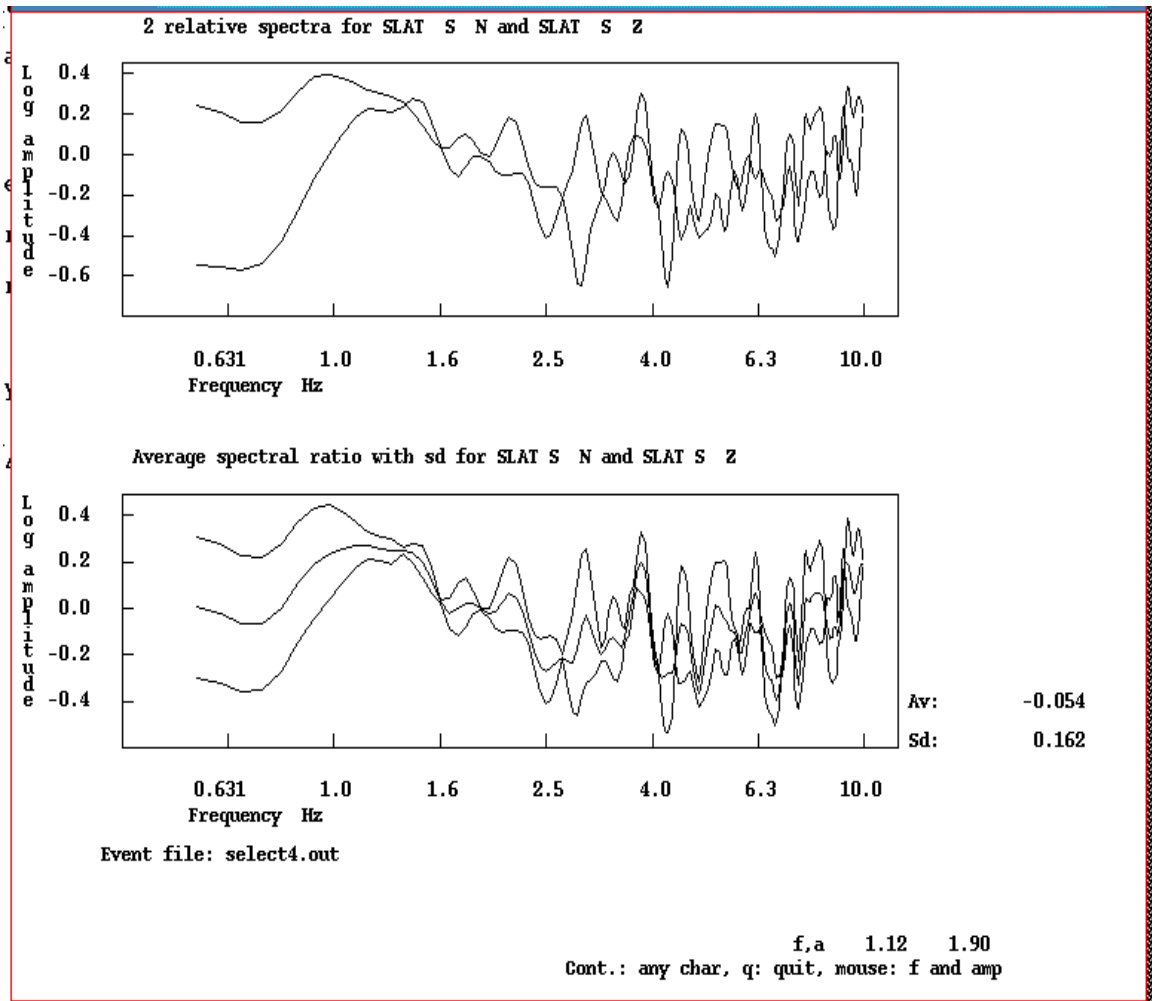


Figure12.37 H/V (SN/SZ) ratio of noise wave result of SLAT station of two earthquakes (EQU10+EQU6), we could see the amplification about 1.90

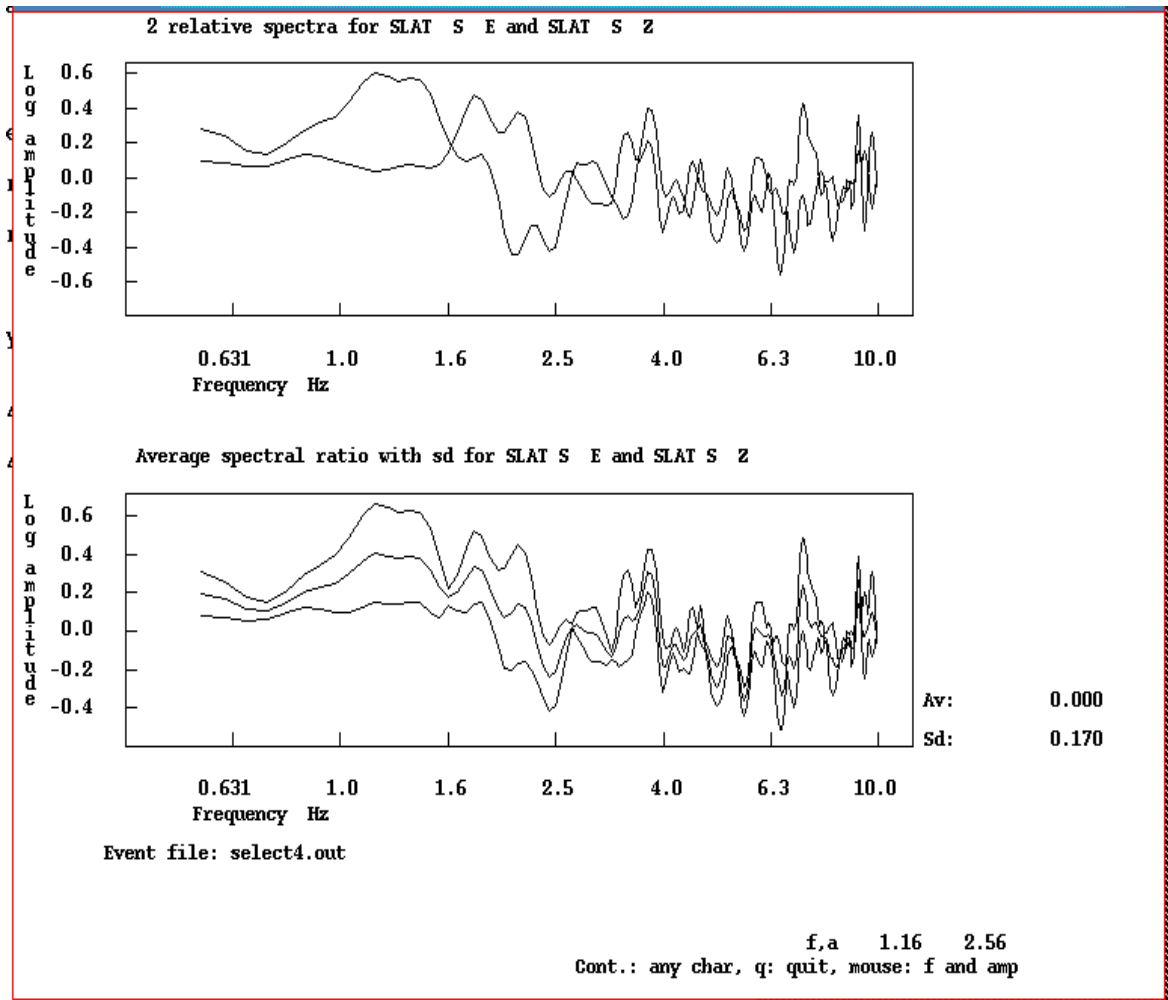


Figure12.38 SE/SZ ratio of noise wave result of SLAT station of two earthquakes (EQU10+EQU6), we could see the amplification about 2.56

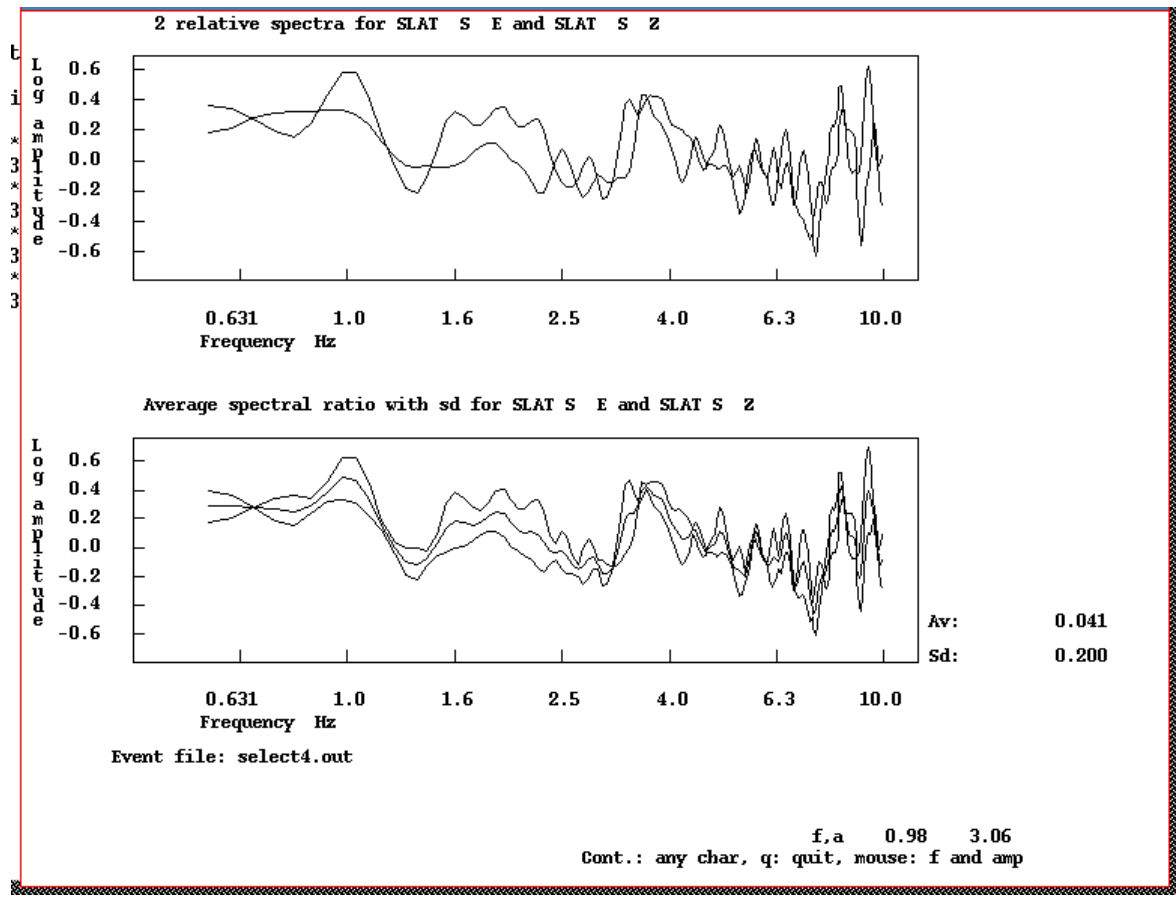


Figure 12.39 The average of SE/SZ ratio of the S-wave recording for two earthquakes (EQU10+EQU6) are recorded by the SLAT station. We could see the amplification about 3.06.

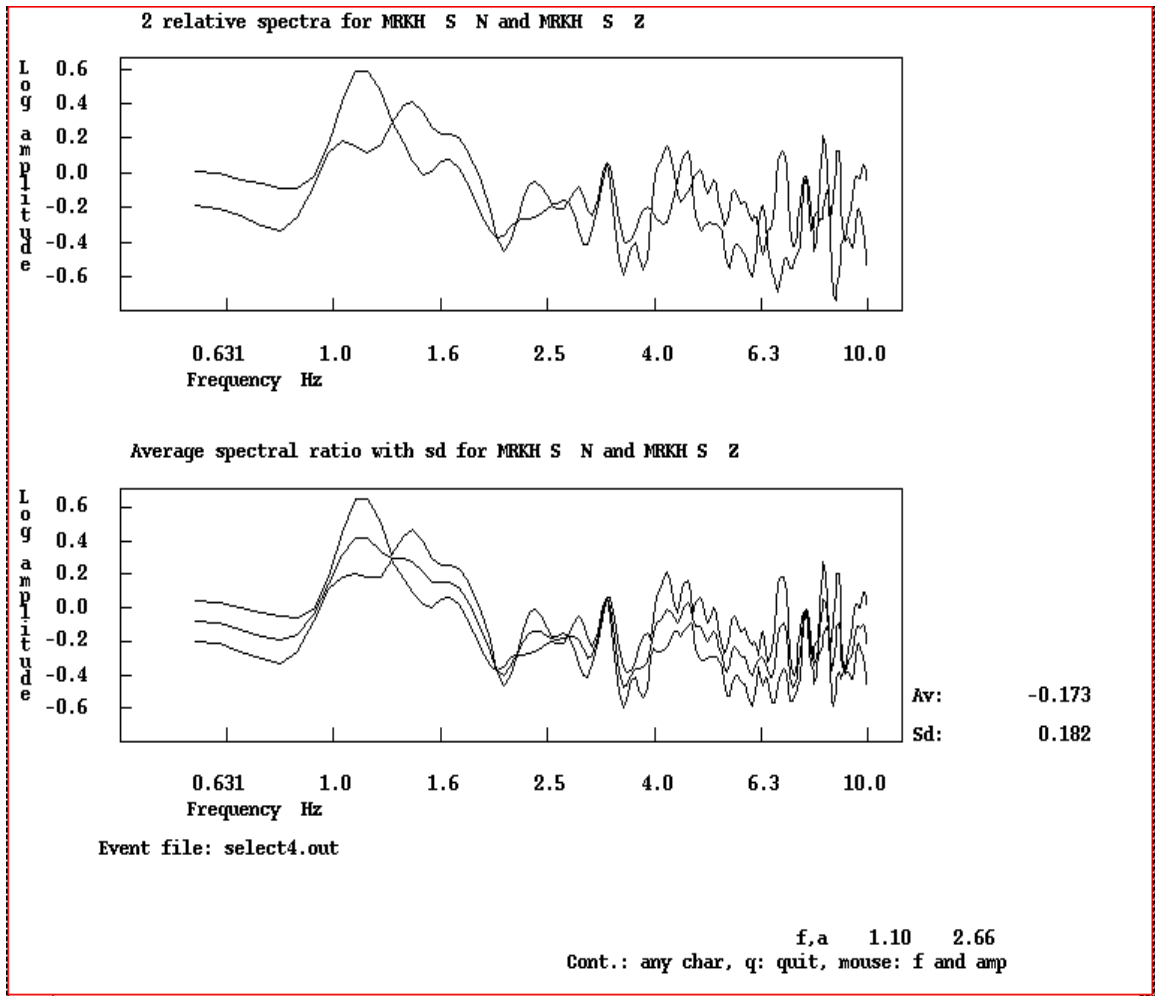


Figure12.40 H/V (SN/SZ) ratio of noise for two earthquakes (EQU10+EQU6) recorded at MRKH station. The amplification factor is about 2.66.

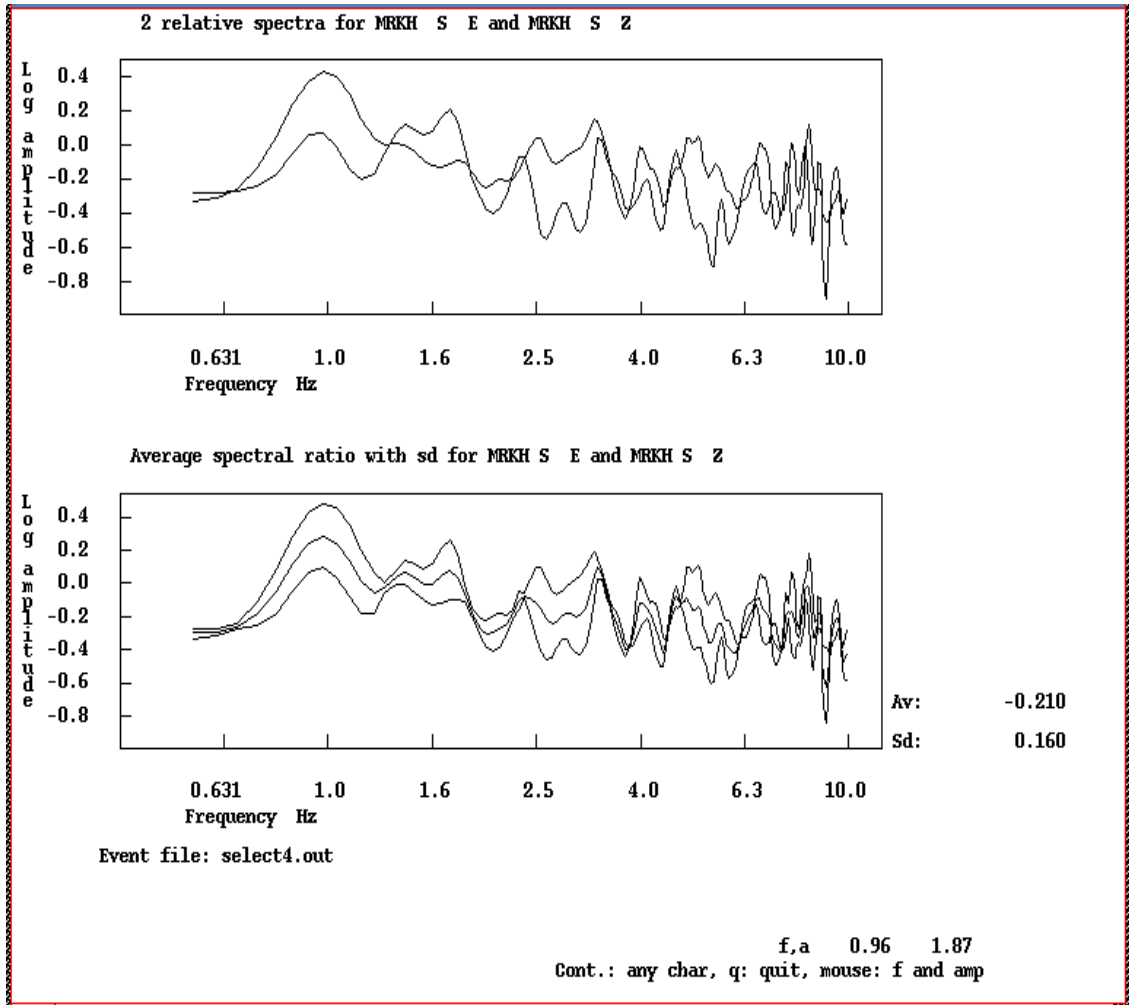


Figure12.41 H/V (SE/SZ) ratio of noise wave result of MRKH station of two earthquakes (EQU10+EQU6), we could see the amplification about 1.87.

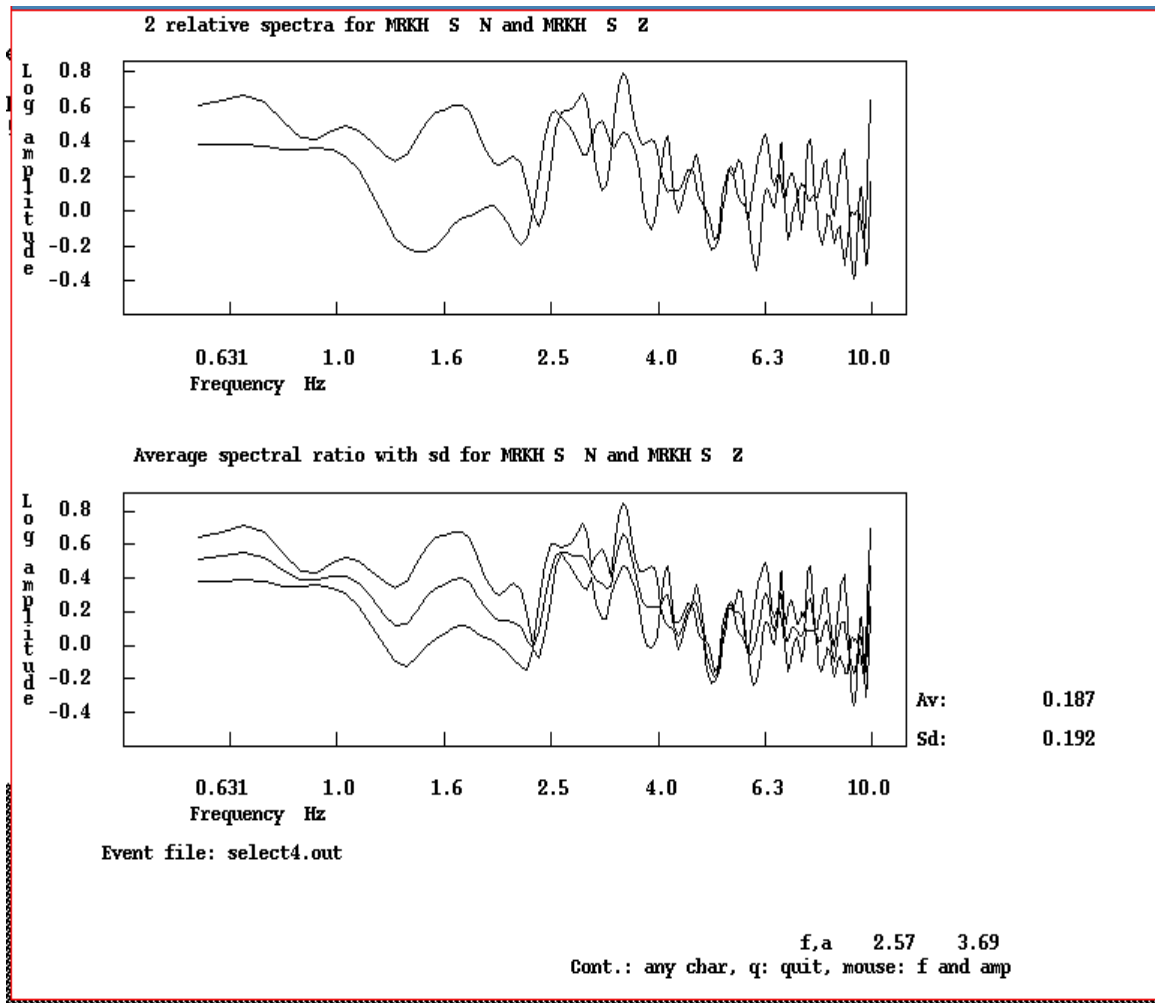


Figure 12.41 HSN / VSZ ratio of S- wave result of MRKH station of two earthquakes (EQU10+EQU6), we could see the amplification about 3.69.

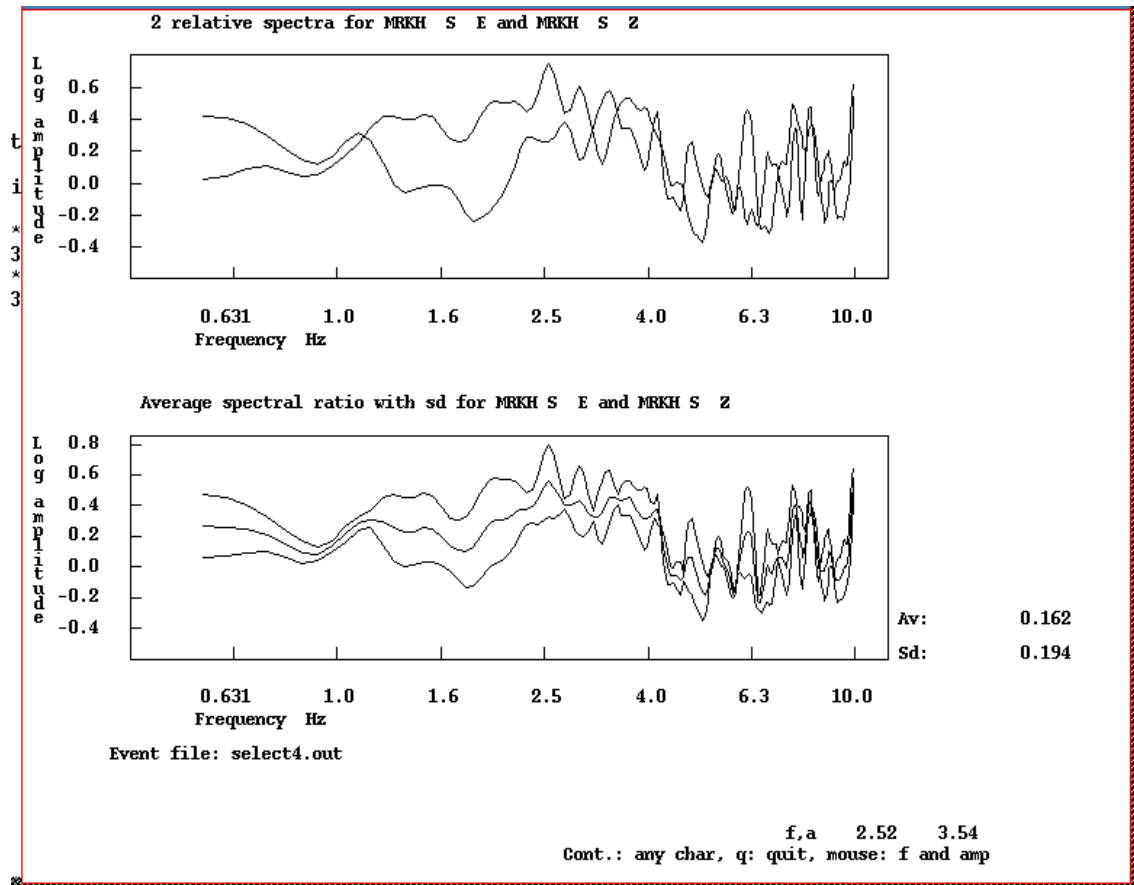


Figure. 12.43 HSE /VSZ ratio of S- wave result of MRKH station of two earthquakes (EQU10+EQU6), we could see the amplification about 3.54.



### **12.3 Analysis of Standard Spectral Ratio (SSR method) of weak motion**

According to assumption in (section 10.1 and 10.2), there are two stations (MRKH and SLAT) were used where are located on sediment (cretaceous sandstone rock) and on hard-rock (granite rock mainly) respectively. The scientific of these two stations is close to each another, the distance between these stations and source is bigger than the distance between them and located sediment and bed rock. These three factors are required for the method. We divide our data in two groups; first group contain earthquake number (10 and 6) and second group contain earthquakes named (2, 3, 4, and 8). Each group we calculated the site response with two approaches; first approach is we calculated the spectral ratio (SEs/SEb and SNs/SNb) of horizontal component of S-wave for station on sediment MRKH(s) verses horizontal component of the station on bed rock (SLAT(b)) was used S-wave.

During the analysis we observed two different earthquakes have the same two spectrums of Hs/Hb ratio which are both of them have the same frequency and amplification factor. Figure 12.45 and 12.46 shows the similarity of these two earthquakes. We could see the sandstone formation have amplified around 1.34 Hz. This similarity shows the amplified at the sandstone formation at the same value as we had before on the site effect estimated by noise recording. This observation led to investigated deep in this two earthquakes have this similarity. In order to check method in the right way we must to show flat response at bedrock (SLAT station). That mean the amplification should be 1 at bedrock. However for all calculated results we have done either in H/V ratio(S-wave and noise wave) approach or on spectral horizontal component of the both stations together when was used S-wave they are showing amplification at SLAT station more than 1.5, also even in one earthquake or average of both earthquakes. On another hand we never see the systematic of resonance frequencies for all testing. furthermore, we observed most of spectrums are showing the peak at low frequencies of spectrum all compares, or on H/V ratio for each station either at one earthquake spectrum or two earthquake together spectrum. Some example are given For all these observations we believe that it is not possible to estimated the site effect at these two stations. The one explanation for that is the station on the bed rock is not good as reference station we can use. That hard rocks exposed at the surface may contain numerous fractures and weathered patches,

making it less compact. Such a site may have its own site response spectra that may not be flat. This would introduce error in the estimation of the site response of area under investigation.

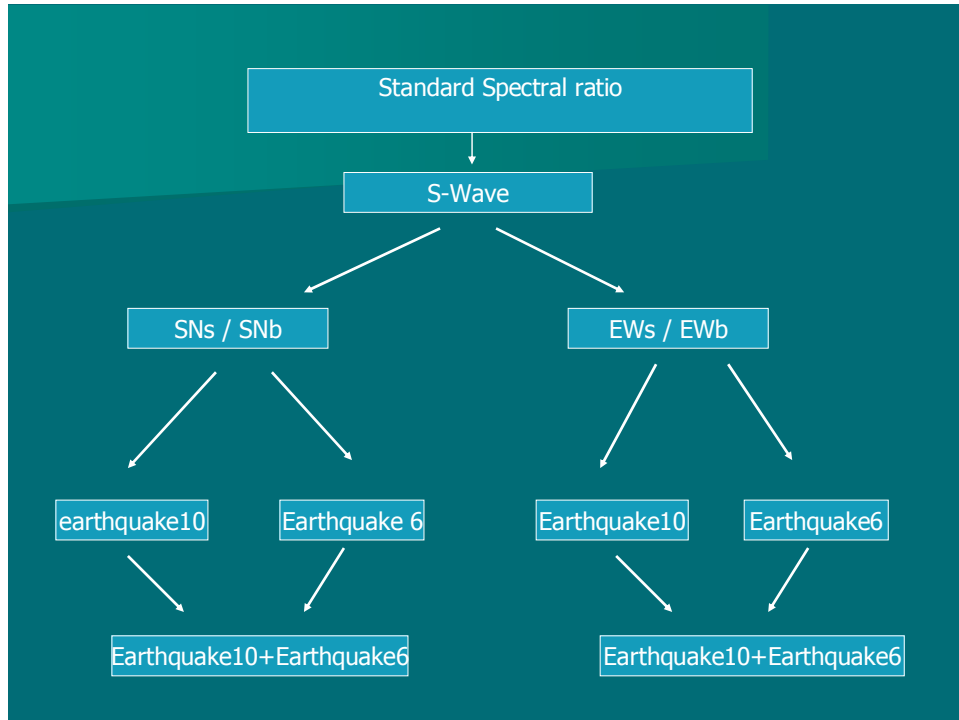


Figure 12.44 sketch shows the structure of analysis of  $H_s/H_b$  standard spectral ratio of the S-wave recording from two earthquakes data (Number 10 and 6).  $H_s/H_b$  horizontal components ratio of two stations one is horizontal components MRKH( $H_s$ ) versus horizontal components of SLAT ( $H_b$ ).

Table 2 H/V ratio of S-wave of the two stations one on sediment (MRKH) and one bedrock (SLAT) of two earthquakes (EQU10+EQU9= 20060911+20040917) recorded, and the H/V ratio of combination for both stations.

Earthquake	Relative station	Fundamental frequency on spectral ratio	Amplification on spectral ratio
EQU10+EQU6(S- wave)	S MRKH s-n/S SLAT s-n	0.97	2.33
EQU10+EQU6(S- wave)	S MRKH e-w/S SLAT e-w	1.33	5.97

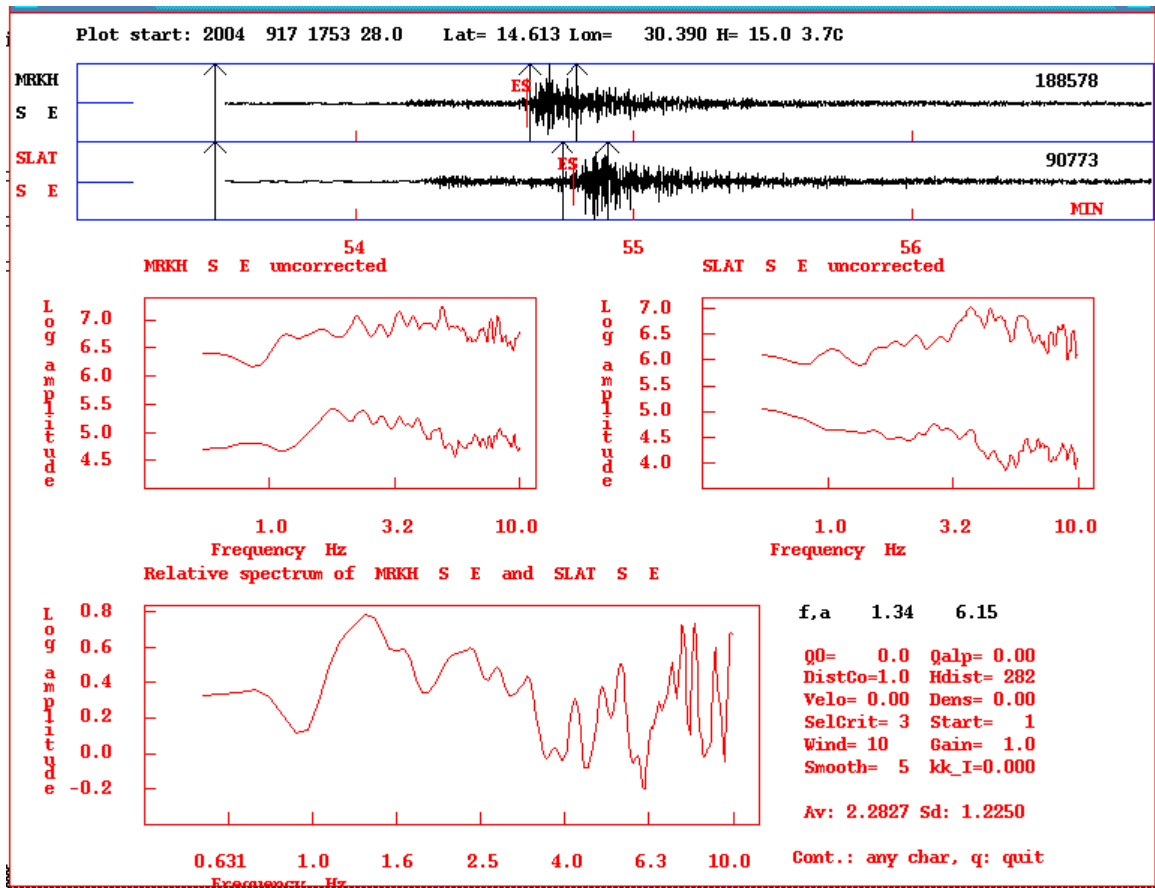


Figure 12.45 S-wave spectral of horizontal components ratio of two stations from earthquake on 2004, the ratio of horizontal components MRKH versus horizontal components of SLAT. We could show the fundamental frequency on spectral ratio and amplification on spectral ratio.

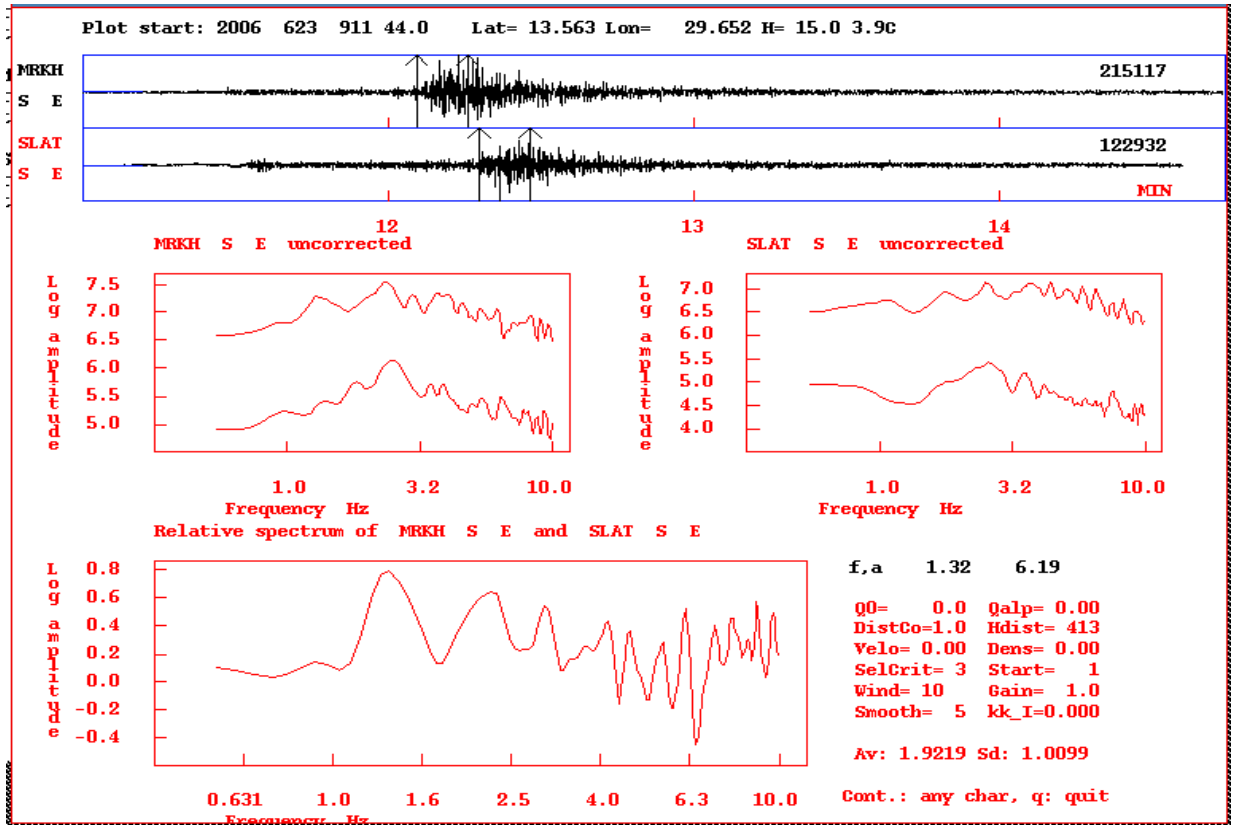


Figure 12.46. S-wave spectral of horizontal components ratio of two stations from earthquake on 2006, the ratio of horizontal components MRKH versus horizontal components of SLAT. We could show the fundamental frequency on spectral ratio and amplification on spectral ratio

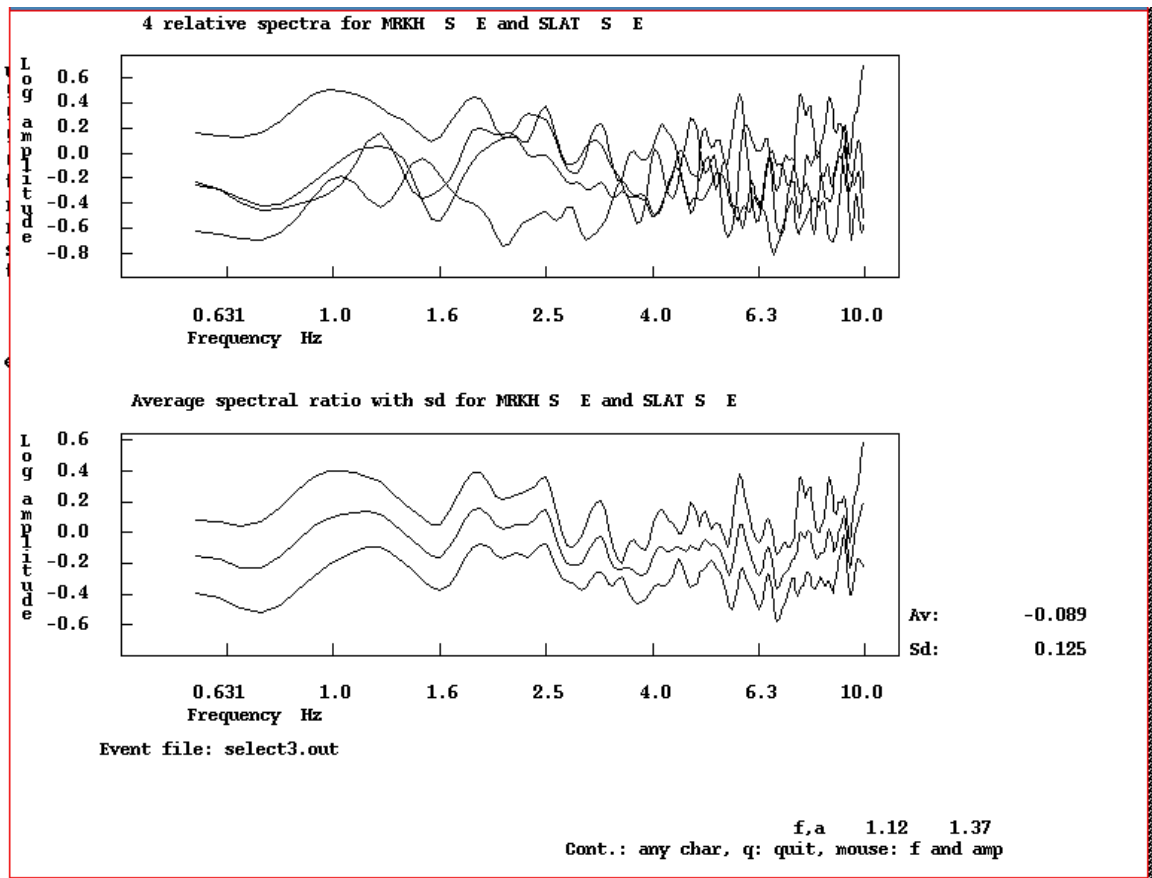


Figure 12.47. The standard spectral ratio  $H_s/H_b$  (SE/SE) ratio of two S-wave of two horizontal component sedimentary rock ( $H_s$ ) and bedrock ( $H_b$ ), of two earthquakes (EQU10+EQU6), we could see the amplification about 1.37.

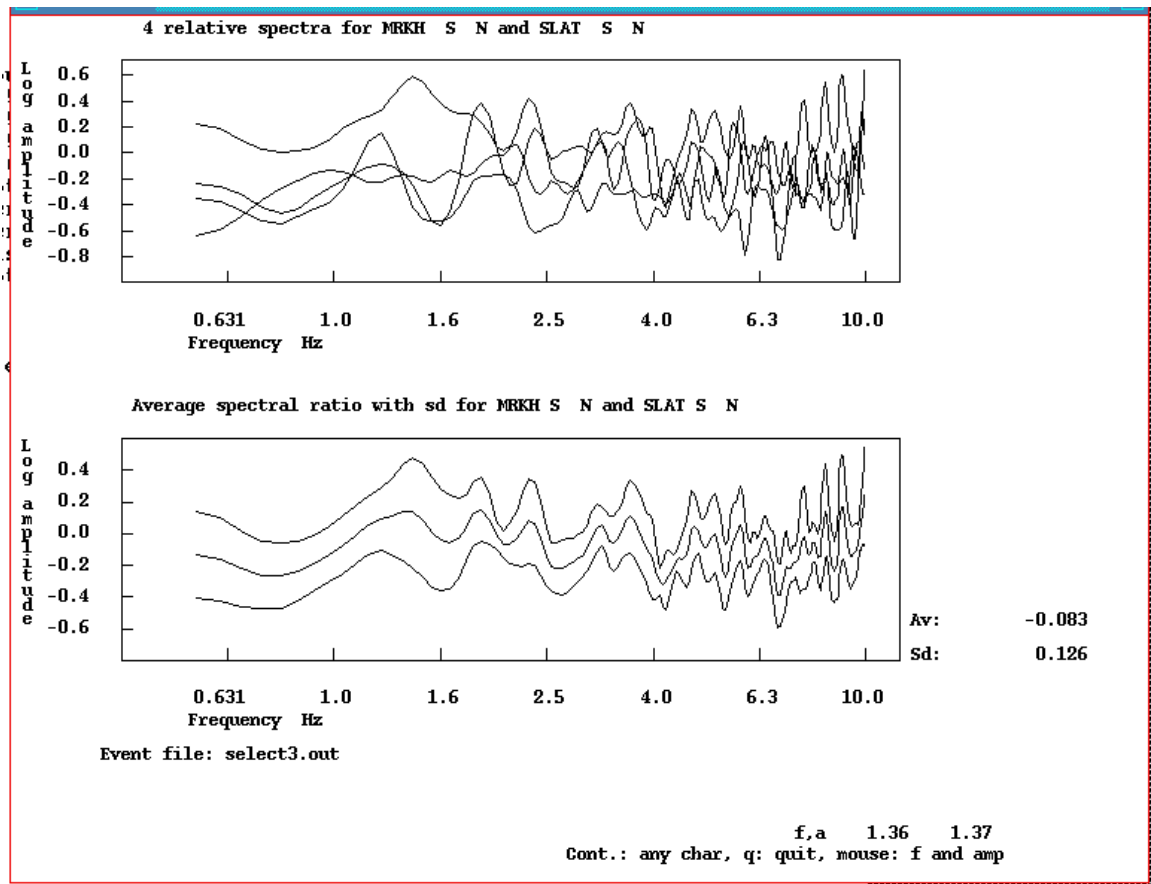


Figure 12.48. H/V (SN/SN) ratio of S-wave result of SLAT station of two earthquakes (EQU10+EQU6), we could see the amplification about 1.37.

## Chapter 13

### Discussions and Conclusions

In chapter six two maps were produced showing fundamental frequency and amplification factors Figure 12.34 and 12.35. Their result shows a clear relation between the fundamental frequencies and the type of underlying sediments. In this section we will discuss the average of our resulting site response spectra on different formations. The data points where ambient noise H/V spectral ratio are analysed, are divided into different groups representing the sedimentary units in the area. Results are discussed as average spectra corresponding to different formations.

Figure 13.1, shows eight spectral ratios for formations. To simplify the result we divide them into two groups; one group on hard rock condition (Basement Khartoum, Basement Omdurman and Basalt named as A, B, C respectively) and second one on a sedimentary unit (named D, E, F, G and H respectively.)

The H/V spectral ratios on hard rock sites (A, B and C) do not represent flat response as expected. The reason for that is probably these areas have thinner layers underlying these sites identified by amplification at high frequencies (Figure 12.12 and 12.19 in chapter six) or sites that are nearby industrial source.

Second part contains sedimentary formation at five sites (D, E, F, G and H). Among them four (D, E, G and H) show peak amplification at low frequencies around 1 to 2 Hz, and the fifth shows a peak at a frequency around 3.8 Hz. We discuss the details of these four figures as following the order of amplitude. First, high amplification factor approximately 9 with low fundamental frequency 0.9 Hz was observed on spectrum H. These sites were located on unconsolidated sediments mainly of mudstone with sandstones with thickness of more than 400m. This is in accordance with observed low frequency amplification (Reiter 1990). Because, all these sites are occurring close to the White Nile River which is thick. The sharp impedance contrast between the sediment and the underlying bedrock gives rise to a clear sharp peak. Figure 13.1 (D) shows the site response on the cretaceous sandstone of the Omdurman formation maximum amplification of a factor of 4 is observed.

The figure 13.1 (G) shows the site response on recently alluvial of the Omdurman. The peak at low frequency less than 1 Hz reaches amplification factor of 3.2. The topmost layer of soil is compact when compared to underlying unconsolidated

sediment. The thickness of this layer is more than 400m [Mohamed 1994]. The frequency on which the amplification occurs is in accordance with this thickness.

In figure 13.1 spectra shown in E and F have a similar shape with amplification around 2.7Hz. As we mentioned before these two formations have similar of layer deposits according to the map by GRAS (1988 and 2006), but were located at different sites on the eastern and western part of the White Nile River. On the sandstone and mudstone of the Gezira formation on Omdurman, the recently constructed buildings have settlement problems. This indicates were mudstone content when compared with the older alluvium at Khartoum (F). Otherwise the two formations have similar deposit and hence the shape their spectra are also similar.

In conclusion, last five sedimentary formations show a good correlation between the geology and the site response. We can, by this method clearly to estimate the local site effects on different types of sediments in the area. The spectra from these sites help characterizing or and thickness of the sediment type sediments.



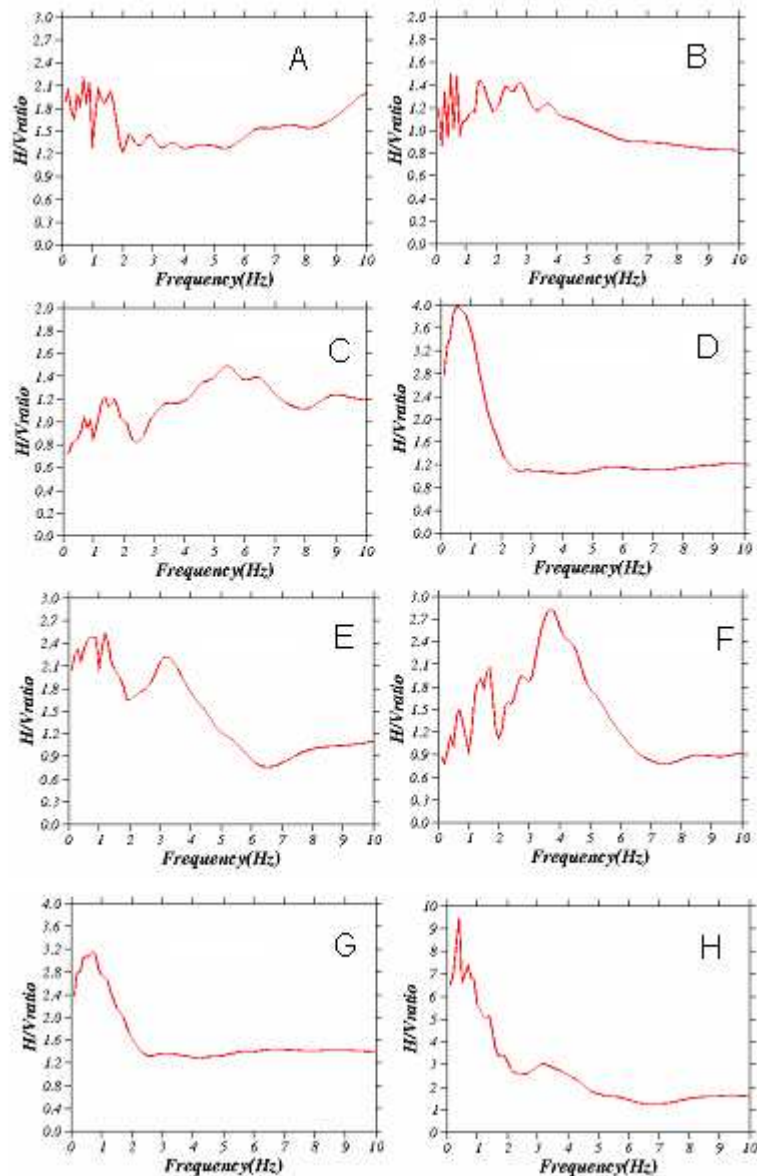


Figure 13.1– Eight site response spectrums represent for eight formations in study area. Each formation has liable following to alphabet as; **A** Basement complex Khartoum, **B** Basement complex Omdurman, **C** Basalt rock Omdurman, **D** Cretaceous sandstone Omdurman formation, **E** Gezira formation Omdurman, **F** Older alluvium Khartoum, **G** Recent Alluvial Omdurman and **H** Recent alluvial Khartoum.

On the following, we correlate the thickness of various formations with the H/V spectral ratios. In figure 12.34, the distribution of the fundamental frequency in the study area revealed a number of anomalies with high or low frequency areas. This has lead us to consider the variation of the thickness of the sediment and there compositional changes at depth. There exists three cross-section based on the borehole data which is given in figure 13.3 and 11.4 [Farah et al, 1997] from this figure it is clear that strong lateral and vertical variations exist in the three cross-

sections. We have correlated our H/V results corresponding to the cross-sections and found that there is a general correlation with the average H/V spectra shown in figure 13.2.

In the following we discuss the H/V spectral ratio results for each of three cross-sections through the data points that fall along them.

**Section A- A<sup>I</sup>**, this section is crossing the area along White Nile river at western bank, trending north–south. The H/V spectral ratios of point M42 is given in appendix C and also seen from the two figure 12.34 and 12.35. The fundamental frequency is around 1.2 Hz with amplification around 5. The sediments under this point have alternating layers of mudstone and sandstone. The sandstone layer is approx 12 m thick. We expected from previous papers (Akatan et al 2004) that in the case of sites which have two subsurface layers. This is reflected as two or more peaks at the spectrum. This is exactly we see in the spectrum computed from the point M42. Points M56, M90, M51 and M91 are the same with frequency less than 1Hz and with amplification around 4. That could be reasonable for these points since we can see that points underlined by thick layers.

At points M03, M05 and M93 show spectra with low frequency around 0.8 to 0.9 Hz and with high amplification about 16 to 18, while point M93 has less amplification around 1.5. The possible explanation for this spectra variation is due to the thickness of the layers under these points. We could see that at points M03 and point M05 both have low frequency which may be due to thickness of mudstone layer while the point M93 has wide band peak with less amplification. Therefore the point M93 was located on thick sandstone layer with high consolidation. Since the areas are flat along this section, and acoustic impedance contrast between mudstone and sandstone layers is high, we believe that the majority of the H/V spectral ratios from these sites have a good agreement with subsurface layers.

**Section B-B<sup>I</sup>** the idea behind this section we observed from figure 21 four anomalies of frequencies and amplification factor. We would like to have explanation for those anomalies now because they are on the same of outcrop. therefore the majority of these points on this section are located in one formation (Omdurman formations). The spectrum of site response at point M82, as we could see, has peak amplification around 0.7Hz with amplification factor around 2. As we observed before in **section A**

those points are located on mudstone have the same frequency spectrum as M82. But it has less amplification when correlated with those points at **section A**. We can explain that those points on section A are located inside the city with more structural noise which might generate high amplitude, where point M82 is far away in quite place. We therefore believe that those points here reliable H/V spectral ratio. At Points M99 and M55 show low frequency below 1 Hz, where we could expect in an area which has a basin or thick sedimentary layers under these points. That is exactly what we observed in our section **B-B'**. But the amplification seems to be wrong because they represent high amplification than we expected. The point M55 may be more reasonable considering this factor. Furthermore the layer under these points characterised by sandstone as a single layer. This may explain these spectra reflected just the frequency. The spectra are computed from points M87, M63 and M13 are shown gradually increasing the frequencies when the depth of mudstone increasing. This is contrasting to what is expected we do not here a reasonable explanation for this excerpt from the fact that this area is highly populated and hence the ground water level more be low. The sections remain until point M03 shows again the spectrum with many peaks which reflect that there is more than one layer under this point.

**Section C - C'** in this section we could see most common formations with variation of with depth layer. The site response spectrum was computed from the point M115 is mostly flat except from a peak at about 14Hz with low amplification. That may be due to thinner layer under this point.

Point M77, shows the site response spectrum with low frequency around 0.9 Hz that could be reasonable if we consider the thickness of the layer under this point. At point M38 and M59 there are high frequencies peak around 4Hz with a low frequency peak that may be due to two observations; one is there points are located on sandstone rock which is highly consolidated at a flat topography and secondly. Furthermore, since these points are located on sandstone, we compared two spectra one from the sandstone formation (D) as we made one the first part (site response with geological formation) and with second one spectrum of these points there have high frequency (D<sup>1</sup>). These two spectra are given in figure 13.2. We recognized that both have a peak at low frequency around 1Hz, while these have different amplifications. Spectrum with these points has also high frequency showing us more

than one peak. Therefore we believe the spectra of these points may reflect the sharp boundaries between two or more layers under these points. The site spectrum of site response just after that anomaly has high amplification with frequency around 1.1Hz. This does not fit with subsurface layers which are located on thick sandstone layer. Through the spectra of points M37, M36 and M10 they are represented almost constant frequency around 1.2Hz but with different amplification. This variation could be due to topography, where the thickness of the layer is 34 meters above the surrounding of the flat area. The level increases gradually, which may be the reason for having high amplifications. We expected at spectrum of point M36 to see high frequency because it located on a thinner mudstone layer under this point.

For preview sections as we could see most of site response spectrum of our section have a good agreement with subsurface layer and characterized of soil formation. Other sites from our data where are not having a crossing section may be the same case as the one have section. Most of site response spectrum from our data result and follow the expression between the fundamental frequencies and thickness of layer (Eq 6., Reiter 1990). The missing agreement between the distribution of the amplification factor at fundamental site frequency and subsurface geology is probably related to the fact that the amplification factor is poorly constrained by the used empirical approach.

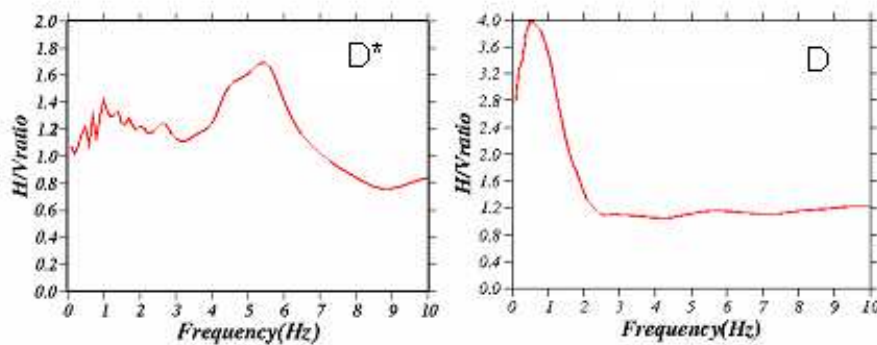


Figure13..2. Two group of the site response spectrum of Cetaceous Sandstone Omdurman formation, **D** is average site response of all sandstone sites and **D\*** is average of site response spectrum of cetaceous sandstone formation located southern Basalt area with high anomalies of frequency.

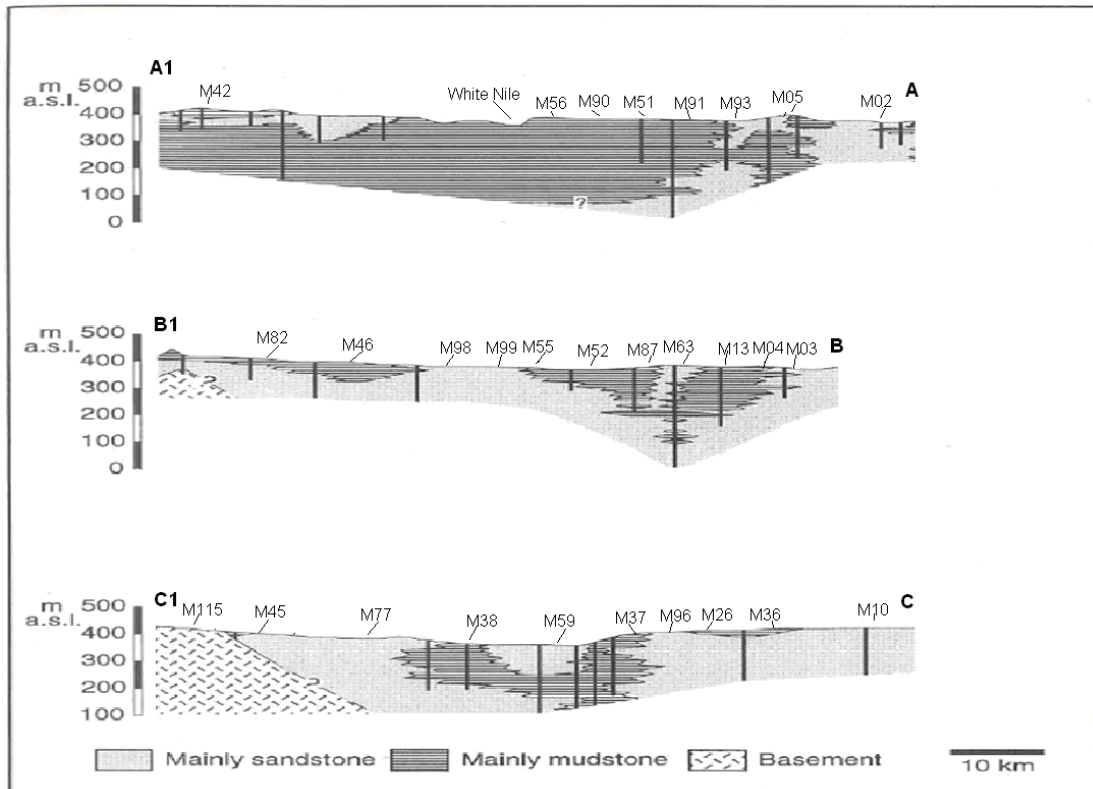


Figure 13.3 Three cross sections shows the sedimentary sequence of the Omdurman area. The locations of these are shown in figure 11.4. On top upper these sections shows the some points our measurements. [After Farah et al 1997].

## Conclusion

As we saw discussed early in chapter on seismicity and the chapter three on geology and tectonics of central Sudan in particularly the geology of Khartoum area, it is clear the study area response to local site effect. Following conclusions can be drawn:

- 1- The obtained site response mainly based on H/V spectral ratio is in generally good agreement with the underlying geology.
- 2- The complexities of the subsurface sedimentary layers are portly reflected in the H/V spectral ratio results.
- 3- The eastern bank of the White Nile shows a low frequency peak with high amplifications.
- 4- Comparison between standard spectral ratio results with the H/V spectral ratio on noise and the weak-motion show poor correlation. This may be due to the earthquake location with response to the recording stations that may not be ideal.

## Acknowledgements

This work would not have been possible without my supervisors Professor Kuvvet Atakan and Professor Jens Haskov, thank you very much for your guidance, support and encouragement during the preparation of this thesis.

I want to say a “great thank you” to Nada Bushra and Dr. Osman for showing me the way to apply for graduate studies in the University of Bergen.

I would like to thank the Norwegian State Educational loan for funding me throughout my studies.

I would also like to thank the people in the Seismology Research Institute in Sudan for helping me in my field work. Special thanks go to Mr. Bader Eldeen for his efforts to help me during the survey.

I wish to express my gratitude towards the people of the Sudanese Seismological Network, Geological Research Authority of Sudan (GRAS) for giving me data. Special thanks to Mr Alhadi for fixing my instruments.

Many thanks go to Mohammed Raessi and Aleksandre kandilarov for helping me in producing the maps with the final results.

Many thanks also go to Louise Wedderkopp Bjerrum , Asude Arslan, Hlompho Malephane, Zoya Zarifi, Gerard and the people of Cake-Club.

## References of PART II

Atakan, k, Bard, P-Y., Kind, F., Moreno, B., Roquette, P., Tendo A., and the SESAME Team (2004), j-SSAME: A standardized software solution for the H/V Spectral ratio Technique. Proceedings of the 13<sup>th</sup> World conference on the Earthquake engineering. Paper No 2270, 1-6 August 2004, Vancouver, Canada, 37pp.

Asi, A. (2000), GBV-116/316(W) operation Manual, GeoSIG Ltd., Glattbrugg.

D. G. Almond 77 - <http://www.jstor.org/view/00804614/ap000572/00a00010/0>.

Igor A. Beresnev, Edward H. Field, Koen Van Den Abeele, and Paul A. Johnson 1994. Magnitude of nonlinear sediment response in Los Angeles Basin during the 1994 Northridge, California, Earthquake. Bulletin seismological society of America August 1998. Vol. 88. No. 4. pp. 881-1097.

Nakamura, Y., 1989. A method for dynamic characteristics estimation of subsurface using microtremor on the ground surface. QR of RTRI 30(1)

Yutaka Nakamura 12WCEE 2000. Clear identification of fundamental idea of Nakamura's technique and its application.

Huey-Chu Huang and Ta-Liang Teng 1999. An Evaluation on H/V Ratio vs. Spectral Ratio for site – response Estimation Using the 1994 Northridge Earthquake Sequence. Pure and applied Geophysics. Pure appl. Geophys. 156 (1999) 631-649 0033\_4553- 194 \$ 1.50 +0.20/0

S.K.Singh, E. Mena, and R. Castro. 1988. Some aspects of source characteristic of 19 September 1985 Michoacán earthquake and ground motion amplification in and near Mexico City from strong motion data. Bulletin of the Seismological Society of America- Vol. 78, N. 2, April 1988, PP.401-1035.

D.H. Lang and J.Schwarz 2005 - Instrumental subsoil classification of Californian strong motion site based on single- station measurement  
[edac.biz/fileamin/Image\\_Archive/PDF-Documents/8NCEE\\_Lang\\_Schwarz.pdf](http://edac.biz/fileamin/Image_Archive/PDF-Documents/8NCEE_Lang_Schwarz.pdf)

I. M. Idriss and H. Bolton Seed 1968. An analysis of ground motions during the 1957 San Francisco earthquake- Bulletin of the Seismological Society of America; December 1968; v. 58; no. 6; p. 2013-2032

Unal Diken and Mete Mirzaoglu 2005. The seismic microzonation map of Yenishir-Bursa, NW of Turkey by means of ambient noise measurements. Journal of Balkan geophysical Society, Vol 8, No.2, May,2005,p. 53-62.

Navarro et al 2001. Surface soil Effects study using short- period Microtremor Observation in Almeria City, Southern Spain. Pure and Applied Geophysics.158 (2001) 2481-2947 0033-4553/01/122481-17 \$ 1.50+1.20/0

Mohammed I A, Wang Jiaying, Liu Tianyou and Farwa D G 2002. Sedimentary Basins in the Western White Nile, Sudan, as Indicated by a Gravity Survey Journal of China University of Geosciences, vol. 13, No, 3 p, 289-296



Jens Havsko and Gerardo Alguacil 2004. Instrumentation in Earthquake Seismology, chapters 3, 4, 5 and 7. © 2004 Springer- ISBN 1-4020-2968-5(HB)

Igor A. Beresnev and Kuo-Liang Wen 1996. Nonlinear soil response A reality. Bulletin of the Seismological Society of America; December 1996; v. 86; no. 6; p. 1964-1978

Kuo-Liang wen Tao-Ming Chang, Che-Min Lin and Hsien –Jen Chiang 2006. Identification of Nonlinear site Response Using the H/V Spectral Ratio Method. Terr.Atmos. Ocean. Sci., Vol.17,No.3,533-533-546, September 2006.

D. Assimki, J. Steidl 2005. Inverse analysis of weak and strong motion downhole array data from the Mw 7.0 Sauriku –Minami earthquake. .Soil Dynamic and Earthquake 27(2007)73-92.

Byau- Heng chin and Keiiti Aki 1991. Simultaneous study of the source, path, and site effects on strong ground motion during the 1989 Loma Prieta earthquake: A preliminary result on pervasive nonlinear site. Bulletin of the Seismological Society of America; October 1991; v. 81; no. 5; p. 1859-19884

Sandra H. Seale and Ralph J. Archuleta 1989. Site amplification and attenuation of strong ground motion. Bulletin of the Seismological Society of America; December 1989; v. 79; no. 6.

Lisa A. Wald and Jim Mori. Evaluation of Methods for Estimating Linear Site-Response Amplifications in the Los Angeles Region 2000. Bulletin of the Seismological Society of America; December 2000; v. 90; no. 6B; p. S32-S42; DOI: 10.1785/0119970170

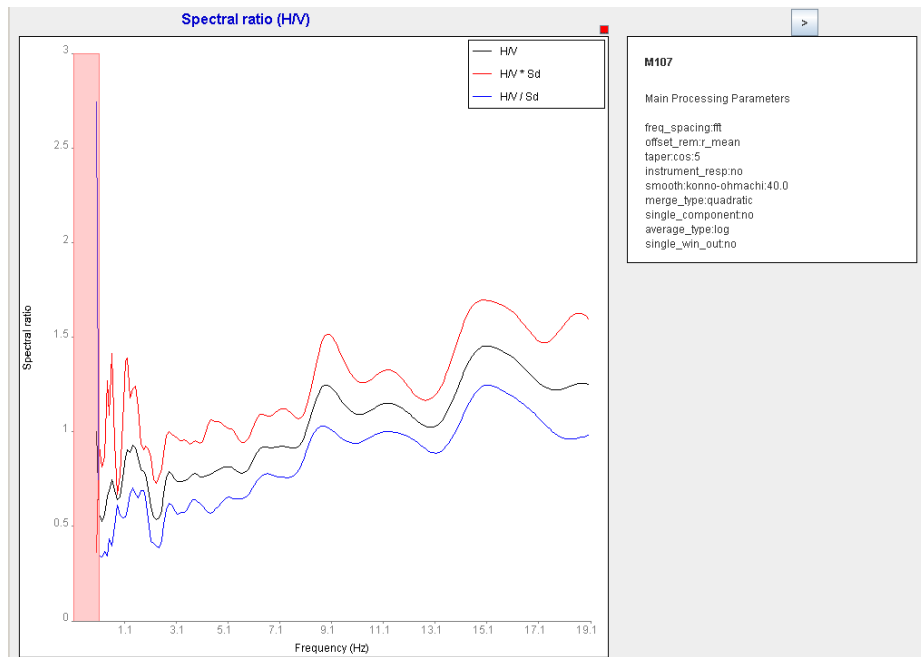
N. Theodulidis, P.-Y. Bard, R. Archuleta and M. Bouchon 1996. Horizontal-to-vertical spectral ratio and geological conditions: The case of Garner Valley Downhole Array in southern California 1996. Bulletin of the Seismological Society of America; April 1996; v. 86; no. 2; p. 306-319

E. A Farah , O.M. Abdullatif, O.M.Kheir and N. Barazi 1997- Groundwater resources in a semi- arid area: a case study from central Sudan –vol,25 No 3, pp-453-466,

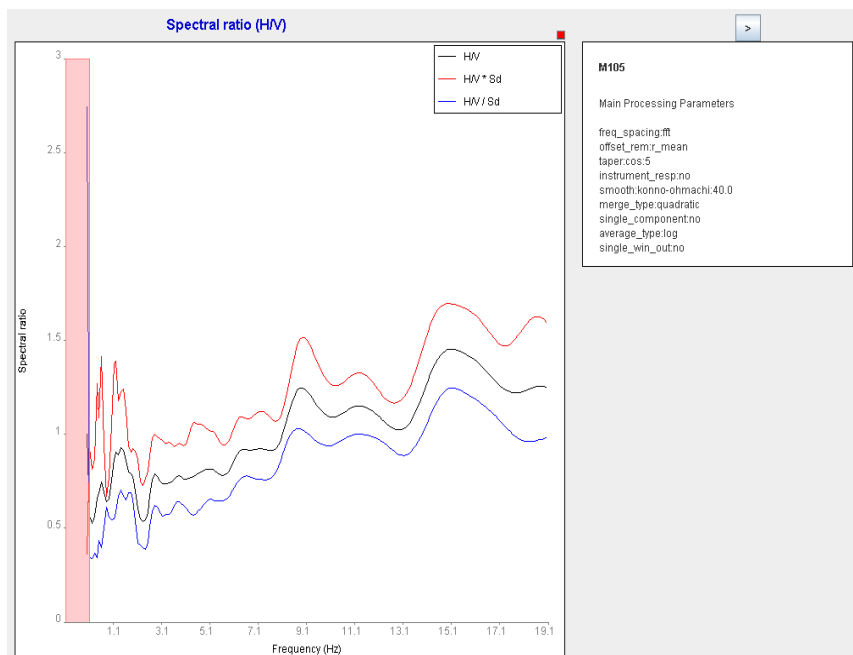
Aleksandre- 2005- Site effects assessment using H/V spectral ration in Bergen – Norway and Plovdiv- Bulgaria (master thesis –2005)

E:A.Farah , E:M:A Mustafa, H:Kumai- Source of ground water recharge at the confluence of the Niles Sudan - Environmental Geology 39(6) April 2000

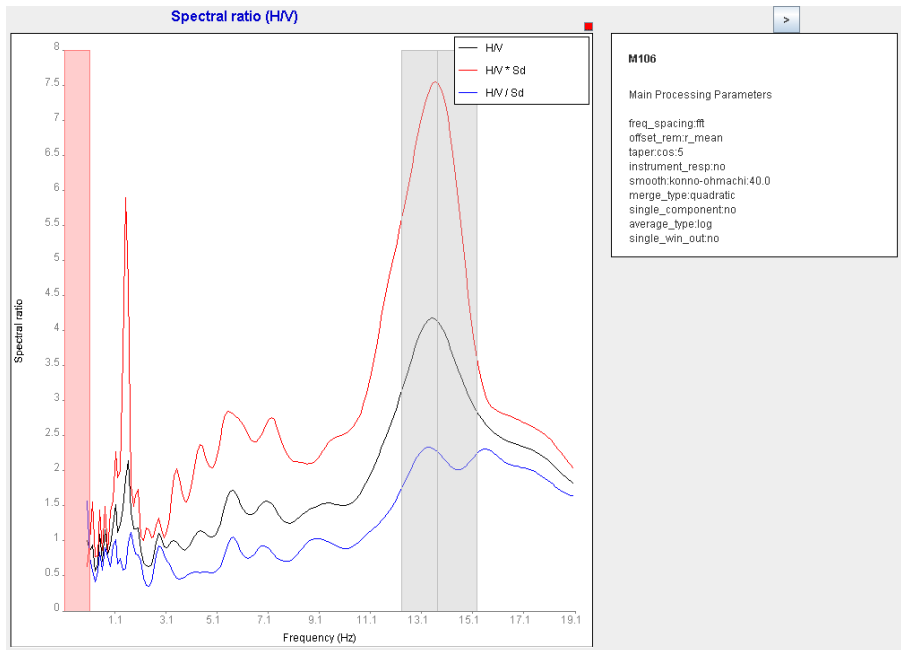
## Appendix A



*This figure shows the site response spectrum computed at points M107, located in basalt rock in central of study area, all show high frequency around 15 Hzr.*



*This figure shows the site response spectrum computed at points M105 located in basalt rock in central of study area, all show high frequency around 15 Hzr.*



*This figure shows the site response spectrum computed at points M106 located in basalt rock in central of study area, all show high frequency around 15 Hzr.*



*This figure shows a view of the forthcoming AlMogran Central Business District at the confluence of the White and Blue Nile in Khartoum.*

## Appendix B

Parameters	Noise script	Signal of S and P Waves script
Selection criteria 1:P, 2:S, 3: from S and P , 4:abs	4	2
Start	0.1	1
Windows length	10,1,1	10,1,1
Number of time to smooth	5	5
Gain factor of channel 1	1	1
Noise spectrum 0:no 1:yes	0	1
Make relative spectra 1:yes 0:no	1	1
Plot pics	1	1
Frequency band to use	0.5 10	0.5 10
Response removal: 0:none, 1:displ., 2;velocity ., 3: acceleration	0	0
Rotate: 0:no, 1:yes	0	0
Q0 and qalpha	0,0,0	0,0,0
Distance correction	0	1
Minimum correlation and sn for kappa	0,0	0,0
Velocity and density	0.0 0.0	0.0 0.0
Magnitude spectrum	0	0
Station and components format	MRKH SE/SZ or SN/SZ	MRKH or SLAT

Table 1. Two scripts of the noise and wave parameters for calculating the spectra in the SPEC program (SEISAN software).

We describe a few commons in spectra from SEISAN manual [Havskov and ottemoller 2005], used the SPEC program which there are two file used to calculated the local site effect in study area; one we used on noise recording and another used the signal with p and S-waves. As we could see above the parameters are used for those two files. We follow the description which is mentioned on SEISAN manual show below.

### The parameters:

**Selection criteria:** determinate how the start the time window is selected. 1: Start with the P-arrival time, 2: Start with the S-arrival time, 3: Start the S- arrival time calculated from the P-arrival time assuming a P to S velocity ratio of 1.78, 4: Start with second after the origin time as given in the CAT file header. When using a P or S- time for start of window, the program uses the first P or S phase found in the CAT file for a given station.

**Start.** Use 1.0 the window shall start exactly at the phase time picked. .

**Window length:** window length in sec for both signal and noise. More than 1, spectra will be made in several windows following the first windows and average spectra will be made. This option can only used if a selection criterion is 4. Used for noise studies or Nakamura studies.

Overlap: windows can overlap (factor>1.0). e.g. 0.9 is equal to 10% overlap.

**Number of times to smooth:** number of time to smooth, 0 means no smoothing.

**Gain factor of the channel 1:** factor that the spectral level for channel 1 is multiplied with. This can be used if the response shape is the same for the two channels and only the levels are different.

**Noise spectrum:** option used to displace the spectrum in window.

Make relative spectra: using to make relative spectra either one station with two components or relative to two stations.

**Plot pics:** the phase pics in the CAT files spec.inp will be plotted.

**Frequency hand used:** lower and upper frequency bands for the spectral plots.

**Response removal:** It is contain the many options that we can calculate displacement, velocity, acceleration power spectral density and determine kappa, more formation about these factors see SEISAN manual version 8.1, [Havskov and ottemoller 2005] . Here we considering out of script (spectra).

**Rotate components:** the option use to adjust our horizontal components if they have specified. Here we used parameter zero because there are no rotation is done.

**Q0, qalpha and kappa:** q-correction  $Q=Q0^{**}qalpha$  used for spectral correction. However here we considering the no Q-correction, because we not used response removal.

**Distance correction alpha:** the spectral amplitude are multiplied by  $R^{**}$  (distance correction) if the distance is zero. That the geometrical spreading and magnitude (moment magnitude). However here also at specs of noise is zero since there is no magnitude determined. For single of body waves we used one.

**Minimum correlation coefficient and minimum signal to noise ratio for kappa:** the minimum correlation coefficient and signal to noise ratio for an event to be included in average kappa. The coefficients are from the linear fit to the flat part of the spectrum. Here we used zero as minimum correlation coefficient of the ratio.

**Velocity and density:** velocity (km/sec) and density (g/cm\*cm) used for calculated moment spectra. Here we used 0, 0 since there no moment spectra are calculated.

**Magnitude spectrum:** this option used if the spectrum level is converted to moment magnitude.

**Stations and components:** station –component pairs used, one pair per line, format 4(a4.1x).

The displace of spectra has three values;

Average in spec (Q): for frequency the average linear 1/Q and corresponding sd is calculated. The upper and lower bounds are calculated by subtracting and adding the sd. These values are then converted back to Q and finally the log is taken. Only the good individual values are used. There is a possibility that the lower bound becomes negative. In that case, the log Q is set to zero. Because the average and upper and lower curves should be symmetric.

Power spectrum: for each frequency the dB values are averaged and upper and lower curves should be symmetric.

Kappa: same as for Power spectrum.

Other spectra: the linear spectra or relative spectra are averaged. The sd used in log spectra are calculated by subtracting log average spectrum from log (average spectrum+sd)

The program has option that we can show the frequency and amplification factor by click on top of average curve which we expected.

*Table 1. shows all the H/V ratio of fundamental frequency and amplification factor with the fundamental frequency on spectral ratio and amplification spectral ratio for two earthquakes.*

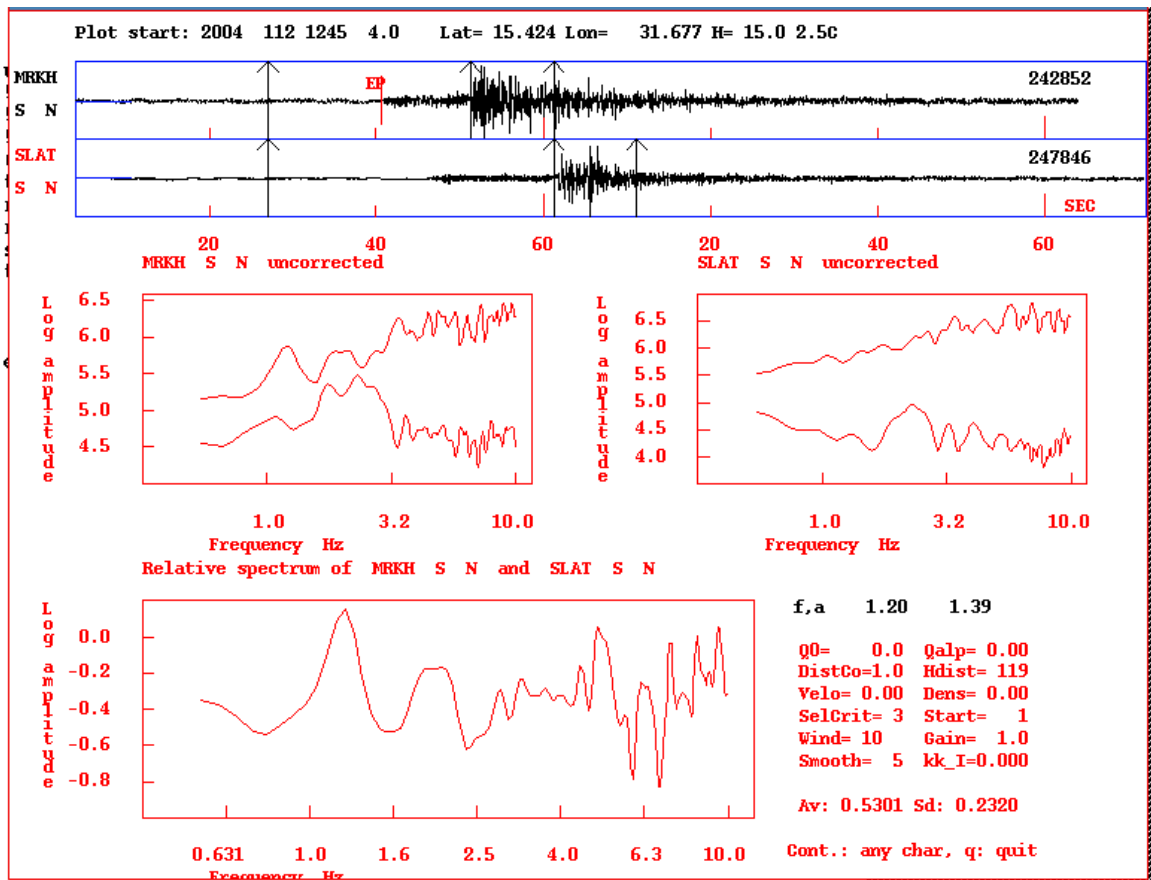
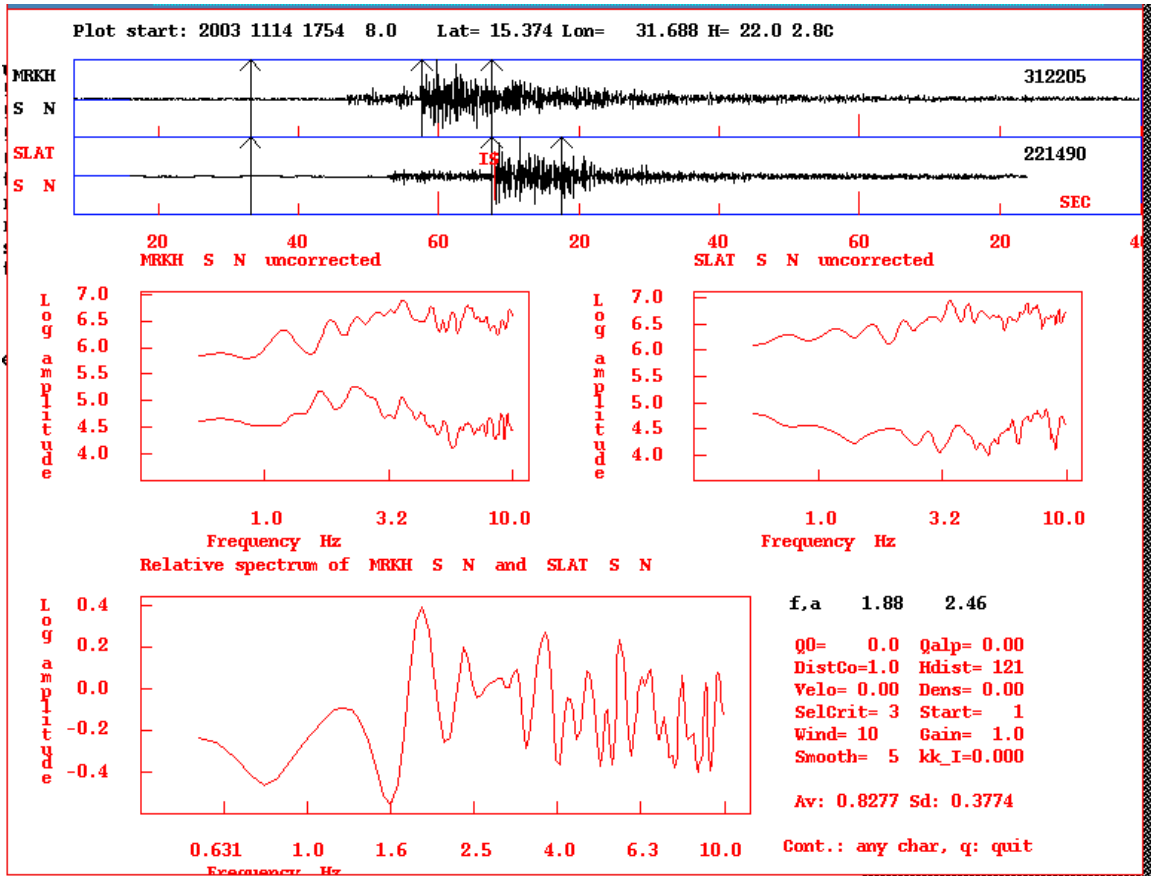
Earthquake	Relative station	Fundamental frequency on spectral ratio	Amplification on spectral ratio
S- wave			
EQU6	S MRKH n-s/S SLAT n-s	1.31	2.33
EQU10	S MRKH n-s/S SLAT n-s	0.97	5,8
EQU6+EQU11(S wave)	AVARAGE	0.97	2.92
EQU1	S MRKH e-w/S SLAT e-w	1.34	6.15
EQU2	S MRKH e-w/S SLAT e-w	1,29	6.19
EQU10+EQU6(S wave)	AVARAGE	1.33	5.97*
Earthquake	Relative station	H/V ratio of frequency	H/V ratio of amplification
EQU6	S MRKH n-s/S MRKH Z	2.49	3.68
EQU10	S MRKH n-s/S MRKH Z	2.82	4.86
EQU10+EQU6(MRKH)	AVARAGE H/V n-s	2.57	3.69*
s wave			
EQU6	S MRKH e-w/S MRKH Z	3.23	3.79
EQU10	S MRKH e-w/S MRKH Z	2.52	5.47
EQU10+EQU6(MRKH s wave)	AVARAGE H/V e-w	2.52	3.54*
Noise			
EQU6	S MRKH n-s/S MRKH Z	1.38	2.60
EQU10	S MRKH n-s/S MRKH Z	1.13	4.05
EQU10+EQU6(MRKH) (noise)	AVARAGE H/V n-s	1.10	2.66*
Noise			
EQU6	S MRKH e-w/S MRKH Z	1.69	1.62

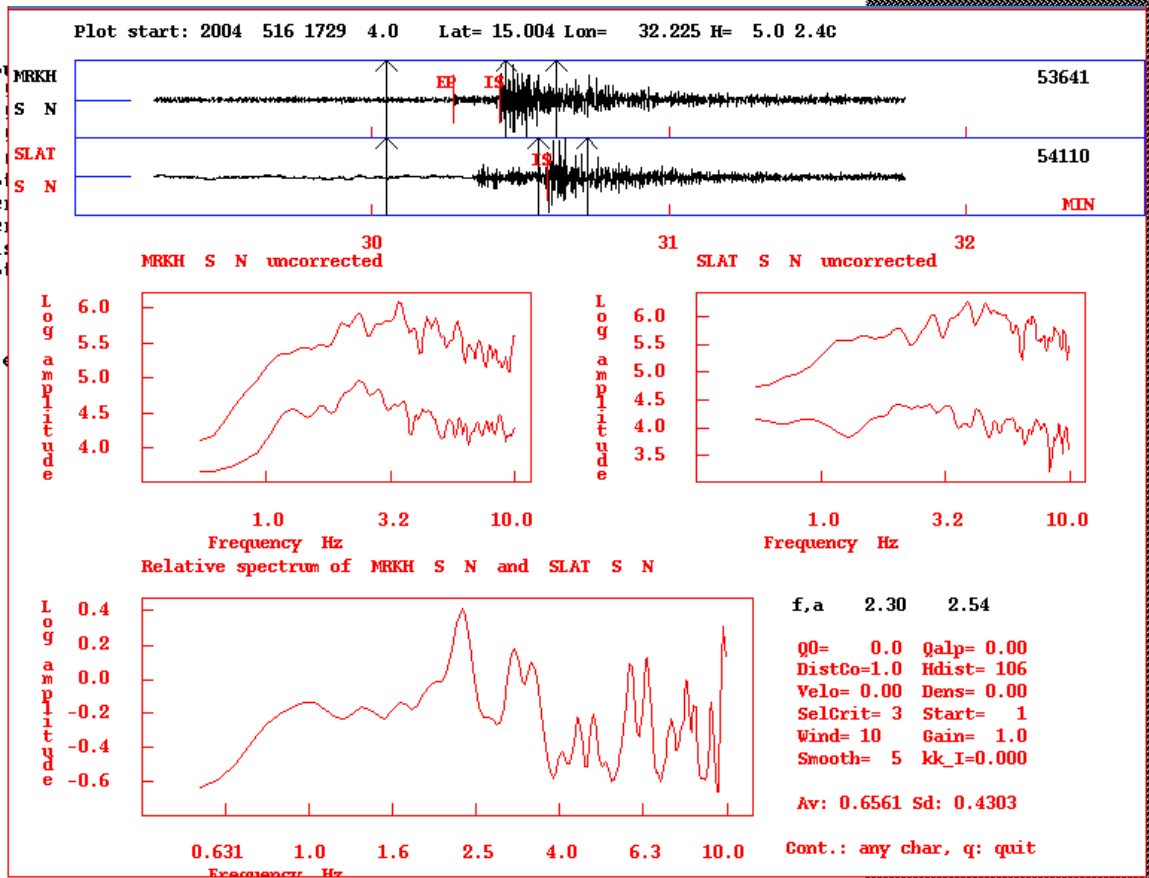
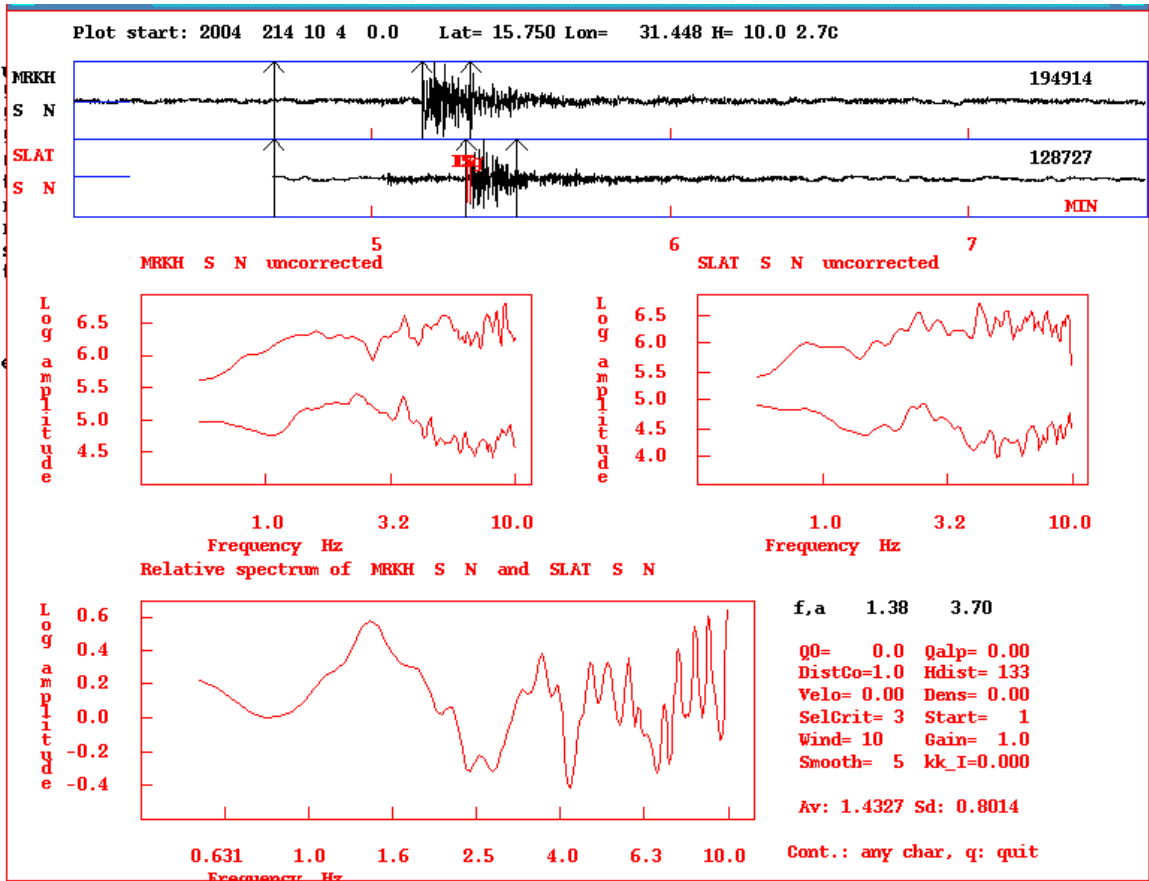
EQU10	S MRKH e-w/S MRKH Z	0.98	2.67
<i>EQU10+EQU6(MRKH)</i> (noise)	<i>AVERAGE H/V e-w</i>	<i>0.96</i>	<i>1.87*</i>
S- wave			
EQU6	S SLAT n-s/S SLAT Z	1.01	7.09
EQU10	S SLAT n-s/S SLAT Z	0.72	4.72
<i>EQU10+EQU6(SLAT)</i> (s wave)	<i>AVERAGE H/V n-s</i>	<i>1.02</i>	<i>4.15</i>
(s -wave)			
EQU6	S SLAT e-w/S SLAT Z	0.99	3.74
EQU10	S SLAT e-w/S SLAT Z	0.98	2.16
<i>EQU10+EQU6(SLAT)</i> (s wave)	<i>AVERAGE H/V e-w</i>	<i>0.98</i>	<i>3.06*</i>
noise			
EQU10	S SLAT n-s/S SLAT Z	1.41	1.83
EQU6	S SLAT n-s/S SLAT Z	0.96	2.41
<i>EQU10+EQU6(SLAT)</i> (noise)	<i>AVERAGE H/V n-s</i>	<i>1.12</i>	<i>1.90*</i>
noise			
EQU10	S SLAT e-w/S SLAT Z	1.15	3.88
EQU6	S SLAT e-w/S SLAT Z	1.75	2.94
<i>EQU10+EQU6(SLAT)</i> (noise)	<i>AVERAGE H/V e-w</i>	<i>1.16</i>	<i>2.56*</i>

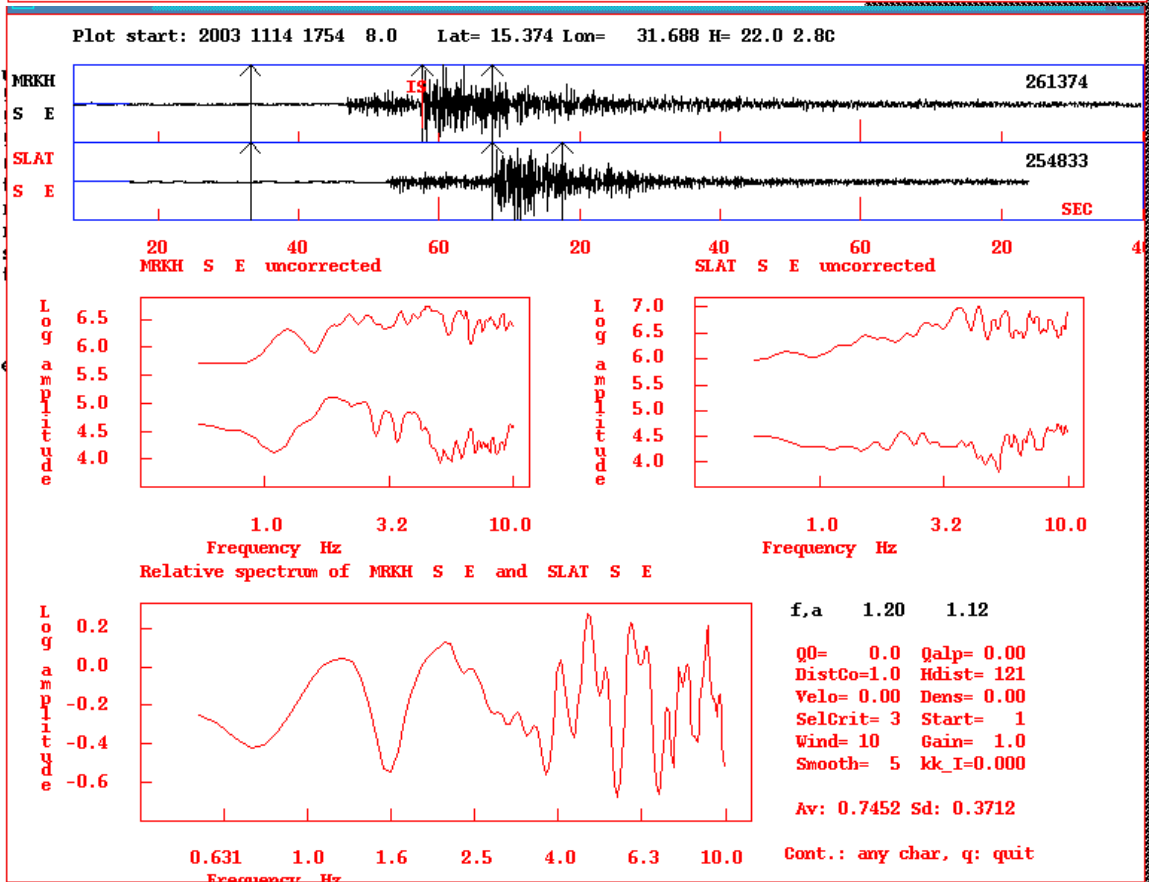
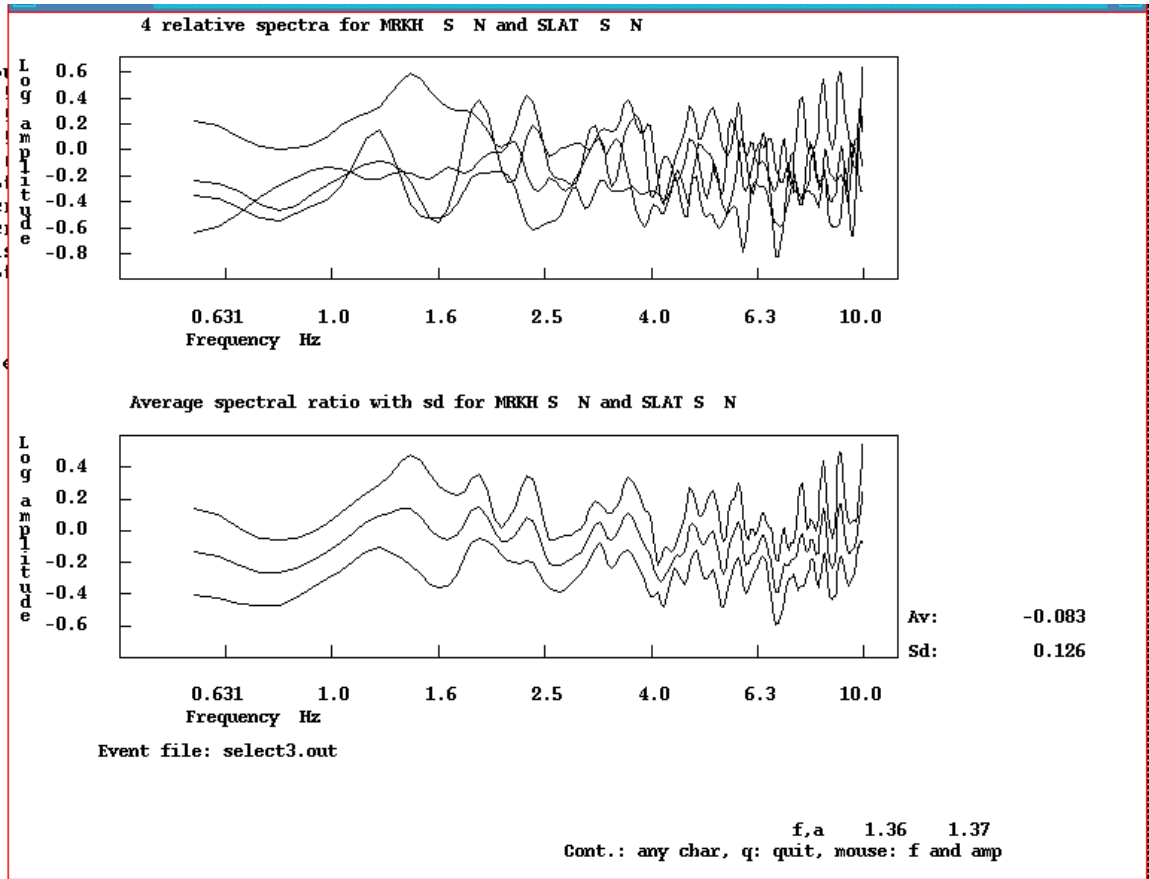
Table 2 shows the details of four standard spectral methods for four earthquakes (2, 3, 4, and 8)

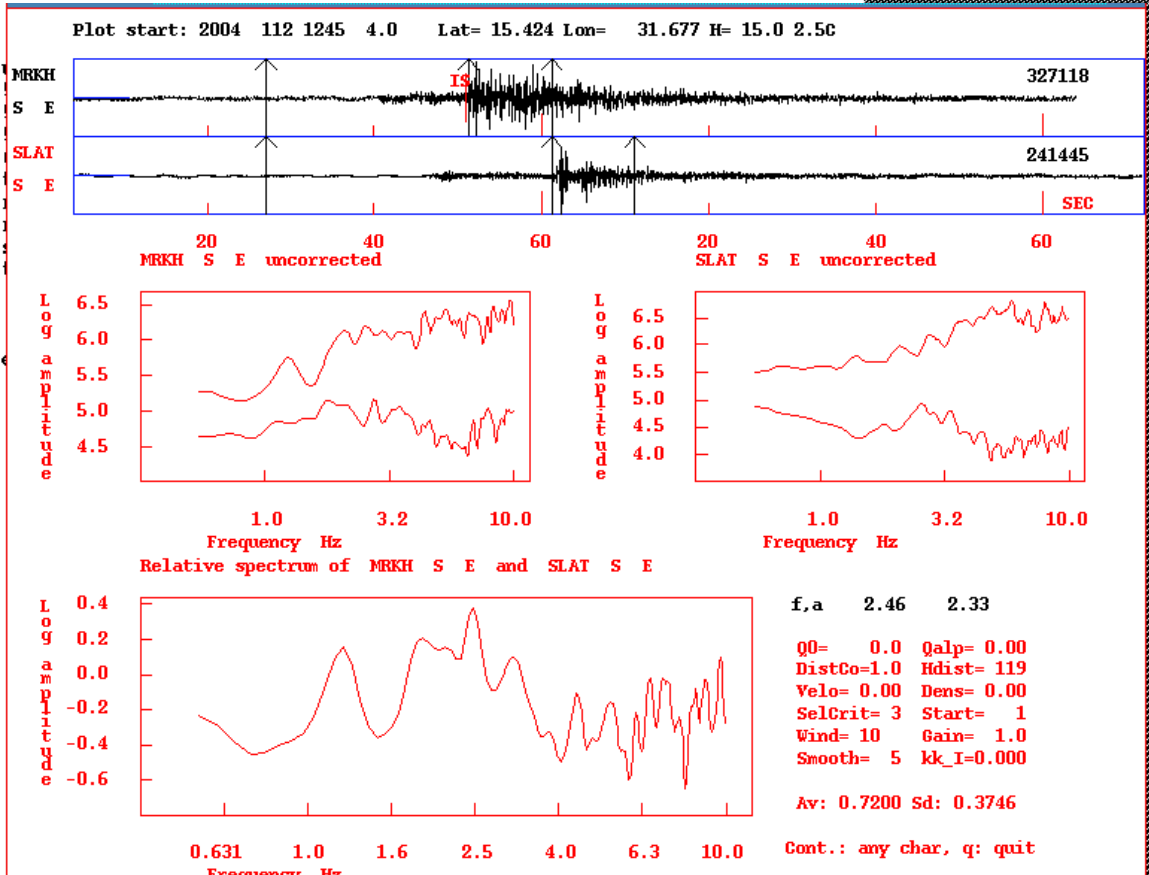
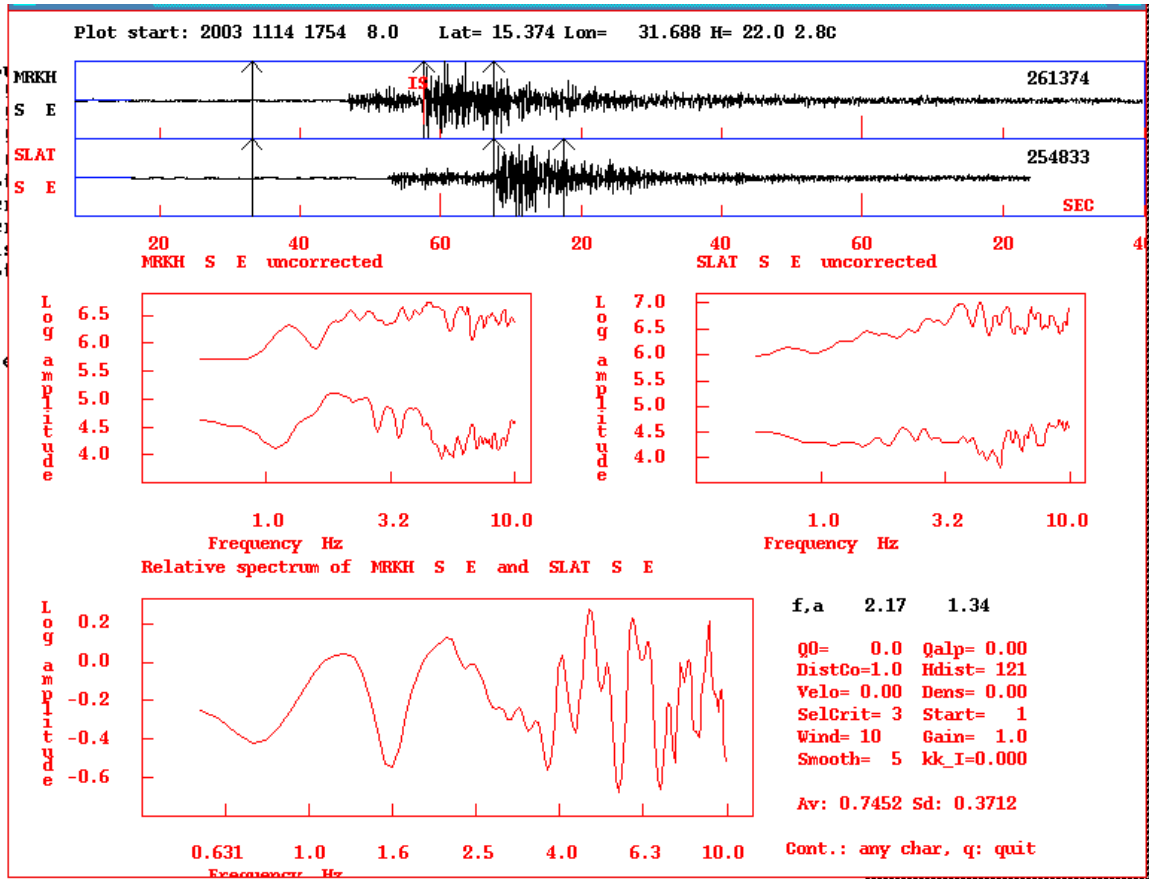
Earthquake	Relative station	Fundamental frequency on spectral ratio	Amplification on spectral ratio
S- wave			
EQU2	S MRKH n-s/S SLAT n-s	1.88	2.46
EQU3	S MRKH n-s/S SLAT n-s	1.20	1.39
EQU4	S MRKH n-s/S SLAT n-s	0.97	2.92
EQU8	S MRKH n-s/S SLAT n-s	1.38	3,70
	AVERAGE	2,30	2,54
EQU2	S MRKH n-s/S SLAT n-s	1.33	5.97*
EQU3	S MRKH n-s/S SLAT n-s	1,36	1,37
EQU4	S MRKH n-s/S SLAT n-s	1,2	1,12
EQU8	AVERAGE	2.57	3.69*
EQU2	S MRKH n-s/S SLAT n-s	2,17	1,34
EQU3	S MRKH n-s/S SLAT n-s	2,46	2,33
EQU4	S MRKH n-s/S SLAT n-s	2.52	3.54*
EQU8	<i>AVERAGE H/V e-w</i>	1,2	1,46

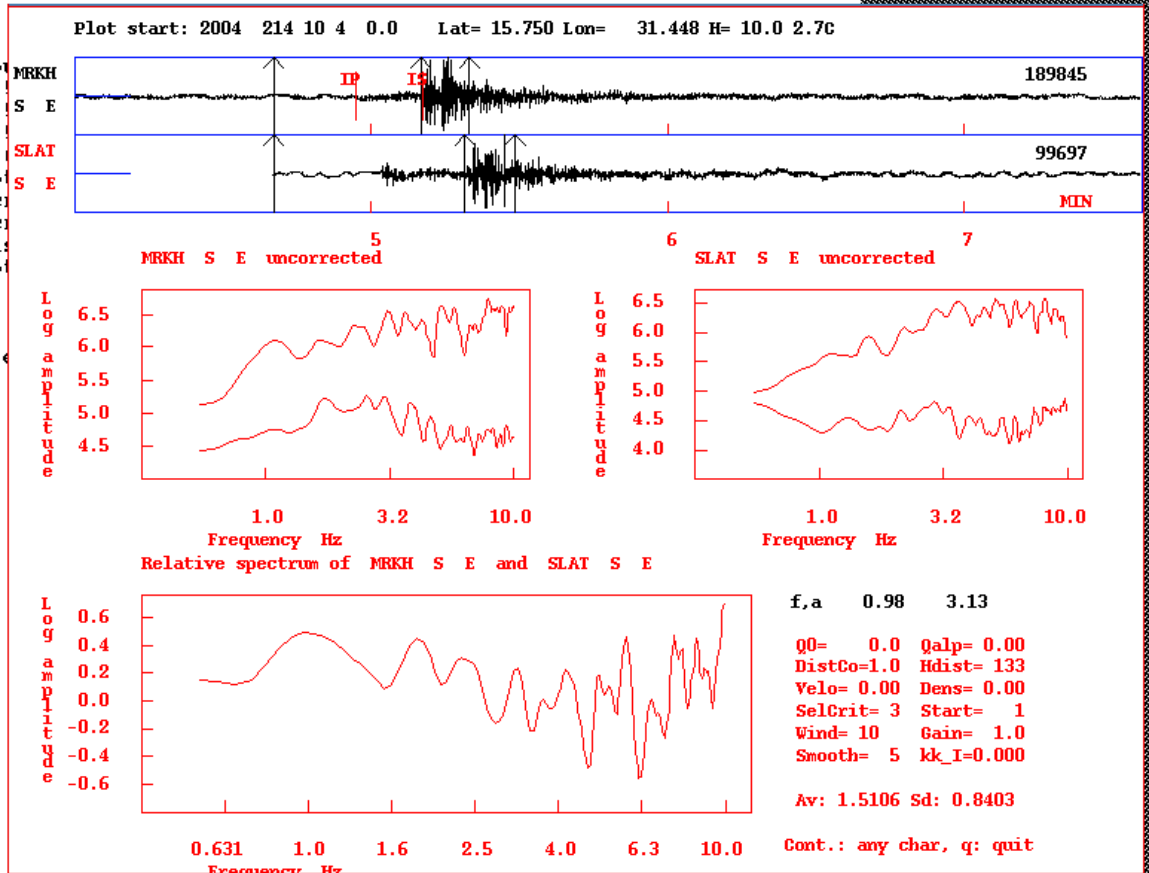
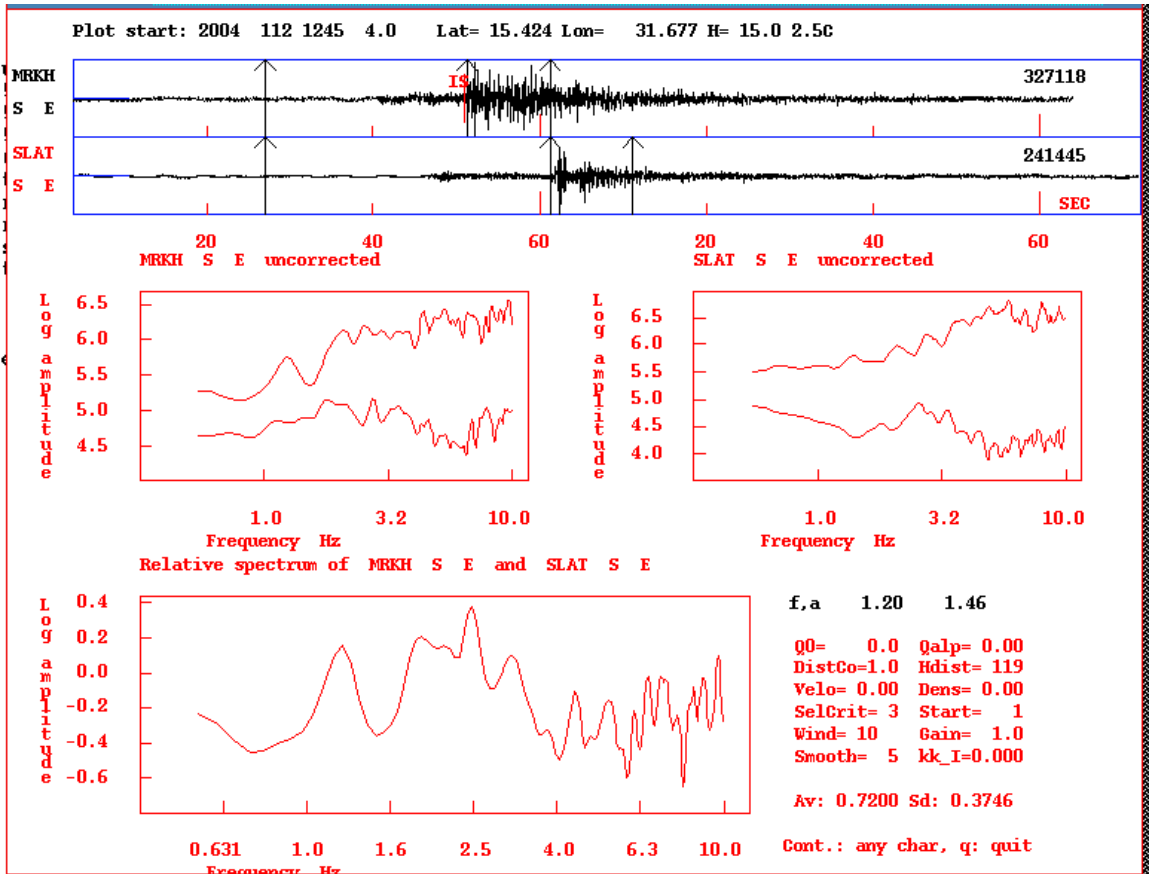




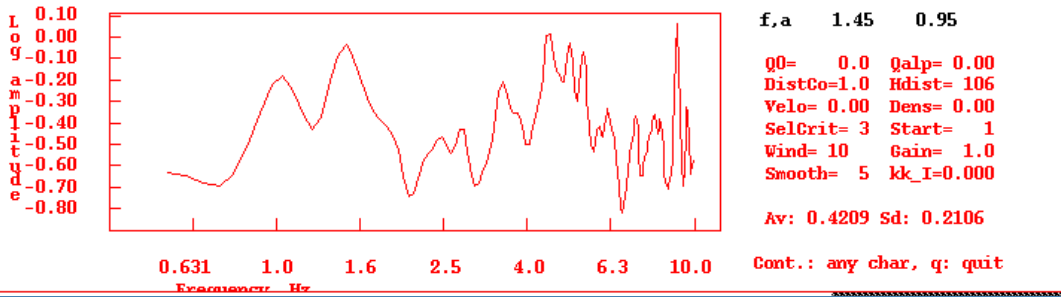
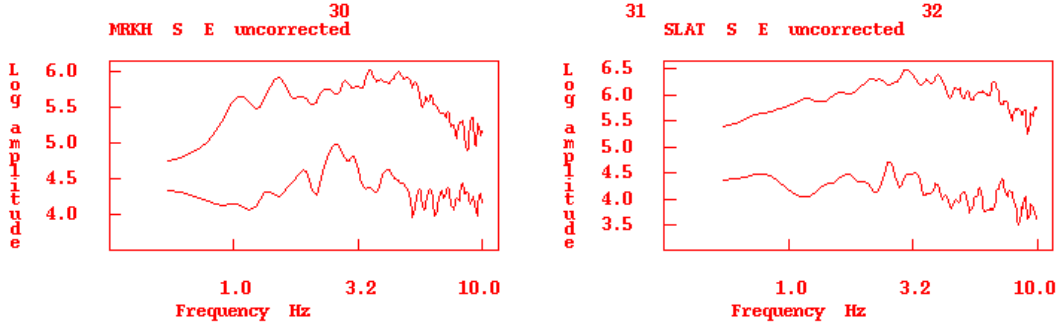
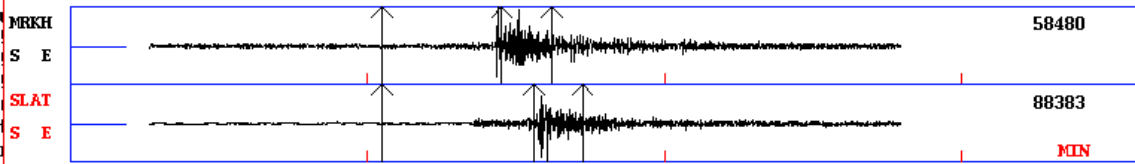




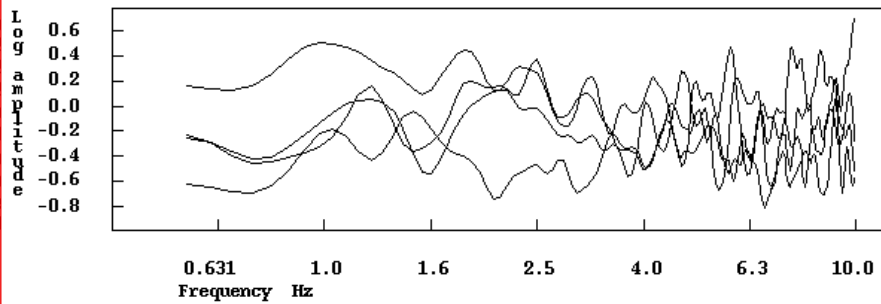




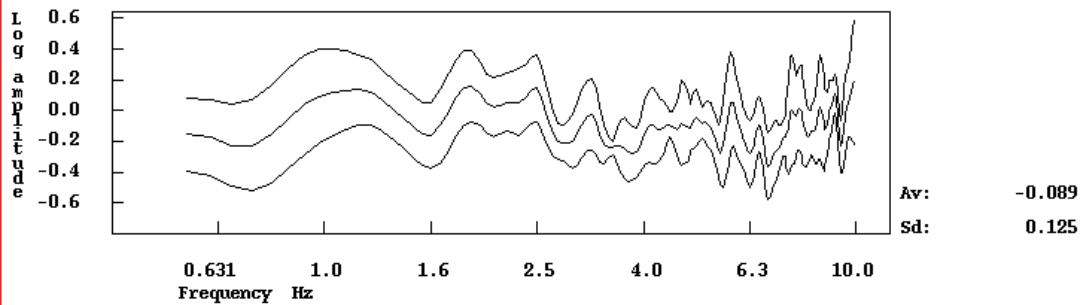
Plot start: 2004 516 1729 4.0 Lat= 15.004 Lon= 32.225 H= 5.0 2.4C



4 relative spectra for MRKH S E and SLAT S E

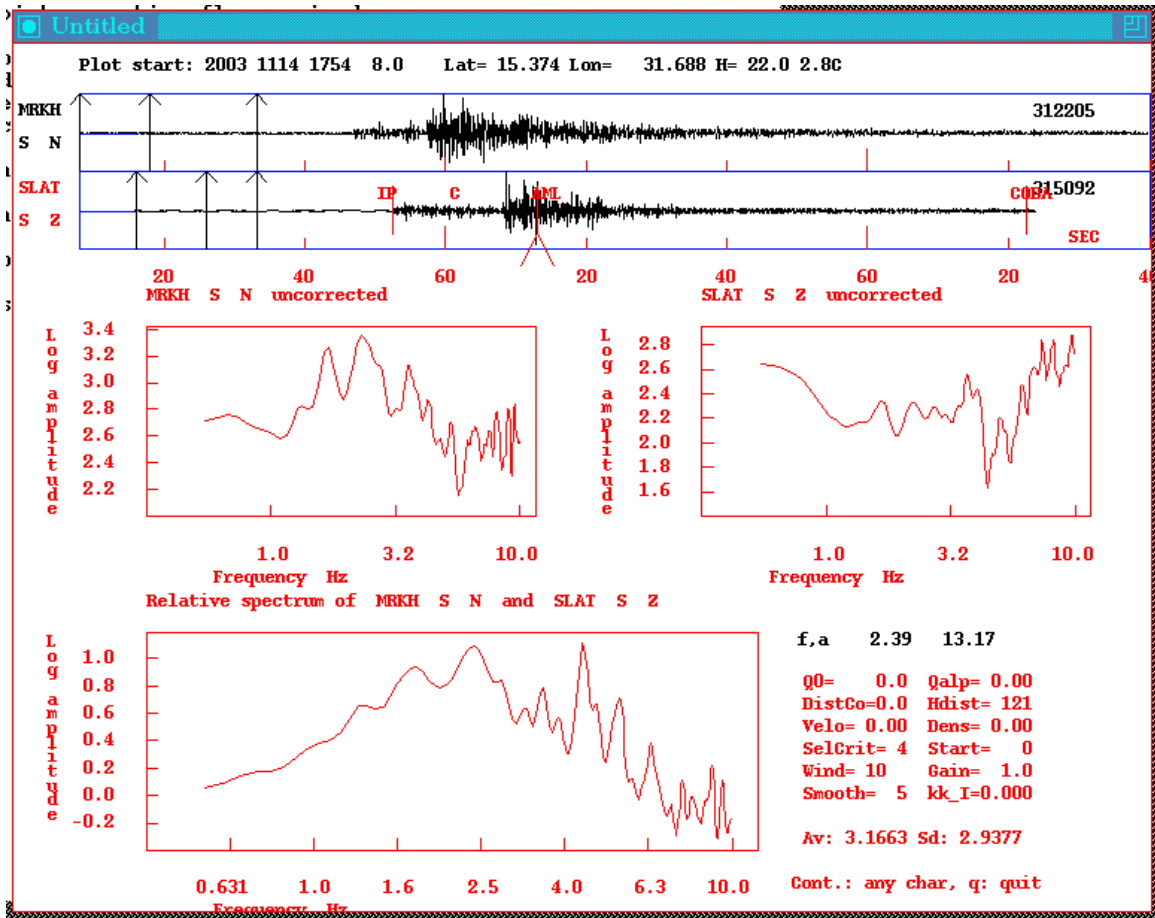


Average spectral ratio with sd for MRKH S E and SLAT S E



Event file: select3.out

f,a 1.12 1.37  
 Cont.: any char, q: quit, mouse: f and amp



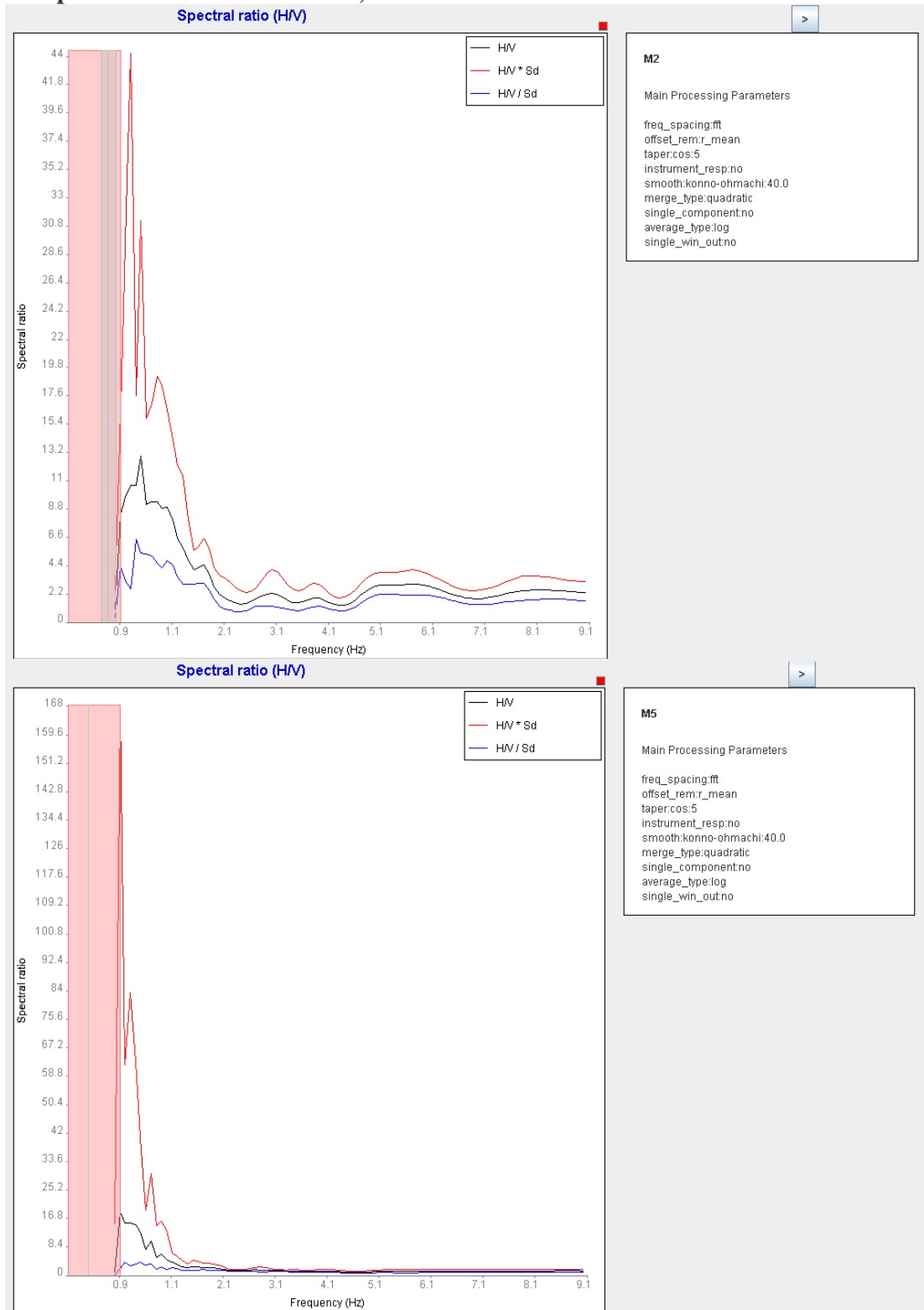


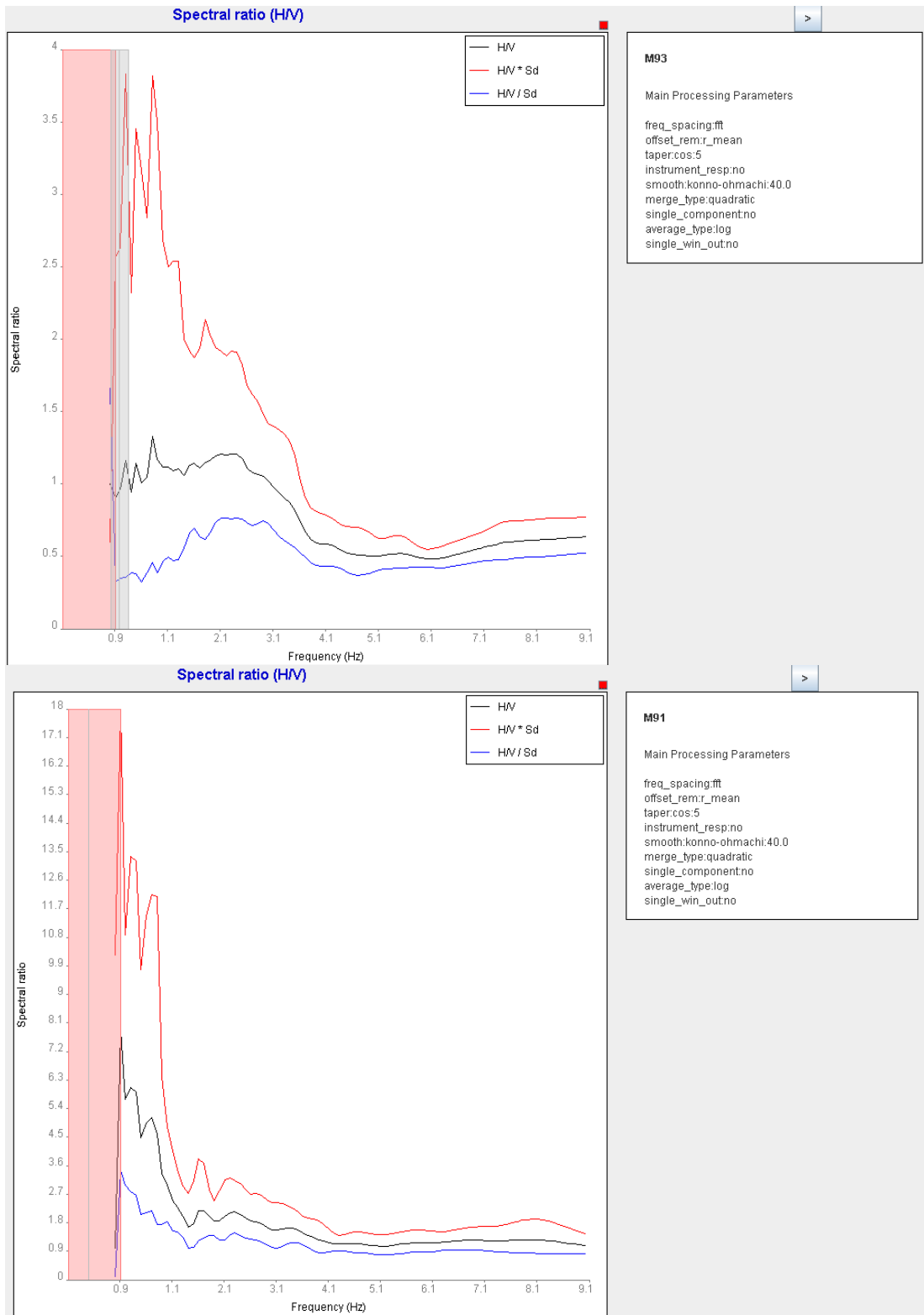


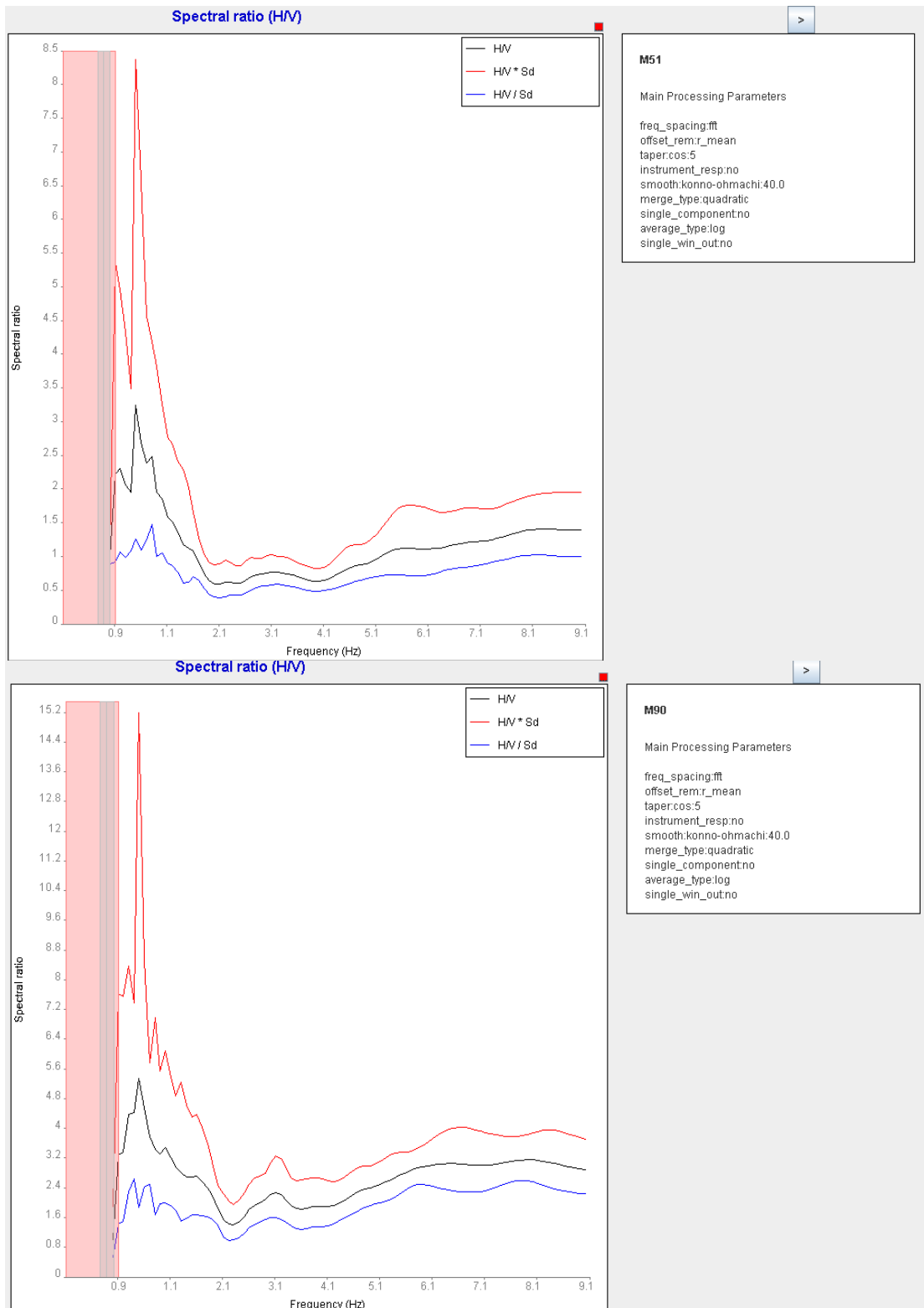
## Appendix C

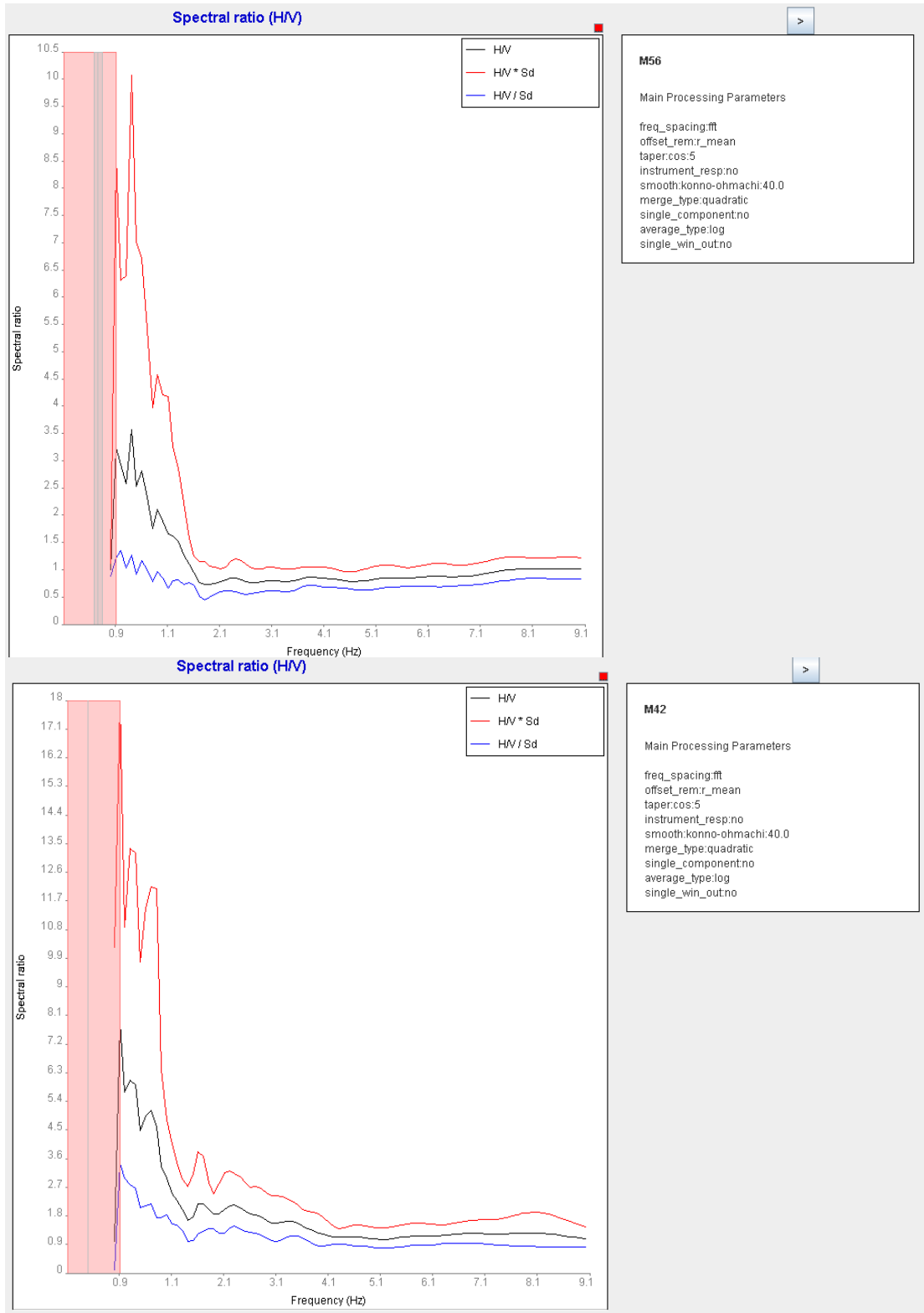
Three cross sections (AA1, BB1 and CC1) shown in figure 11.4. That we described some of points on each section and correlation the subsurface layer with spectrum of these points on each section.

### The points on the section A-A1;

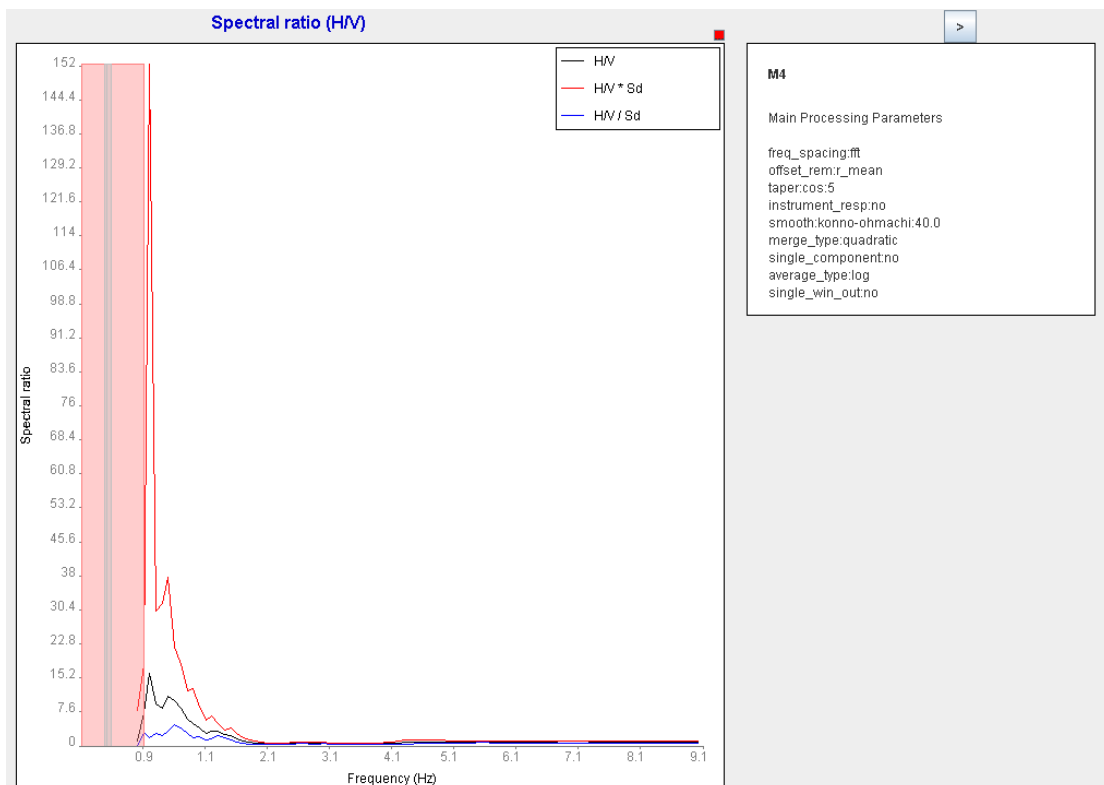
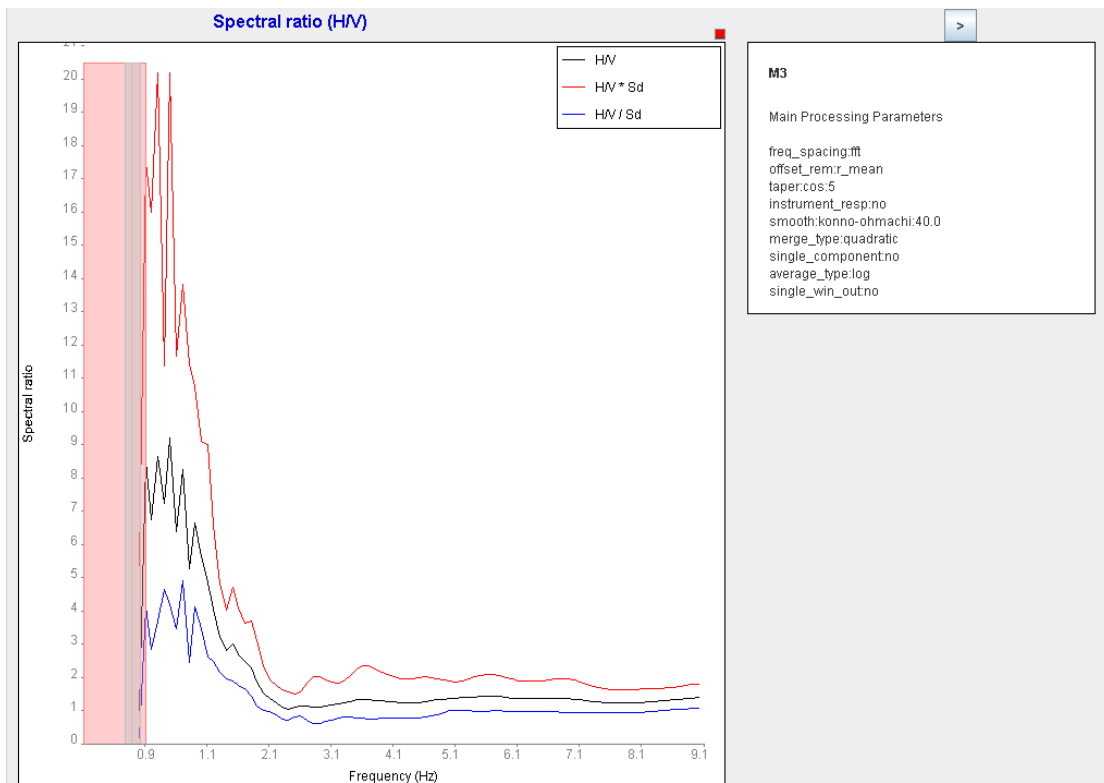


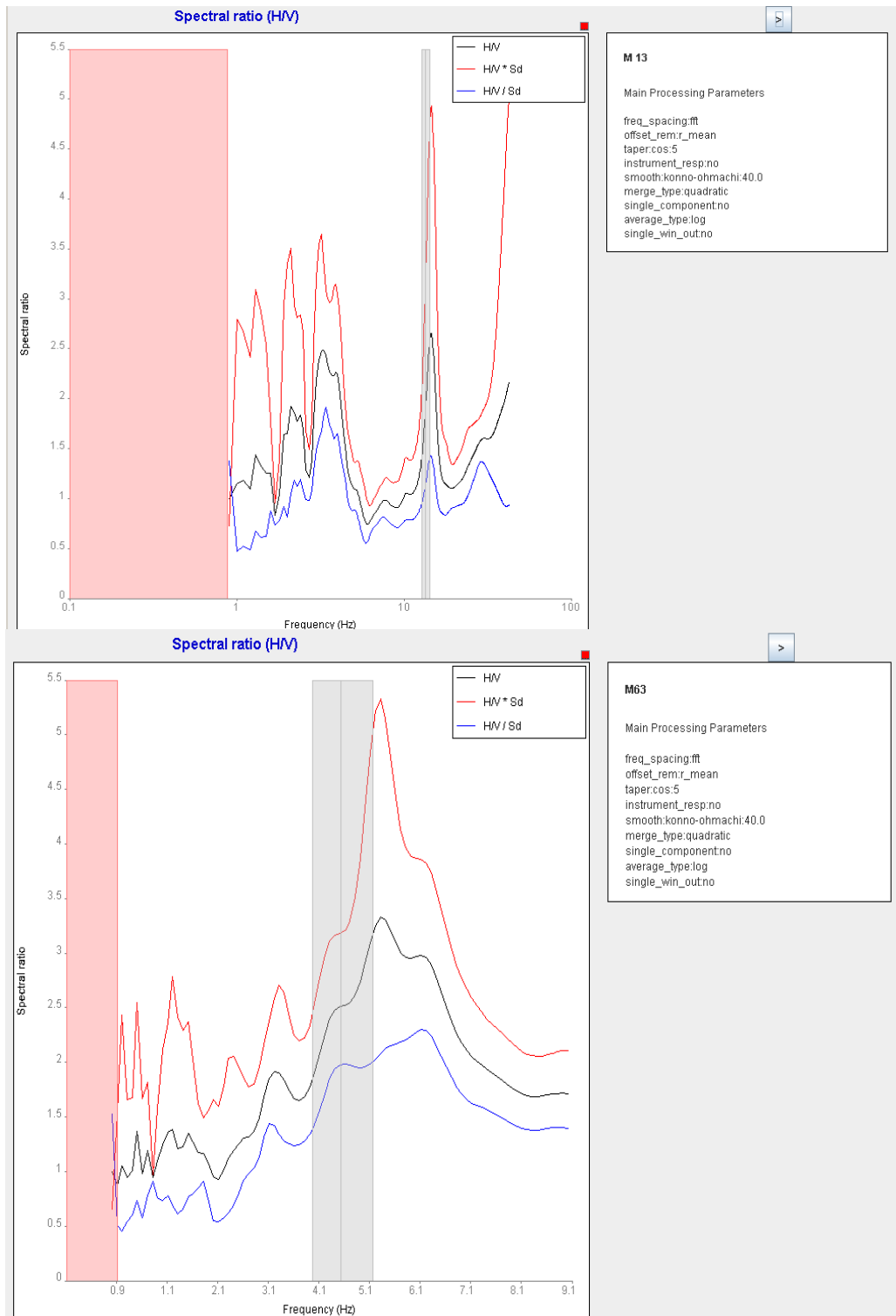


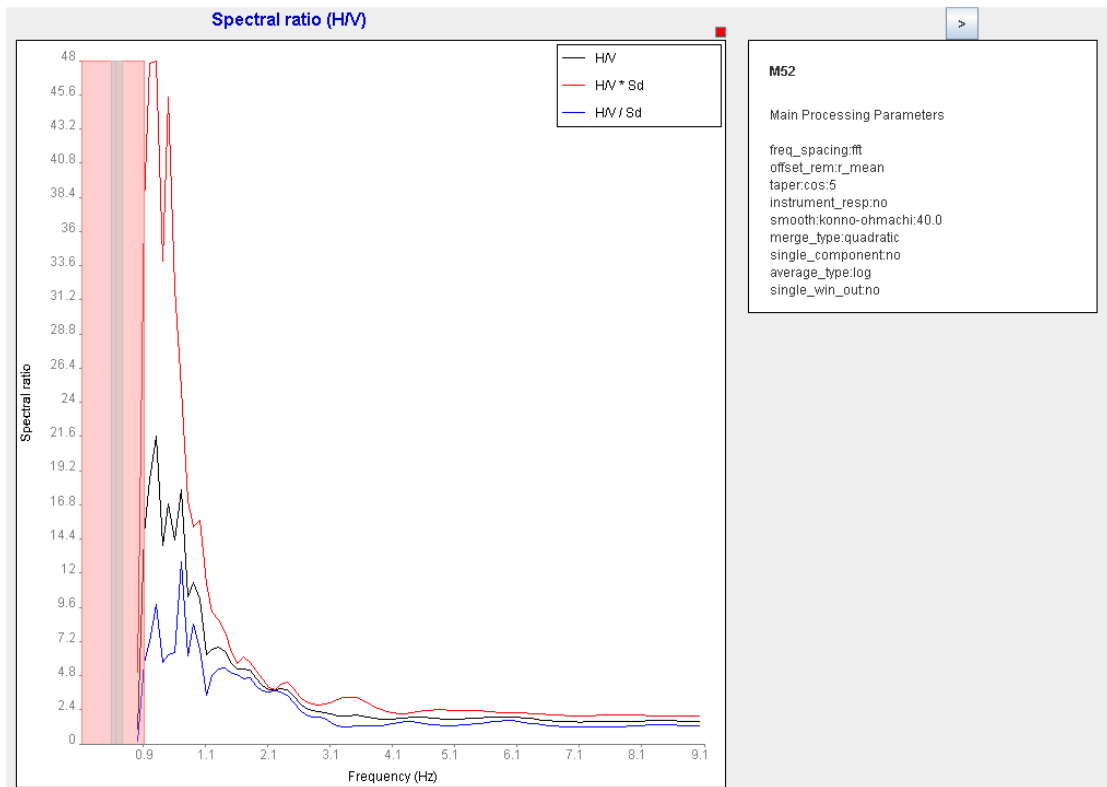
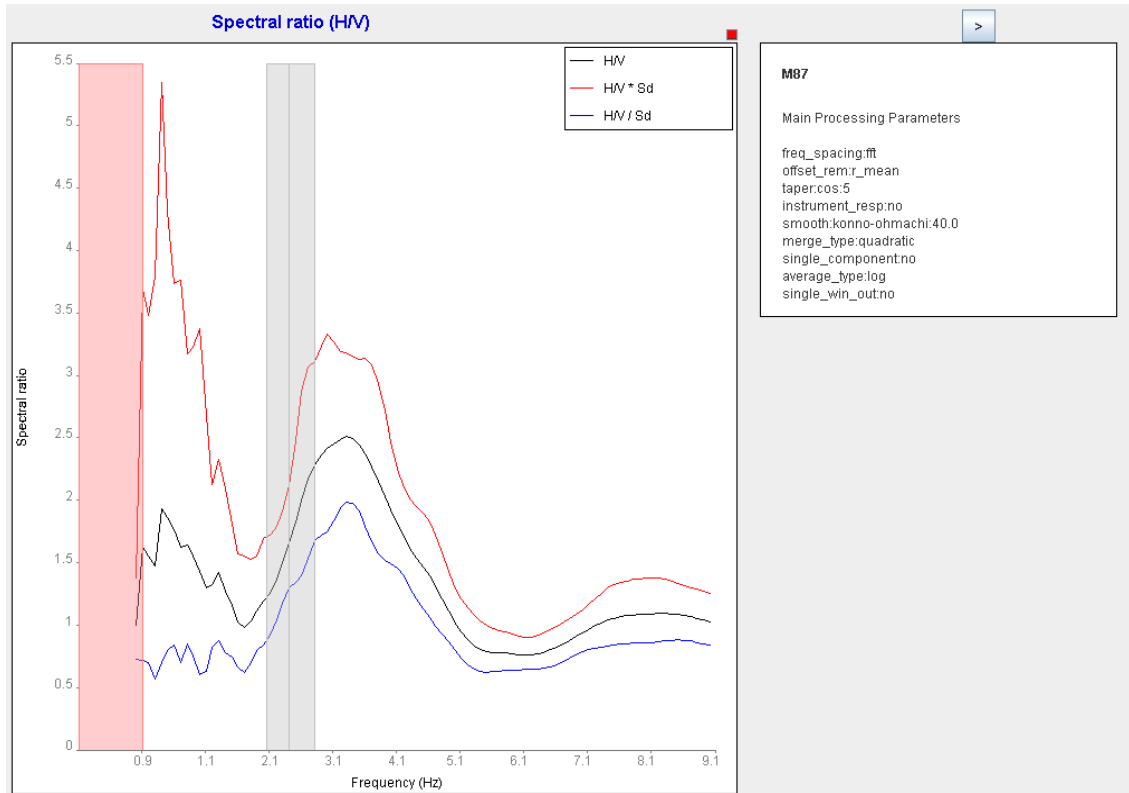


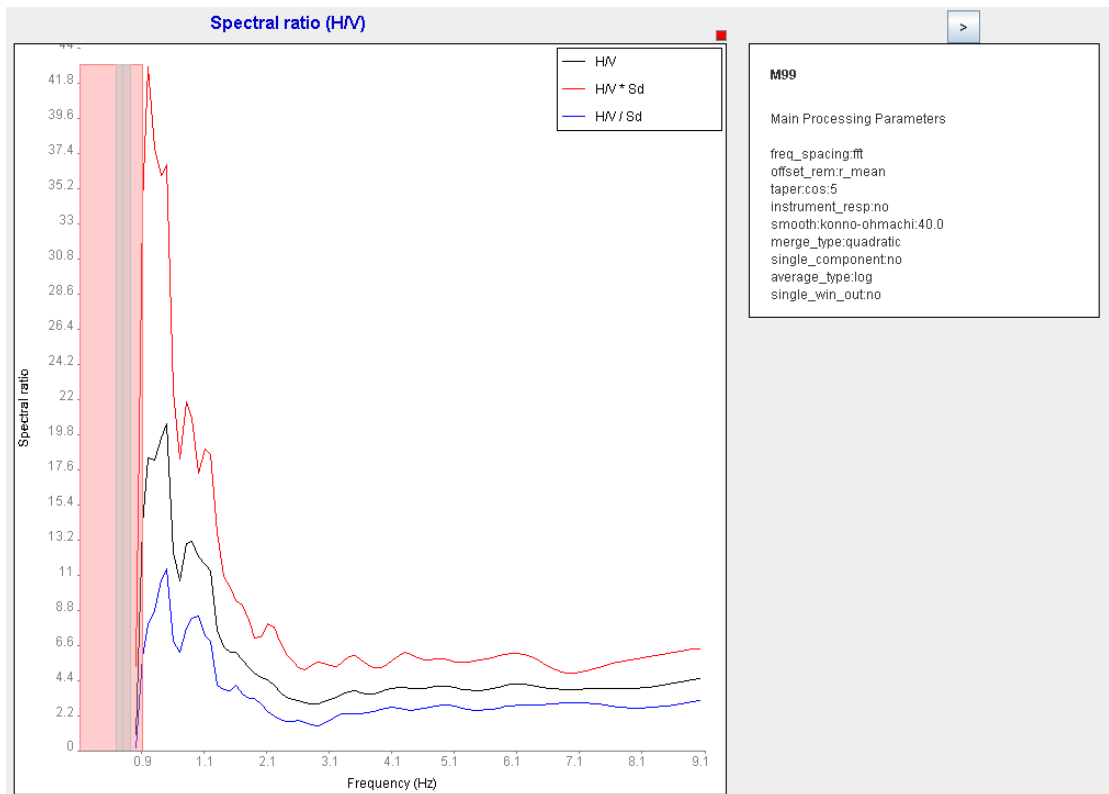
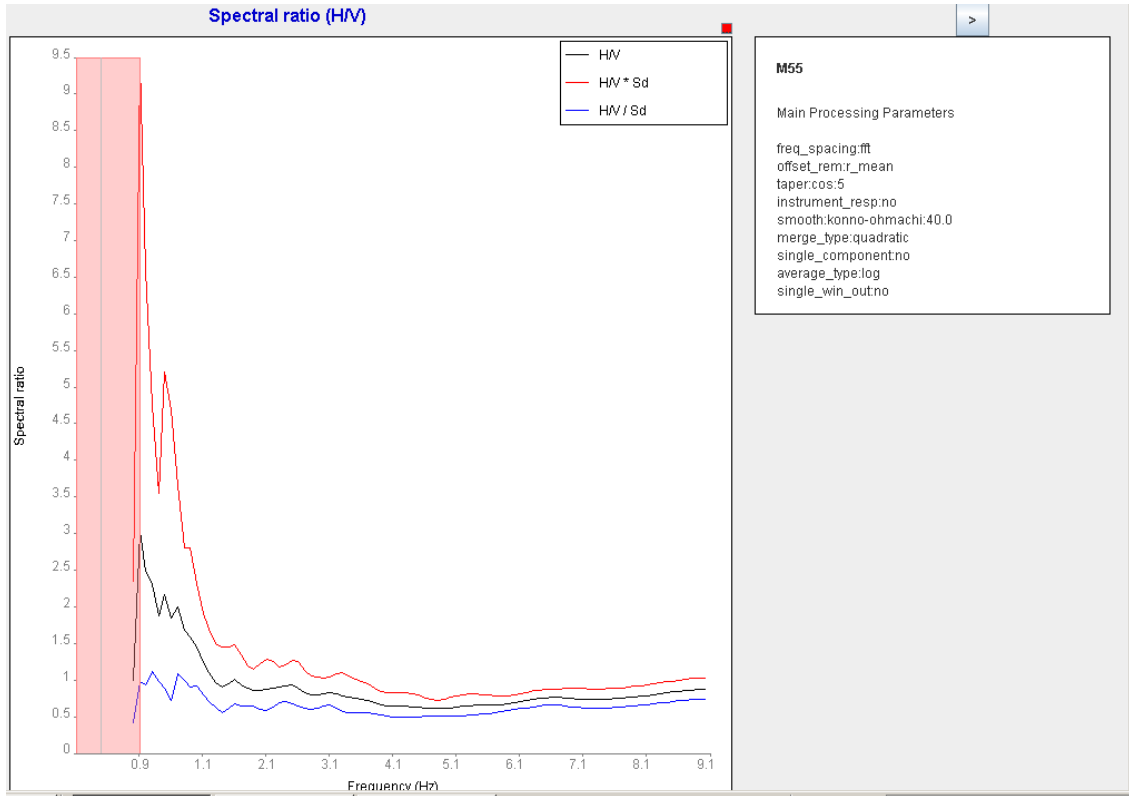


# Cross Section B-B1

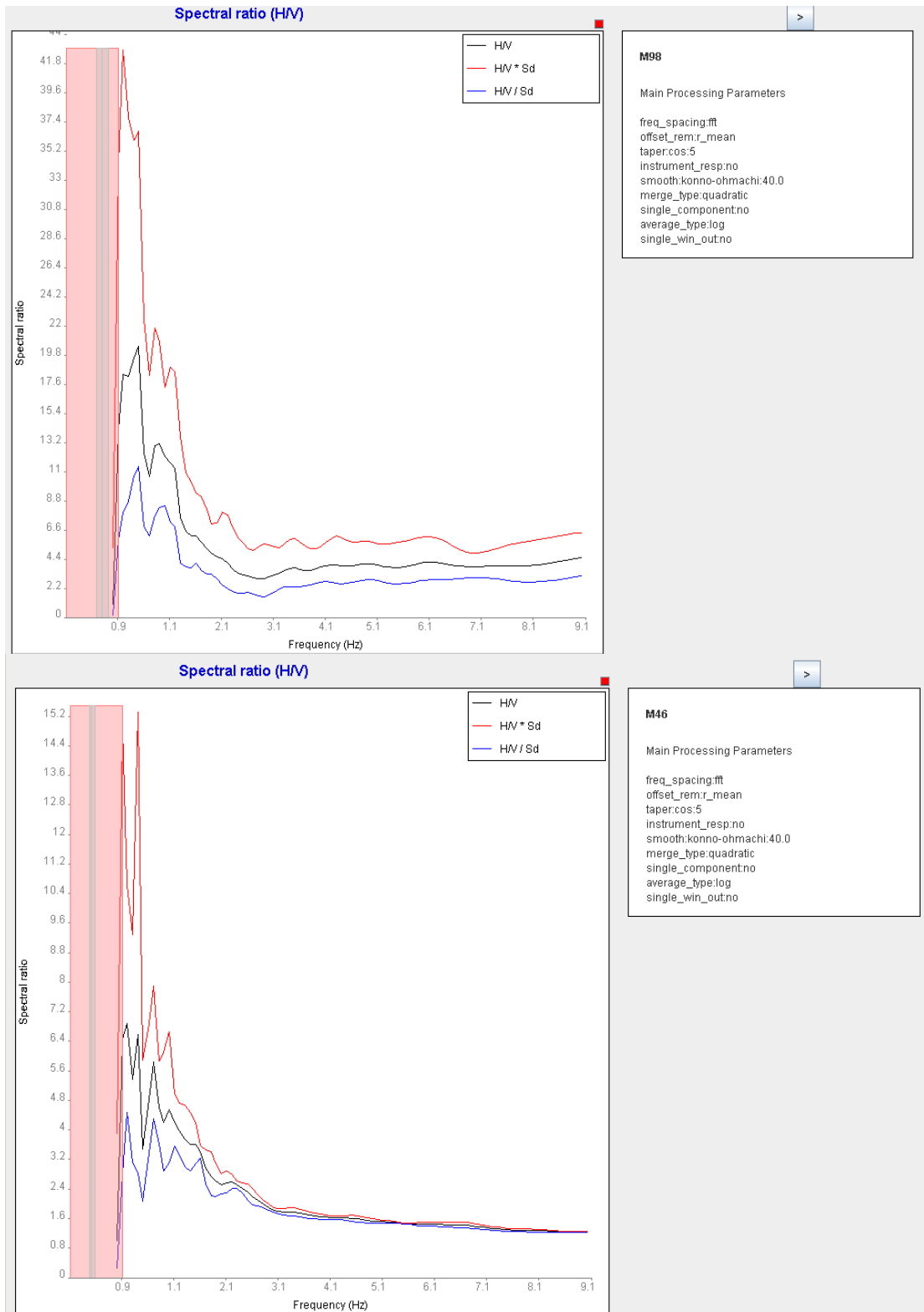


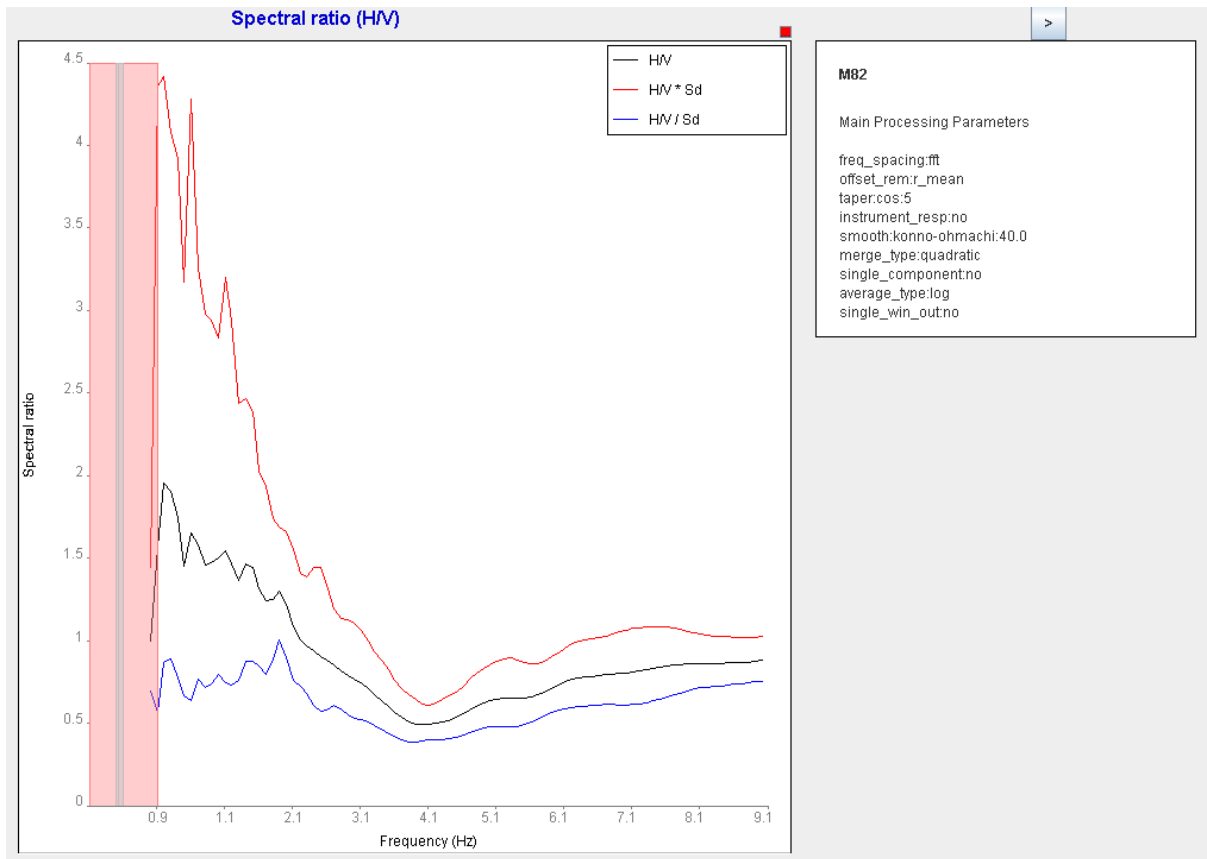












## Cross section C-C1

